Springer Tracts in Modern Physics
Volume 195

Springer
Berlin
Heidelberg
New York
Hong Kong
London
Milan
Paris
Tokyo

Springer Tracts in Modern Physics

Springer Tracts in Modern Physics provides comprehensive and critical reviews of topics of current interest in physics. The following fields are emphasized: elementary particle physics, solid-state physics, complex systems, and fundamental astrophysics.
Suitable reviews of other fields can also be accepted. The editors encourage prospective authors to correspond with them in advance of submitting an article. For reviews of topics belonging to the above mentioned fields, they should address the responsible editor, otherwise the managing editor.
See also springeronline.com

Konrad Kleinknecht

Uncovering *CP* Violation

Experimental Clarification in the Neutral K Meson and B Meson Systems

With 61 Figures

Springer

Professor Konrad Kleinknecht
Johannes-Gutenberg-Universität
Institut für Physik
55099 Mainz, Germany
E-mail: konrad.kleinknecht@uni-mainz.de

Library of Congress Cataloging-in-Publication Data

Kleinknecht, K. (Konrad), 1940-
Uncovering CP Violation : experimental clarification in the neutral K meson and B meson systems / Konrad Kleinknecht.
p. cm. - - (Springer tracts in modern physics, ISSN 0081-3869 ; v. 195)
Includes bibliographical references and index.
ISBN 3-540-40333-7 (acid-free paper)
1. CP violation (Nuclear physics) I. Title. II. Springer tracts in modern physics ; 195.

QC1.S797 vol. 195
[QC793.3.V5]
539 s- -dc22
[539.7'25] 2003060995

Physics and Astronomy Classification Scheme (PACS):
11.30, 12.15, 14.65, 29.30, 29.40

ISSN print edition: 0081-3869
ISSN electronic edition: 1615-0430
ISBN 3-540-40333-7 Springer-Verlag Berlin Heidelberg New York

Springer-Verlag Berlin Heidelberg New York
a member of BertelsmannSpringer Science+Business Media GmbH

springeronline.com

Typesetting: Camera-ready copy from the author using a Springer LaTeX macro package
Production: LE-TeX Jelonek, Schmidt & Vöckler GbR, Leipzig
Cover concept: eStudio Calamar Steinen
Cover production: *design &production* GmbH, Heidelberg

Printed on acid-free paper SPIN: 10855407 56/3141/YL 5 4 3 2 1 0

To the memory of René Turlay (1932–2002)

Codiscoverer of $\mathcal{CP}$ violation

Preface

This world, with all its events, even the most minute, has before been produced and destroyed, and will again be produced and destroyed, without any bounds and limitations.

David Hume, *Dialogues Concerning Natural Religion* (1779), Part VIII

The discovery of $\mathcal{CP}$ violation in decays of neutral K mesons by Jim Christenson, Jim Cronin, Val Fitch and René Turlay in 1964 came as a complete surprise to us. At that time, the structure of the weak interaction had become clear, as a V–A interaction with built-in parity violation; the second neutrino, with muon flavor, had been found; and the eightfold way had been formulated as a flavor SU(3) symmetry of the three known quarks. However, this phenomenon of $\mathcal{CP}$ violation did not fit into the picture and was a small $\mathcal{O}(10^{-3})$ effect, completely different from the 100% parity violation as seen in the neutrino helicity.

Forty years later, we have a rather clear picture of how this observed $\mathcal{CP}$ violation in K meson decays fits into the framework of weak interactions between six quarks. In addition, $\mathcal{CP}$ violation has now been observed in a second neutral meson system, the B^0 system. This book describes how, over this long period of time, experimenters invented and built ingenious detectors in order to clarify the question, of whether $\mathcal{CP}$ violation was a completely new phenomenon outside the known interactions or an integral part of the weak interaction. This endeavor required the detection of decay amplitudes which are 10^5 times weaker than those of normal weak decays.

I was introduced to the field of K mesons by Jack Steinberger when he had just come to CERN from Columbia University in 1965. At that time, our first experiment on the interference between $\mathcal{CP}$-violating and $\mathcal{CP}$-conserving amplitudes took one year. Today, experiments at B factories will go on for another 10 years in order to elucidate further this intriguing phenomenon.

I thank my colleagues over many years in the CERN–Aachen–Torino, CERN–Heidelberg, NA31 and NA48 collaborations for the good spirit in which we did these experiments.

I also thank Mrs. Silvia Müller and Dr. Andreas Hirstius for their help with the manuscript and the figures.

Mainz, August 2003 *Konrad Kleinknecht*

Konrad Kleinknecht: Uncovering $\mathcal{CP}$ Violation, STMP 195, VII–IX (2003)

Contents

1 Introduction

1.1 Matter–Antimatter Asymmetry in the Universe

One of the surprising facts in our present understanding of the development of the Universe is the complete absence of "primordial" antimatter from the Big Bang about 13.7 billion years ago. The detection of charged cosmic-ray particles by magnetic spectrometers borne by balloons, satellites, and the space shuttle has shown no evidence for such primordial (high-energy) antibaryons; nor has the search for gamma rays from antimatter–matter annihilation yielded any such observation. In the early phases of the expanding Universe, a hot (10^{32} K) and dense plasma of quarks, antiquarks, leptons, antileptons and photons coexisted in equilibrium. This plasma expanded and cooled down, and matter and antimatter could recombine and annihilate into photons. If all interactions were symmetric with respect to matter and antimatter, and if baryon and lepton numbers were conserved, then all particles would finally convert to photons, and the expansion of the Universe would shift the wavelength of these photons to the far infrared region.

This cosmic microwave background radiation was indeed observed by Penzias and Wilson in 1965 [1], and its wavelength distribution corresponds exactly to Planck black-body radiation at a temperature of 2.73 K (see Fig. 1.1). The density of this radiation is about 5×10^2 photons/cm^3.

However, this radiation is not the only remnant of the Big Bang; there is also a small amount of baryonic matter left over, at a density of 6×10^{-8} nucleons/cm^3, about 10^{-10} of the photon density. This phenomenon can only be explained if the three conditions of Sakharov [2] are fulfilled:

- there must be an interaction violating $\mathcal{CP}$ invariance, where $\mathcal{C}$ is the particle–antiparticle transformation and $\mathcal{P}$ the space inversion operation;
- there must be an interaction violating the conservation of baryon number;
- there must be phases of the expansion without thermodynamic equilibrium.

The first condition was shown to be fulfilled when, in 1964, J. Christenson, J. Cronin, V. Fitch and R. Turlay discovered $\mathcal{CP}$ violation [3] in decays of neutral K mesons. The second criterion would imply that protons are not stable; searches for such a decay have been unsuccessful, showing that the lifetime of the proton is longer then 10^{31} years. The third condition can be

Konrad Kleinknecht: Uncovering $\mathcal{CP}$ Violation, STMP 195, 1–2 (2003)

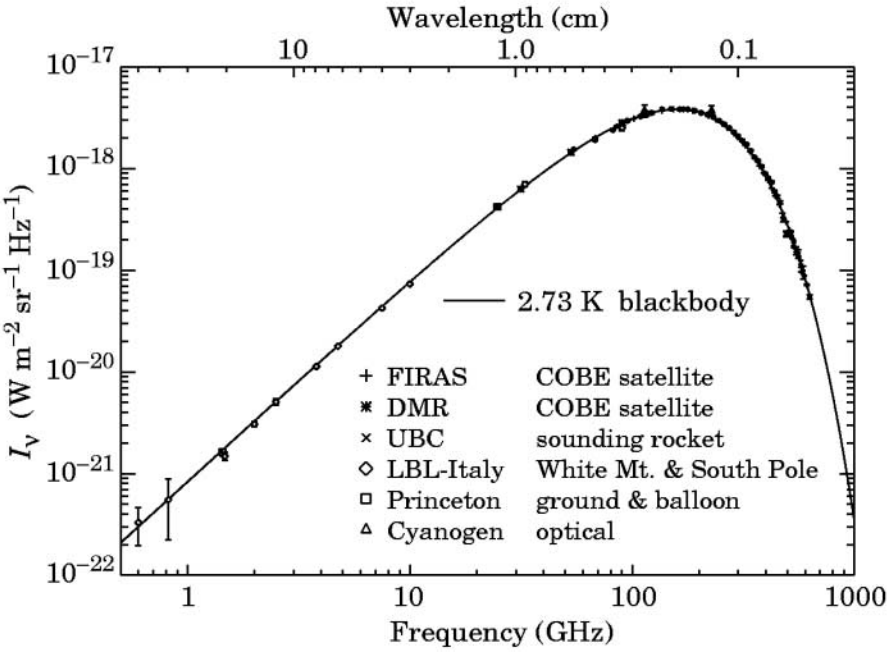

Fig. 1.1. Frequency distribution of the cosmic microwave background variation, as measured by the COBE satellite and earth-based experiments.

met in cosmological models by inflationary fast expansion or by a first-order phase transition in the electroweak interaction of the Standard Model.

In the following, we shall concentrate on the observed $\mathcal{CP}$ violation, which could in principle lead to a small surplus of matter, the observed baryon asymmetry of 10^{-10} in the Universe.

References

1. A. A. Penzias, R. Wilson, *Astrophys. J.* **142**, 419 (1965) 1
2. A. D. Sakharov, *JETP Lett.* **5**, 24 (1967) 1
3. J. H. Christenson, J. W. Cronin, V. L. Fitch, R. Turlay, *Phys. Rev. Lett.* **13**, 138 (1964) 1

2 Symmetries

Symmetries and conservation laws have long played an important role in physics. The simplest examples of macroscopic relevance are the laws of conservation of energy and momentum, which are due to the invariance of forces under translation in time and space, respectively. Both are continuous transformations. In the domain of quantum phenomena, there are also conservation laws corresponding to discrete transformations. One of these is reflection in space (the "parity operation") $\mathcal{P}$ [1]. The second discrete transformation is particle–antiparticle conjugation $\mathcal{C}$ [2]. This transforms each particle into its antiparticle, whereby all additive quantum numbers change their sign. A third transformation of this kind is time reversal $\mathcal{T}$, which reverses momenta and angular momenta [3]. This corresponds formally to an inversion of the direction of time. According to the $\mathcal{CPT}$ theorem of Lüders and Pauli [4, 5], there is a connection between these three transformations such that, under rather weak, assumptions in a local field theory all processes are invariant under the combined operation $\mathcal{C} \cdot \mathcal{P} \cdot \mathcal{T}$.

2.1 Discrete Symmetries in Classical Physics

2.1.1 Parity $\mathcal{P}$

The parity operation consists in reversing the direction of the position vector $\boldsymbol{r} = (X, Y, Z)$ in Cartesian coordinates. This corresponds to reflection in a plane mirror, followed by a rotation by 180°. Symmetry under parity operation is therefore also called mirror symmetry.

The parity operation reverses the direction of all polar vectors derived from the position vector; in particular, this is the case for the momentum $\boldsymbol{p} = m\boldsymbol{v} = m\mathrm{d}\boldsymbol{r}/\mathrm{d}t$ and the acceleration $\boldsymbol{a} = \mathrm{d}^2\boldsymbol{r}/\mathrm{d}t^2$. Therefore, the Newtonian force $\boldsymbol{F} = \mathrm{d}\boldsymbol{p}/\mathrm{d}t$ is also reversed under the parity operation.

This must be also the case for the Lorentz and Coulomb forces on a particle with charge q moving with velocity $\boldsymbol{v}$:

$$\boldsymbol{F} = q(\boldsymbol{E} + \boldsymbol{v} \times \boldsymbol{B}) \,. \tag{2.1}$$

Since the charge q is invariant under $\mathcal{P}$, and the force $\boldsymbol{F}$ and the velocity $\boldsymbol{v}$ change sign, the electric field strength $\boldsymbol{E}$ must change sign and the magnetic field strength $\boldsymbol{B}$ must remain unchanged.

Konrad Kleinknecht: Uncovering $\mathcal{CP}$ Violation, STMP 195, 3–12 (2003)

For the electric potential $\boldsymbol{A}$,we obtain, from the relations

$$\boldsymbol{E} = -\mathrm{grad}\, V - \partial \boldsymbol{A}/\partial t, \tag{2.2}$$

$$\boldsymbol{B} = \mathrm{rot}\, \boldsymbol{A}, \tag{2.3}$$

the result that $\boldsymbol{A}$ changes sign and V remains invariant, since the spatial differential operator changes sign under the parity operation.

We therefore have four classes of quantities with different transformation behavior under $\mathcal{P}$: axial vectors or pseudovectors such as $\boldsymbol{B}$ and the angular momentum $\boldsymbol{J} = \boldsymbol{r} \times \boldsymbol{p}$, and scalars such as V, which remain invariant under $\mathcal{P}$; and polar vectors such as $\boldsymbol{r}$, $\boldsymbol{p}$, $\boldsymbol{F}$, $\boldsymbol{E}$ and $\boldsymbol{A}$, and pseudoscalars such as $\boldsymbol{E} \cdot \boldsymbol{B}$, which change sign under $\mathcal{P}$.

2.1.2 Time Reversal $\mathcal{T}$

This operation consists in reversing the sign of the time axis t. Under this operation $t \to -t$, the velocity $\boldsymbol{v}$, the momentum $\boldsymbol{p}$ and the angular momentum $\boldsymbol{J}$ change sign, while the force $\boldsymbol{F}$ remains unchanged under $\mathcal{T}$. From the fact that the Coulomb and Lorentz forces are invariant, we derive the result that $\boldsymbol{E} \to \boldsymbol{E}$ and $\boldsymbol{B} \to \boldsymbol{B}$ under $\mathcal{T}$; for the potentials, $V \to V$ but $\boldsymbol{A} \to -\boldsymbol{A}$.

2.1.3 Dipole Moments

Elementary particles with spin may have electric or magnetic dipole moments. The spin $\boldsymbol{s}$ has the dimensions of an angular momentum, and therefore remains unchanged under parity and changes sign under time reversal.

The potential energy of an electric or magnetic dipole in an external field is proportional to the scalar product of the electric or magnetic moment with the strenght of the external electromagnetic field. Since the moments must be parallel to the spin, the potential energy is given by

$$-d_{\mathrm{e}} \boldsymbol{s} \cdot \boldsymbol{E} \quad \text{for the electric case} \tag{2.4}$$

and

$$-d_{\mathrm{m}} \boldsymbol{s} \cdot \boldsymbol{B} \quad \text{for the magnetic case} \tag{2.5}$$

Here d_{e} and d_{m} are the electric and magnetic dipole moments. If we onsider the transformation properties of $\boldsymbol{s}$, $\boldsymbol{E}$ and $\boldsymbol{B}$ under $\mathcal{P}$ and $\mathcal{T}$, it turns out that for both operations $d_{\mathrm{m}} \to d_{\mathrm{m}}$ and $d_{\mathrm{e}} \to -d_{\mathrm{e}}$. This means that observation of a nonvanishing electric dipole moment would violate any invariance under parity and time-reversal transformations.

In classical physics, all processes are invariant under parity and under time reversal. In the case of mirror symmetry, this means that a physical experiment will lead to the same result as a mirror-imaged experiment, since the equations of classical physics are left-right symmetric. In a similar way,

the classical motion of one particle can be reversed, e.g. by playing a film backwards, and this inversion of the motion corresponds formally to time reversal. Again, the laws of motion are invariant under $\mathcal{T}$, and the reversed motion follows the same path backwards as forwards.

Of course, this is no longer the case if many particles move and interact with each other; in this case the second law of thermodynamics ensures that entropy is increasing, thus defining an arrow of time.

2.2 Discrete Symmetries in Quantum Systems

2.2.1 Particle–Antiparticle Conjugation

In relativistic quantum mechanics, the Dirac equation requires that for each solution describing a particle, there is a second solution with opposite charge, describing the antiparticle. The antiparticle of the electron, the positron, was found in 1933 [7], and the antiproton was found in 1955 [8]. The particle–antiparticle conjugation $\mathcal{C}$ transforms the field ϕ of the particle into a related field $\phi^\dagger$ which has opposite quantum numbers: the charge, lepton number, baryon number, strangeness, beauty, etc. for the antiparticle are opposite in sign to the values for the particle.

Invariance under the $\mathcal{C}$ transformation is always valid in the strong and electromagnetic interactions. This means, in particular, that the visible spectral lines from atoms and their antiatom partners are identical, and we cannot use these lines to identify antimatter in the Universe.

This would be especially important in the science-fiction scenario in which a man-made spacecraft sets out to meet a distant civilization, where it would be advisable to know whether the other planet was made of matter or antimatter. In this case another means of differentiation would have to be found.

2.2.2 Violation of Mirror Symmetry – Parity Violation in Weak Interactions

Lee and Yang [10] suggested that of the four interactions – strong, electromagnetic, weak and gravitational – the weak interaction might violate mirror symmetry when it was described by a combination of vector and axial-vector currents in the Lagrangian (V–A theory). The interference of these two currents could lead to pseudoscalar observables which would change sign under the parity operation. One such observable is the scalar product of an axial vector (such as the spin of a particle) with a polar vector (such as the momentum of another particle in the final state). If the expectation value of this pseudoscalar is measured to be nonvanishing, then parity is violated.

An experiment on the beta decay of cobalt-60 [11] measured exactly such an observable, the scalar product of the spin $5\hbar$ of the ^{60}Co nucleus and the direction of the electron from its beta decay into an excited state of ^{60}Ni

with nuclear spin $4\hbar$. The ^{60}Co nuclei were polarized by embedding them in a cerium–magnesium crystal, where the magnetic moments were aligned by a weak external magnetic field of about 0.05 T. In the strong magnetic field inside this paramagnet, the ^{60}Co nuclei are polarized through hyperfine interactions if the temperature is low enough (0.01 K) to avoid thermal demagnetization. The polarization was measured through the asymmetry of γ rays from the cascade decay of the ^{60}Ni state. The measurement then required the detection of the electron direction relative to the polarization of the Co nuclei. The experimenters found that the electron was emitted preferentially in a direction opposite to the external magnetic field, and that this effect disappeared when the crystal was warmed and the nuclear polarization disappeared. Thus, at low temperature, a nonzero pseudoscalar is observed, demonstrating parity violation.

Other experiments lead to similar results. The helicity $h = \boldsymbol{s} \cdot \boldsymbol{p}/|\boldsymbol{s} \cdot \boldsymbol{p}|$ of the neutrino emitted in the weak electron capture by ^{152}Eu was measured in an experiment by Goldhaber and Grodzins [15] to be negative; the neutrino is "left-handed", i.e. the spin is aligned antiparallel to the momentum. Similarly, measurements of the polarization of electrons from β^- decay showed a negative value, with a modulus increasing with the velocity of the electron, v/c. Positrons from β^+ decay were found to have a positive polarization that increases with v/c.

2.2.3 Violation of $\mathcal{C}$ Symmetry, and $\mathcal{CP}$ Invariance

In the realm of weak decays of particles, supporting evidence for the violation of mirror symmetry came from the observation that parity is violated in the decay $\pi^+ \to \mu^+ \nu_\mu$, and that the muon neutrino from this decay is left-handed [12, 13]. The $\mathcal{P}$-conjugate process, i.e. $\pi^+ \to \nu_\mu \mu^+$, with a right-handed neutrino, does not occur. The same is true for the $\mathcal{C}$-conjugate process, $\pi^- \to \mu^- \overline{\nu_\mu}$, with a left-handed antineutrino. However, if we combine the $\mathcal{C}$ and $\mathcal{P}$ operations, we arrive at a process $\pi^- \to \mu^- \overline{\nu_\mu}$ with a right-handed antineutrino, which proceeds at the same rate as the original π^+ decay, with a left-handed muon neutrino. Evidently, in weak interactions, $\mathcal{P}$ and $\mathcal{C}$ are violated, while it seemed at the time of those experiments that the process was invariant under the combined operation $\mathcal{C} \cdot \mathcal{P}$. This argument can be visualized as in Fig. 2.1. Here the $\mathcal{P}$ mirror and the $\mathcal{C}$ mirror act on a left-handed neutrino, both leading to unphysical states, a right-handed neutrino and a left-handed antineutrino. Only the combined $\mathcal{CP}$ mirror leads to a physical particle, the right-handed antineutrino. This argument was made by Landau [14], suggesting that the real symmetry was $\mathcal{CP}$ invariance.

2.2.4 $\mathcal{CP}$ Invariance and Neutral K Mesons

One consequence of this postulated $\mathcal{CP}$ invariance was predicted by Gell-Mann and Pais [9] for the neutral K mesons: there should be a long-lived

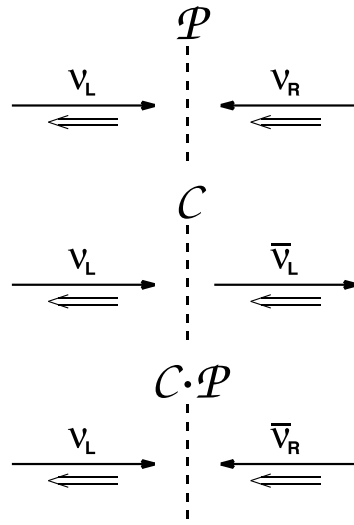

Fig. 2.1. The mirror image of a left-handed neutrino under $\mathcal{P}$, $\mathcal{C}$ and $\mathcal{CP}$ mirror operations

partner to the known V^0 $\left(K_1^0\right)$ particle of short lifetime (10^{-10}s). According to this proposal, these two particles are mixtures of the two strangeness eigenstates $K^0(\mathbb{S}=+1)$ and $\overline{K^0}(\mathbb{S}=-1)$ produced in strong interactions. Weak interactions do not conserve strangeness, and the physical particles should be eigenstates of $\mathcal{CP}$ if the weak interactions are $\mathcal{CP}$-invariant. These eigenstates are described as follows (where we choose the phases such that $\overline{K^0}=\mathcal{CP}K^0$):

$$\mathcal{CP}K_1=\mathcal{CP}\left[\frac{1}{\sqrt{2}}\left(K^0+\overline{K^0}\right)\right]=\frac{1}{\sqrt{2}}\left(\overline{K^0}+K^0\right)=K_1\ , \tag{2.6}$$

$$\mathcal{CP}K_2=\mathcal{CP}\left[\frac{1}{\sqrt{2}}\left(K^0-\overline{K^0}\right)\right]=\frac{1}{\sqrt{2}}\left(\overline{K^0}-K^0\right)=-K_2\ . \tag{2.7}$$

Because $\mathcal{CP}\,|\pi^+\pi^-\rangle=|\pi^+\pi^-\rangle$ for π mesons in a state with angular momentum zero, i.e. the two-pion state has a positive $\mathcal{CP}$ eigenvalue, a decay into $\pi^+\pi^-$ is allowed for the K_1 but forbidden for the K_2; hence the longer lifetime of K_2, which was indeed confirmed when the K_2 was discovered [16, 17].

2.2.5 Discovery of $\mathcal{CP}$ Violation

In 1964, however, Christenson, Cronin, Fitch and Turlay [18] discovered that the long-lived neutral K meson also decays to two charged pions with a branching ratio of 2×10^{-3}.

The motivation of this experiment was twofold: the experimenters wanted to check on an effect found by Adair et al[19]. when the latter observed

interactions of long-lived kaons (K_2) in hydrogen, and they wanted to test $\mathcal{CP}$ invariance by searching for the decay of K_2 into two pions. Adair et al. had found anomalous regeneration of short-lived kaons (K_1) above expectation. "Regeneration" is an effect due to the different strong interactions of the two components of a long-lived kaon, K^0 and $\overline{K^0}$. This leads to a creation of a coherent K_1 component when a K_2 beam traverses matter (see Sect. 5.3). The anomalous effect above expectation was still observed in the experiment of Christenson et al. when the (K_2) beam hit a hydrogen target.

Therefore, Christenson et al. emptied the target and looked for $K_2 \to \pi^+\pi^-$ decays from the vacuum. To their surprise, they found such decays, which meant that $\mathcal{CP}$ invariance was broken in this decay.

The magnetic spectrometer used by Christenson et al. is shown in Fig. 2.2. On each side of the spectrometer, one charged particle is detected through spark chambers in front of and behind the magnet. The two vector momenta $\boldsymbol{p}_i$ $(i = 1, 2)$ of the two particles are measured. Assuming the mass of the particles to be the pion rest mass m_π their energies can be obtained from

$$E_i^2 = \boldsymbol{p}_i^2 + m_\pi^2 \,. \tag{2.8}$$

The invariant mass of the pair is

$$m_{\pi\pi} = \sqrt{[(E_1 + E_2)^2 - (\boldsymbol{p}_1 + \boldsymbol{p}_2)^2]} \,, \tag{2.9}$$

and the kaon momentum is

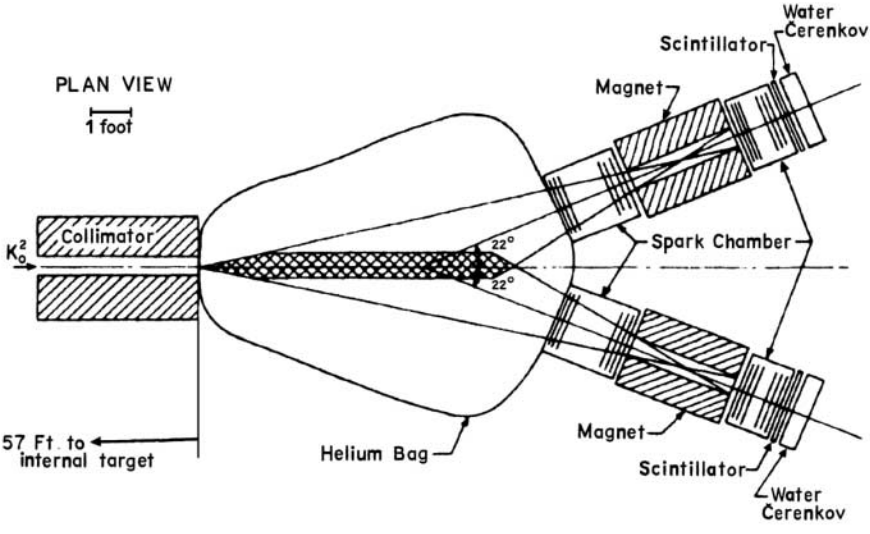

Fig. 2.2. The experimental setup used by Christenson et al. [18] for the discovery of $\mathcal{CP}$ violation

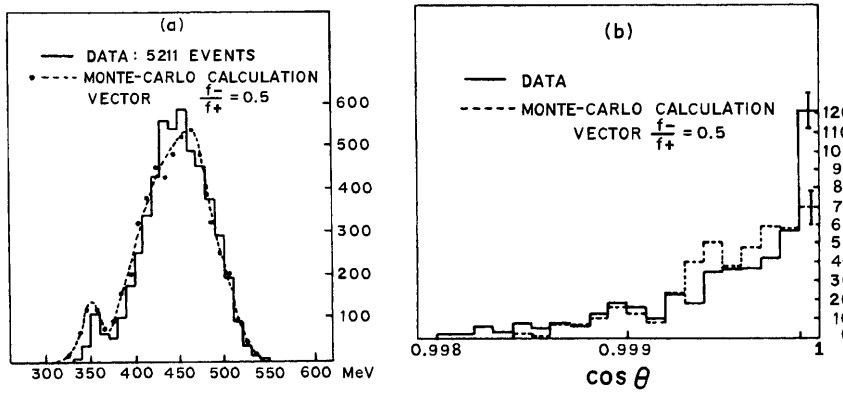

Fig. 2.3. (**a**) Experimental distribution of m^* compared with Monte Carlo calculation. The calculated distribution is normalized to the total number of observed events. (**b**) Angular distribution of those events in the range $490 < m^* < 510$ MeV. The calculated curve is normalized to the number of events in the total sample.

$$\boldsymbol{p}_{\mathrm{K}} = \boldsymbol{p}_1 + \boldsymbol{p}_2 \ . \tag{2.10}$$

From the reconstructed kaon momentum, the intersection of the kaon flight path with the target plane gives an indication of whether this was a two-body decay coming from the target or a three-body decay with an escaping neutrino.

In the latter case, the direction of $\boldsymbol{p}_{\mathrm{K}}$ does not point back to the target source. The result of the experiment is shown in Fig. 2.3. A significant peak of $\mathrm{K} \to \pi^+\pi^-$ decays coming from the target direction ($\cos\theta = 1$) is seen, while the background of three-body decays outside the peak can be extrapolated under the signal, and represents only ∼20% of the data in the signal region: there is a signal at the level of 2×10^{-3} of all decays, and $\mathcal{CP}$ is violated.

From then on the long-lived K meson state was called $\mathrm{K_L}$ because it was no longer identical to the $\mathcal{CP}$ eigenstate $\mathrm{K_2}$. However, the physical long-lived state $\mathrm{K_L}$ was a superposition of a predominant $\mathrm{K_2}$ amplitude and a small admixture of a $\mathrm{K_1}$ amplitude, $\mathrm{K_L} = (\mathrm{K_2} + \varepsilon \mathrm{K_1})/\sqrt{1+|\varepsilon|^2}$ where the admixture parameter ε is determined by experiment to satisfy $|\varepsilon| \sim 2 \times 10^{-3}$ (3.21) . Similarly, the short-lived state was called $\mathrm{K_S}$, and $\mathrm{K_S} = (\mathrm{K_1} + \varepsilon \mathrm{K_2})/\sqrt{1+|\varepsilon|^2}$. The $\mathcal{CP}$ violation that manifested itself by the decay $\mathrm{K_L} \to \pi^+\pi^-$ was confirmed subsequently in the decay $\mathrm{K_L} \to \pi^0\pi^0$ [20, 21], and by a charge asymmetry in the decays $\mathrm{K_L} \to \pi^\pm e^\mp \nu$ and $\mathrm{K_L} \to \pi^\pm \mu^\mp \nu$ [22, 23].

2.3 Discrete Symmetries in Quantum Mechanics

The three discrete symmetries $\mathcal{P}$, $\mathcal{C}$ and $\mathcal{T}$ are described by the operators $\mathcal{P}$ for the parity transformation, $\mathcal{C}$ for particle–antiparticle conjugation and

$\mathcal{T}$ for time reversal. Invariance of an interaction described by a Hamiltonian $\mathcal{H}$ under a symmetry operation means that $\mathcal{H}$ commutes with the relevant operator, e.g. $[\mathcal{H}\ ,\ \mathcal{P}\ ] = 0$. According to experimental evidence, the strong and electromagnetic interactions are $\mathcal{P}$- and $\mathcal{C}$-invariant. The corresponding operators are unitary, i.e. the Hermitian conjugate is equal to the inverse:

$$\mathcal{C}^\dagger = \mathcal{C}^{-1}\ , \tag{2.11}$$

$$\mathcal{P}^\dagger = \mathcal{P}^{-1}\ . \tag{2.12}$$

For two states $|\psi\rangle$ and $|\varphi\rangle$, such a unitary transformation does not change the product:

$$\langle\psi\ |\ \varphi\rangle \quad = \quad \langle\psi'\ |\ \varphi'\rangle\ , \tag{2.13}$$

where $|\psi'\rangle$ and $|\varphi'\rangle$ are the transformed states.

By defining the intrinsic parity of the proton as $+1$, a phase convention for the fields can be chosen, such that the parity operator $\mathcal{P}$ has only eigenvalues of $+1$ or -1, and all particles have intrinsic parities ± 1 as quantum numbers. These conserved quantities, which correspond to discrete symmetries, are multiplicative quantum numbers.

The third discrete symmetry, time reversal, is a special case. The corresponding operator $\mathcal{T}$ is not unitary, but antiunitary. Here the bracket $\langle\psi|\varphi\rangle$ is not conserved by the $\mathcal{T}$ transformation, but rather

$$\langle\psi'|\varphi'\rangle \quad = \quad \langle\psi|\varphi\rangle^*\ . \tag{2.14}$$

Probability is still conserved, i.e.

$$|\langle\psi'|\varphi'\rangle| \quad = \quad |\langle\psi|\varphi\rangle|\ , \tag{2.15}$$

but the phases are not. The fact that $\mathcal{T}$ is antiunitary can be deduced, from the Schrödinger equation for a free particle, where the time derivative is odd under $\mathcal{T}$ while the Laplace operator Δ is even. This can be reconciled with $\mathcal{T}$ invariance only if $\mathcal{T}$ makes the changes $\mathrm{i} \to -\mathrm{i}$ and $\psi \to \psi^*$.

$\mathcal{CPT}$, the product of all three discrete transformations, being a product of two unitary and one antiunitary operator, is also antiunitary. According to the $\mathcal{CPT}$ theorem of Lüders (1954) and Pauli (1955), and, Jost (1957) [4, 5, 6], a field theory with Lorentz invariance, locality and the commutation relations given by the spin–statistics theorem is $\mathcal{CPT}$-invariant. At present there is no realistic field theory which violates $\mathcal{CPT}$ invariance.

As a consequence of this theorem, violation of one of the three discrete symmetries implies a violation of a complementary one. If $\mathcal{CP}$ is violated, then $\mathcal{T}$ is also violated.

The experimental consequences of $\mathcal{CPT}$ invariance are the equality of the masses, lifetimes and magnetic dipole moments of a particle and its antiparticle. These equalities have been tested with great precision, as shown in Table 2.1.

Table 2.1. Comparison of masses m, lifetimes τ, and magnetic g-factors of particle and antiparticles

Particle	$\lvert m-\overline{m}\rvert/m$	$\lvert\tau-\overline{\tau}\rvert/\tau$	$\lvert g-\overline{g}\rvert/g$
e	$< 4\times10^{-8}$		$(-0.5\pm2.1)\times10^{-12}$
μ		$(1\pm8)\times10^{-5}$	$(-2.6\pm1.6)\times10^{-8}$
π	$(2\pm5)\times10^{-4}$	$(5.5\pm7.1)\times10^{-4}$	
p	$< 10^{-8}$		
K^0	$< 5\times10^{-18}$		

A very special case in this context is that of the masses of the neutral K mesons. The mass difference between the long-lived $\mathrm{K_L}$ and the short-lived $\mathrm{K_S}$ can be measured in interference experiments. This difference is due to second-order weak interactions and, therefore, is very small, about $\Delta m = (3.480\pm0.007)\times10^{-6}$ eV, which means that $\Delta m/m_{\mathrm{K}} < 10^{-14}$. From this, one can deduce very stringent limits on the mass difference between the K^0 and $\overline{\mathrm{K}^0}$, of order 10^{-18}.

Thus, from experimental evidence, there is no doubt about the validity of $\mathcal{CPT}$ invariance.

References

1. E. Wigner, *Z. Phys.* **43**, 624 (1927) 3
2. G. C. Wick, *Ann. Rev. Nucl. Sci.* **8**, 1 (1958) 3
3. E. Wigner, *Nachr. Akad. Wiss. Göttingen* **31**, 546 (1932) 3
4. G. Lüders, *Kgl. Danske Videnskab. Selskab, Matfys. Medd.* **28(5)**, 1 (1954) 3, 10
5. W. Pauli, n *Niels Bohr and the Development of Physics* ed. W. Pauli, Pergamon, Oxford 2nd edn. (1955), p.30 3, 10
6. R. Jost, *Helv. Phys. Acta* **30**, 209 (1957) 10
7. C. D. Anderson, *Science* **76**, 238 (1932); *Phys. Rev.* **43**, 491 (1933) 5
8. O. Chamberlain, E. Segre, C. Wiegand, T. Ypsilantis, *Phys. Rev.* **100**, 947 (1955) 5
9. M. Gell-Mann, A. Pais, *Phys. Rev.* **97**, 1387 (1955) 6
10. T. D. Lee, C. N. Yang, *Phys. Rev.* **104**, 254 (1956) 5
11. C. S. Wu *et al.*, *Phys. Rev.* **105**, 1413 (1957) 5
12. R. L. Garwin, L. M. Lederman, M. Weinrich, *Phys. Rev.* **105**, 1415 (1957) 6
13. J. I. Friedman, V. L. Telegdi, *Phys. Rev.* **105**, 1681 (1957) 6
14. L. D. Landau, *Nucl. Phys.* **3**, 127 (1957) 6
15. M. Goldhaber, L. Grodzins, A. W. Sunyar, *Phys. Rev.* **109**, 1015 (1958) 6
16. M. Bardon *et al.*, *Ann. Phys. NY* **5**, 156 (1958) 7
17. D. Neagu *et al.*, *Phys. Rev. Lett.* **6**, 552 (1961) 7
18. J. H. Christenson, J. W. Cronin, V.L. Fitch, R. Turlay, *Phys. Rev. Lett.* **13**, 138 (1964) 7, 8
19. R. Adair *et al.*, *Phys. Rev.* **132**, 2285 (1963) 7

20. J. M. Gaillard *et al.*, *Phys. Rev. Lett.* **18**, 20 (1967) 9
21. J. W. Cronin *et al.*, *Phys. Rev. Lett.* **18**, 25 (1967) 9
22. S. Bennett *et al.*, *Phys. Rev. Lett.* **19**, 993 (1967) 9
23. D. Dorfan *et al.*, *Phys. Rev. Lett.* **19**, 987 (1967) 9

3 Mixing and Decay of Neutral Mesons

3.1 Particle–Antiparticle Mixing

Neutral mesons (represented by N^0 in this chapter) with a characteristic quantum number, such as the strangeness $\mathbb{S}$ for K^0 mesons, charm $\mathbb{C}$ for D^0 mesons and beauty $\mathbb{B}$ for B_s^0 and B_d^0 mesons, have the particular property that they can mix with their antiparticles, which carry an opposite-sign quantum number. Weak interactions do not conserve any of these quantum numbers ($\mathbb{S}$, $\mathbb{C}$, $\mathbb{B}$); consequently N^0 and $\overline{\mathrm{N}^0}$ can mix by second-order weak transitions through intermediate states such as $2\pi, 3\pi, \pi\mu\nu, \pi e\nu$ (for K^0), or $\pi\mathrm{K}$ (for B^0). The states that obey an exponential decay law are linear superpositions of N^0 and $\overline{\mathrm{N}^0}$,

$$\alpha\,|\mathrm{N}^0\rangle + \beta\,|\overline{\mathrm{N}^0}\rangle = \begin{pmatrix}\alpha\\ \beta\end{pmatrix} . \tag{3.1}$$

The time-dependent Schrödinger equation then becomes a matrix equation

$$\mathrm{i}\frac{\mathrm{d}}{\mathrm{d}t}\begin{pmatrix}\alpha\\ \beta\end{pmatrix} = X\begin{pmatrix}\alpha\\ \beta\end{pmatrix} , \tag{3.2}$$

where $X_{ik} = M_{ik} - \mathrm{i}\Gamma_{ik}/2$, and M_{ik} and Γ_{ik} are Hermitian matrices, called mass matrix and decay matrix, respectively. Both of the latter two matrices are Hermitian: $M = M^\dagger$ and $\Gamma = \Gamma^\dagger$. However X is not Hermitian. The elements of the matrix X are

$$\begin{aligned} X_{11} &= \langle \mathrm{N}^0|\mathcal{H}|\mathrm{N}^0\rangle , \quad & X_{22} &= \langle \overline{\mathrm{N}^0}|\mathcal{H}|\overline{\mathrm{N}^0}\rangle , \\ X_{12} &= \langle \mathrm{N}^0|\mathcal{H}|\overline{\mathrm{N}^0}\rangle , \quad & X_{21} &= \langle \overline{\mathrm{N}^0}|\mathcal{H}|\mathrm{N}^0\rangle \end{aligned} \tag{3.3}$$

where $\mathcal{CPT}$ invariance requires the diagonal elements to be equal: $X_{11} = X_{22}$. The matrix has the form

$$X = \begin{pmatrix} m - \frac{\mathrm{i}}{2}\Gamma & m_{12} - \frac{\mathrm{i}}{2}\Gamma_{12} \\ m_{12}^* - \frac{\mathrm{i}}{2}\Gamma_{12}^* & m - \frac{\mathrm{i}}{2}\Gamma \end{pmatrix} . \tag{3.4}$$

The off-diagonal elements of the matrices are given by

$$\Gamma_{21} = 2\pi \sum \varrho_F \langle \overline{\mathrm{N}^0}|\mathcal{H}_\mathrm{W}|F\rangle\langle F|\mathcal{H}_\mathrm{W}|\mathrm{N}^0\rangle , \tag{3.5}$$

Konrad Kleinknecht: Uncovering $\mathcal{CP}$ Violation, STMP 195, 13–20 (2003)

where the sum runs over all possible physical intermediate states F, which have a phase space density ϱ_F. Similarly,

$$M_{21} = \langle \overline{\mathrm{N}^0} | \mathcal{H}_\mathrm{W} | \mathrm{N}^0 \rangle + \sum_n \frac{\langle \overline{\mathrm{N}^0} | \mathcal{H}_\mathrm{W} | n \rangle \langle n | \mathcal{H}_\mathrm{W} | \mathrm{N}^0 \rangle}{m_{\mathrm{N}^0} - m_n} \,, \tag{3.6}$$

where the sum extends over all possible virtual intermediate states n.

The eigenvalue equations for X yield two eigenstates, which can be labeled by their mass: h for the higher mass, l for the lower mass. These eigenstates are the physical particles with a definite mass and an exponential lifetime distribution. The eigenvalues M_h and M_l of the matrix X are

$$\begin{aligned} M_h &= m_h - \frac{\mathrm{i}}{2} \Gamma_h \,, \\ M_l &= m_l - \frac{\mathrm{i}}{2} \Gamma_l \end{aligned} \tag{3.7}$$

We denote the differences between the physical quantities by $\Delta\Gamma = \Gamma_h - \Gamma_l$ and $\Delta m = m_h - m_l > 0$ and denote the average values by

$$\Gamma = \frac{\Gamma_h + \Gamma_l}{2} \,, \tag{3.8}$$

$$m = \frac{m_h + m_l}{2} \,. \tag{3.9}$$

For the B^0 – $\overline{\mathrm{B}^0}$ system and the D^0 – $\overline{\mathrm{D}^0}$ system, the two decay widths Γ_h and Γ_l are expected to be nearly equal (because the numbers of final states for the decay are very similar). In these cases it is customary to introduce the dimensionless quantities

$$x = \frac{\Delta m}{\Gamma} \tag{3.10}$$

and

$$y = \frac{\Delta\Gamma}{2\Gamma} \,. \tag{3.11}$$

Here x is positive by definition, and y varies between -1 and $+1$. For heavy systems such as B^0, $|y|$ is expected to be much less than 1, while for the K^0 systemm, y is found experimentally to be close to -1, since here the decay width of the lighter state is 600 times larger then that of the heavier state. Therefore, for the K^0 system, the lighter state is called $\mathrm{K_S}$ ("short-lived") and the heavier state $\mathrm{K_L}$ ("long-lived"). Table 3.1 gives a summary of various parameters of oscillating meson pairs.

3.2 Decays of Neutral Mesons

3.2.1 Time-Dependent Schrödinger equation

From the time-dependent Schrödinger equation for mixed states given above, it follows that

$$\frac{\mathrm{d}}{\mathrm{d}t}\left(|\alpha|^2+|\beta|^2\right) = -\left(\alpha^*\beta^*\right) \mathit{\Gamma} \begin{pmatrix}\alpha\\ \beta\end{pmatrix} . \tag{3.12}$$

Since both of the neutral mesons N^0 and $\overline{\mathrm{N}^0}$ decay, the left-hand side of this equation is negative for any α or β. Therefore $\mathit{\Gamma}$ is positive definite, in particular $\mathit{\Gamma}_{11}, \mathit{\Gamma}_{22}$ and $\det \mathit{\Gamma}$ are positive.

The physical particles, which have a definite mass and lifetime, are mixtures of the eigenstates N^0 and $\overline{\mathrm{N}^0}$ of the strong interaction, which carry definite values of their characteristic quantum numbers strangeness $\mathbb{S}$, charm $\mathbb{C}$, and beauty $\mathbb{B}$.

If the weak interaction through which these particles decay is invariant under a discrete symmetry, say $\mathcal{CP}$, then the physical particles are eigenstates of this symmetry because $\mathcal{H}_{\mathrm{W}}$ commutes with $\mathcal{CP}$.

The effect of discrete symmetries on N^0 and $\overline{\mathrm{N}^0}$ is the following: $\mathcal{CP}$ is unitary, and there is an arbitrary phase a:

$$\begin{aligned}\mathcal{CP}|\mathrm{N}^0\rangle &= \mathrm{e}^{\mathrm{i}a}|\overline{\mathrm{N}^0}\rangle ,\\ \mathcal{CP}|\overline{\mathrm{N}^0}\rangle &= \mathrm{e}^{-\mathrm{i}a}|\mathrm{N}^0\rangle .\end{aligned} \tag{3.13}$$

$\mathcal{CPT}$, however, is antiunitary, and, with an arbitrary phase b,

$$\begin{aligned}\mathcal{CPT}|\mathrm{N}^0\rangle &= \mathrm{e}^{\mathrm{i}b}|\overline{\mathrm{N}^0}\rangle ,\\ \mathcal{CPT}|\overline{\mathrm{N}^0}\rangle &= \mathrm{e}^{\mathrm{i}b}|\mathrm{N}^0\rangle .\end{aligned} \tag{3.14}$$

For $\mathcal{T}$, which is also antiunitary, we obtain

Table 3.1. Parameters of the four neutral oscillating meson pairs [1]. (See Sects. 5.6.10, 6.6 and 6.7)

	$\mathrm{K}^0/\overline{\mathrm{K}^0}$	$\mathrm{D}^0/\overline{\mathrm{D}^0}$	$\mathrm{B}^0/\overline{\mathrm{B}^0}$	$\mathrm{B}_\mathrm{s}^0/\overline{\mathrm{B}_\mathrm{s}^0}$
τ (ps)	89.59 ± 0.04 ; $51\,700 \pm 400$	0.4117±0.0027	1.542 ± 0.016	1.461±0.057
$\mathit{\Gamma}$ (s^{-1})	5.61×10^{9}	2.4×10^{12}	$(6.41\pm0.16)\times10^{11}$	$(6.7 \pm 0.3)\times10^{11}$
$y = \Delta\mathit{\Gamma}/(2\mathit{\Gamma})$	−0.9966	$\lvert y\rvert < 0.06$	$\lvert y\rvert \lesssim 0.01$	−(0.01–0.10)
Δm (s^{-1})	$(5.286\pm0.011)\times10^{9}$	$< 7\times10^{10}$	$(4.89\pm0.08)\times10^{11}$	$> 14.4\times10^{12}$
Δm (eV)	$(3.480\pm0.007)\times10^{-6}$	$< 5\times10^{-6}$	$(3.22\pm0.05)\times10^{-4}$	$> 8.6\times10^{-3}$
$x = \Delta m/\mathit{\Gamma}$	0.945±0.002	< 0.03	0.76±0.02	21–40

$$\begin{aligned}\mathcal{T}|\mathrm{N}^0\rangle &= \mathrm{e}^{\mathrm{i}(b-a)}|\overline{\mathrm{N}^0}\rangle \\ \mathcal{T}|\overline{\mathrm{N}^0}\rangle &= \mathrm{e}^{\mathrm{i}(b+a)}|\mathrm{N}^0\rangle\end{aligned} \tag{3.15}$$

We choose the arbitrary phase a to be equal to 0 here, such that the eigenstates of $\mathcal{CP}$ are

$$\begin{aligned}|\mathrm{N}_+\rangle &= \frac{1}{\sqrt{2}}\left(|\mathrm{N}^0\rangle + |\overline{\mathrm{N}^0}\rangle\right) , \\ |\mathrm{N}_-\rangle &= \frac{1}{\sqrt{2}}\left(|\mathrm{N}^0\rangle - |\overline{\mathrm{N}^0}\rangle\right) ,\end{aligned} \tag{3.16}$$

with the property that they have $\mathcal{CP}$ eigenvalues $+1$ and -1:

$$\begin{aligned}\sqrt{2}\,\mathcal{CP}|\mathrm{N}_+\rangle &= \mathcal{CP}|\mathrm{N}^0\rangle + \mathcal{CP}|\overline{\mathrm{N}^0}\rangle = |\overline{\mathrm{N}^0}\rangle + |\mathrm{N}^0\rangle = \sqrt{2}\,|\mathrm{N}_+\rangle \\ \sqrt{2}\,\mathcal{CP}|\mathrm{N}_-\rangle &= \mathcal{CP}|\mathrm{N}^0\rangle - \mathcal{CP}|\overline{\mathrm{N}^0}\rangle = |\overline{\mathrm{N}^0}\rangle - |\mathrm{N}^0\rangle = -\sqrt{2}\,|\mathrm{N}_-\rangle\end{aligned} \tag{3.17}$$

Historically, in the K^0 system, $|\mathrm{N}_+\rangle$ was designated by $|\mathrm{K}_1\rangle$, and $|\mathrm{N}_-\rangle$ by $|\mathrm{K}_2\rangle$.

Discrete symmetries impose certain conditions on the elements of the mass and decay matrix. $\mathcal{CPT}$ invariance requires the masses and lifetimes of the particle and antiparticle to be equal, i.e. $X_{11} = X_{22}$, or $M_{11} = M_{22}$ and $\Gamma_{11} = \Gamma_{22}$, for the diagonal elements. $\mathcal{CP}$ invariance requires that $|X_{12}| = |X_{21}|$. In the following, we assume $\mathcal{CPT}$ invariance.

The eigenvalue equation for the matrix X yields

$$\Delta\mu = \Delta m - \frac{i}{2}\Delta\Gamma = 2\sqrt{X_{12}X_{21}} . \tag{3.18}$$

The corresponding eigenvectors of X are written

$$\begin{aligned}|\mathrm{N}_h\rangle &= p|\mathrm{N}^0\rangle - q|\overline{\mathrm{N}^0}\rangle , \\ |\mathrm{N}_l\rangle &= p|\mathrm{N}^0\rangle + q|\overline{\mathrm{N}^0}\rangle ,\end{aligned} \tag{3.19}$$

or in the form of the corresponding relations

$$\begin{aligned}|\mathrm{N}^0\rangle &= \frac{1}{2p}\left(|\mathrm{N}_h\rangle + |\mathrm{N}_l\rangle\right) , \\ |\overline{\mathrm{N}^0}\rangle &= \frac{-1}{2q}\left(|\mathrm{N}_h\rangle - |\mathrm{N}_l\rangle\right) .\end{aligned} \tag{3.20}$$

Unitarity requires $|p|^2 + |q^2| = 1$, and $\mathcal{CP}$ invariance would mean $p = q = 1/\sqrt{2}$. In the case of $\mathcal{CP}$ noninvariance, an asymmetry parameter can be defined by

$$\varepsilon = \frac{p-q}{p+q} \quad \text{or} \quad \frac{p}{q} = \frac{1+\varepsilon}{1-\varepsilon} \tag{3.21}$$

and we obtain

$$\varepsilon = \frac{\frac{1}{2}\Im m\, \Gamma_{12} + \mathrm{i}\,\Im m\, M_{12}}{\Delta m - \frac{i}{2}\Delta\Gamma} \,, \tag{3.22}$$

where $\Im m\, M_{12} \gg \Im m\, \Gamma_{12}$ for the K meson system, and therefore

$$\arg\,\varepsilon \simeq \arctan \frac{2\,\Delta m}{\Gamma_{\mathrm{S}}} \tag{3.23}$$

In this case the two physical states are not orthogonal, and we obtain

$$\langle \mathrm{N}_l | \mathrm{N}_h \rangle = \frac{2\,\Re e\,\varepsilon}{1 + |\varepsilon|^2} \,. \tag{3.24}$$

For the eigenstates of the time-dependent Schrödinger equation, the time evolution obeys an exponential decay law, as can be shown in the Wigner–Weisskopf approximation. Here, the time T is measured in the rest frame given by the common mass defined by the strong and electromagnetic interactions. The time evolution is given by

$$\begin{aligned} |\mathrm{N}_h(t)\rangle &= \mathrm{e}^{-\mathrm{i}m_h t - \frac{1}{2}\Gamma_h t}\, |\mathrm{N}_h(0)\rangle \,, \\ |\mathrm{N}_l(t)\rangle &= \mathrm{e}^{-\mathrm{i}m_l t - \frac{1}{2}\Gamma_l t}\, |\mathrm{N}_l(0)\rangle \,. \end{aligned} \tag{3.25}$$

In this way, N_h decays as $\exp(-\Gamma_h t)$ and N_l as $\exp(-\Gamma_l t)$, while the phases of the two states evolve with different frequency, and this difference will show up in any interference effect between the two decaying mesons.

On the other hand, if initially a pure flavor state N^0 or $\overline{\mathrm{N}^0}$ is produced, the decay law is not exponential but shows oscillations. If we define the complex quantities

$$\begin{aligned} \mathrm{i}M_h = \gamma_h &= \mathrm{i}m_h + \frac{\Gamma_h}{2} \,, \\ \mathrm{i}M_l = \gamma_l &= \mathrm{i}m_l + \frac{\Gamma_l}{2} \,, \end{aligned} \tag{3.26}$$

for the heavy (h) and light (l) meson states, then the amplitude for an initially pure state N^0 at time $t = 0$ is given by (3.19), and at a finite time t the two components evolve according to (3.25). At this time, the state is

$$\psi_{\mathrm{N}} = \frac{1}{2}\left(\mathrm{N}^0 \left(\mathrm{e}^{-\gamma_h t} + \mathrm{e}^{-\gamma_l t} \right) - \frac{q}{p} \overline{\mathrm{N}^0} \left(\mathrm{e}^{-\gamma_h t} - \mathrm{e}^{\gamma_l t} \right) \right) \,. \tag{3.27}$$

The probability of finding an $\overline{\mathrm{N}^0}$ after a time t, starting from an initially pure N^0 state is

$$P(\mathrm{N}^0 \to \overline{\mathrm{N}^0}) = \frac{1}{4}\left|\frac{q}{p}\right|^2 \left[\mathrm{e}^{-\Gamma_h t} + \mathrm{e}^{-\Gamma_l t} - 2\mathrm{e}^{-\Gamma t} \cos\left(\Delta m\, t\right) \right] \,. \tag{3.28}$$

If we express this in the unified variables $T = \Gamma t, x$ and y, this reads

$$P(\mathrm{N}^0 \to \overline{\mathrm{N}^0}) = \frac{1}{2}\left|\frac{q}{p}\right|^2 \mathrm{e}^{-T}\left(\cosh yT - \cos xT\right) \ . \tag{3.29}$$

Similarly, the probability of finding an N^0 in an initially pure N^0 state is

$$P(\mathrm{N}^0 \to \mathrm{N}^0) = \frac{1}{2}\mathrm{e}^{-T}\left(\cosh yT + \cos xT\right) \ . \tag{3.30}$$

The difference between these two probabilities is then

$$\begin{aligned} &P(\mathrm{N}^0 \to \mathrm{N}^0) - P(\mathrm{N}^0 \to \overline{\mathrm{N}^0}) \\ &= \frac{1}{2}\mathrm{e}^{-T}\left(\cosh yT + \cos xT\right) - \frac{1}{2}\mathrm{e}^{-T}\left(\left|\frac{q}{p}\right|^2 \cosh yT - \left|\frac{q}{p}\right|^2 \cos xT\right) \\ &= \frac{1}{2}\mathrm{e}^{-T}\left[\cosh yT\left(1 - \left|\frac{q}{p}\right|^2\right) + \cos xT\left(1 + \left|\frac{q}{p}\right|^2\right)\right] \ . \end{aligned} \tag{3.31}$$

The two states N_h and N_l are not orthogonal, but their overlap δ is

$$\delta = \langle N_h | N_l \rangle = |p|^2 - |q|^2 = \frac{1 - \left|\frac{q}{p}\right|^2}{1 + \left|\frac{q}{p}\right|^2} = \frac{2\,\Re e\,\varepsilon}{1 + |\varepsilon|^2} \, . \tag{3.32}$$

From this result, we obtain

$$P(\mathrm{N}^0 \to \mathrm{N}^0) - P(\mathrm{N}^0 \to \overline{\mathrm{N}^0}) = \frac{1}{2}\mathrm{e}^{-T}\left(1 + \left|\frac{q}{p}\right|^2\right)\left(\delta \cosh yT + \cos xT\right) \ . \tag{3.33}$$

Similarly,

$$P(\mathrm{N}^0 \to \mathrm{N}^0) + P(\mathrm{N}^0 \to \overline{\mathrm{N}^0}) = \frac{1}{2}\mathrm{e}^{-T}\left(1 + \left|\frac{q}{p}\right|^2\right)\left(\cosh yT + \delta \cos xT\right) \ , \tag{3.34}$$

and the flavor asymmetry at time T in an initially pure flavor state becomes

$$A(T) = \frac{P(\mathrm{N}^0 \to \mathrm{N}^0) - P(\mathrm{N}^0 \to \overline{\mathrm{N}^0})}{P(\mathrm{N}^0 \to \mathrm{N}^0) + P(\mathrm{N}^0 \to \overline{\mathrm{N}^0})} = \frac{\cos xT + \delta \cosh yT}{\cosh yT + \delta \cos xT} \, . \tag{3.35}$$

This function behaves very differently, for the four different systems.

3.2.2 Decay Asymmetries and $\mathcal{CP}$

We define the decay amplitudes of neutral mesons to a final state f as

$$\begin{aligned} A_f &= \langle f | T | \mathrm{N}^0 \rangle \ , \\ \overline{A_f} &= \langle f | T | \overline{\mathrm{N}^0} \rangle \ . \end{aligned} \tag{3.36}$$

The decay amplitudes of the mass eigenstates are then

$$\begin{aligned} A_f^h &= pA_f - q\overline{A_f}\ , \\ A_f^l &= pA_f + q\overline{A_f}\ , \end{aligned} \tag{3.37}$$

and we define the complex quantity

$$\lambda_f = \frac{q\overline{A_f}}{pA_f}\ . \tag{3.38}$$

The moduli for the decay of N^0 to f and the decay of $\overline{\mathrm{N}^0}$ to its $\mathcal{CP}$ conjugate state $\overline{f}$ are equal if $\mathcal{CP}$ is conserved, and vice versa:

$$\begin{aligned} |A_f| &= |\overline{A_{\overline{f}}}|\ , \\ |A_{\overline{f}}| &= |\overline{A_f}|\ . \end{aligned} \tag{3.39}$$

(If f is a $\mathcal{CP}$ eigenstate, this is simplified to $|A_f| = |\overline{A_f}|$).

Now $\mathcal{CP}$ violation may occur in three different ways:

1. $\mathcal{CP}$ violation in the mixing, if $|q/p| \neq 1$, called "indirect $\mathcal{CP}$ violation".
2. $\mathcal{CP}$ violation in the decay amplitudes, when (3.39) is not valid, called "direct $\mathcal{CP}$ violation".
3. $\mathcal{CP}$ violation in the interference, when the phase of the expression

$$A_f \overline{A_f^*} A_{\overline{f}} \overline{A_{\overline{f}}^*} p^2/q^2 \tag{3.40}$$

is not zero.

These three types of $\mathcal{CP}$ violation are characterized by the following details:

1. *$\mathcal{CP}$ violation in the mixing* . This type of $\mathcal{CP}$ violation will show up if the mass eigenstates of a neutral meson system are different from the $\mathcal{CP}$ eigenstates, i.e. if $|q/p| \neq 1$ (or $\varepsilon \neq 0$) and if there is a relative phase between M_{12} and Γ_{12}. For the neutral kaon system, this is evident from the existence of the decay $\mathrm{K_L} \to \pi^+\pi^-$, where $|\varepsilon| \sim 2 \times 10^{-3}$, and from the charge asymmetry in semileptonic decays δ_L which is proportional to $2\,\Re e\,\varepsilon$. For the neutral B system, this effect could be seen also in the charge asymmetry of semileptonic decays

$$a_\mathrm{SL} = \frac{\Gamma(\overline{\mathrm{B}^0}(t) \to l^+\nu X) - \Gamma(\mathrm{B}^0(t) \to l^-\nu X)}{\Gamma(\overline{\mathrm{B}^0}(t) \to l^+\nu X) + \Gamma(\mathrm{B}^0(t) \to l^-\nu X)}\ . \tag{3.41}$$

This asymmetry is expected to be small in the Standard Model, of order $\Delta\Gamma/\Delta m$ or $\mathcal{O}(10^{-3})$.

2. *$\mathcal{CP}$ violation in the decay amplitude.* This effect appears if the decay amplitude A_f of the neutral meson N^0 to a final state f is different from the amplitude $\overline{A_{\overline{f}}}$ of the antiparticle $\overline{\mathrm{N}^0}$ to the charge-conjugate state $\overline{f}$, i.e. $|\overline{A_{\overline{f}}}/A_f| \neq 1$. In the neutral-kaon decay to two π mesons, this is realized by the interference of two decay amplitudes, one with $\Delta I = 1/2$ to an isospin $I = 0$ state, and another with $\Delta I = 3/2$ to an isospin $I = 2$ state. The amplitude of direct $\mathcal{CP}$ violation is denoted by ε' and proceeds through penguin diagram processes. The observed magnitude of this amplitude is $|\varepsilon'| \sim 4 \times 10^{-6}$. In the neutral B meson system, the required two decay amplitudes with different weak phases and different strong phases could be a penguin diagram and a tree diagram, e.g. for the decay to the final state $\mathrm{K}^-\pi^+$ or $\mathrm{K}^+\pi^-$. The $b \to s$ penguin diagram has a dominant contribution from a top quark loop, with a weak coupling $V_{tb}^* V_{ts}$ and an isospin-1/2 ($\mathrm{K}\pi$) state. The tree diagram for $b \to u + (\overline{u}s)$ has a coupling $V_{ub}^* V_{us}$ and leads to $I = 1/2$ or $3/2$ states. The observed quantity is the decay asymmetry:

$$a = \frac{N(\overline{\mathrm{B}^0} \to \mathrm{K}^-\pi^+) - N(\mathrm{B}^0 \to \mathrm{K}^+\pi^-)}{N(\overline{\mathrm{B}^0} \to \mathrm{K}^-\pi^+) + N(\mathrm{B}^0 \to \mathrm{K}^+\pi^-)} \,. \tag{3.42}$$

   However, the asymmetries are of limited magnitude because the penguin amplitude is much smaller than the tree amplitude, and also the observation is difficult because of the small branching ratios of the decays. These ratios are $\mathrm{BR}(\mathrm{B} \to \mathrm{K}\pi) \sim 1.5 \times 10^{-5}$ and $\mathrm{BR}(\mathrm{B} \to \pi\pi) \sim 4 \times 10^{-6}$.
3. *$\mathcal{CP}$ violation in the interference.* Here the time dependence of the decay of an initially pure flavor state to a final state f is different for an initial particle or antiparticle. The final state can be a $\mathcal{CP}$ eigenstate such as $\pi^+\pi^-$ ($\mathcal{CP} = +$) or $J/\Psi\mathrm{K_S}$ ($\mathcal{CP} = -$). In the Kaon system, the observed effect is $\Im m\, \varepsilon \sim 1.6 \times 10^{-3}$, while in the B^0 system, it is a very large asymmetry of order $\mathcal{O}(1)$.

References

1. K. Hagiwara *et al.*, Review of Particle Physics, *Phys. Rev. D* **66**, 010001 (2002) 15

4 Models of $\mathcal{CP}$ Violation

After the discovery of $\mathcal{CP}$ violation in K decay, a host of theoretical models was proposed to allocate this phenomenon to known interactions. Assuming $\mathcal{CPT}$ invariance of all interactions, the observed $\mathcal{CP}$-violating effects in K decay imply also $\mathcal{T}$ violation (the experimental data of Chap. 5 are even sufficient to prove $\mathcal{T}$ violation without $\mathcal{CPT}$ invariance). In general, with $\mathcal{CPT}$ invariance, there are four combinations of violations possible:

(a) $\mathcal{T}$-conserving, $\mathcal{C}$-violating and $\mathcal{P}$-violating;
(b) $\mathcal{T}$-violating, $\mathcal{C}$-conserving and $\mathcal{P}$-violating;
(c) $\mathcal{T}$-violating, $\mathcal{C}$-violating and $\mathcal{P}$-conserving;
(d) $\mathcal{T}$-violating, $\mathcal{C}$-violating and $\mathcal{P}$-violating.

Parity conservation in strong and electromagnetic interactions has been tested, for example by looking for a circular polarization in γ rays from nuclear transitions. The presence of a wrong-parity admixture in one of the nuclear states involved will cause a small amplitude for a γ transition with abnormal multipolarity that can interfere with the dominant amplitude and cause such a circular polarization. In the experiments of Lobashov et al. [18], polarizations of the order of 10^{-5} have been measured. These are consistent with being due to the two-nucleon force np $\rightarrow$ pn induced by the weak interaction (see [19] for a review).

From many experiments of a similar nature, one can infer that the strong and electromagnetic interactions are not of type (a), (b) or (d). Therefore, if the source of the $\mathcal{CP}$-violating phenomena is located in the strong or the electromagnetic interaction, there must be a part of one of those interactions that belongs to class (c), i.e. $\mathcal{C}$- and $\mathcal{T}$-violating, but $\mathcal{P}$-conserving.

The proposed models can be grouped into the following four categories:

1. Millistrong $\mathcal{CP}$ violation models [1, 2, 3] postulate the existence of $\mathcal{C}$- and $\mathcal{T}$-violating terms of order 10^{-3} in the strong interaction. The process $\mathrm{K_L} \rightarrow \pi^+\pi^-$ is supposed to occur by the interference of two amplitudes: first, the $\mathrm{K_L}$ decays via the normal $\mathcal{CP}$-conserving weak interaction, with $\Delta\mathbb{S} = 1$, into an intermediate state X, and then this state decays into $\pi^+\pi^-$ by a $\mathcal{T}$-violating strong interaction. The amplitude of the process is of order $G_{\mathrm{F}}\, a$, where G_{F} is the Fermi coupling constant and a is the

Konrad Kleinknecht: Uncovering $\mathcal{CP}$ Violation, STMP 195, 21–26 (2003)

coupling of this $\mathcal{CP}$-violating strong interaction. From the experimental value of $|\eta_{+-}|$, one can conclude that $a \approx 10^{-3}$.

2. Electromagnetic $\mathcal{CP}$ violation models [4, 5, 6, 7] require large parts of the electromagnetic interaction of hadrons to be $\mathcal{C}$- and $\mathcal{T}$-violating, but $\mathcal{P}$-conserving. A two-step process $\mathrm{K_L} \to \mathrm{X} \to 2\pi$ could then occur through the interference of a weak and an electromagnetic $\mathcal{CP}$-violating amplitude. The product of G_{F} with the fine structure constant α is not too far from $G_{\mathrm{F}} \times 10^{-3}$, as required by the magnitude of $|\eta_{+-}|$.
3. Milliweak models assume that a part, of the order of 10^{-3}, of the weak interaction is $\mathcal{CP}$-violating and is responsible for the observed effects. The decay $\mathrm{K_L} \to 2\pi$ is then a one-step process, hence the name "direct $\mathcal{CP}$ violation", and $\mathcal{CP}$ or $\mathcal{T}$ violations of the order of 10^{-3} should show up in other weak processes [8, 9, 10, 11, 12, 13, 14, 15, 16]. In these models, based on two doublets of quarks, $\mathcal{CP}$ violation is introduced in different ways. In one example [16], $\mathcal{CP}$ violation is due to the Higgs couplings, with flavor-changing neutral currents allowed; in another one [14], it is due to right-handed weak currents. A bold alternative was considered in 1973 by Kobayashi and Maskawa [20]: they saw that if there are three doublets of quarks, there is a possibility of $\mathcal{CP}$ violation in the 3×3 weak quark mixing. Today, with six quarks observed, this seems the most natural model.
4. The superweak model [17] postulates a new $\Delta\mathbb{S} = 2$ $\mathcal{CP}$-violating interaction that has a coupling (coupling constant g) smaller than the second-order weak interaction. This interaction could induce a transition $\mathrm{K_L} \to \mathrm{K_S}$, with a subsequent decay $\mathrm{K_S} \to 2\pi$. More precisely, this interaction would cause a first-order transition matrix element

$$\mathcal{M}_{\mathrm{SW}} = \langle \overline{K} | \mathcal{H}_{\mathrm{SW}} | K \rangle \sim g G_{\mathrm{F}} \ . \tag{4.1}$$

The mass difference itself is related to the second-order weak matrix element

$$\mathcal{M}_{\overline{\mathrm{K}}\mathrm{K}} = \sum_n \frac{\langle \overline{\mathrm{K}} | \mathcal{H}_{\mathrm{W}} | n \rangle \langle n | \mathcal{H}_{\mathrm{W}} | K \rangle}{E_{\mathrm{K}} - E_n + i\varepsilon} \ . \tag{4.2}$$

where n is an intermediate state with energy E_n and $\mathcal{H}_{\mathrm{W}}$ is the weak Hamiltonian. In order that the $\mathcal{CP}$-violating amplitude for $\mathrm{K_L} \to 2\pi$ relative to the $\mathcal{CP}$-conserving amplitude should be of the observed magnitude, the ratio $\mathcal{M}_{\mathrm{SW}}/\mathcal{M}_{\overline{\mathrm{K}}\mathrm{K}}$ must be of the order of 10^{-3}. Since $\mathcal{M}_{\mathrm{SW}} \approx g G_{\mathrm{F}}$ and $\mathcal{M}_{\overline{\mathrm{K}}\mathrm{K}} \sim G_{\mathrm{F}}^2 m_p^2$ where the proton mass m_p is used as a cutoff in the integration, this yields $g \sim G_{\mathrm{F}} m_p^2 \approx 10^{-8}$.
This superweak interaction can be detected only in the $\mathrm{K_L}$–$\mathrm{K_S}$ and $\mathrm{B^0}$–$\overline{\mathrm{B^0}}$ systems because these are the only known pairs of states with such a small difference in energy that they are sensitive to forces weaker than the second-order weak interaction. The clear prediction of this model is that there is no direct $\mathcal{CP}$ violation in the decay.

For models other than the superweak one, violations of $\mathcal{CP}$ or $\mathcal{T}$ should manifest themselves in other reactions of particles or nuclei. One observable is the electric dipole moment (EDM) of the neutron. Most milliweak models predict this EDM to be of order 10^{-23} ecm to 10^{-24} ecm, while the superweak model predicts 10^{-29} ecm. The present experimental upper limit is 0.63×10^{-25} ecm.

One of the milliweak models which is rather clear in its predictions should be noted: this is the idea of Kobayashi and Maskawa (KM) dating from 1973 [20]. At the time of the discovery of $\mathcal{CP}$ violation, only three quarks were known, and there was no possibility of explaining $\mathcal{CP}$ violation as a genuine phenomenon of weak interactions with left-handed charged currents and an absence of flavor-changing neutral currents. This situation remained unchanged with the introduction of a fourth quark because the 2×2 unitary weak quark mixing matrix has only one free parameter, the Cabibbo angle, and no nontrivial complex phase. However, as remarked by Kobayashi and Maskawa, the picture changes if six quarks are present. In this case the 3×3 unitary mixing matrix V_{ik} naturally contains a phase δ, in addition to three mixing angles (Chap. 7). It is then possible to construct $\mathcal{CP}$-violating weak amplitudes from "box diagrams" of the form shown in Fig. 4.1.

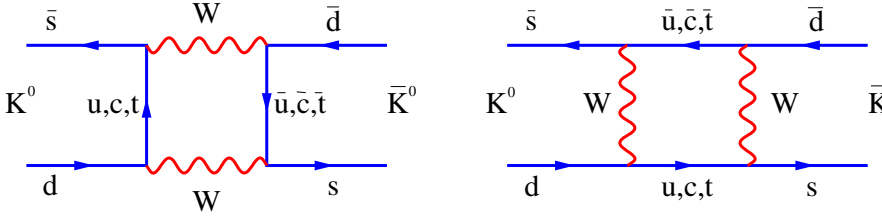

Fig. 4.1. Box diagram for K^0–$\overline{K^0}$ mixing connected with the $\mathcal{CP}$-violating parameter ε

In the K^0–$\overline{K^0}$ system, this amplitude is proportional to the product of the four weak coupling constants $G_F^2 V_{ts} V_{ts}^* V_{td} V_{td}^*$. If there is a nontrivial phase δ in the unitary mixing matrix, then the product is a complex number, with the imaginary part depending on the phase δ. This leads to time-reversal ($\mathcal{T}$) violation and to $\mathcal{CP}$ violation. The $\mathcal{CP}$-violating mixing parameter for the kaon system, ε, is given by

$$\varepsilon = \frac{G_F^2 f_K^2 m_K m_W^2}{G\sqrt{2}\pi^2 \Delta m} B_K \Im m(V_{td} V_{ts}^*) F(m_t^2, m_c^2) \,. \tag{4.3}$$

Here G_F is the Fermi constant, f_K the kaon decay constant, B_K the kaon bag factor (0.80 ± 0.15), and $F(M_t^2, m_c^2)$ the loop function due to interference of the top and charm graphs, given by

$$F(m_t^2, m_c^2) = \Re e\,(V_{cs}^* V_{cd})\left[\eta_1 S_0\left(m_c^2\right) - \eta_3 S_0\left(m_c^2, m_t^2\right)\right] - \Re e\,(V_{ts}^* V_{td})\,\eta_2 S_0\left(m_t^2\right)\ , \tag{4.4}$$

where $S_0(m_t^2)$ is a kinematical factor.

For the B_d^0–$\overline{B_d^0}$ mixing, a similar box graph applies, with the s quark replaced by a b quark. Here the amplitude is proportional to $G_F^2 V_{tb} V_{tb}^* V_{td} V_{td}^*$. Analogous diagrams can be calculated for B_s^0 ($b\overline{s}$) mixing and for D^0 ($c\overline{d}$) mixing.

All $\mathcal{CP}$-violating amplitudes in the KM model are proportional to the following product of the three mixing angles and the phase δ, (Chap. 7),

$$J = |V_{us} V_{ub} V_{cb} \sin\delta| \tag{4.5}$$

A necessary consequence of this model of $\mathcal{CP}$ violation is the non equality of the relative decay rates for $K_L \to \pi^+\pi^-$ and $K_L \to \pi^0\pi^0$. This "direct $\mathcal{CP}$ violation" is due to "penguin diagrams" of the form given in Fig. 4.2 for kaon decays. The amplitude for this direct $\mathcal{CP}$ violation is denoted by ε'. In kaon decays, it will show up in the interference of two decay amplitudes, with the final two-pion state having isospin 0 or 2 (A_0 and A_2 in (5.21)). With six quarks, the weak quark mixing through flavor change can carry a nontrivial phase δ in the mixing matrix, and therefore can induce a $\mathcal{CP}$-violating difference between weak decay amplitudes, such that $|A_f| \neq |\overline{A_f}|$. This model gives an explicit origin of direct $\mathcal{CP}$ violation with a predictable size. In the kaon system, these asymmetries are very small because of the small value of $|J| \sim 3 \times 10^{-5}$, the suppression of $\Delta I = 3/2$ currents, and the partial cancellation of two penguin graphs, called Q_6 and Q_8, shown in Fig. 4.2. However, in the B^0 system, the asymmetries of the decay rates to $\mathcal{CP}$ eigenstates can be very large. Examples are the decays $B^0 \to J/\Psi K_S$ and $B^0 \to \pi^+\pi^-$.

The main models which could be tested experimentally were the KM model and the superweak model, and the decisive question was the existence or non existence of direct $\mathcal{CP}$ violation. For the kaon system in the superweak model $\varepsilon' = 0$, and the decay rates of K_L to $\pi^+\pi^-$ and to $\pi^0\pi^0$ are equal. The predicted value of ε' within the KM model can be estimated if one infers the

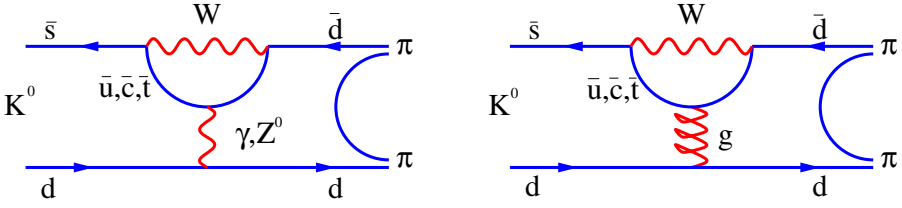

Fig. 4.2. Penguin diagrams for $K^0 \to 2\pi$ decay with direct $\mathcal{CP}$ violation (amplitude ε'). The graphs correspond to the Wilson operators Q_8 and Q_6 and give rise to amplitudes with opposite signs.

magnitude of the mixing angles from other experiments and if the hadronic matrix elements for box graphs and penguin graphs are calculated. Typical values of $|\varepsilon'/\varepsilon|$ are in the range $+(0.2 - 3)\times 10^{-3}$ for three generations of quarks. A measurement of this quantity to this level of precision therefore becomes the *experimentum crucis* for our understanding of $\mathcal{CP}$ violation. If ε' is orthogonal to ε, then a measurement of the phases of η_{+-} and of η_{00} can help to detect a finite value of $\Im m(\varepsilon'/\varepsilon)$. If, however, the phase of ε' is close to that of ε, and since $|\varepsilon'/\varepsilon| \ll 1$ to a good approximation, we obtain

$$\frac{\varepsilon'}{\varepsilon} \simeq \Re e\left(\frac{\varepsilon'}{\varepsilon}\right) = \frac{1}{6}\left(1 - \frac{|\eta_{00}|^2}{|\eta_{+-}|^2}\right) . \tag{4.6}$$

Various methods have been used to calculate the value of $\Re e(\varepsilon'/\varepsilon)$. Owing to the difficulties in calculating hadronic matrix elements in the penguin diagrams, which involve long-distance effects, the task turns out to be very difficult. In particular, the partial cancellation of the two penguin graphs with different signs is a severe problem. The following results have been obtained recently:

1. The Dortmund group has used the $1/N_{\mathrm{C}}$ expansion and chiral perturbation theory (χPT). This group quotes a range of $1.5 \times 10^{-4} < \varepsilon'/\varepsilon < 31.6 \times 10^{-4}$ [21] from scanning the complete range of input parameters.
2. The Munich group has used a phenomenological approach in which as many parameters as possible are taken from experiment. The result [22] is $1.5\times 10^{-4} < \varepsilon'/\varepsilon < 28.8\times 10^{-4}$ from a scanning of the input parameters, and $\varepsilon'/\varepsilon = (7.7^{+6.0}_{-3.5}) \times 10^{-4}$ using a Monte Carlo method to determine the error.
3. The Rome group has used lattice calculation results for the electromagnetic penguin graph Q_8, but the gluonic penguin Q_6 cannot be computed. This group quotes $-13 \times 10^{-4} < \varepsilon'/\varepsilon < 37 \times 10^{-4}$ [23].
4. The Trieste group has used a phenomenological chiral quark model to calculate ε'/ε. Their result is $\varepsilon'/\varepsilon = (22 \pm 8) \times 10^{-4}$ [24]. This group's results also reproduces the $\Delta I = 1/2$ enhancement rule.
5. The Valencia Group also uses chiral perturbation theory to determine the final state interactions and isospin violating effects [25]. This group obtains the value $\varepsilon'/\varepsilon = (17^{+9.6}_{-7.3}) \times 10^{-4}$.

It is hoped that reliable hadronic matrix elements will be obtained in the near future by lattice gauge theory calculations.

References

1. J. Prentki, M. Veltman, *Phys. Lett.* **15**, 88 (1965) 21
2. L. B. Okun, *Sov. J. Nucl. Phys.* **1**, 670 (1965) 21
3. T. D. Lee, L. Wolfenstein, *Phys. Rev. B* **138**, 1490 (1965) 21

4. J. Bernstein, G. Feinberg, T. D. Lee, *Phys. Rev. B* **139**, 1650 (1965) 22
5. S. Barshay, *Phys. Lett.* **17**, 78 (1965) 22
6. F. Salzman, G. Salzman, *Phys. Lett.* **15**, 91 (1965) 22
7. B. Arbuzov, A. T. Filipov, *Phys. Lett.* **20**, 537; *Phys. Lett.* **21**, 771 (1965) 22
8. L. Wolfenstein, *Nuovo Cimento* **42**, 17 (1966) 22
9. W. Alles, *Phys. Lett.* **14**, 348 (1965) 22
10. S. L. Glashow, *Phys. Rev. Lett.* **14**, 35 (1964) 22
11. F. Zachariasen, G. Zweig, *Phys. Lett.* **14**, 794 (1965) 22
12. S. N. Lotsoff, *Phys. Lett.* **14**, 344 (1965) 22
13. R. G. Sachs, *Phys. Rev. Lett.* **13**, 286 (1964) 22
14. R. N. Mohapatra, *Phys. Rev. D* **6**, 2023 (1972); R. Mohapatra and J. Pati, *Phys. Rev. D* **11**, 566 (1975) 22
15. A. Pais, *Phys. Rev. D* **8**, 625 (1973) 22
16. T. D. Lee, *Phys. Rev. D* **8**, 1226 (1973); P. Sikivie, *Phys. Lett.* **65B**, 141 (1976) 22
17. L. Wolfenstein, *Phys. Rev. Lett.* **13**, 562 (1964) 22
18. V. M. Lobashov *et al.*, *Phys. Lett. B* **25**, 104 (1967) 21
19. E. M. Henley, *Ann. Rev. Nucl. Sci.* **19**, 367 (1969) 21
20. M. Kobayashi, T. Maskawa, *Prog. Theor. Phys.* **49**, 652 (1973) 22, 23
21. T. Hambye, G.O. Köhler, E.A. Paschos, P.H. Soldan, *Nucl. Phys. B* **564**, 391 (2000). 25
22. S. Bosch *et al.*, *Nucl. Phys. B* **565**, 3 (2000) 25
23. M. Ciuchini and G. Martinelli, *Nucl. Phys. Proc. Suppl.* **99B**, 27 (2001) 25
24. S. Bertolini, M. Fabbrichesi, J.O. Eeg, *Phys. Rev.*D **63**, 056009 (2001) 25
25. E. Pallante, A. Pich, I. Scimemi, *Nucl. Phys. B* **617**, 441 (2001) 25

5 The Neutral K Meson System

5.1 Mass Eigenstates and $\mathcal{CP}$ Eigenstates

The eigenstates of strangeness are K^0 ($\mathbb{S} = +1$) and $\overline{\mathrm{K}^0}$ ($\mathbb{S} = -1$), the $\mathcal{CP}$ eigenstates are K_1 (with $\mathcal{CP}$ eigenvalue $+1$) and K_2 ($\mathcal{CP}$ eigenvalue -1), and the mass eigenstates are

$$|\mathrm{K_S}\rangle = p\,|\mathrm{K}^0\rangle + q|\overline{\mathrm{K}^0}\rangle \quad (\mathbf{S}\text{hort-lived})\,, \tag{5.1}$$

$$|\mathrm{K_L}\rangle = p\,|\mathrm{K}^0\rangle - q|\overline{\mathrm{K}^0}\rangle \quad (\mathbf{L}\text{ong-lived})\,, \tag{5.2}$$

where $\mathrm{K_L}$ is the heavier state (h), from experiment. The lifetimes of the two eigenstates are very different. While the short-lived particle ($\mathrm{K_S}$) has a mean lifetime of $(0.8959 \pm 0.0004) \times 10^{-10}$ s, the long-lived particle $\mathrm{K_L}$ has a lifetime of $(5.17 \pm 0.04) \times 10^{-8}$ s, i.e. 600 times larger. This is due to the fact that the dominant $\mathcal{CP}$-conserving decays are $\mathrm{K_S} \to 2\pi$ and $\mathrm{K_L} \to 3\pi, \pi e\nu, \pi\mu\nu$, with a much smaller phasespace for the three-body decays. Using the parameter $\varepsilon = (p-q)/(p+q)$, (5.1) and (5.2) can also be written

$$|\mathrm{K_S}\rangle = \frac{1}{\sqrt{1+|\varepsilon|^2}}(|\mathrm{K}_1\rangle + \varepsilon|\mathrm{K}_2\rangle)\,, \tag{5.3}$$

$$|\mathrm{K_L}\rangle = \frac{1}{\sqrt{1+|\varepsilon|^2}}(|\mathrm{K}_2\rangle + \varepsilon|\mathrm{K}_1\rangle)\,. \tag{5.4}$$

The long-lived state is therefore mainly a state with $\mathcal{CP}$ eigenvalue -1, with a small (2×10^{-3}) admixture of a $\mathcal{CP}$ $+1$ state K_1. The two mass eigenstates are not orthogonal if $\mathcal{CP}$ is violated, because $\langle \mathrm{K_S}|\mathrm{K_L}\rangle = 2\,\Re e\,\varepsilon$.

5.2 Isospin Decomposition

In $\mathrm{K_{S,L}} \to 2\pi$ decays, the angular momentum of the pions vanishes. The spatial part of the wave function is therefore symmetric, and since pions are bosons, the isospin wave function must be symmetric too. The two symmetric combinations of two $I = 1$ states have $I = 0$ and $I = 2$, and the four transition amplitudes that exist are

Konrad Kleinknecht: Uncovering $\mathcal{CP}$ Violation, STMP 195, 27–93 (2003)

$$\langle 0|T|\mathrm{K_S}\rangle\,, \qquad \langle 2|T|\mathrm{K_S}\rangle\,, \qquad \langle 0|T|\mathrm{K_L}\rangle\,, \qquad \langle 2|T|\mathrm{K_L}\rangle\,. \tag{5.5}$$

These can be reduced to three complex numbers by normalizing to the amplitude $\langle 0|T|\mathrm{K_S}\rangle$:

$$\varepsilon_0 = \frac{\langle 0|T|\mathrm{K_L}\rangle}{\langle 0|T|\mathrm{K_S}\rangle}\,, \tag{5.6}$$

$$\varepsilon_2 = \frac{1}{\sqrt{2}}\frac{\langle 2|T|\mathrm{K_L}\rangle}{\langle 0|T|\mathrm{K_S}\rangle}\,, \tag{5.7}$$

$$\omega = \frac{\langle 2|T|\mathrm{K_S}\rangle}{\langle 0|T|\mathrm{K_S}\rangle}\,. \tag{5.8}$$

The experimentally observable quantities are

$$\eta_{+-} = \frac{\langle \pi^+\pi^-|T|\mathrm{K_L}\rangle}{\langle \pi^+\pi^-|T|\mathrm{K_S}\rangle}\,, \tag{5.9}$$

$$\eta_{00} = \frac{\langle \pi^0\pi^0|T|\mathrm{K_L}\rangle}{\langle \pi^0\pi^0|T|\mathrm{K_S}\rangle}\,, \tag{5.10}$$

$$\delta_\mathrm{L} = \frac{\Gamma(\mathrm{K_L}\to\pi^- l^+\nu) - \Gamma(\mathrm{K_L}\to\pi^+ l^-\nu)}{\Gamma(\mathrm{K_L}\to\pi^- l^+\nu) + \Gamma(\mathrm{K_L}\to\pi^+ l^-\nu)}\,. \tag{5.11}$$

Relating the isospin states to the physical 2π states

$$\langle 0| = \frac{1}{\sqrt{3}}\langle\pi^-\pi^+| - \frac{1}{\sqrt{3}}\langle\pi^0\pi^0| + \frac{1}{\sqrt{3}}\langle\pi^+\pi^-|\,, \tag{5.12}$$

$$\langle 2| = \frac{1}{\sqrt{6}}\langle\pi^-\pi^+| + \sqrt{\frac{2}{3}}\langle\pi^0\pi^0| + \frac{1}{\sqrt{6}}\langle\pi^+\pi^-|\,. \tag{5.13}$$

we obtain

$$\eta_{+-} = \frac{\varepsilon_0 + \varepsilon_2}{1 + (1/\sqrt{2})\omega}, \tag{5.14}$$

$$\eta_{00} = \frac{\varepsilon_0 - 2\varepsilon_2}{1 - \sqrt{2}\omega}. \tag{5.15}$$

Because of the validity of the $\Delta I = 1/2$ rule for $\mathcal{CP}$-conserving weak nonleptonic decays, $\omega \ll 1$ and therefore can be neglected.

A suitable choice for the phase of the $\mathrm{K}^0 \to 2\pi(I=0)$ amplitude is obtained by choosing this amplitude to be real except for final-state interactions between two pions, leading to a phase shift δ_0:

$$\langle 0|T|\mathrm{K}^0\rangle = \mathrm{e}^{\mathrm{i}\delta_0} A_0 \qquad \text{and } A_0 \text{ real.} \tag{5.16}$$

Similarly,

$$\langle 2|T|\mathrm{K}^0\rangle = \mathrm{e}^{\mathrm{i}\delta_2} A_2\,. \tag{5.17}$$

With these choices, we obtain

$$\varepsilon_0 = \varepsilon \,, \tag{5.18}$$

$$\varepsilon_2 = \frac{\mathrm{i}}{\sqrt{2}} \mathrm{e}^{\mathrm{i}(\delta_2 - \delta_0)} \frac{\Im m\, A_2}{A_0} = \varepsilon' \,. \tag{5.19}$$

Therefore, representing ε and ε' in the complex plane, we obtain the triangle relations

$$\eta_{+-} = \varepsilon + \varepsilon' \,, \qquad \eta_{00} = \varepsilon - 2\varepsilon' \,. \tag{5.20}$$

In this way, η_{+-}, η_{00} and $3\epsilon'$ form a triangle in the complex plane, the Wu–Yang triangle. The $\mathcal{CP}$-violating decay amplitude ε' is due to interference of $\Delta I = 1/2 (A_0)$ and $\Delta I = 3/2 (A_2)$ amplitudes:

$$\varepsilon' = \frac{\mathrm{i}\, \Im m\, A_2}{2A_0} \mathrm{e}^{\mathrm{i}(\delta_2 - \delta_0)} \,. \tag{5.21}$$

Its phase is given by the $\pi\pi$ phase shifts in the $I = 0$ and $I = 2$ states, δ_0 and δ_2 (assuming $\mathcal{CPT}$ invariance):

$$\arg(\varepsilon') = (\delta_2 - \delta_0) + \frac{\pi}{2} \,. \tag{5.22}$$

The $\pi\pi$ phase shifts have been measured precisely in pion-scattering experiments. The results obtained are $\delta_2 = (-7.2 \pm 1.3)^\circ$ [3] and $\delta_0 = (39 \pm 5)^\circ$ [4]. Using dispersion relation calculations or chiral perturbation theory, these results can be used to extract $\arg(\varepsilon')$. The results are $(42.3 \pm 1.5)^\circ$ [1] and $(46.0 \pm 3.6)^\circ$ [2].

The decomposition of the observable decay amplitude into ε and ε' corresponds to a separation of the $\mathcal{CP}$-violating effects due to the mass and decay matrices (represented by ε), which are seen also in the impurity of the $\mathrm{K_L}$ and $\mathrm{K_S}$ states, from $\mathcal{CP}$ violation in the transition matrix element (represented by ε').

The phase of ε is given by (3.22) and (3.23):

$$\arg \varepsilon = \Phi_\mathrm{D} + \arctan\left(2\frac{\Delta m}{\Gamma_\mathrm{S}}\right) \,, \tag{5.23}$$

where $\Delta m = m_\mathrm{L} - m_\mathrm{S}$ and

$$\Phi_\mathrm{D} = -\arctan\left(\frac{\Im m\, \Gamma_{12}}{2\, \Im m\, M_{12}}\right). \tag{5.24}$$

If there is no strong $\mathcal{CP}$ violation in the channels $\mathrm{K} \to 2\pi(\mathrm{I} = 2), \mathrm{K} \to \pi \mathrm{l} \nu$, and $\mathrm{K} \to 3\pi$, Φ_D is very small. This can be deduced from the Bell–Steinberger unitarity relation. If the final states of the $\mathrm{K_L}$ and $\mathrm{K_S}$ decays are designated by $|F\rangle$, then

$$\Gamma_\mathrm{S} = \sum_F |\langle F|T|\mathrm{K_S}\rangle|^2 \,, \tag{5.25}$$

$$\Gamma_\mathrm{L} = \sum_F |\langle F|T|\mathrm{K_L}\rangle|^2 \,. \tag{5.26}$$

Unitarity leads to the relation

$$\mathrm{i}\,(M_\mathrm{S} - M_\mathrm{L}^*)\,\langle \mathrm{K_S}|\mathrm{K_L}\rangle = \sum_F \langle F|T|\mathrm{K_L}\rangle^* \langle F|T|\mathrm{K_S}\rangle\ . \tag{5.27}$$

The mass matrix elements are then (with $\mathcal{CPT}$ invariance assumed)

$$X_{11} = X_{22} = \frac{M_\mathrm{S} + M_\mathrm{L}}{2} \tag{5.28}$$

$$X_{12} = \frac{(M_\mathrm{S} - M_\mathrm{L})(1+\varepsilon)}{2(1-\varepsilon)} \tag{5.29}$$

$$X_{21} = \frac{(M_\mathrm{S} - M_\mathrm{L})(1-\varepsilon)}{2(1+\varepsilon)}. \tag{5.30}$$

Ignoring all final states but 2π or assuming $\Im m\, \Gamma_{12} = 0$, we obtain the following from the unitarity relation or from (3.22):

$$\arg\,\varepsilon = \arctan\left(2\frac{\Delta m}{\Gamma_\mathrm{S}}\right) = \Phi_{\mathrm{sw}} \tag{5.31}$$

where Φ_{sw} designates the phase in the superweak model

When we add other final states of $\mathcal{CP}$-violating decays, the phase is shifted by Φ_D, and an upper limit can be obtained from the unitarity relation:

$$\Phi_\mathrm{D} \le \frac{0.75}{\Gamma_\mathrm{S}|\eta_{+-}|} \sum_F \sqrt{\Gamma_{F,\mathrm{CPV}} \cdot \Gamma_{F,\mathrm{CPC}}} \tag{5.32}$$

where the sum runs over all states $F \neq 2\pi$ and the root is taken of the product of the $\mathcal{CP}$-violating (CPV) and $\mathcal{CP}$-conserving (CPC) decay rates.

Present limits on $\mathcal{CP}$-violating processes in these decays show that contributions from semileptonic decays are negligible. Using the limits on $\Delta Q = \Delta\mathbb{S}$-violating amplitudes, we obtain

$$|\Phi_\mathrm{D}(\mathrm{K_{e3}})| < 0.07^\circ\ , \qquad |\Phi_\mathrm{D}(\mathrm{K_{\mu 3}})| < 0.05^\circ\ . \tag{5.33}$$

In the same way, the upper limit on the $\mathcal{CP}$-violating $\mathrm{K_S} \to \pi^+\pi^-\pi^0$ decay [5],

$$\frac{\Gamma(\mathrm{K_S} \to \pi^+\pi^-\pi^0)}{\Gamma_\mathrm{S}} < 4.1 \times 10^{-7}\ , \tag{5.34}$$

allows us to set the limit

$$|\Phi_D(\pi^+\pi^-\pi^0)| < 0.2^\circ\ . \tag{5.35}$$

Similarly, from the limit [7] $\Gamma(\mathrm{K_S} \to 3\pi^0)/\Gamma_\mathrm{S} < 1.3 \times 10^{-6}$ it follows that

$$|\Phi_D(3\pi^0)| < 0.4^\circ\ . \tag{5.36}$$

New, more sensitive experiments will improve this limit. If we use the experimental values of Δm and Γ_S from Sect. 5.6, then $\arg \varepsilon = (43.4 \pm 0.1 \pm 0.4)°$, where the first error comes from the uncertainties of Δm and Γ_S and the second error from the uncertainty of Φ_D.

Another independent observable is the charge asymmetry

$$\delta_L = \frac{1-|x|^2}{|1-x|^2} 2\,\Re e\,\varepsilon\,, \tag{5.37}$$

where $x = g/f$ is the ratio of the $\Delta Q = -\Delta\mathbb{S}$ to the $\Delta Q = \Delta\mathbb{S}$ amplitude (Sects. 5.4.2 and 5.6.9).

5.3 K_L–K_S Regeneration

The term *regeneration* was introduced by Pais and Piccioni [8] to designate the creation of short-lived K_S mesons when long-lived K_L mesons traverse matter. It was predicted that this process would happen if the short- and long-lived K-mesons were two different linear combinations of the K^0 and $\overline{K^0}$, the eigenstates of strangeness ($\mathbb{S} = +1$ and $\mathbb{S} = -1$). Because strong interactions conserve strangeness, several reactions that the $\overline{K^0}$ can undergo (e.g. $\overline{K^0}p \to \Lambda\pi^+$) have no counterpart for the K^0. Therefore the total cross sections of the $\overline{K^0}$ on the nucleons p and n are both bigger than the corresponding total cross sections of the K^0 on the nucleons and as a consequence, the total cross section of the $\overline{K^0}$ on any nucleus N also obeys the inequality $\sigma_\tau(\overline{K^0}N) \geqq \sigma_\tau(K^0N)$, which can become an equality in the asymptotic region. The optical theorem relates the total cross section σ_τ to the forward scattering amplitude $f(0)$ by $\Im m\, f(0) = (k/4\pi)\sigma_\tau$, where $k = p/h$ is the wavenumber of the K meson. Therefore, at any finite momentum we have $|\Im m\, \overline{f}(0)| > |\Im m\, f(0)|$, where $\overline{f}$ designates the $\overline{K^0}$ scattering amplitude.

Assuming for the moment that the real part of $f(0)$ is not correspondingly bigger than $\Re e\, \overline{f}(0)$, it follows that $|\overline{f}(0)| > |f(0)|$. An incident long-lived K is described by 5.4. By interaction of the K_L with matter, the two components of K_L, namely K^0 and $\overline{K^0}$, are altered differently, and the state emerging is

$$\begin{aligned} |\psi_f(\theta)\rangle &= \frac{f(\theta)p|K^0\rangle - \overline{f}(\theta)q|\overline{K^0}\rangle}{\sqrt{|p|^2+|q|^2}} \\ &= \frac{f(\theta)-\overline{f}(\theta)}{2}|K_S\rangle + \frac{f(\theta)+\overline{f}(\theta)}{2}|K_L\rangle\,. \end{aligned} \tag{5.38}$$

Now, if $f(\theta) \neq \overline{f}(\theta)$, then the emerging state contains a K_S component; this component is "regenerated" from the K_L beam. In particular, in the forward direction ($\theta = 0$), the amplitude of K_S regenerated by one scattering center is proportional to $f(0) - \overline{f}(0)$.

If we now consider two scattering centers, these two scatterers will act coherently if $d(p_S \cos\theta - p_L) \ll 1$, where p_S and p_L are the momenta of the

K_S and K_L respectively, d is the distance between the two scattering centers along the K_L direction, and θ is the scattering angle between the incoming K_L and outgoing K_S [9, 10]. Using the momentum transfer $p_S - p_L = \Delta m\, m_L/p_L$ (following from energy conservation), we can obtain from this relation the coherence length, i.e. the distance d_{max} along the K_L direction at which two scattering centers can still interfere fully coherently for forward regeneration

$$d_{max} \approx \frac{1}{p_S - p_L} = \frac{p_L}{m_L \Delta m} , \tag{5.39}$$

and the maximum scattering angle for coherent regeneration,

$$\theta^2 \lesssim 2\frac{(p_S - p_L)}{p_S} \approx 10^{-14} . \tag{5.40}$$

The coherence length is of the order of several K_S mean decay lengths, and the momentum transfer is of the order of 10^{-6} eV/c.

We therefore expect different classes of regeneration:

1. Coherent regeneration , or "transmission regeneration", in the forward direction at angles $\theta \leqq 10^{-7}$ rad: coherent addition of amplitudes from an extended region several centimeters in length.
2. Elastic ("diffraction") regeneration from nuclei: incoherent addition of intensities from different nuclei, but coherent action of the nucleons inside the nucleus: typical recoil momenta of $p^* \sim 50$ MeV/c, and a Gaussian angular distribution at small momentum transfers.
3. Inelastic regeneration : momentum transfers so big as to break up the nucleus or to transfer it to an excited state.

In the present context, the interest in the regeneration amplitudes is due to the fact that in the study of $\mathcal{CP}$-violating effects, regeneration proves to be a powerful tool: it is possible to generate coherent mixtures of K_L and K_S waves and to study interference effects between the $\mathcal{CP}$-conserving decay $K_S \to 2\pi$ from regenerated K_S and the $\mathcal{CP}$-violating decay $K_L \to 2\pi$. This method has been used extensively [11, 12, 13, 14, 15, 16]. Also, the regeneration amplitudes measured by detecting $K_S \to \pi^+\pi^-$ have been used to obtain an absolute normalization for the decay rate of $K_L \to \pi^0\pi^0$ [21]. Finally, the decay time distribution of $K \to \pi e \nu$ decays from a coherent K_L, K_S mixture has been used to measure the phase relation between the outgoing K_S and incoming K_L, the "regeneration phase" [16, 18, 19, 20].

The connection between the "elementary" scattering amplitude $f(\theta) - \overline{f}(\theta)$ and the macroscopically observed regeneration probability for coherent regeneration (class 1 above) can be expressed in the following way: we define the state emerging from a block of matter of length L placed in a pure K_L beam as

$$|\psi_f\rangle = |K_L\rangle + \varrho(L)|K_S\rangle . \tag{5.41}$$

Then $\varrho(L)$ is obtained by summing all contributions from individual scattering centers. The result is [10]

$$\varrho = \pi \mathrm{i} \frac{f(0) - \overline{f}(0)}{k} \Lambda_{\mathrm{S}} N \frac{1 - \mathrm{e}^{(\mathrm{i}(\Delta m/\Gamma_{\mathrm{S}}) - (1/2))l}}{1/2 - \mathrm{i}(\Delta m/\Gamma_{\mathrm{S}})} \ , \tag{5.42}$$

where

$f(0)$ and $\overline{f}(0)$	are, respectively, the K^0 and $\overline{\mathrm{K}^0}$ scattering amplitudes in the forward direction;
$k = p_{\mathrm{K}}/\hbar$	is the kaon wave number;
$\Lambda_{\mathrm{S}} = \beta\gamma\tau_{\mathrm{S}}$	is the mean decay length of the $\mathrm{K_S}$;
N	is the density of scattering centers;
$\Delta m = m_{\mathrm{L}} - m_{\mathrm{S}}$	is the $\mathrm{K_L}$–$\mathrm{K_S}$ mass difference;
$\Gamma_{\mathrm{S}} = \hbar/\tau_s$	is the $\mathrm{K_S}$ decay rate; and
$l = L/\Lambda_{\mathrm{S}}$	is the length of the regenerator in units of the $\mathrm{K_S}$ decay length.

This expression for ϱ contains two factors: a nuclear part

$$\pi \mathrm{i} \frac{f(0) - \overline{f}(0)}{k} \Lambda_{\mathrm{S}} N \ , \tag{5.43}$$

and a geometrical part $G(L)$ depending on the length L of the regenerator. Therefore the phase of ϱ is usually split into two parts:

$$\Phi_{\varrho} = \arg(\varrho) = \Phi_f + \Phi_{\Delta m} \ , \tag{5.44}$$

where

$$\Phi_f = \arg\left\{ \mathrm{i} \left[f(0) - \overline{f}(0) \right] \right\} \tag{5.45}$$

is the nuclear regeneration phase and

$$\Phi_{\Delta m} = \arg \frac{1 - \mathrm{e}^{(\mathrm{i}(\Delta m/\Gamma_{\mathrm{S}}) - (1/2))l}}{1/2 - \mathrm{i}(\Delta m/\Gamma_{\mathrm{S}})} \ , \tag{5.46}$$

is the phase of the geometrical factor.

The nuclear regeneration phase can be calculated from a dispersion integral over the amplitude $f(0) - \overline{f}(0)$ as a function of the kaon momentum p_{K}. If it is assumed that this difference is determined by a single ω meson exchange process (Regge behavior), then the decrease of $f(0) - \overline{f}(0)$ follows a power law $(p_{\mathrm{K}})^{\alpha}$. In this simplified case, the phase Φ_f is related to the exponent α by the relation $\Phi_f = -(\pi/2)(1+\alpha)$. However, this is only true if the decrease of the amplitude $f(0) - \overline{f}(0)$ follows this power law exactly up to infinite momentum. This is due to the fact that the phase is obtained from a dispersion relation integral over the amplitude up to infinite momentum [43].

5.4 Interference Between Decay Amplitudes of K_L and K_S

An arbitrary coherent mixture of K_L and K_S states will show interference phenomena when decaying into 2π and in other common decay channels. According to Sect. 3.2.1 the eigentime development of K_L is

$$|K_L\rangle \to |K_L\rangle\, e^{-iM_L\tau} \ , \tag{5.47}$$

where $M_L = m_L - (i/2)\Gamma_L$, and correspondingly for K_S. An arbitrary mixture

$$|\psi(0)\rangle = a_S|K_S\rangle + a_L|K_L\rangle \tag{5.48}$$

will develop into

$$|\psi(\tau)\rangle = a_S\, e^{-iM_S\tau}\, |K_S\rangle + a_L\, e^{-iM_L\tau}\, |K_L\rangle \ . \tag{5.49}$$

5.4.1 2π Decay

The 2π decay amplitude is therefore

$$\begin{aligned} \langle 2\pi|T|\psi(\tau)\rangle &= a_S\, e^{-iM_S\tau}\, \langle 2\pi|T|K_S\rangle + a_L\, e^{-iM_L\tau}\, \langle 2\pi|T|K_L\rangle \\ &= \langle 2\pi|T|K_S\rangle a_S\, e^{-iM_S\tau} + a_L\eta\, e^{-iM_L\tau} \ , \end{aligned} \tag{5.50}$$

where $\eta = \eta_{+-}$ for $\pi^+\pi^-$ decay and $\eta = \eta_{00}$ for $\pi^0\pi^0$ decay. The observed decay rate is proportional to

$$\begin{aligned} R(\tau) = |a_S|^2\, e^{-\Gamma_S\tau} + |a_L\,\eta|^2\, e^{-\Gamma_L\tau} \\ + 2|a_S||a_L||\eta|\, e^{-(\Gamma_L+\Gamma_S)(\tau/2)} \cos\left(\Delta m\,\tau + \Phi\right) \ . \end{aligned} \tag{5.51}$$

where $\Phi = \arg(a_S) - \arg(\eta a_L)$. We obtain for various initial conditions of the mixture:

1. For an initially pure K^0 state ($a_S = 1 = a_L$),

$$R_1(\tau) = e^{-\Gamma_S\tau} + |\eta|^2\, e^{-\Gamma_L\tau} + 2|\eta|\, e^{-(\Gamma_L+\Gamma_S)(\tau/2)} \cos\left(\Delta m\,\tau - \arg\eta\right) \ . \tag{5.52}$$

2. For an initially pure $\overline{K^0}$ state, the interference term changes sign.
3. For an incoherent mixture of K^0 (intensity N_K) and $\overline{K^0}$ (intensity $N_{\overline{K}}$, the interference term is multiplied by the "dilution factor"

$$\frac{N_K - N_{\overline{K}}}{N_K + N_{\overline{K}}} \ . \tag{5.53}$$

Measurement of the interference term under these conditions is called the *vacuum interference method*.

4. For the coherent mixture behind a regenerator, $a_S = \varrho, a_L = 1$, and we obtain

$$R_2(\tau) = |\varrho|^2 \, \mathrm{e}^{-\Gamma_S \tau} + |\eta|^2 \, \mathrm{e}^{-\Gamma_L \tau} + 2|\varrho||\eta| \, \mathrm{e}^{-(\Gamma_L + \Gamma_S)(\tau/2)} \cos\left(\Delta m \, \tau + \Phi_\varrho - \arg \eta\right). \quad (5.54)$$

If the K_L beam passes through two regenerators characterized by regeneration amplitudes ϱ_1 and ϱ_2 and if the downstream ends of these two slabs of matter are placed at a separation G along the beam direction, corresponding to a time in the K rest system of $\tau_G = G m_K/(c p_K)$, where p_K is the kaon momentum, then the state behind the second regenerator is proportional to

$$|\psi\rangle = |K_L\rangle \, \mathrm{e}^{-\mathrm{i} M_L \tau_G} + \varrho_1 |K_S\rangle \, \mathrm{e}^{-\mathrm{i} M_S \tau_G} + \varrho_2 |K_S\rangle \, \mathrm{e}^{-\mathrm{i} M_L \tau_G} \quad (5.55)$$

and the 2π decay amplitude directly behind the second regenerator is

$$\langle 2\pi|T|\psi\rangle \propto \varrho_1 \, \mathrm{e}^{-\mathrm{i} M_S \tau_G} + \varrho_2 \, \mathrm{e}^{-\mathrm{i} M_L \tau_G} + \eta \, \mathrm{e}^{-\mathrm{i} M_L \tau_G}. \quad (5.56)$$

Neglecting for simplicity the $\mathcal{CP}$-violating terms, which is justified if $|\varrho_1/\eta| \gg 1$ and $|\varrho_2/\eta| \gg 1$ are chosen, the 2π decay rate becomes

$$I_{2\pi} = |\langle 2\pi|T|\psi\rangle|^2 \propto |p_1|^2 \, \mathrm{e}^{-\Gamma_S \tau_G} + |p_2|^2 + 2|p_1||p_2| \, \mathrm{e}^{-\Gamma_S(\tau_G/2)} \cos\left(\Delta m \, \tau_G + \Phi_{\varrho_1} - \Phi_{\varrho_2}\right). \quad (5.57)$$

5.4.2 Semileptonic Decays

The phenomenological Lagrangian for the semileptonic decay $K \to \pi l \nu$ is

$$L_{\Delta \mathbb{S}=1} = S_\lambda^* j_\lambda + S_\lambda j_\lambda^*, \quad (5.58)$$

where S_λ is the hadron current and j_λ is the lepton current

$$j_\lambda = \mathrm{i} \sum_{l=e,\mu} \psi_l^+ \gamma_4 \gamma_\lambda (1 + \lambda_5) \psi_{\nu l} \quad (5.59)$$

in the notation of Lee and Wu [22]. The structure of S is, a priori, unknown. It may contain any of the five Lorentz-invariant operators for vector, axial-vector, scalar, tensor or pseudoscalar interactions. Experiments are consistent with V–A interactions and the absence of the other interactions. The hadron current S_λ can then be decomposed unambiguously into a vector part $\boldsymbol{S}_\lambda^V$ and an axial-vector part $\boldsymbol{S}_\lambda^A$:

$$S_\lambda = S_\lambda^{\mathrm{V}} + S_\lambda^{\mathrm{A}}. \quad (5.60)$$

With the convention that the relative parity of the K and π mesons is + 1, the K_{l3} decays are governed by the matrix element of $\boldsymbol{S}_\lambda^{\mathrm{V}}$, while the $K_{\pi 2}$

decays are related to the axial-vector part $\boldsymbol{S}^{\mathrm{A}}_{\lambda}$. For the vector part relevant to K_{l3} decay, Lorentz invariance requires that only two form factors enter; these are denoted by

$$f_+ \text{ and } f_- \quad \text{for } \mathrm{K}^0 \to \pi^- l^+ \nu_l \ , \tag{5.61}$$

$$g_+ \text{ and } g_- \quad \text{for } \overline{\mathrm{K}^0} \to \pi^- l^+ \nu_l \ , \tag{5.62}$$

$$\overline{f_+} \text{ and } \overline{f_-} \quad \text{for } \overline{\mathrm{K}^0} \to \pi^+ l^- \overline{\nu}_l \ , \tag{5.63}$$

$$\overline{g_+} \text{ and } \overline{g_-} \quad \text{for } \mathrm{K}^0 \to \pi^+ l^- \overline{\nu}_l \ , \tag{5.64}$$

where l denotes a lepton (muon or electron). The matrix element for the first reaction is given by

$$\langle \pi^- | S_\lambda(\chi) | \mathrm{K}^0 \rangle = \frac{1}{2} \sqrt{E_{\mathrm{K}} E_\pi} [(\mathrm{K}_\lambda + \pi_\lambda) f_+(q^2) + (\mathrm{K}_\lambda - \pi_\lambda) f_-(q^2)] \, \mathrm{e}^{(\mathrm{i}q\cdot x)} \ , \tag{5.65}$$

where K_λ and π_λ are the four-momenta of the kaon and pion, E_{K} and E_π their energies, and q^2 the square of the momentum transfer $q_\lambda = K_\lambda - \pi_\lambda$. Corresponding expressions hold for the other three reactions.

As discussed in [22],

1. $\mathcal{CPT}$ invariance requires $f_\pm = -f_\pm^*$ and $\overline{g_\pm} = -g_\pm^*$.
2. $\mathcal{T}$ invariance allows one to chose all four form factors to be real.
3. The $\Delta Q = \Delta \mathbb{S}$ rule forbids the decays $\overline{\mathrm{K}^0} \to \pi^- l^+ \nu_l$ and $\mathrm{K}^0 \to \pi^+ l^- \nu$, i.e. $g_\pm = \overline{g_\pm} = 0$; the degree of violation of this rule is measured by the parameter $x = g_+/f_+$.
4. The $\Delta I = 1/2$ rule relates the matrix elements of the two members of an isospin doublet by a Clebsch–Gordan coefficient:

$$\sqrt{2} M(\mathrm{K}^+ \to \pi^0 l^+ \nu) = M(\mathrm{K}^0 \to \pi^- l^+ \nu) \ . \tag{5.66}$$

From the Gell-Mann–Nishijima relation for hadrons,

$$Q = \frac{B + \mathbb{S}}{2} + I_3 \ , \tag{5.67}$$

where Q is the charge, B the baryon number, $\mathbb{S}$ the strangeness and I_3 the third isospin component, we conclude that for transitions between mesons ($B = 0$),

$$\Delta Q = \frac{\Delta \mathbb{S}}{2} + \Delta I_3 . \tag{5.68}$$

If $\Delta I = 1/2$, then for a transition with $\Delta \mathbb{S} = 1$, $\Delta Q = \Delta \mathbb{S}$ also holds; in particular, this means $g_\pm = \overline{g_\pm} = 0$. If we take for simplicity the electron decay, where the form factors f_- and g_- vanish, the decay amplitudes for $|\mathrm{K_S}\rangle$ and $|\mathrm{K_L}\rangle$ can be written as follows:

$$\begin{aligned}
\langle\pi^- e^+\nu|T|\mathrm{K_S}\rangle &\propto (1+\varepsilon)\langle\pi^- e^+\nu|T|\mathrm{K}^0\rangle + (1-\varepsilon)\langle\pi^- e^+\nu|T|\overline{\mathrm{K}^0}\rangle \\
&= (1+\varepsilon)f + (1-\varepsilon)g\ , \\
\langle\pi^- e^+\nu|T|\mathrm{K_L}\rangle &\propto (1+\varepsilon)f - (1-\varepsilon)g, \\
-\langle\pi^- e^+\nu|T|\mathrm{K_S}\rangle &\propto (1+\varepsilon)g^* + (1-\varepsilon)f^*\ , \\
-\langle\pi^- e^+\nu|T|\mathrm{K_L}\rangle &\propto (1+\varepsilon)g^* - (1-\varepsilon)f^*\ .
\end{aligned}$$

Taking an arbitrary coherent mixture of K_L and K_S denoted by $|\psi(\tau)\rangle$ as above (5.49), its decay amplitudes

$$A^{\pm}(\tau) = \langle\pi^{\pm} e^{\mp}\nu|T|\psi(\tau)\rangle \tag{5.69}$$

are given by

$$\begin{aligned}
A^+(\tau) &\propto a_{\mathrm{S}}\,\mathrm{e}^{-\mathrm{i}M_{\mathrm{S}}\tau}\left[(1+\varepsilon)+(1-\varepsilon)\,x\right] \\
&\quad + a_{\mathrm{L}}\,\mathrm{e}^{-\mathrm{i}M_{\mathrm{L}}\tau}\left[(1+\varepsilon)+(1-\varepsilon)\,x\right]\ , \qquad (5.70)\\
-A^-(\tau) &\propto a_{\mathrm{S}}\,\mathrm{e}^{-\mathrm{i}M_{\mathrm{S}}\tau}\left[(1+\varepsilon)\,x^*+(1-\varepsilon)\right] \\
&\quad + a_{\mathrm{L}}\,\mathrm{e}^{-\mathrm{i}M_{\mathrm{L}}\tau}\left[(1+\varepsilon)^*+(1-\varepsilon)\right]\ . \qquad (5.71)
\end{aligned}$$

The corresponding decay rates for the two charge states are $N^{\pm}(\tau) = |A^{\pm}(\tau)|^2$, and if we call the ratio of the initial K_S and K_L components $R = a_S/a_L$, we obtain the following for the difference between the charge states:

$$\begin{aligned}
N^+ - N^- \approx 4(1-|x|^2)\{&\Re e\,\varepsilon\left[\mathrm{e}^{-\Gamma_L\tau} + |R|^2\,\mathrm{e}^{-\Gamma_S\tau}\right] \\
&+ |R|\,\mathrm{e}^{-\overline{\Gamma}\tau}(1+|\varepsilon|^2)\cos\left(\Delta m\,\tau+\Phi_R\right)\}\ . \qquad (5.72)
\end{aligned}$$

we also obtain

$$\begin{aligned}
&N^+ + N^- \qquad (5.73)\\
&\quad\approx \mathrm{e}^{-\Gamma_L\tau}[(1+|\varepsilon|^2)(1+|x|^2) - 2\,\Re e\,x\,(1-|\varepsilon|^2) - 4\,\Im m\,x\,\Im m\,\varepsilon] \\
&\quad + 2|R|^2\,\mathrm{e}^{-\Gamma_S\tau}[(1+|\varepsilon|^2)(1+|x|^2) + 2\,\Re e\,x\,(1-|\varepsilon|^2) + 4\,\Im m\,x\,\Im m\,\varepsilon] \\
&\quad + 8|R|\,\mathrm{e}^{-\overline{\Gamma}\tau}\{\Re e\,\varepsilon(1+|x|^2)\cos\left(\Delta m\,\tau+\Phi_R\right) \\
&\quad - \left[2\,\Im m\,\varepsilon\,\Re e\,x - \left(1-|\varepsilon|^2\right)\,\Im m\,x\right]\sin\left(\Delta m\tau+\Phi_R\right)\}\ , \qquad (5.74)
\end{aligned}$$

where $\overline{\Gamma} = (1/2)(\Gamma_S + \Gamma_L)$.

In the limit where $\Re e\,\varepsilon \ll 1, \Im m\,x \ll 1$ and $\tau > 3/\Gamma_S$, the expression for the charge asymmetry $\delta(\tau) = (N^+ - N^-)/(N^+ + N^-)$ can be simplified:

$$\delta(\tau) = 2\frac{1-|x|^2}{|1-x|^2}\left[\Re e\,\varepsilon + |R|\,\mathrm{e}^{-(1/2)(\Gamma_S-\Gamma_L)\tau}\cos\left(\Delta m\,\tau+\Phi_R\right)\right]. \tag{5.75}$$

For an initially pure K_L beam ($R = 0$), the asymmetry is independent of the decay time:

$$\delta_{\mathrm{L}} = 2\,\Re e\,\varepsilon\,\frac{1-|x|^2}{|1-x|^2}\,. \tag{5.76}$$

For an initial incoherent mixture of K^0 (N_{K}) and $\overline{\mathrm{K}^0}$ ($N_{\overline{\mathrm{K}}}$) the quantity $|R|$ has to be replaced by $(N_{\mathrm{K}} - N_{\overline{\mathrm{K}}})/(N_{\mathrm{K}} + N_{\overline{\mathrm{K}}})$, i.e. by the same dilution factor as for 2π interference in a short-lived beam.

For the coherent mixture created by a regenerator, R is given by the regeneration amplitude ϱ, and Φ_R by the regeneration phase Φ_ϱ.

5.5 Detection of K^0 Decays

The main decay modes originating from K^0's in a neutral beam and their respective branching ratios are [23]

$$\begin{array}{lll}
\mathrm{K_L} \to \pi^\pm e^\mp \nu & (38.79 \pm 0.27)\% & \mathrm{K_{e3}}\ ; \\
\mathrm{K_L} \to \pi^\pm \mu^\mp \nu & (27.18 \pm 0.25)\% & \mathrm{K}_{\mu 3}\ ; \\
\mathrm{K_L} \to \pi^+\pi^-\pi^0 & (12.58 \pm 0.19)\% & \mathrm{K}_{\pi 3}\ ; \\
\mathrm{K_L} \to \pi^0\pi^0\pi^0 & (21.08 \pm 0.27)\% & \mathrm{K}_{\pi 3}\ ; \\
\mathrm{K_S} \to \pi^+\pi^- & (68.60 \pm 0.27)\% & \mathrm{K}_{\pi 2}\ ; \\
\mathrm{K_S} \to \pi^0\pi^0 & (31.40 \pm 0.27)\% & \mathrm{K}_{\pi 2}\ .
\end{array}$$

The experimental problem is to detect the rare $\mathcal{CP}$-violating decay modes $\mathrm{K_L} \to \pi^+\pi^-$ and $\mathrm{K_L} \to \pi^0\pi^0$, with branching ratios of order 10^{-3} in this overwhelming background of other decays and to measure their decay rate and, by interference, their phase relation to $\mathcal{CP}$-conserving decay amplitudes. In addition, the $\mathcal{CP}$ impurity in the $\mathrm{K_L}$ state can be obtained by measuring the charge asymmetry in the semileptonic decay modes.

5.5.1 Charged Decay Modes

The two charged decay products in $\pi^+\pi^-$ and semileptonic decays are usually recorded in a magnetic spectrometer consisting of a wide-aperture magnet and at least three layers of position-measuring detectors. The measurement of the track position was done originally by optical spark chambers [11, 12, 13, 25], and then by wire spark chambers with magnetostrictive readout [14], by counters only [26, 27], by multiproportional wire chambers [24, 27, 28] and by drift chambers [67, 68]. As an example, Fig. 5.1 shows a spectrometer [24] used for the detection of medium-energy kaons from a 24 GeV/c extracted proton beam at the CERN proton synchrotron. Here the magnet has an aperture of 240×60 cm^2. This permits observation of K decays with a K momentum from 5 to 15 GeV/c over a 9m long decay path upstream of the magnet with a geometrical acceptance around 25%, depending on the decay mode. Most important for the measurement of interference phenomena between $\mathrm{K_S}$ and $\mathrm{K_L}$ decays extending over at least 20 $\mathrm{K_S}$ mean lifetimes in the Kaon rest frame is the fact that this geometric acceptance varies smoothly and by

not more than 50% over 10 K_S mean lifetimes. The acceptance has to be computed by Monte Carlo methods, which is one of the ultimate limitations of the experiment.

In this spectrometer, the vector momenta $\boldsymbol{p}_i$ $(i = 1, 2)$ of the charged decay products are measured by three multiwire proportional chambers, each equipped with a horizontal and a vertical signal wire plane. The wire spacing is 2 mm, corresponding to a measurement error of ± 0.7 mm; the wire diameter is 20 μm. The chambers can be used with a time resolution of 40 ns, thus permitting operation in regions of charged-particle flux ten times higher than the fluxes sustainable by spark chambers, with recovery times of ~ 1 μs. Furthermore, since the chambers are dc operated, they do not require additional scintillation counters, permitting a reduction of the matter in the path of the detected particles to 0.3 g/cm^2 for the total apparatus. The readout time of an electronically accepted event is 10 μs, and more than 1000 events can be recorded during one machine burst of 350 ms duration.

The energies of the particles are obtained from the calculated vector momenta $\boldsymbol{p}_i$, assuming their rest mass to be m_π, as

$$E_i = \sqrt{\boldsymbol{p}_i^2 + m_\pi^2} \; . \tag{5.77}$$

The invariant mass of the pair is obtained as

$$m_{\pi\pi} = \sqrt{(E_1 + E_2)^2 - (\boldsymbol{p}_1 + \boldsymbol{p}_2)^2} \; , \tag{5.78}$$

and the kaon momentum to be $\boldsymbol{p}_{\mathrm{K}} = \boldsymbol{p_1} + \boldsymbol{p_2}$. The lifetime of the kaon from the target (position along the beam z_{T}) to the decay vertex (z_{V}) in the kaon rest system is given by $\tau = (z_{\mathrm{V}} - z_{\mathrm{T}}) m_{\mathrm{K}} / (c p_z)$, where m_{K} is the kaon mass, c the light velocity and p_z the component of $\boldsymbol{p}_{\mathrm{K}}$ along the beam line.

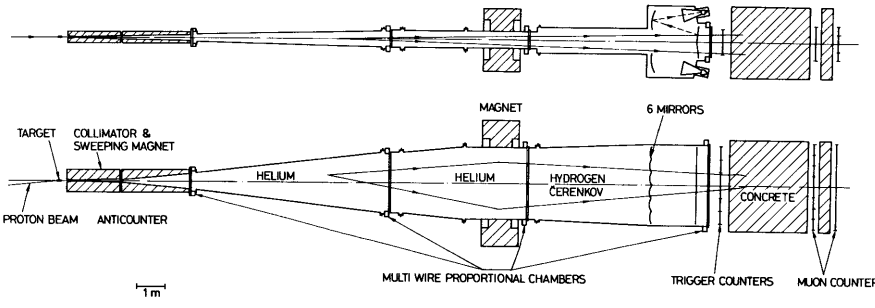

Fig. 5.1. Magnetic spectrometer for detecting two charged decay products of neutral K mesons, side view (*top*) and top view (*bottom*). The spectrometer, consisting of a magnet and 3×2 planes of proportional chambers, measures the momenta of the two charged particles; the Cerenkov counter identifies electrons from K_{e3} decay and the muon hodoscopes detect muons from $K_{\mu 3}$ decay [24].

Two sets of information can be used to separate 2π and leptonic decays. First the invariant mass $m_{\pi\pi}$ is required to be equal to m_{K} within the experimental resolution for 2π decay (Fig. 5.2), while leptonic decays show a broad $m_{\pi\pi}$ distribution, owing to the wrong assignment of a pion mass to the lepton and to the missing neutrino energy. Second, all experimenters use lepton identification in order to identify these decay modes. This can be done by several methods.

The most frequently used methods for electron identification at intermediate energies, around 10 GeV, are Cerenkov counters, and identification through comparison of the energy deposition in electromagnetic and hadronic showers. Threshold gas Cerenkov counters identify electrons by their high velocity, whereas Cerenkov emission by pions is avoided by a suitable choice of refractive index n; the threshold momentum is $p_{\mathrm{th}} = m_{\pi}/\sqrt{2(n-1)} = 8.4\ \mathrm{GeV}/c$ for hydrogen at atmospheric pressure.
At high energies, i.e. for electrons with energies between 10 GeV and 100 GeV, electron identification in calorimetric detectors works on the principle that for a particle of momentum p, the energy E deposited in a calorimeter by an electron (or photon) is much higher than for a hadron of the same momentum. With a suitable calibration of the calorimeter E/p is near unity for

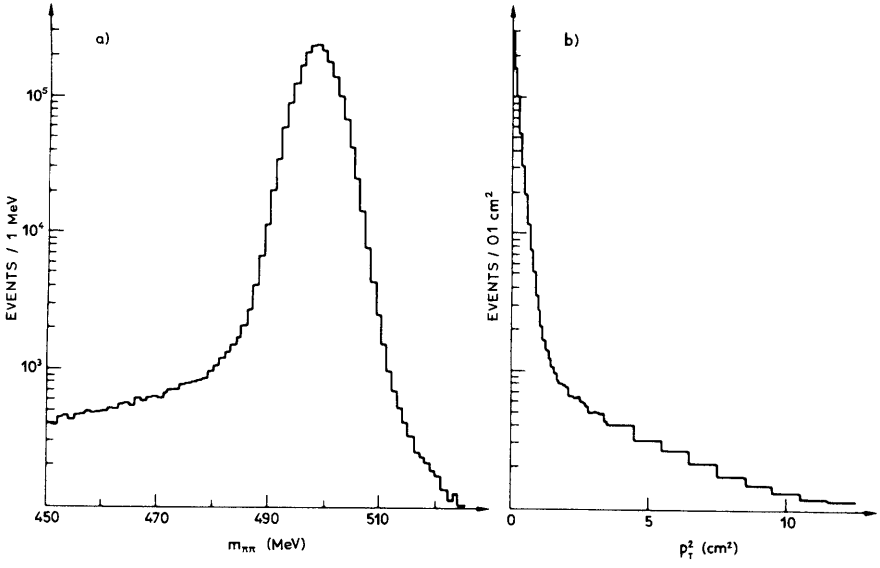

Fig. 5.2. (**a**) Invariant-$\pi^+\pi^-$-mass distribution of two-prong events recorded in the apparatus of Fig. 5.1 after removing most of the three-body leptonic $\mathrm{K_L}$ decays identified through the Cerenkov or muon counters. (**b**) Distribution as a function of p_t^2, the squared distance of the reprojected K momentum in the target plane from the target center [28]

electrons and less than 0.9 for hadrons because part of the hadronic energy is used for nuclear excitation or nuclear spallation, and therefore remains undetected. Also, the width of an electromagnetic shower is much smaller than that of a hadronic shower produced by pions.

For the identification of muons, on the other hand, one uses their penetration through several ($\sim$ 8) interaction lengths of material in order to distinguish them from pions interacting in this absorber. For an absorber of 900 g/cm^2 of light concrete, the minimum momentum of a penetrating muon is 1.5 GeV/c, and the penetration probability of a Pion through a hadronic cascade is 0.6% at 4 GeV/c momentum. In addition to this kind of misidentification of a pion, there is the possibility of pion decay in flight.

Once the 2π decay mode has been identified, one has to know, in general, whether the K_S or K_L from which the decay products originate has undergone scattering on its way from its production to the decay point. In the case of a short-lived beam produced by protons interacting in a target near to the detector, this can be done by calculating the distance of the intercept of the reprojected kaon momentum p_K in the target plane from the target center, p_t. Unscattered events cluster around $p_t = 0$, as shown in Fig. 5.2. In the case of a long-lived beam, one uses the component of p_K transverse to the beam, p_t, or the angle θ between the kaon direction p_K and the beam direction in order to separate transmitted and coherently regenerated ($\theta = 0 = p_t$) kaons from events due to kaons that have undergone scattering, or diffractive or inelastic regeneration.

This analysis is straightforward for 2π decays, but substantially more complicated for semileptonic decays, since the neutrino momentum escapes detection. Not only is it impossible, in the case of semileptonic events, to separate coherently regenerated ones from incoherently regenerated kaons, but there is also a twofold ambiguity in the kaon momentum. These difficulties can be solved by comparing the experimental distributions in momentum on a statistical basis with the corresponding distributions calculated by Monte Carlo methods from hypotheses about the "real" distributions.

5.5.2 Neutral Decay Modes

The detection of the neutral decay mode $K_L \to \pi^0\pi^0 \to 4\gamma$ is complicated by the presence of the decay $K_L \to 3\pi^0 \to 6\gamma$ with a 21% branching ratio. This decay can simulate 4γ events for kinematic reasons, e.g. if two γ rays are missed by the detector. Very specific kinematic features of the $2\pi^0$ decay were therefore used in the early medium-energy experiments in order to obtain a clean $K_L \to 2\pi^0$ signal [29, 30, 31, 32, 34].

In the apparatus (Fig. 5.3) of the Princeton group [30] used in the very early phase of $\mathcal{CP}$ experiments, this was achieved by measuring with great precision the energy and direction of one γ ray of the four γ's from $2\pi^0$ decay. This photon can have a transverse momentum relative to the K_L direction of up to 240 MeV/c, since its parent π^0 has a momentum of exactly

209 MeV/c in the K_L rest system. The γ's from the background reaction $K_L \rightarrow 3\pi^0 \rightarrow 6\gamma$, however, are restricted to a transverse momentum below 167 MeV/c. Consequently, the apparatus of the Princeton group included a pair spectrometer for the precise measurement the of momentum, direction and transverse momentum of one γ ray converted in a converter one-tenth of a radiation length thick with standard deviations of 3%, 3 mrad, and 5 MeV/c, respectively. In the spectrometer, positions of the e^+ and e^- trajectories bent by an 18inch × 72inch aperture magnet were recorded by five optical spark chambers. The remaining three γ rays were converted in a large optical spark chamber containing six radiation lengths of lead.

Using the energy and direction of the spectrometer γ ray, the conversion points of the three other γ rays, and the decay vertex of the K_L computed from the spectrometer γ-ray direction and the beam path, the decay can be reconstructed with two constraints.

As an alternative, the design of the detector (Fig. 5.4) of the Aachen–CERN–Torino group [29] has been guided by the idea of measuring accurately the energies of all four γ rays and the direction of at least two γ's of the four from $K_L \rightarrow \pi^0\pi^0 \rightarrow 4\gamma$ decay. The upstream part of the detector is the "direction-measuring" region, totaling four spark chamber modules of four wire planes each. Every module is preceded by a lead converter foil one-

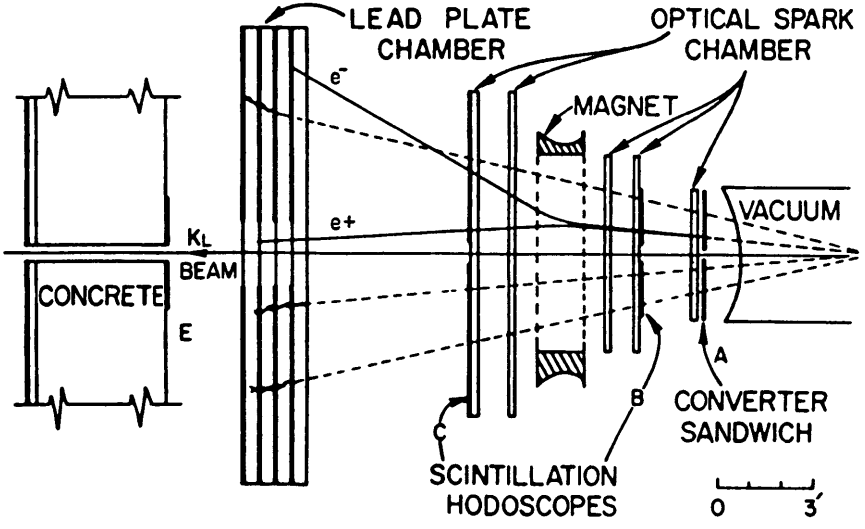

Fig. 5.3. Apparatus of the Princeton group for the detection of $K_L \rightarrow 2\pi^0$ decays. The rare $K_L \rightarrow 2\pi^0 \rightarrow 4\gamma$ decays are selected by requiring one γ ray converted in the converter A to have a transverse momentum $p_t > 170$ MeV/c, as measured in the magnetic pair spectrometer. The other three γ rays are detected in the lead-plate chamber [30]

tenth of a radiation length thick, and the directions of the wires in the four planes are at 0°, 45°, 90°, and 135° relative to the vertical inorder to avoid ambiguities in the track reconstruction from the sparks. The spatial resolution of the spark chambers is equal to the scattering error in a lead converter one-tenth of a radiation length thick for a γ energy of 1 GeV, i.e. the average energy of γ's from $K_L \to 2\pi^0$ decay in the beam. In the downstream part of the detector the remaining γ rays are converted either in one of the two lead plates one-quarter of a radiation length thick in front of two further spark chamber modules or in an array of 61 hexagonal lead-glass prisms 13 radiation lengths thick. These total absorption counters made of lead glass permit an energy measurement of the γ rays with a resolution (standard deviation) of $\sigma_E/E = 3.3\%/\sqrt{E_\gamma}$, where E_γ is measured in GeV. A spark chamber trigger requires at least two channels in each of the vertical and horizontal counter arrays behind the fourth module; the energy deposited in at least three of the six outer sectors (see Fig. 5.4) of the lead glass counter array must exceed 450 MeV. The tracks of the e^+e^- pair from a γ converted in the first four modules are used to determine the decay point, and this position is used together with the conversion points of the other γ rays to determine their directions. Gamma rays are then paired such that the invariant mass of the pair is as close as possible to the π^0 mass. The π^0 mass, the 4γ invariant mass m, the angle θ between the total visible momentum and the beam path, and p_γ, the largest of the transverse momenta of the γ rays, can be used as constraints in the kinematical selection of $2\pi^0$ decays.

For kaon energies between 40 GeV and 200 GeV, totally absorbing electromagnetic calorimeters are used. These calorimeters consist of scintillating crystals, Cerenkov lead glass counters, or liquid-noble-gas detectors with or without lead radiators. Their longitudinal thickness is around 25 radia-

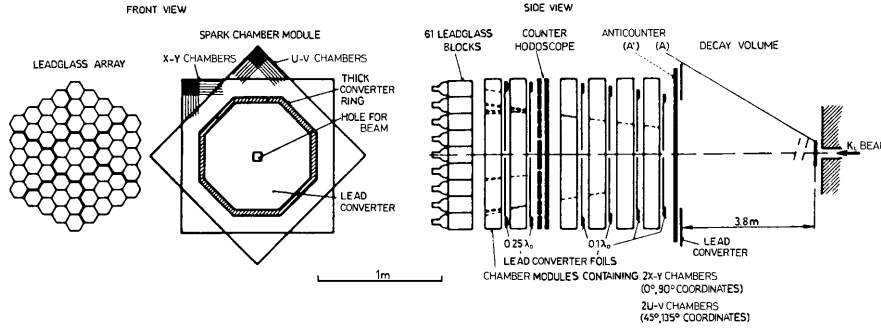

Fig. 5.4. Apparatus of the Aachen–CERN–Torino group for the measurement of the $K_L \to 2\pi^0$ decay rate. This detector consists of a direction-measuring part (four chamber modules upstream), where at least two γ rays are required to convert, and an energy-measuring part (two chamber modules and a lead glass wall), where the energies of all four γ rays are recorded [29]

tion lengths, and their transverse segmentation corresponds to the transverse width of an electromagnetic shower, given by the Molière radius R_{M} of the material. In this way, the energies E_i and the transverse positions (x_i, y_i) of each of the four photon-induced showers are measured in the calorimeter. This is the only information available for reconstructing all variables describing the decay. In principle the invariant mass of the four photons can be calculated using the relation

$$M^2 = E^2 - \boldsymbol{p}^2 = \left(\sum_{i=1}^{4} E_i\right)^2 - \left(\sum_{i=1}^{4} \boldsymbol{p}_i\right)^2 \tag{5.79}$$

$$= \sum_{i \neq j} (E_i E_j - E_i E_j \cos\theta_{ij}) \tag{5.80}$$

$$= 2 \sum_{i<j} E_i E_j \frac{\theta_{ij}^2}{2} \,. \tag{5.81}$$

The opening angle θ_{ij} between two photons can be obtained from the transverse distance r_{ij} between the impact points in the calorimeter,

$$r_{ij} = \sqrt{(x_i - x_j)^2 + (y_i - y_j)^2} \,, \tag{5.82}$$

and the distance z of the K meson decay point from the calorimeter. Using these variables, the invariant four-photon mass can be written as

$$M = \frac{1}{z} \sqrt{\sum_{i<j} E_i E_j r_{ij}^2} \,. \tag{5.83}$$

This relation can be used to calculate the distance of the decay point of the kaon from the calorimeter by using the kaon mass as a constraint:

$$z = \frac{1}{M_{\mathrm{K}}} \sqrt{\sum_{i<j} E_i E_j r_{ij}^2} \,. \tag{5.84}$$

With this knowledge about the decay point, the invariant mass of any pair (i, j) of photons can then be calculated:

$$M_{ij} = \frac{1}{z} r_{ij} \sqrt{E_i E_j} \,. \tag{5.85}$$

Of the three possible combinations, the one where both masses are closest to the π^0 mass is chosen. A scatter plot of m_{12} versus m_{34} shows a signal at (m_{π^0}, m_{π^0}) if the four photons come from the decay $\mathrm{K_L} \to \pi^0\pi^0$, while for events from the decay $\mathrm{K_L} \to 3\pi^0$, with four detected photons, the invariant masses are spread over a large region around this point (Fig. 5.34). It is possible to extract the amount of background in the signal region by extrapolating the observed level of background events into this signal region, with

the help of Monte Carlo simulations of the $K_L \to 3\pi^0$ background. In high-energy experiments, the background can then be reduced to a level below one percent.

5.5.3 Detectors Measuring Charged and Neutral Decay Modes Simultaneously

For the measurement of the parameter ε' of direct $\mathcal{CP}$ violation, the ratio of the decay rates of K_L into charged ($\pi^+\pi^-$) and neutral ($\pi^0\pi^0$) two-pion states has to be measured with great precision. For this purpose, experimentalists reduce systematic normalization uncertainties by measuring charged and neutral decays (from K_L and K_S mesons) simultaneously.

Four such experiments have been constructed for high-energy K meson beams, two of them at CERN (NA31 and NA48) and two at Fermilab (E731 and kTeV).

One experiment has been designed to detect K mesons of a few hundred MeV/c momentum arising from the annihilation of stopping antiprotons in a hydrogen target at the Low Energy Antiproton Ring (LEAR) at CERN (CPLEAR).

5.5.4 NA31

This detector [33], situated in a K_L or K_S beam from the CERN SPS, was based on calorimetry and was designed for good stability and high efficiency. The K_L beam was produced by a 450 GeV proton beam with a production angle of 3.6 mrad in the year 1986 and 2.5 mrad in the years 1988 and 1989. In the year 1986, a K_S beam was also produced by a 450 GeV proton beam with a production angle of 3.6 mrad. In the years 1988 and 1989, the proton energy for the K_S beam was 360 GeV and the production angle 4.5 mrad.

A schematic illustration of the beam layout and the apparatus is shown in Fig. 5.5. The principal features can be summarized as follows:

- both the K_L and the K_S beam are in vacuum;
- to adjust the steeply falling vertex distribution of the K_S decays to the almost flat vertex distribution of the K_L decays, the K_S target is located on a train, that can be positioned at 41 stations in the decay volume;
- an anticounter with a 7 mm lead converter in the K_S beam is used to veto decays in the collimator, defines the upstream edge of the decay region, and provides for the relative calibration of the $2\pi^0$ and $\pi^+\pi^-$ energy scales to a precision better than $\pm 10^{-3}$;
- four ring-shaped anticounters around the decay region detect photons and thus reduce unwanted three-body decays;
- two wire chambers spaced 25 m apart, with ± 0.5 mm resolution in each projection, track charged pions;

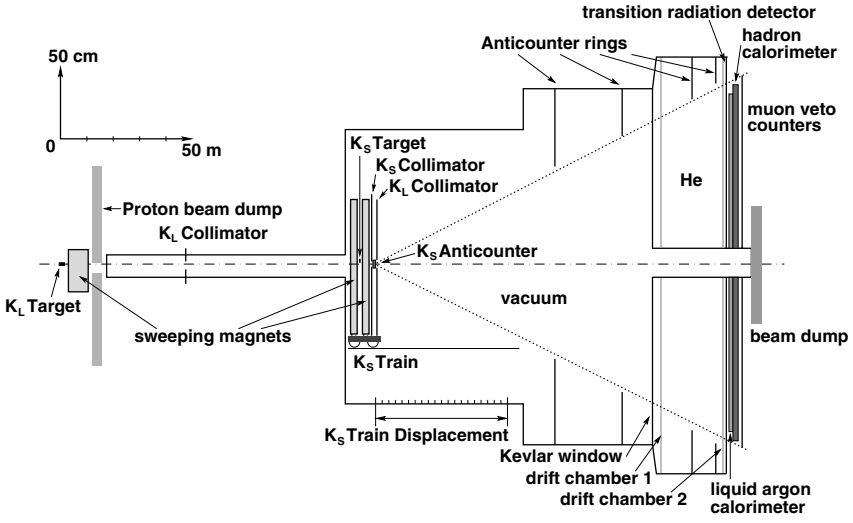

Fig. 5.5. Beam layout and detector in the NA31 experiment. The setup contains a movable target for the production of the K_S mesons, and a liquid-argon calorimeter; it does not contain a magnet

- a hodoscope of scintillation counters triggers on $\pi^+\pi^-$ decays detected by a coincidence of hits in opposite quadrants;
- a liquid-argon/lead sandwich calorimeter with strip readout detects photons with ± 0.5 mm position resolution and an energy resolution of $\sigma_E/E = 10\%/E \oplus 7.5\%/\sqrt{E} \oplus 0.6\%$;
- a plane of scintillation counters, installed in the liquid argon after 13 radiation lengths of material, triggers on $2\pi^0$ decays;
- an iron/scintillator sandwich calorimeter measures the energy of charged pions with $\pm 65\%/\sqrt{E}$ energy resolution;
- two planes of scintillator, after a total of 3 m of iron equivalent, reject $K^0 \to \pi\mu\nu$ decays.

In order to obtain the maximum solid angle for the decay particles, no magnetic analysis of charged-pion momenta was done. The energies of the two pions and their opening angle are used to measure the invariant mass of the charged pair.

The NA31 experiment collected K_L and K_S decays in alternating time periods. In each case the charged and neutral decays were collected simultaneously.

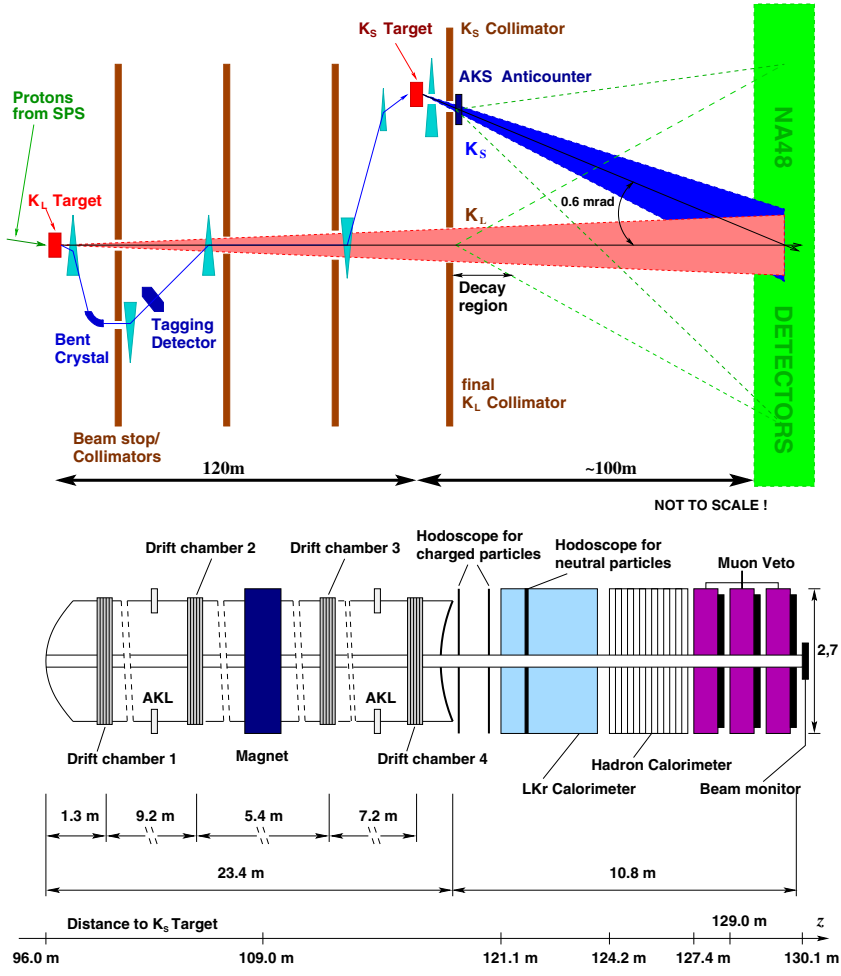

Fig. 5.6. Beam layout and detector in the NA48 experiment

5.5.5 NA48

This experiment (Fig. 5.6 was the successor to the NA31 experiment and also built at CERN. The experiment was exposed to a simultaneous nearly collinear K_L/K_S beam, derived from a 450 GeV/c proton beam from the SPS.

The K_S beam was produced by using a fraction of the protons that did not interact with the K_L target.

In the NA48 experiment [68], the charged and neutral decay modes of K_L and K_S mesons could be measured simultaneously. Charged particles from decays were measured by a magnetic spectrometer composed of four drift

chambers with a dipole magnet (inducing a transverse momentum kick of 265 MeV/c in the horizontal plane) between the second and the third chamber. These chambers and their interconnecting beam tube were aligned along the bisector between the converging K_S and K_L beam axes. The volume between the drift chambers was filled with helium. Each chamber consisted of eight planes of sense wires, two horizontal, two vertical and two along each of the 45° directions. In the third chamber, only the horizontal and vertical planes were instrumented. The average efficiency per plane was 99.5%, with a radial uniformity better than ±0.2%. The space point resolution was ≈95 μm. The momentum resolution was $\sigma_p/p = 0.48\% \oplus 0.009\% \times p$, where the momentum p is in GeV/c. The $\pi\pi$ invariant mass resolution is 2.5 MeV.

The magnetic spectrometer was followed by a scintillator hodoscope, composed of two planes segmented into horizontal and vertical strips. Fast logic combine the strip signals (arranged in four quadrants) for use in the first level of the $\pi^+\pi^-$ trigger, with a time resolution of 200 ps.

A liquid-krypton (LKr) calorimeter was used to reconstruct $K \to 2\pi^0$ decays. This was a quasi-homogeneous detector with an active volume of ∼10 m^3 of liquid krypton. Cu–Be–Co ribbon electrodes of size 40 μm × 18 mm × 125 cm defined 13212 cells (each with a 2 cm × 2 cm cross section) in a structure of longitudinal projective towers pointing to the center of the decay region. The calorimeter was ∼27 radiation lengths long and fully contained electromagnetic showers with energies up to 100 GeV. The energy resolution of the calorimeter was $\sigma_E/E = (3.2 \pm 0.2)\%/E \oplus (9 \pm 1)\%/\sqrt{E} \oplus (0.42 \pm 0.05)\%$ where E is in GeV. The LKr calorimeter was also used, together with an iron-scintillator calorimeter, to measure the total deposited energy for triggering purposes.

Finally, at the end of the beam line, three planes of muon counters behind 80 cm of iron were used to identify $K_L \to \pi\mu\nu$ ($K_{\mu 3}$) decays.

5.5.6 E731

This detector was constructed at Fermilab. A K_L beam was produced by 800 GeV/c protons from the Tevatron. The experiment used the regeneration technique to produce the K_S beam (see Sect. 5.3). In this technique, a double-beam of K_L mesons is created at the K_L target. Four B_4C-blocks were located in the lower half of the double beam to regenerate K_S mesons from the K_L mesons. The layout of the experiment is shown in Fig. 5.7.

The photons from neutral decays were detected with a lead glass calorimeter. The calorimeter was composed of ∼800 blocks of lead glass (Schott F-2) arranged in a circular array with holes for the two beams. The dimensions of the blocks were 5.82 cm × 5.82 cm × 60.17 cm. The calorimeter had a length of ∼18.7 radiation lengths. The diameter of the array was ∼1.8 m. The energy resolution of the calorimeter was $\sigma_E/E = 5\%/\sqrt{E} \oplus 2.5\%$. The average position resolution was about 2.8 mm, varying from 1.5 mm for a particle near the block's edge to 4 mm for a particle in the center of a block.

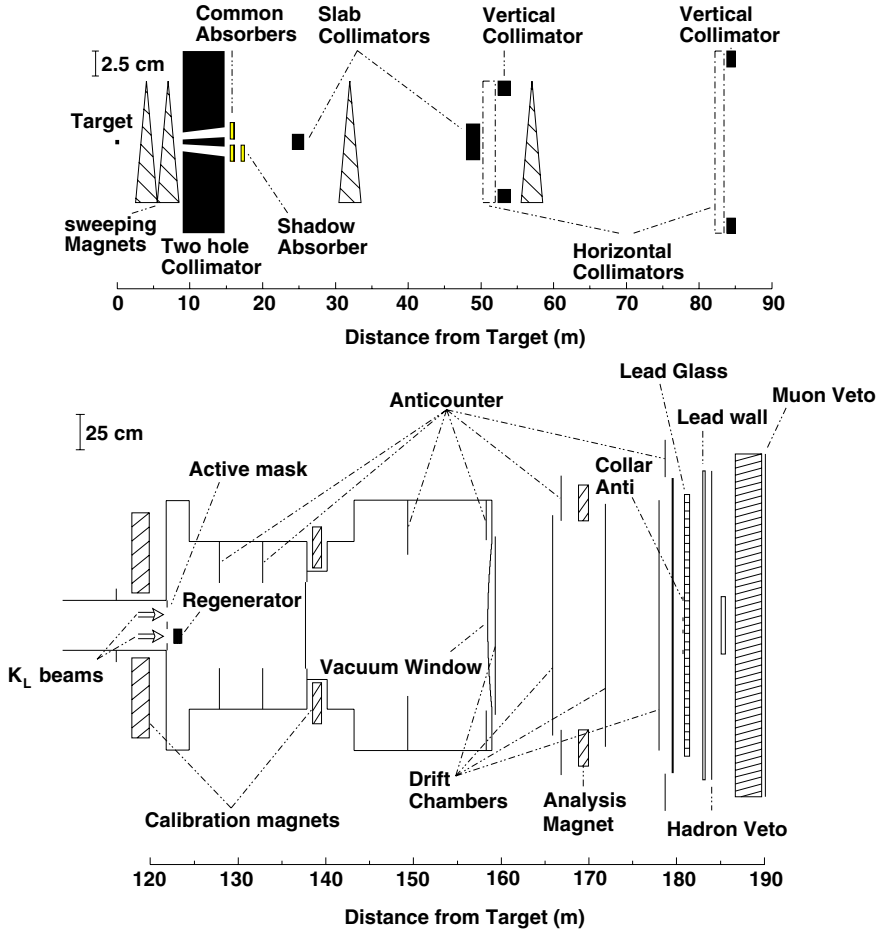

Fig. 5.7. The E731 beam and detector

The trajectories of charged particles were measured with a charged-particle spectrometer. This consisted of four drift chambers with a momentum-analyzing magnet between the second and the third chamber. Helium bags were placed between the chambers to reduce the effects of multiple scattering. There were four planes of sense wires per chamber, two in the horizontal and two in the vertical direction. The smallest chamber measured $1.26 \times 1.26\ \mathrm{m}^2$, with 101 sense wires per plane. The largest chamber measured $1.77 \times 1.77\ \mathrm{m}^2$, with 140 sense wires per plane. The momentum resolution of the charged-particle spectrometer was $\sigma_p/p = 0.45[1 \oplus p/(37.5\ \mathrm{GeV}/c)]\%$. Charged and neutral decays were collected separately in alternating time periods, but $\mathrm{K_L}$ and $\mathrm{K_S}$ decays were collected together.

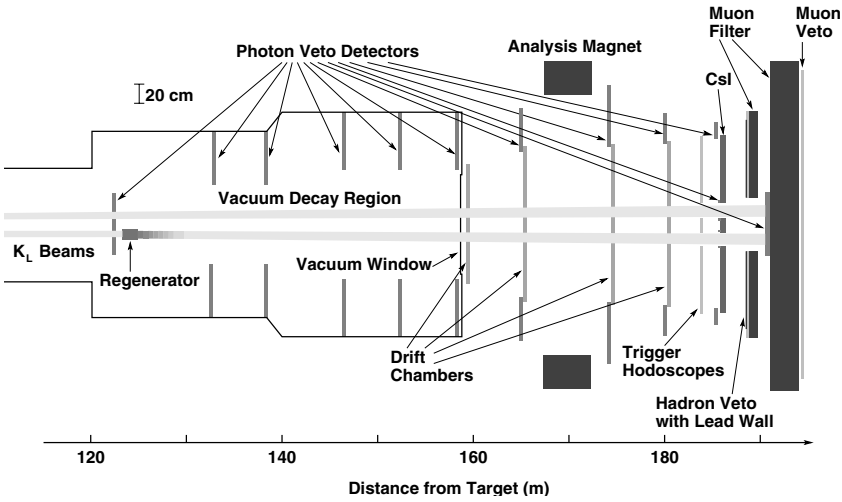

Fig. 5.8. The kTeV beam and detector

5.5.7 kTeV

The kTeV experiment at the 800 GeV/c Tevatron was the successor to the E731 experiment and uses a similar regeneration technique to produce the K_S beam. Like the NA48 experiment, the kTeV detector could simultaneously measure the charged and neutral decays of the K_L and K_S mesons. Figure 5.8 shows the experimental setup of the kTeV experiment. The K_L "double beam" entered from the left, one half continuing as K_L, the other half producing a K_S beam by regeneration. The regenerator in the kTeV experiment was made of blocks of plastic scintillator. These blocks were viewed by photomultiplier tubes to reject inelastically or quasi-elastically scattered kaons.

The evacuated decay volume extended over 40 m, or about 7 K_S mean lifetimes at 100 GeV/c, followed by the first drift chamber. All chambers had two insensitive areas in order to let the two beams pass through. The analysis magnet was located between the second and the third drift chamber and provided a horizontal momentum kick of 412 MeV/c. Each of the four drift chambers had two horizontal and two vertical planes of sense wires. There were a total of 16 planes and 1972 wires in the drift chambers. As in the E731 detector, the smallest chamber measured 1.26×1.26 m^2, with 101 sense wires per plane and the largest chamber measured 1.77×1.77 m^2, with 140 sense wires per plane. The typical single-hit position resolution of the drift chambers was about 110 μm in either direction, which lead to a mean mass resolution of 2.2 MeV for the reconstructed kaon mass obtained from the $\pi^+\pi^-$ decay mode. The momentum resolution for a charged particle

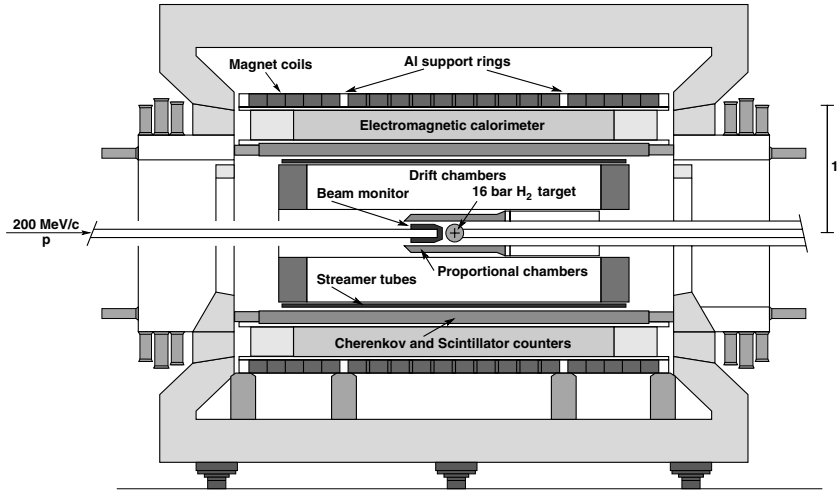

Fig. 5.9. The CPLEAR detector

was $\sigma_p/p = 0.17\% \oplus 0.0071\% \times p$ (in GeV/c). The average inefficiency for reconstructing a hit pair was about 3.7%.

The four photons from the $2\pi^0$ were detected in an electromagnetic calorimeter made of pure cesium iodide. The calorimeter consisted of 3100 blocks arranged in a square array of 1.9 m side length. The blocks had two sizes: 2.5 × 2.5 cm^2 in the central region (2232 blocks) and 5 × 5 cm^2 in the outer region (868 blocks). All blocks are 50 cm, or ∼27 radiation lengths, long. Two 15 cm square holes allowed the passage of the K_L and the K_S beam through the calorimeter. The light collection uniformity of the crystals was within 5%. The calorimeter had an energy resolution of $\sigma_E/E = 2\%/\sqrt{E} \oplus 0.4\%$. The average position resolution for electrons was about 1.2 mm for clusters in the smaller crystals and 2.4 mm for the larger crystals.

5.5.8 CPLEAR

In contrast to the four detectors described in the previous sections, the CPLEAR detector measured decays from kaons produced in $\bar{p}p$ annihilations at rest obtained from the low energy $\bar{p}$ ring LEAR at CERN. The antiprotons were stopped in a 16 bar hydrogen gas target and formed a protonium before annihilation. In annihilation reactions of the type $\bar{p}p \to K^0K^-\pi^+$ and $\bar{p}p \to \overline{K^0}K^+\pi^-$, the charged kaon was identified through the time of flight and track curvature in a solenoidal magnetic field ("tagging"). This tag was used as a trigger for detecting the decay products of the neutral K meson

associated with the K^+ or K^-. A unique property of this scheme is that the strangeness of the neutral K meson is known from the charge of the tagged K^+ or K^-.

As shown in Fig. 5.9, the CPLEAR experiment had a cylindrical, onion-type, setup. The target region was followed by two proportional chambers. The inner proportional chamber had 576 wires and the outer one 768 wires. Six cylindrical drift chambers, starting at a radius of 25.46 cm and going out to a radius of 50.95 cm, provided the main tracking information for charged particles. The number of readout strips of the inner cathode of the drift chambers varied between 275 (innermost chamber) and 510 (outermost chamber). For the outer cathode, the number of readout strips varied between 285 (innermost chamber) and 520 (outermost chamber). All cathode strips were inclined at different stereo angles with respect to the anode wires. The strip efficiency was about 90%. The outermost tracking detector was a streamer tube detector. It consisted of 384 discrete tubes, 2.52 m long and 1.65×1.65 cm^2 in cross section. The tubes were located at radii between 56.8 cm and 62.0 cm. The offline track-finding efficiency was better than 99% and the wire positions were determined with an accuracy of about 10 μm. The mean mass resolution achieved for the invariant kaon mass in the $\pi^+\pi^-$ final state was 13.6 MeV/c^2. The resolution of the (missing mass)^2 relative to the primary Kπ pair was 0.082(GeV/c^2)^2. By applying kinematically and/or geometrically constrained fits, the K^0 momentum resolution σ_{p_t}/p_t was improved from 5.5% to 0.25%.

The tracking detectors were followed by the particle identification detector (PID). This detector was used for charged-kaon identification and e/π separation. It consisted of 32 trapezoidal sectors and was located at radii between 62.5 cm and 75.0 cm. Each sector was composed of two layers (inner, 3.0 cm thick; outer, 1.4 cm thick) of plastic scintillators with an 8 cm thick liquid threshold Cerenkov detector in between. The kaon identification efficiency was about 75% for kaon momenta greater than 350 MeV/c. The probability of faking a kaon signal was smaller than 6×10^{-3}. Using the $\mathrm{d}E/\mathrm{d}x$ information from the first scintillator, a good K/π separation was possible up to 500 MeV/c. The two charged tracks from the decays $\overline{K^0} \to \pi^+\pi^-$, $\pi^+e^-\nu$, $\pi^+\mu^-\nu$ were reconstructed and the decay vertex was calculated. Using this vertex and the annihilation point in the hydrogen target, the proper time for decay of the kaon was obtained.

The electromagnetic calorimeter had the form of a barrel and was an assembly of 18 lead plates alternating with sampling chambers, which consisted of small-cross-section tubes and pickup strips. It was located at radii between 75 cm and 100 cm. The calorimeter had a total thickness of $\sim$6 radiation lengths, an energy resolution of $\sigma_E/E \approx 13\%/\sqrt{E}$ and a position resolution of $\sim$5 mm for the photon conversion points. The photon detection efficiency was (90 ± 1)% for photon energies above 200 MeV. For photons

with energies below 200 MeV the efficiency dropped significantly and was only about 60% for 100 MeV photons.

All subdetectors were embedded in a 3.6 m long, 2 m diameter solenoid magnet, which provided a 0.44 T uniform field.

5.6 Elucidation of $\mathcal{CP}$ Violation in K^0 Decays (I): Search for $\Im m(\varepsilon'/\varepsilon)$

5.6.1 Interference Experiments Behind a Regenerator

Even after the discovery by the Princeton group, some doubts remained about whether $\mathcal{CP}$ invariance really had to be given up. One idea for saving $\mathcal{CP}$ was the hypothesis that together with the two pions emitted in the K_L decay, there was a scalar meson emitted with such a small mass that it was not noticed in the invariant $\pi^+\pi^-$ mass. Two experiments were set up at CERN in order to check if the decay amplitude for $K_L \to \pi^+\pi^-$ showed time-dependent interference with the amplitude for $K_S \to \pi^+\pi^-$ from coherently regenerated K_S in the K_L beam [12, 13]. Since the K_S wave regenerated from the K_L wave has a fixed phase relation to the K_L wave, the decay amplitudes for the decay of K_L and regenerated K_S to a common final state must interfere with each other. In both experiments, magnetic spectrometers with spark chambers were used as tracking devices. Both experiments showed clearly that the decay amplitude of the regenerated K_S interferes with the decay amplitude of the K_L transmitted through the regenerator. The proper time distribution of decays downstream of the regenerator clearly displayed the exponential K_S decay, the K_L decays (nearly constant per time interval), and an interference term with oscillatory behavior. The beat frequency of this oscillation term $\cos(\Delta m\,\tau - \Phi)$ was found to be about half of the inverse of the K_S lifetime, 10^{-10} s. These experiments demonstrated that the final state in the decay $K_L \to \pi^+\pi^-$ was the same as in the $K_S \to \pi^+\pi^-$ decay, and therefore the conclusion that there was $\mathcal{CP}$ violation became unavoidable.

Apart from the determination of the mass difference Δm and the K_S lifetime, these measurements also offered the possibility of studying the phase Φ_{+-} of the amplitude ratio η_{+-}. However, this value was not directly accessible since in the interference term, the phase shift measured is the difference $\Phi_{+-} - \Phi_f$, where Φ_f is the nuclear regeneration phase

$$\Phi_f = \mathrm{i}\,\arg(f(0) - \overline{f}(0))\,, \tag{5.86}$$

where $f(0)$ and $\overline{f}(0)$ are the forward scattering amplitudes for K^0 and $\overline{K^0}$ on a nucleus. Attempts were made to calculate the phase Φ_f from data on K^+ and K^- scattering by using isospin symmetry but the uncertainties in these calculations remained substantial.

5.6.2 The Significance of the Phase Φ_{+-}

The phase of $\eta_{+-}, \Phi_{+-} = \arg(\eta_{+-})$, was a possible clue that would help to disentangle the two components of $\mathcal{CP}$ violation, since

$$\eta_{+-} = \varepsilon + \varepsilon' \,. \tag{5.87}$$

If ε', the parameter of direct $\mathcal{CP}$ violation, was comparable in size to ε, and if its phase was orthogonal to ε, then the phase of η_{+-} would deviate in a detectable way from the phase of ε, which is mainly determined by the experimentally measurable values of Δm and $\Gamma_S = 1/\tau_S$ (see Sect. 5.2):

$$\arg(\varepsilon) = \arctan\left(\frac{2\Delta}{\Gamma_S}\right) + \Phi_D = \Phi_{SW} + \Phi_D \tag{5.88}$$

With the present values of Δm and Γ_S (Sect. 5.6.10), $\Phi_{SW} = (43.4 \pm 0.1)°$.

A significant deviation of the measured value of Φ_{+-} from Φ_{SW} would be evidence for a nonvanishing component $\Im m(\varepsilon'/\varepsilon)$ and against the superweak model of $\mathcal{CP}$ violation.

5.6.3 K_L–K_S Mass Difference

Measurements of the K_L–K_S mass difference $\Delta m = m_L - m_S$ make use of the different propagation of the K_S and K_L waves with time (Sect. 5.4.1). If τ is the eigentime in the K rest frame, then K_L propagates in accordance with $\exp(-\mathrm{i}m_L\tau)$ and K_S with $\exp(-\mathrm{i}m_S\tau)$. The interference term of the two waves is then proportional to $\exp(\mathrm{i}\,\Delta m\,\tau)$, i.e. to $\cos(\Delta m\,\tau)$. All experiments measure such an interference term to determine Δm.

The traditional method is the varying-gap method, first used by the Princeton group [35]. Here, a K_L beam traverses two slabs of matter placed in series along the beam at a distance G apart, thus regenerating coherent forward K_S amplitudes ϱ_1 and ϱ_2, and the intensity of K_S decays behind the second slab is measured as a function of the distance G between the slabs; this intensity is given in Sect. 5.4.1. A severe problem in this experiment, which compares $K \to 2\pi$ decay intensities for different flight times τ_G, is the monitoring of the K_L beam flux. This monitoring has been done [36, 37] by recording K_{e3} decays or by recording neutrons in the beam or charged particles from the proton target. However, corrections are needed because dead-time effects in the chambers vary with gap distance and possibly with time. The Aachen–CERN–Torino group [38] has avoided these problems by monitoring the K_L flux by recording $K_S \to \pi^+\pi^-$ decays, i.e. by reserving a part of the K_L beam cross section for measuring the K_L flux multiplied by $|\varrho_2|^2$ and using another part for measuring $|\varrho_1|^2 \exp(-\Gamma_S\tau_G)$. This fixed-triple-gap method has given $\Delta m = (0.542 \pm 0.006) \times 10^{10}\ \mathrm{s}^{-1}$, and this result is independent of Γ_S.

A variant of this method has been used by the CERN–Heidelberg–Dortmund group [39]. Here, a quarter of the beam cross section is sacrificed for monitoring coherently regenerated $K_S \to \pi^+\pi^-$ decays. The intensities R_1 and R_2 for two distances between the two regenerators relative to the respective monitor events M_1 and M_2 are measured. The ratio of exposure times in the two positions was chosen to be 3:1 to minimize the statistical error.

The fixed distance in space transforms (via the broad K_L momentum spectrum) to a distribution of gap flight times in the K^0 rest system; therefore the ratio $(R_1/M_1)/(R_2/M_2)$ as a function of the K_S momentum shows the typical interference (see Fig. 5.10). The result of this experiment is $\Delta m = (0.534 \pm 0.003) \times 10^{10}\ s^{-1}$ for $\Gamma_S = 1.120 \times 10^{10}$ s. The error is reduced to ± 0.00255 if the result is used in conjunction with a vacuum interference experiment done in the same apparatus [28].

A second measurement, using a quite different method has been reported by the same group [40]. Here, the charge asymmetry in K_{e3} and $K_{\mu 3}$ decays at short distances from a K^0 production target was measured. This charge asymmetry (see Sect. 5.4.2) is given by

$$\delta(\tau) = 2\frac{1-|x|^2}{|1-x|^2}\left[e^{-\overline{\Gamma}\tau}\,\frac{N_K - N_{\overline{K}}}{N_K + N_{\overline{K}}}\,\cos(\Delta m\,\tau) + \Re e\,\varepsilon\right]. \tag{5.89}$$

Of the total data on semileptonic decays, 6×10^6 K_{e3} decays and 2×10^6 $K_{\mu 3}$ decays at times $\tau < 12.75 \times 10^{-10}$ s were relevant to the measurement of the mass difference, while the rest of the data was used to determine the long-term asymmetry due to $\mathcal{CP}$ violation (see Sect. 5.6.9). The dilution factor was obtained from the size of the interference term in the vacuum interference experiment [28] (see Sect. 5.6.5). The results of the fit to the data displayed in Figs. 5.11 and 5.12, including a $(0.45 \pm 0.10)\%$ shift due to radiative corrections in K_{e3}, are in units of $10^{10}s^{-1}$: $\Delta m = 0.5341 \pm 0.0043$ and $\Delta m = 0.529 \pm 0.010$, respectively. More recently, new results from the high-energy experiments at Fermilab E731 [41], E773 [44] and kTeV [45] have been obtained for the interference term behind a regenerator. The most precise experiment in this series reports a value of 0.5261 ± 0.0015 if the lifetime τ_S is 0.8959×10^{-10} s. The corresponding vertex distribution is shown in Fig. 5.17. Additional information on the mass differencehas been obtained from interference experiments (Sects. 5.6.5, 5.6.6 and 5.6.7). However, in those experiments, the measured value of Δm is correlated with the value of the phase difference Φ_{+-}.

5.6.4 Rate of $K_L \to \pi^+\pi^-$ Decay

This rate has been measured in two different ways. The first was by recording the number of $K_L \to \pi^+\pi^-$ decays in a certain decay volume together with leptonic decays $K_L \to \pi e \nu$ in the same volume. A Monte Carlo calculation of

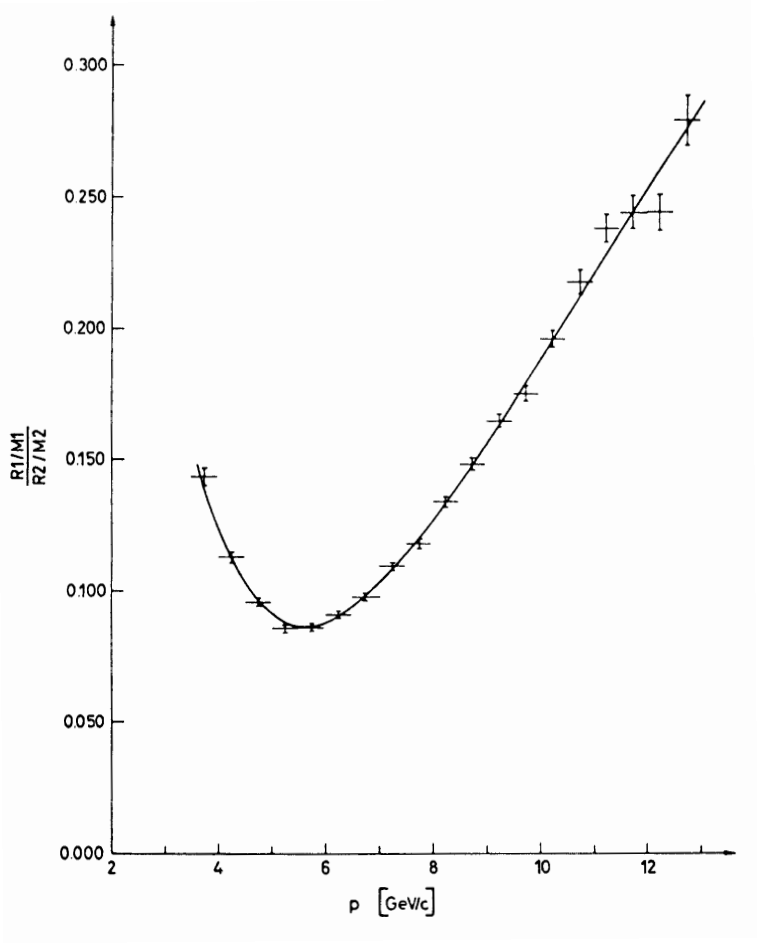

Fig. 5.10. Normalized intensity of $K \to \pi^+\pi^-$ decays behind a two-regenerator setup as a function of the kaon momentum, showing destructive interference between the two coherent K_S waves regenerated in the first and second slabs of copper [39]

the relative detection efficiency of the apparatus for $K_{\pi 2}$ ($\varepsilon_{\pi 2}$) and K_{e3} (ε_{e3}) decays is of crucial importance here; in particular, one needs to know the matrix element for K_{e3} decay, and the influence of this uncertainty will be more pronounced if the apparatus selects a small fraction of the Dalitz plot. Essentially all older measurements were made in this way; here $|\eta_{+-}|$ was obtained from the relation

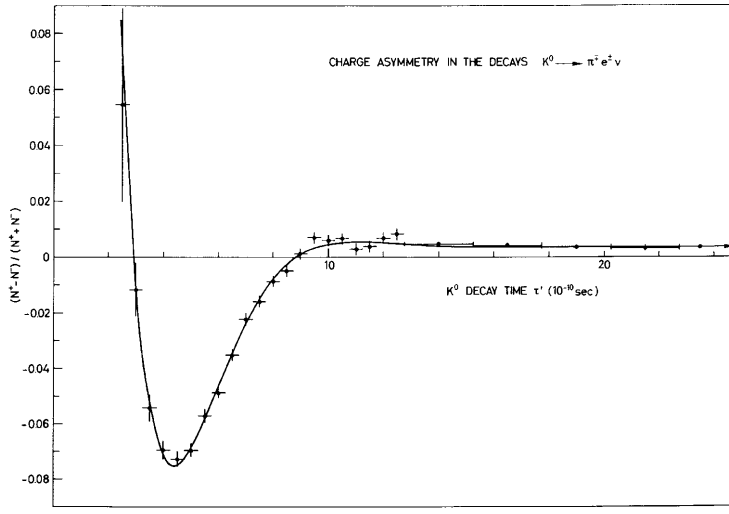

Fig. 5.11. Eigentime dependence of charge asymmetry in K_{e3} decays from initially pure strangeness states, showing interference of K_S and K_L decay amplitudes [40]

$$|\eta_{+-}|^2 = \frac{N(K_L \to \pi^+\pi^-)\,\varepsilon_{e3}}{N(K_L \to \pi e\nu)\,\varepsilon_{\pi 2}} \frac{\Gamma(K_L \to \pi e\nu)}{\Gamma(K_L \to \text{all})} \frac{\Gamma(K_L \to \text{all})}{\Gamma(K_S \to \text{all})} \frac{\Gamma_S}{\Gamma(K_S \to \pi^+\pi^-)} \,. \tag{5.90}$$

The second method can only be used in a short-lived K^0 beam. Strangeness eigenstates K^0 (and $\overline{K^0}$) are produced by an external proton beam hitting a nuclear target. The K_S and K_L components of the K^0 state propagate with time differently, but both decay into π^+ and π^-. Their two decay amplitudes interfere in the way described in Sect. 5.4.1. At decay times comparable to the K_S lifetime τ_S, the resulting intensity of $K \to \pi^+\pi^-$ decays is mainly due to $K_S \to \pi^+\pi^-$ decay, and at late times ($\tau > 15\tau_S$) it is due to $K_L \to \pi^+\pi^-$ decay. The observation of the time distribution will give therefore $|\eta_{+-}|^2$ as the ratio of the $\pi^+\pi^-$ rate at long times to the rate extrapolated back to $\tau = 0$. Here also, a Monte Carlo calculation is needed to allow comparison of the detection efficiencies for the same two-body decay $K \to 2\pi$ at different points of the decay volume.

Four experiments have been reported between 1967 and 1974:

1. The experiment on vacuum interference by the CERN–Heidelberg group [28] has given $|\eta_{+-}| = (2.30 \pm 0.035) \times 10^{-3}$ with $\Gamma_S = (1.119 \pm 0.006) \times 10^{10}\ s^{-1}$ from the fit.

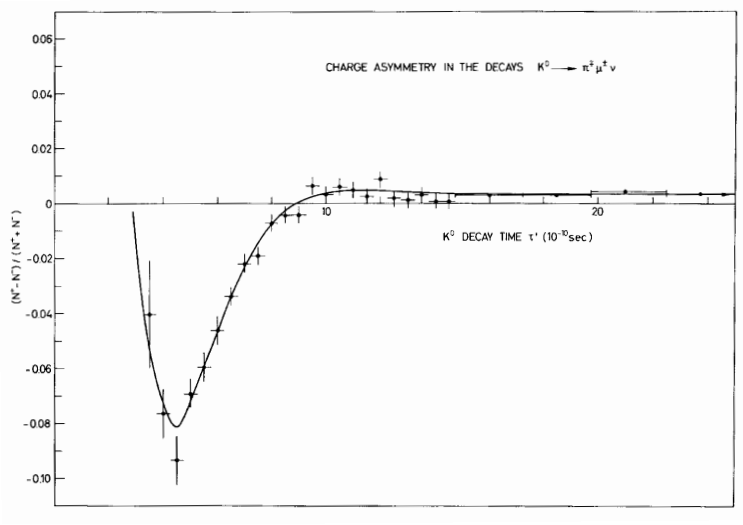

Fig. 5.12. Eigentime dependence of charge asymmetry in $K_{\mu 3}$ decays from initially pure strangeness states, showing interference of K_S and K_L decay amplitudes [40]

2. The same group reports [28] an independent measurement using K_{e3} decays for normalization, with the result $|\eta_{+-}| = (2.30 \pm 0.06) \times 10^{-3}$ using $\Gamma_S = 1.119 \times 10^{10}\ s^{-1}$.
3. The Colorado–SLAC–Santa Cruz group [46] reported on a measurement in a K_L beam by normalizing in two ways:
   - comparing the $K_L \to \pi^+\pi^-$ rate with the $K_L \to \pi e \nu$ rate, and
   - comparing it with $K_L \to \pi^+\pi^-\pi^0$ events.

   The results of both normalizations agree well and give together $|\eta_{+-}| = (2.23 \pm 0.05) \times 10^{-3}$ for $\tau_S = 0.862 \times 10^{10}$ s. Using $\Gamma_S = 1.120 \times 10^{10}\ s^{-1}$, the result is $|\eta_{+-}| = (2.27 \pm 0.05) \times 10^{-3}$.
4. A Dubna group [47] finds $|\eta_{+-}| = (2.05 \pm 0.11) \times 10^{-3}$, using K_{e3} for normalization.

The older experiments, before 1967,were designed in general to have a small detection efficiency for K_{e3} decays in order to obtain a small background-K_{e3}-to-signal ($K_{\pi 2}$) ratio. There is a discrepancy between the pre-1967 and the post-1973 experiments that cannot be negated. It is therefore not possible to take an average of the old and new data; one must choose between them. The facts that the vacuum interference experiment depends less critically on Monte Carlo calculations and that the SLAC experiment has two independent normalizations that give consistent results favor the newer group of results. The agreement between the CERN–Heidelberg vacuum interference experiment and the SLAC result using, along with other normalizations, the conventional normalization by K_{e3} also removes the possibility

that there might be a deep physical reason for obtaining different results from the two methods. The average from the group of four experiments, corrected for the average value of the K_S lifetime ($\tau_S = 0.89594 \times 10^{-10}$ s),is

$$|\eta_{+-}| = (2.279 \pm 0.025) \times 10^{-3} \,. \tag{5.91}$$

Recently, CPLEAR [48] also reported a value of $|\eta_{+-}|$ from its data obtained with strangeness-tagged kaons. The result is $(2.287 \pm 0.035) \times 10^{-3}$ for our best value of the K_S lifetime.

Taking all experiments together, we obtain the average value

$$|\eta_{+-}| = (2.281 \pm 0.020) \times 10^{-3} \,. \tag{5.92}$$

5.6.5 Measurements of the Phase Φ_{+-} in Interference Experiments Behind a Regenerator

The relative phase between the two amplitudes of the decays $K_L \to \pi^+\pi^-$ and $K_S \to \pi^+\pi^-$ has been measured by two distinct methods.

The first consists of measuring the interference of the $K_L \to \pi^+\pi^-$ amplitude with the coherently regenerated $K_S \to \pi^+\pi^-$ amplitude behind a slab of material (the regenerator). The experiments require (*a*) the measurement of the $\pi^+\pi^-$ intensity as a function of the K^0 eigentime behind the regenerator, which is given in Sect. 5.4.1, and (*b*) the measurement of the charge asymmetry δ in leptonic K^0 decays as a function of the K eigentime τ behind the regenerator, given in Sect. 5.4.2. Experiment (*a*) gives the interference phase $\Phi_{+-} - \Phi_\varrho$, and experiment (*b*) the phase of the regeneration amplitude Φ_ϱ.

One of the early experiments in this series was the one by the Columbia group at Brookhaven [17, 20]. Using a proportional wire spectrometer to detect $\pi^+\pi^-$ and leptonic decays at the same time, this group obtained the time distribution of $\pi^+\pi^-$ events behind a carbon regenerator shown in Fig. 5.13. The figure shows also the corresponding time distribution of events from the K^0 momentum interval $5 < p < 6$ GeV/c. There is a deep minimum arising from destructive interference at $\tau \sim 6.5 \times 10^{-10}$. The charge asymmetry of K_{e3} and $K_{\mu 3}$ decays as a function of the K^0 eigentime behind the regenerator, which follows (5.75), is shown in Fig. 5.14. The regeneration phase Φ_ϱ extracted from this asymmetry can be used together with the combined phase $\Phi_\varrho - \Phi_{+-}$ obtained from the 2π interference to obtain the value

$$\Phi_{+-} = (45.5 \pm 2.8)^\circ + 120^\circ \frac{\Delta m - 0.5348 \times 10^{10}\ \mathrm{s}^{-1}}{\Delta m} \,. \tag{5.93}$$

The latest and most precise experiment of this type has been done by the kTeV collaboration [45] (see also [41]) in an experiment at Fermilab with an 800 GeV/c proton beam. The detector is described in Sect. 5.5.7; 5×10^9 events were recorded in 1996–97.

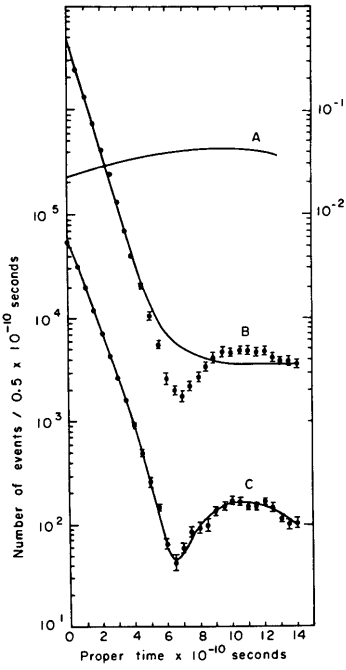

Fig. 5.13. Time distribution of $K \to \pi^+\pi^-$ decays behind a carbon regenerator [17]. (A) Detection efficiency for kaon momentum interval $5 < p_K < 6$ GeV/c. (B) Efficiency-corrected data summed over p_K; the *curve* shows the fit without interference. (C) Data for $5 < p_K < 6$ GeV/c with fit including interference

Using the x and y planes of the four drift chambers, a vertex of the two charged tracks is reconstructed, with a resolution of about 30 cm in the z position along the beam. Background from K_{e3} semileptonic decays was reduced by a factor of 1000 by requiring, for each of the two tracks, the energy E in the CsI calorimeter to be less than 85% of the measured momentum p. The $K_{\mu 3}$ background eas reduced by the muon veto counters. The reconstructed $\pi\pi$ invariant mass was required to be in the range 488 – 508 MeV. Figure 5.15b shows the invariant-mass distribution for events behind the regenerator. The rms resolution of the invariant-mass distribution is 1.6 MeV. Decays originating from a K_L transmitted through the regenerator or from a K_S regenerated coherently in the regenerator were selected by requiring the momentum $\boldsymbol{p}$ of the pion pair to point back to the proton target. For this purpose, the transverse momentum $\boldsymbol{p}_t$ of the pair relative to the line connecting the target and the impact point of the momentum $\boldsymbol{p}$ at the regenerator exit face was calculated. The distribution of p_t^2 is shown in Fig. 5.16b for the regenerator beam. Events with $p_t^2 < 250$ MeV$^2/c^2$ have been selected. There are about 9×10^6 events. Their z decay distribution

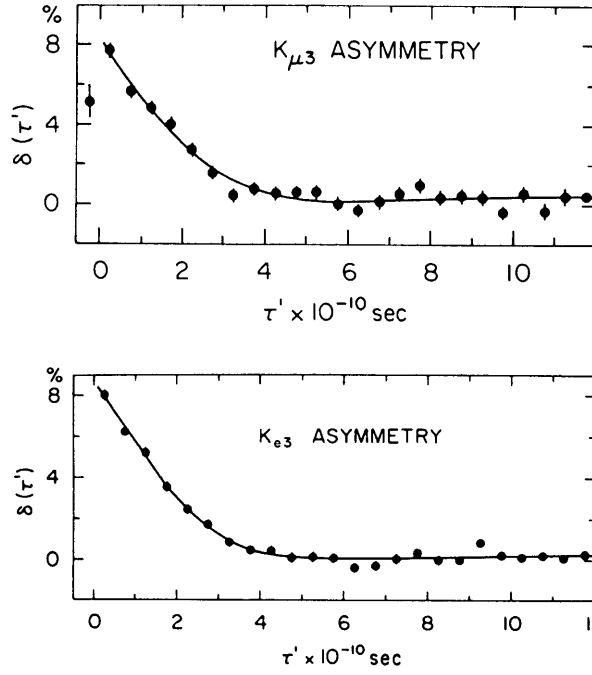

Fig. 5.14. Charge asymmetry of semileptonic decays behind a carbon regenerator for $K_{\mu 3}$ (*upper graph*) and K_{e3} (*lower graph*) displaying interference of the regenerated K_S wave with the transmitted K_L wave [20]

in the restricted kaon momentum interval from 40 to 50 GeV/c is shown in Fig. 5.17. The corresponding decay time distribution was fitted with the formula (5.54). The nuclear regeneration amplitude $F = \mathrm{i}(f(0) - \overline{f}(0))/k$ was assumed to decrease with the kaon momentum $\boldsymbol{p}$ according to a power law $F(p) = F(70\ \mathrm{GeV}/c)(p/70\ \mathrm{GeV}/c)^{\alpha}$. This was motivated by a Regge model, where the difference between the K and $\overline{\mathrm{K}}$ scattering amplitudes would be described by one single ω meson exchange trajectory. In this model, the phase of the regeneration amplitude is given by $\Phi_F = -(\pi/2)(1+\alpha)$. In the fit, Φ_{+-}, Δm, Γ_S and α were free parameters, and Φ_F was assumed to be given by the Regge model. The results are

$$\Phi_{+-} = 44.12^\circ \pm 0.72^\circ\ (\mathrm{stat}) \pm 1.20^\circ\ (\mathrm{syst}) \tag{5.94}$$

$$= 44.12^\circ \pm 1.40^\circ\ , \tag{5.95}$$

$$\Delta m = (5288 \pm 23) \times 10^6 \mathrm{s}^{-1}\ , \tag{5.96}$$

$$\tau_S = (89.58 \pm 0.08\ (\mathrm{stat})) \times 10^{-12}\ \mathrm{s}\ , \tag{5.97}$$

$$\chi^2 = 223.6 \quad \text{for 197 degrees of freedom}\ . \tag{5.98}$$

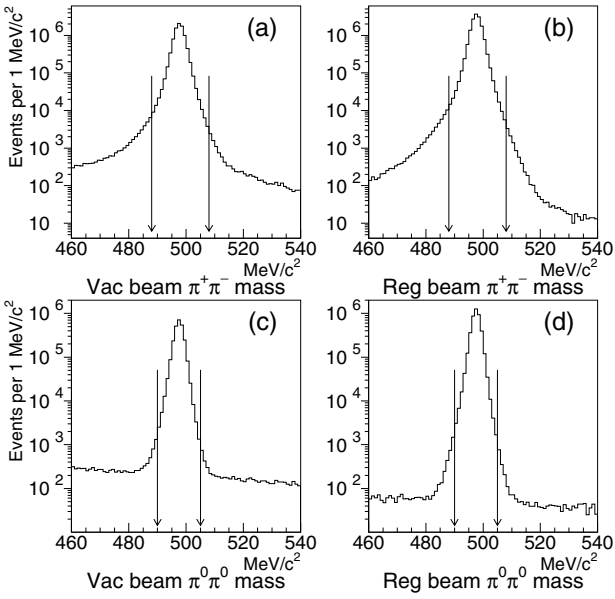

Fig. 5.15. Invariant-mass distributions for (**a**) vacuum beam $\pi^+\pi^-$, (**b**) regenerator beam $\pi^+\pi^-$, (c) vacuum beam $\pi^0\pi^0$, (**d**) regenerator beam $\pi^0\pi^0$. The *vertical arrows* indicate the accepted mass range. All other analysis cuts have benn applied. (kTeV experiment [45])

The systematic error in Φ_{+-} includes a 0.25° uncertainty from the fact that the relation between the regeneration phase and the momentum dependence of the regeneration amplitude through a dispersion relation integral is incomplete. It has been argued [43] that this uncertainty is larger, more than one degree, because of the limited momentum range in which the regeneration amplitude was measured (Sect. 5.3).

5.6.6 Measurements of Φ_{+-} in Vacuum Interference Experiments

The other method for measuring Φ_{+-} is the vacuum interference method mentioned above (Sect. 5.4.1), where one observes the $K \to \pi^+\pi^-$ distribution obtained from an initially pure strangeness state. The information on Φ_{+-} is contained in the interference term proportional to $\cos(\Delta m - \Phi_{+-})$, and the time at which the two interfering amplitudes are equal is $\sim 12\tau_S$, so that the correlation of Φ_{+-} with Δm is rather strong. This method requires high precision in the experiments on the mass difference described in Sect. 5.6.3. An error of $\pm 0.002 \times 10^{10}$ s^{-1} in Δm induces an uncertainty of 1.2° in Φ_{+-}.

Three experiments of this type have been done in the intermediate-energy domain [28, 49, 50]. An analysis of the latest and most precise of those has

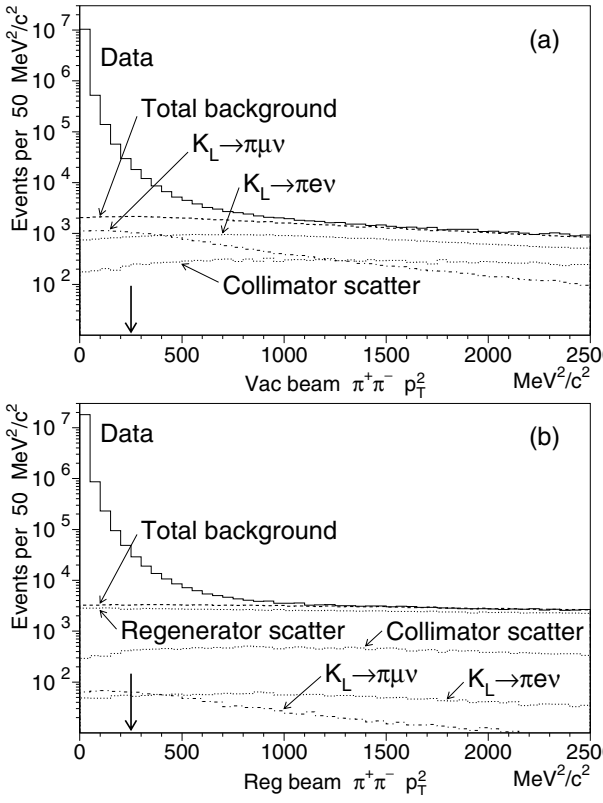

Fig. 5.16. Data on p_t^2 distribution after all other $K \to \pi^+\pi^-$ selection cuts have been applied, for (**a**) the vacuum beam and (**b**) the regenerator beam. The Monte Carlo predictions for the background components are overlaid. Events with $p_t^2 < 250$ MeV$^2/c^2$ (*vertical arrow*) are included in the final $K \to \pi^+\pi^-$ sample. (kTeV experiment, [45])

been performed by the CERN–Heidelberg group [28]. The apparatus, situated in a 75 mrad short neutral beam derived from 24 GeV/c protons, has been described in Sect. 5.5.1. The time distribution of 6×10^6 $K_{S,L} \to \pi^+\pi^-$ decays is shown in Fig. 5.18; *(curve a)*, together with the fitted time distribution, as given in Sect. 5.4.1. The result of this fit is

$$\Phi_{+-} = (49.4^\circ \pm 1.0^\circ) + 305^\circ \frac{(\Delta m - 0.540 \times 10^{10}\ \mathrm{s}^{-1})}{\Delta m}\ , \tag{5.99}$$

$$|\eta_{+-}| = (2.30 \pm 0.035) \times 10^{-3}\ , \tag{5.100}$$

$$\Gamma_S = (1.119 \pm 0.006) \times 10^{-10}\ \mathrm{s}^{-1}\ , \tag{5.101}$$

$$\chi^2 = 421 \quad \text{for 444 degrees of freedom}\ . \tag{5.102}$$

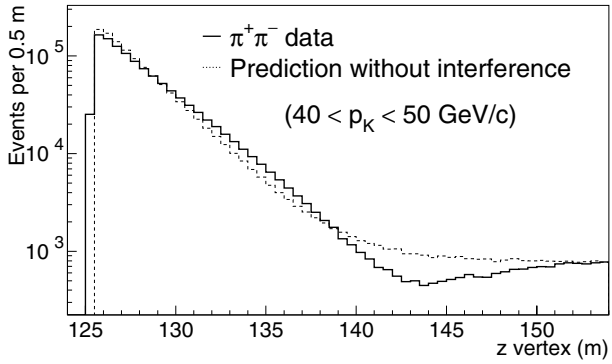

Fig. 5.17. z decay distribution of $K \to \pi^+\pi^-$ decays in the regenerator beam, for the restricted momentum range 40–50 GeV/c. The Monte Carlo prediction (*dashed line*) is without the interference term that is proportional to "$2|\varrho||\eta|$" (kTeV experiment [45])

In the high-energy domain, this method has also been used by the NA31 collaboration. In a 3.6 mrad neutral beam derived from 450 GeV protons, kaons of mean momentum around 100 GeV were allowed to decay. Two different target positions were chosen, at distances of 48 m and 33.6 m from the defining collimator of the neutral beam, which marked the upstream end of the decay volume. Kaons that decayed along 50 m in an evacuated tank were detected further downstream at about 120 m from the final collimator, by the NA31 detector (Sect. 5.5.4, Fig. 5.5). The measured time distribution of $\pi^+\pi^-$ decays is shown in Fig. 5.19, with the extracted interference term in the inset. There are 2.24×10^6 and 0.57×10^6 $\pi^+\pi^-$ events in the data for the target in the near and far positions, respectively; the corresponding numbers of $\pi^0\pi^0$ events are 1.81×10^6 and 0.31×10^6. The phases were extracted from a fit to the time distribution of the ratio of the data in the near and far positions of the target (Fig. 5.20).

The results are

$$\Phi_{+-} = (46.9^\circ \pm 1.4^\circ) + 310^\circ \frac{(\Delta m - 0.5351 \times 10^{10} s^{-1})}{\Delta m} + 270^\circ \frac{(\tau_S - 0.8922 \times 10^{-10}\ \mathrm{s})}{\tau_S} \qquad (5.103)$$

and

$$\Phi_{00} = (47.1^\circ \pm 2.1^\circ) + 310^\circ \frac{(\Delta m - 0.5351 \times 10^{10} s^{-1})}{\Delta m} + 225^\circ \frac{(\tau_S - 0.8922 \times 10^{-10}\ \mathrm{s})}{\tau_S}\,. \qquad (5.104)$$

The difference between the two phases comes out to be

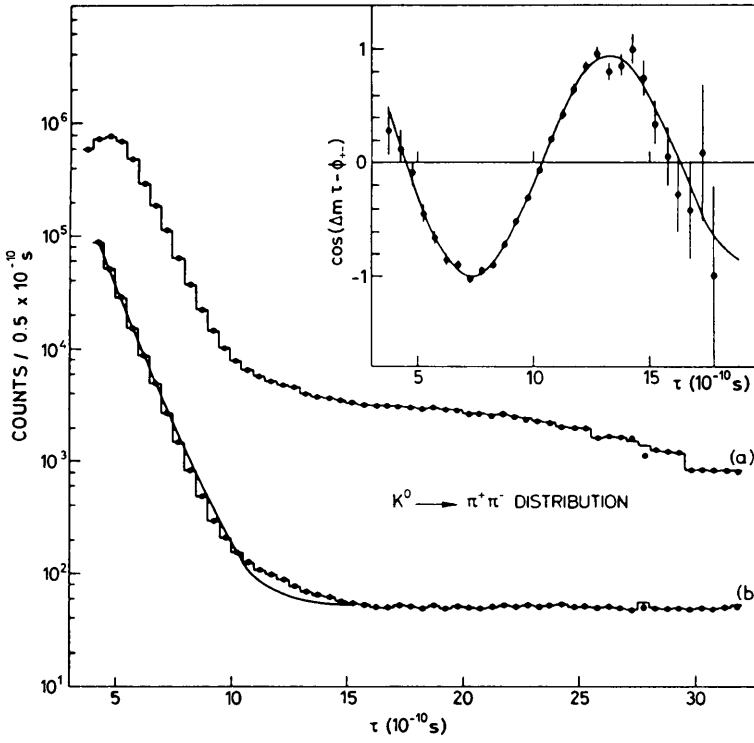

Fig. 5.18. Time distribution of $K \to \pi^+\pi^-$ events from a coherent mixture of K_L and K_S produced in pure strangeness states [28]. *Curve a* events (*histogram*) and fitted distribution (*dots*). *Curve b* events corrected for detection efficiency (*histogram*), and fitted distribution with interference term (*dots*) and without interference term (*curve*). *Inset*: interference term as extracted from data (*dots*) and fitted term (*line*). (CERN–Heidelberg experiment [28])

$$\Phi_{00} - \Phi_{+-} = 0.2^\circ \pm 2.6^\circ \pm 1.2^\circ \; . \tag{5.105}$$

5.6.7 Measurements of the Phase Difference $\Phi_{00} - \Phi_{+-}$

For small $|\varepsilon'/\varepsilon|$, this phase difference is related to ε'/ε by the equation

$$\Phi_{00} - \Phi_{+-} = -3\,\Im m\left(\frac{\varepsilon'}{\varepsilon}\right) \; . \tag{5.106}$$

In this way, the component of ε' orthogonal to the direction of ε can be measured. In the absence of $\mathcal{CPT}$ violation and for small $|\varepsilon'/\varepsilon|$, both of the phases Φ_{00} and Φ_{+-} are close to the superweak phase $\Phi_{\rm sw}$ (5.31).

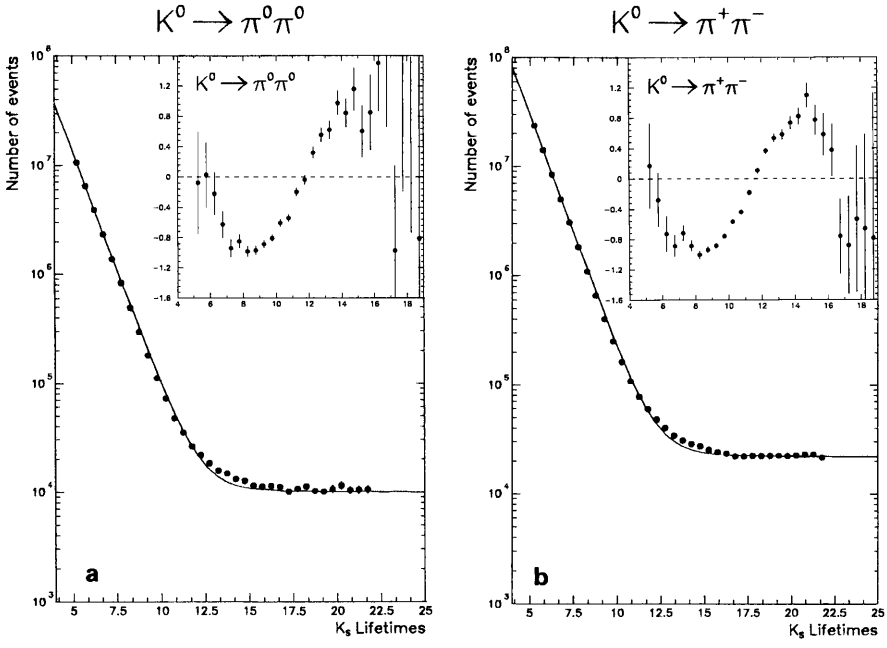

Fig. 5.19. The rates of decay of kaons to charged and neutral pions as a function of the K_S lifetime. The fitted lifetime distributions with the interference term removed are superimposed. The *insets* show the interference terms extracted from the data. (NA31 experiment [51])

The measurement of this phase difference by the NA31 experiment (Sect. 5.6.6) was improved by the simultaneous measurement of the time distributions of $\pi^+\pi^-$ and $\pi^0\pi^0$ decays behind a regenerator in the kTeV experiment [45] (Sect. 5.6.5). Here, the uncertainty arising from the phase of coherent regeneration (which is the determining uncertainty in the Φ_{+-} measurement) cancels in the comparison of the two decay modes. The authors of [45] conclude that

$$\Phi_{00} - \Phi_{+-} = (0.39 \pm 0.50)^\circ \,. \tag{5.107}$$

Together with an earlier measurement by E731/E773 [44] and the NA31 measurement (5.105), this gives

$$\Phi_{00} - \Phi_{+-} = (0.36 \pm 0.43)^\circ \,. \tag{5.108}$$

5.6.8 Measurement of Φ_{+-} from a Tagged Pure Strangeness State

The CPLEAR experiment (Sect. 5.5.8) offers the unique feature of tagging a pure neutral strangeness state K^0 or $\overline{K^0}$ produced in a $\overline{p}p$ annihilation at rest

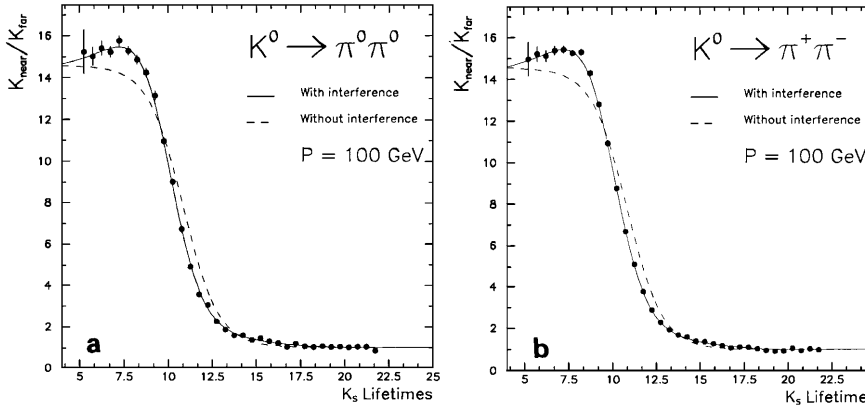

Fig. 5.20. Ratio distributions averaged over momenta and scaled to 100 GeV. The *solid line* is the result of the fit with interference; the *dashed line* is the expectation without interference

by identifying a charged kaon produced in the same reaction. Compared with the vacuum interference experiments (Sect. 5.6.6), this offers the advantage of a full-size interference term, whereas, in the vacuum interference experiments, an incoherent mixture of (predominantly) K^0 and $\overline{K^0}$ forms the initial state, and the interference term is diluted.

The interference term is visualized by measuring the decay-rate asymmetry for decays into $\pi^+\pi^-$,

$$A_{+-}(\tau) = \frac{\overline{N}(\tau) - N(\tau)}{\overline{N}(\tau) + N(\tau)} \tag{5.109}$$

$$= 2\,\Re e\,\varepsilon - 2\,|\eta_{+-}|\mathrm{e}^{-(1/2)\Gamma_S\tau}\cos(\Delta m\,\tau - \Phi_{+-})\,. \tag{5.110}$$

In the corresponding experimental distribution, the background was subtracted and the events were appropriately weighted taking into account the tagging efficiencies for K^0 and $\overline{K^0}$. The result is shown in Fig. 5.21 [48]. The result of a fit to these data gives values for Φ_{+-} and $|\eta_{+-}|$, which are correlated with the values chosen for Δm and τ_S, respectively.

The correlation parameters are

$$\delta\Phi_{+-} = 0.30(\Delta m - 0.5301 \times 10^{10}\ \mathrm{s}^{-1}) \tag{5.111}$$

and

$$\delta|\eta_{+-}| = 0.09(\tau_S - 0.8934 \times 10^{-10}\ \mathrm{s})\,. \tag{5.112}$$

For the values of Δm and τ_S chosen by the authors of [48], the results are

$$\Phi_{+-} = 43.19^\circ \pm 0.53^\circ\ (\mathrm{stat}) \pm 0.28^\circ\ (\mathrm{syst}) \pm 0.42^\circ\ (\Delta m)\,, \tag{5.113}$$

$$|\eta_{+-}| = [2.264 \pm 0.023\ (\mathrm{stat}) \pm 0.026\ (\mathrm{syst})] \times 10^{-3}\,. \tag{5.114}$$

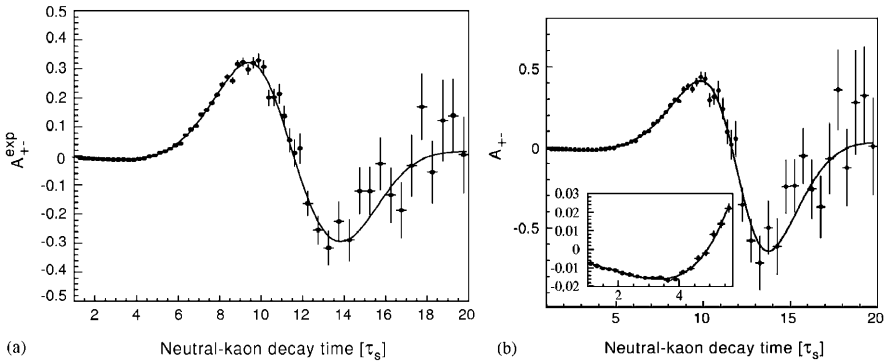

Fig. 5.21. (**a**) The measured decay-rate asymmetry, $A_{+-}^{exp}(\tau)$; the data points include residual background. (**b**) The decay-rate asymmetry, $A_{+-}(\tau)$; the data points are background subtracted. In both cases the continuous curve is the result of the fit (CPLEAR experiment, [52])

A similar asymmetry is obtained for decays to $\pi^0\pi^0$, although with less statistical weight. Figure 5.22 shows the decay time distribution (Fig. 5.22a) and the $\mathcal{CP}$ asymmetry as measured (Fig. 5.22b). From the corresponding fit, the following values of the $\mathcal{CP}$ parameters in the neutral mode have been extracted:

$$\Phi_{00} = 42.0^\circ \pm 5.6^\circ \text{ (stat)} \pm 1.9^\circ \text{ (syst)} \,, \tag{5.115}$$

$$|\eta_{00}| = [2.47 \pm 0.31 \text{ (stat)} \pm 0.24 \text{ (syst)}] \times 10^{-3} \,. \tag{5.116}$$

5.6.9 Charge Asymmetry in Semileptonic Decays

This asymmetry $\delta_{\rm L}$ is the third manifestation of $\mathcal{CP}$ violation (5.37). This asymmetry measures the $\mathcal{CP}$ impurity of the long-lived kaon state; $\delta_{\rm L} = 2\Re e\, \varepsilon(1-|x|^2)/(|1-x|^2)$, where x is the $\Delta\mathbb{S} = \Delta Q$ violation parameter. Considerable precision was achieved in the first ten years of experimentation after 1964: for the K_{e3} mode, two experiments, by the Princeton group [53] and by the CERN–Heidelberg group [54], have been reported; for the $K_{\mu 3}$ mode, results have been obtained from Stanford [56] and one from the CERN–Heidelberg group [54], and a Brookhaven–Yale group [57] obtained a result for a mixture of both decay modes. Recently, two new results on this asymmetry have been reported by the kTeV and NA48 collaborations. Tha most siugnificant features of these results are:

1. Event numbers of up to 298 million events in the K_{e3} mode and 15 million events in the $K_{\mu 3}$ mode.

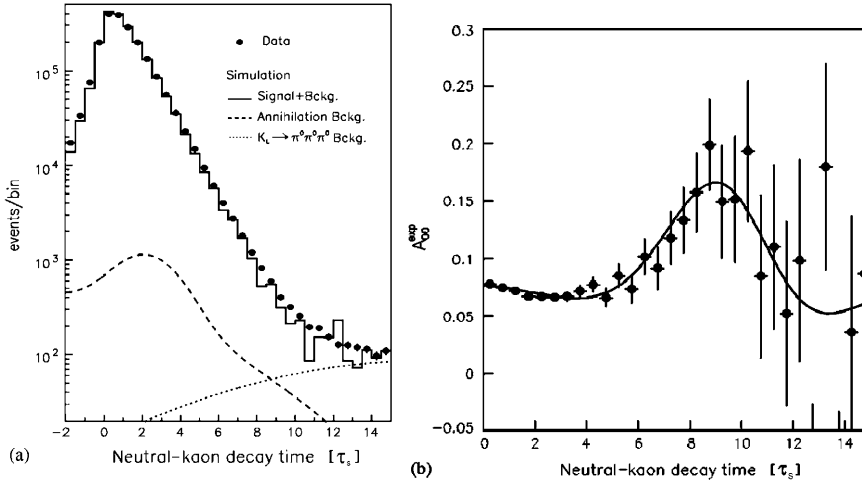

Fig. 5.22. (**a**) The measured decay time distribution for $\overline{\mathrm{K}^0}(\mathrm{K}^0) \to \pi^0\pi^0$, overlaid with the result of the simulation of this decay (*solid line*) and the various background channels. The background is shown separately for the contributions from $\overline{\mathrm{p}}\mathrm{p}$ annihilations (*dashed line*) and $\mathrm{K_L} \to \pi^0\pi^0\pi^0$ decays (*dotted line*). (**b**) The measured asymmetry $A_{00}^{\mathrm{exp}}(\tau)$. The *solid line* shows the result of the fit. (CPLEAR experiment [52])

2. An apparatus design such that the decay products (π and electron) traverse only minute amounts of matter (about 0.3 – 0.4 g cm^{-2}), thus diminishing corrections due to secondary interactions of these particles.
3. The precision of the $\mathrm{K}_{\mu 3}$ asymmetry measurements is a factor of 4 below the value for $\mathrm{K}_{\mathrm{e}3}$, making a comparison between the two possible. Table 5.1 gives the results; the average $\delta_{\mathrm{L}} = (3.316 \pm 0.053) \times 10^{-3}$.

The charge asymmetries for $\mathrm{K}_{\mathrm{e}3}$ and $\mathrm{K}_{\mu 3}$ decays are equal to within 8%: $\delta_{\mathrm{L}}^{e}/\delta_{\mathrm{L}}^{\mu} = 1.04 \pm 0.08$. Assuming the validity of the $\Delta Q = \Delta\mathbb{S}$ rule, which is supported by the present experiments, we obtain $\Re e\,\varepsilon = (1.658 \pm 0.026) \times 10^{-3}$. If we use the most precise tests of the $\Delta Q = \Delta\mathbb{S}$ rule by the CPLEAR experiment [52], there is a small correction

$$\frac{1-|x|^2}{|1-x|^2} = 0.996 \pm 0.012\,. \tag{5.117}$$

5.6.10 Parameters of $\mathcal{CP}$ Violation in the K^0 System: $\Im m(\varepsilon'/\varepsilon)$

$\mathrm{K_S}$ lifetime. We take the average of the older measurements from the Particle Data Group 2002 [23], $\tau_{\mathrm{S}} = (0.8941 \pm 0.0009) \times 10^{-10}$ s, and combine this with the two new measurements by the kTeV collaboration,

Table 5.1. Charge asymmetry measurements in K_{l3} decays. The $K_{\mu 3}$ and K_{e3} average value is $\delta_L = (3.316 \pm 0.053) \times 10^{-3}$ ([a] See also [26], [b] See also [27])

Group and reference	Year	Decay mode	Result ($\times 10^3$)	δ ($\times 10^3$)
Columbia [59]	1969	K_{e3}	2.46 ± 0.59	
Columbia–Harvard CERN [60]	1970	K_{e3}	3.46 ± 0.33	K_{e3} average
San Diego–Berkeley [61]	1972	K_{e3}	3.6 ± 1.8	3.322 ± 0.055
Princeton [53]	1973	K_{e3}	3.18 ± 0.38	
CERN–Heidelberg [54]	1974	K_{e3}	3.41 ± 0.18	
kTeV [55]	2002	K_{e3}	$3.322 \pm 0.058 \pm 0.047$	
NA48 [7]	2003	K_{e3}	$3.317 \pm 0.070 \pm 0.072$	
Brookhaven–Yale [57]	1973	$K_{e3} + K_{\mu 3}$	3.33 ± 0.50	
SLAC–Berkeley [62]	1969	$K_{\mu 3}$	5.8 ± 1.7	
Berkeley [63]	1972	$K_{\mu 3}$	6.0 ± 1.4	$K_{\mu 3}$ average
Stanford [56]	1972	$K_{\mu 3}$	2.78 ± 0.51	3.19 ± 0.24
CERN–Heidelberg [54]	1974	$K_{\mu 3}$	3.13 ± 0.29	

$(0.8965 \pm 0.0007) \times 10^{-10}$ s [45], and by the NA48 collaboration, $(0.89598 \pm 0.0007) \times 10^{-10}$ s [64]. Our grand average is

$$\tau_S = (0.8959 \pm 0.0004) \times 10^{-10} \text{ s} . \tag{5.118}$$

We use this value in the following sections.

Mass difference Δm. Combining the values from the CERN–Heidelberg experiments [38, 39, 40] with those from Fermilab E731 and E773 [41, 44], from CPLEAR [48, 65, 66] and from the most precise single measurement by kTeV [45], we obtain

$$\Delta m = (0.5286 \pm 0.0011) \times 10^{10} \text{ s}^{-1} . \tag{5.119}$$

Superweak phase. From the two parameters given above, we obtain the phase of ε in the superweak model,

$$\Phi_{sw} = \arctan\left(\frac{2\,\Delta m}{\Gamma_S}\right) = (43.4 \pm 0.1)^\circ . \tag{5.120}$$

Moduli of the Amplitudes η_{+-} and η_{00}. From Sect. 5.6.4, we conclude

$$|\eta_{+-}| = (2.281 \pm 0.020) \times 10^{-3} . \tag{5.121}$$

Absolute measurements of the amplitude η_{00} are much less precise. A recent average including the CPLEAR result is

$$|\eta_{00}| = (2.23 \pm 0.11) \times 10^{-3} . \tag{5.122}$$

Phase Φ_{+-}. In all measurements, this phase is extracted from an interference term with a beat frequency Δm. The correlation with the value of Δm varies

from experiment to experiment. Even after the first round of experiments, ten years after the discovery of $\mathcal{CP}$ violation, it became clear that there was no evidence for direct $\mathcal{CP}$ violation from a comparison of the measured phase Φ_{+-} with the superweak phase $\Phi_{\rm SW}$. From the two most precise experiments at that time, the phase, evaluated for the mass difference $\Delta m = (0.5286 \pm 0.0011) \times 10^{10}\ {\rm s}^{-1}$ and the K_S lifetime given above, we have $\Phi_{+-} = (43.0 \pm 1.2)^\circ$ from the CERN–Heidelberg group [28] and $\Phi_{+-} = (44.1 \pm 2.8)^\circ$ from Carithers et al. [17]. Together these results yield $(43.2 \pm 1.1)^\circ$, in very good agreement with $\Phi_{\rm SW} = (43.4 \pm 0.1)^\circ$. From the difference of these two phases, $\Delta\Phi = (0.2 \pm 1.1)^\circ$, one can deduce a value for the component of the direct $\mathcal{CP}$ violation ε' transverse to ε, such that

$$\Im m\left(\frac{\varepsilon'}{\varepsilon}\right) = \tan\Delta\Phi = -(3 \pm 19) \times 10^{-3}\ . \tag{5.123}$$

This negative result, although supporting $\mathcal{CPT}$ invariance, showed at that time, in 1975, how difficult it would be to find direct $\mathcal{CP}$ violation in the imaginary part of ε'/ε. Experimental activity then shifted to other fields of particle physics, the discovery of neutral currents in 1973 put the focus of interest on neutrino physics, and the discovery of charmed quarks opened the way to explain $\mathcal{CP}$ violation as a consequence of weak quark mixing in a six-quark scheme.

Only in 1983 did a new group of experimenters see the chance of measuring the real part of ε'/ε, because at the higher energies of the Super Proton Synchrotron (SPS) at CERN (450 GeV protons) and the Tevatron at Fermilab (800 GeV protons), the detection of photons in the energy range of 20–100 GeV became much easier and a measurement of the decay $K_L \to \pi^0\pi^0$ with high precision became feasible. In the course of these new experiments the measurement of the phase Φ_{+-} was resumed, and results came from NA31 [51], E731 [41], E773 [44] and kTeV [45]. Taking these results together with the pre-1975 data and the result from CPLEAR [48], we obtain the world average

$$\Phi_{+-} = (43.3 \pm 0.4)^\circ \tag{5.124}$$

using the values for Δm and τ_S above. This result is in excellent agreement with the value of $\Phi_{sw} = (43.4 \pm 0.1)^\circ$. Since the interference experiments were evaluated without assuming $\mathcal{CPT}$ invariance, this constitutes a stringent test of $\mathcal{CPT}$ invariance. The difference is $\Phi_{+-} - \Phi_{\rm SW} = -(0.1 \pm 0.4)^\circ$. At the same time, this result can again be used to constrain the component of ε' orthogonal to ε:

$$\Im m\left(\frac{\varepsilon'}{\varepsilon}\right) = -(1.7 \pm 7.0) \times 10^{-3}\ . \tag{5.125}$$

Therefore, at this level of 10^{-2} relative to the amplitude for $\mathcal{CP}$ violation by mixing, ε, there is no evidence for a direct $\mathcal{CP}$ violation amplitude ε' orthogonal to ε. Our interest now shifts to the component of ε' parallel to ε, i.e. to $\Re e(\varepsilon'/\varepsilon)$.

5.7 Elucidation of $\mathcal{CP}$ Violation in K^0 Decays (II): Discovery of Direct $\mathcal{CP}$ Violation in $\Re e(\varepsilon'/\varepsilon)$

5.7.1 Significance of the Double Ratio R

A measurement of decay rates with the required precision of 10^{-3} is only possible by measuring the ratio of rates in the same beam in the same time interval. The real part of ε'/ε is connected with the amplitude ratios of $\mathcal{CP}$-violating K_L decays to $\mathcal{CP}$-conserving K_S decays η_{00} and η_{+-}. From the Wu–Yang triangle relations (5.20) $\eta_{00} = \varepsilon - 2\varepsilon'$ and $\eta_{+-} = \varepsilon + \varepsilon'$, we obtain

$$\Re e\left(\frac{\varepsilon'}{\varepsilon}\right) = \frac{1}{6}\left(1 - \left|\frac{\eta_{00}}{\eta_{+-}}\right|^2\right) . \tag{5.126}$$

A measurement of the double ratio

$$R = \frac{|\eta_{00}|^2}{|\eta_{+-}|^2} = \frac{\Gamma(K_L \to 2\pi^0)/\Gamma(K_L \to \pi^+\pi^-)}{\Gamma(K_S \to 2\pi^0)/\Gamma(K_S \to \pi^+\pi^-)} \tag{5.127}$$

to a precision of about 0.3% is therefore required to distinguish between the two remaining models, the KM milliweak model and the superweak model. Since the KM model predicts values of $\Re e(\varepsilon'/\varepsilon)$ in the range between 0.2×10^{-3} and 3×10^{-3}, the precision required for detecting a signal of direct $\mathcal{CP}$ violation depends on the actual value. If the largest prediction is realized in nature, a precision of $\delta R = 5 \times 10^{-3}$ would be sufficient for a threee-standard-deviation observation. If, however, the lowest value is realized, a precision of $\delta R = 0.4 \times 10^{-3}$ would be needed, corresponding to samples of several million events for each of the four decay modes.

5.7.2 The NA31 Experiment: First Evidence for Direct $\mathcal{CP}$ Violation

The first observation of direct $\mathcal{CP}$ violation was made by a collaboration of physicists at CERN in 1988 [58]. The experiment, called "North Area No. 31", or NA31, was based on the concurrent detection of $2\pi^0$ and $\pi^+\pi^-$ decays. Collinear beams of K_L and K_S were employed alternately. The beam layout and the apparatus were described in Sect. 5.5.4. Data were taken at a rate of 1000 events/machine burst in 1986 and 1987. The $K^0 \to 2\pi^0 \to 4\gamma$ decays were reconstructed from the measured positions and energies of the photons. From these positions and energies, the distance z of the kaon decay vertex from the calorimeter was calculated, as described in Sect. 5.5.2. Using the vertex position, the invariant masses of two-photon pairs were obtained. Of the three possible combinations, the one fitting the $2\pi^0$ hypothesis best was chosen. The $\gamma\gamma$ invariant masses were used to reduce the background, which was primarily due to $K_L \to 3\pi^0 \to 6\gamma$ decays with two photons escaping

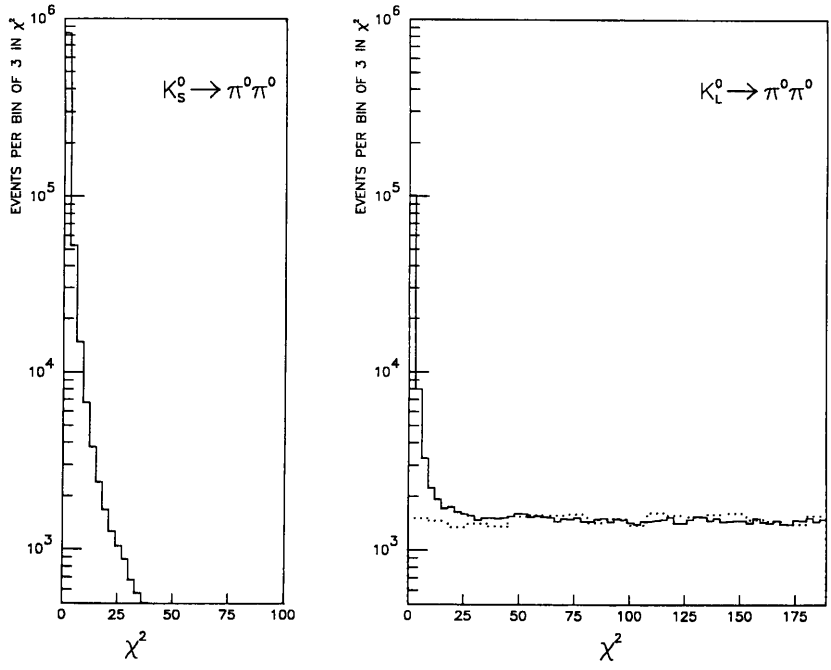

Fig. 5.23. Number of accepted 4γ events as a function of χ^2, for the $K_S \to \pi^0\pi^0$ and $K_L \to \pi^0\pi^0$ data, and a Monte Carlo calculation of the background originating from $K_L \to 3\pi^0$ decays (*dotted*). The signal region was taken as $\chi^2 < 9$. (NA31 experiment [58])

detection. This background is uniformly distributed in a two-dimensional scatter plot of photon-pair masses, while the $2\pi^0$ signal peaks at a point S where both photon pairs have the π^0 mass, with a 2 MeV resolution. Signal and background events were counted in equal-area χ^2 contours around S. Figure 5.23 shows the χ^2 distribution of events in the K_S beam and in the K_L beam. The signal region was taken as $\chi^2 < 9$. Background in the K_L data was subtracted by linear extrapolation into the signal region, and amounts to about 4%, while it is negligible in the K_S data.

The $K^0 \to \pi^+\pi^-$ decays were reconstructed from the four space points of the two pion tracks in two wire chambers with four layers each. From these tracks, the position of the decay vertex along the beam was reconstructed with a precision of better than 1 m. The energies E_1, E_2 of the two pions were obtained from the energies deposited in the liquid-argon electromagnetic calorimeter and the iron–scintillator hadronic calorimeter. The K^0 energy was then calculated, using the kaon mass and the opening angle θ of the two tracks as constraints, from the ratio E_1/E_2:

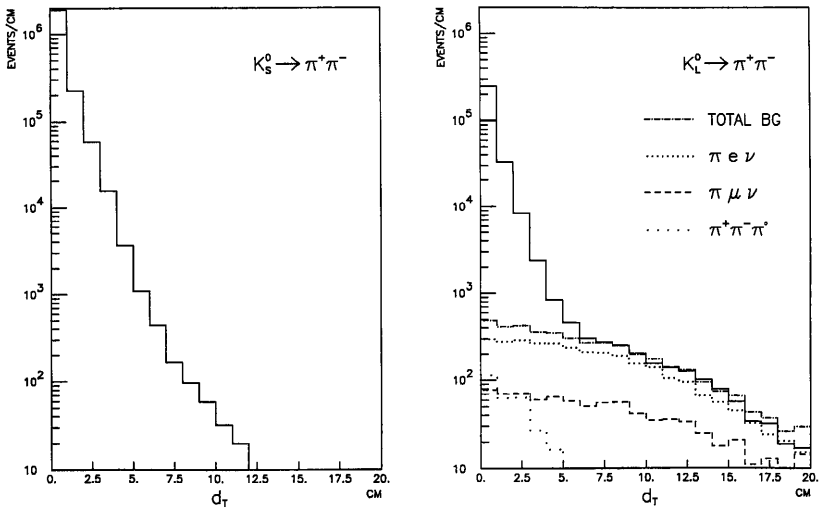

Fig. 5.24. Event distribution for charged decays as a function of the distance d_T between the decay plane and the production target, for K_S and K_L decays and for various background components. (NA31 experiment [58])

$$E_K = \sqrt{\frac{A}{\theta^2}\left(m_K^2 - Am_\pi^2\right)}\,, \tag{5.128}$$

where

$$A = \frac{E_1}{E_2} + \frac{E_2}{E_1} + 2\,. \tag{5.129}$$

Background from $\Lambda \to p\pi^-$ decays was suppressed by requiring $0.4 < E_1/E_2 < 2.5$, and background from $K^0 \to \pi e\nu$ (K_{e3}) decay was reduced by comparing, for each track, the energy deposited in the front half of the electromagnetic calorimeter with the energy deposited in the hadron calorimeter.

After cuts on the invariant $\pi^+\pi^-$ mass and on the transverse location of the center of energy relative to the center of the neutral beam, a residual background of three-body decays needed to be subtracted.

Figure 5.24 shows the transverse distance d_T between the decay plane, as reconstructed from the two tracks, and the K^0 production target, at the longitudinal position of the target. For K_S decays, this distributions peaks at $d_T = 0$ with a resolution given by the measurement error and multiple scattering. For K_L decays, in addition to this component of two-body decays from the target, there is a broader distribution mixed in, due to three-body decays. The signal region was taken to be $d_T < 5$ cm, and the three-body background was extrapolated from a control region $7 < d_T < 12$ cm. This background amounts to $(6.5 \pm 2.0) \times 10^{-3}$ of the signal, including systematic uncertainties.

The remaining event sample contained 109×10^3 of $K_L \to \pi^0\pi^0$, 295×10^3 of $K_L \to \pi^+\pi^-$, 932×10^3 of $K_S \to \pi^0\pi^0$ and 2300×10^3 of $K_S \to \pi^+\pi^-$. In order to equalize the acceptance for K_S decays (with an average decay length of 6 m) to that for the uniformly distributed K_L decays, the K_S data were taken with the K_S target displaced in 1.2 m steps over 48 m such that the distribution of K_S decays became effectively uniform in the fiducial region. This makes the double ratio essentially insensitive to acceptance corrections. The double ratio was evaluated in 10×32 bins in energy and vertex position. The weighted average, after all corrections, is

$$R = 0.980 \pm 0.004\ (\text{stat}) \pm 0.005\ (\text{syst})\ . \tag{5.130}$$

The corresponding result for the direct-$\mathcal{CP}$-violation parameter is [58]

$$\Re e\left(\frac{\varepsilon'}{\varepsilon}\right) = (33.0 \pm 11.0) \times 10^{-4}\ . \tag{5.131}$$

This, with three-standard-deviation significance, shows that the $\mathcal{CP}$-odd K_2 decays to two pions, and was the first evidence of direct $\mathcal{CP}$ violation.

In further measurements with the NA31 detector, the event numbers recorded were considerably increased, by a factor of four, thus decreasing the statistical error. In addition, the background from K_{e3} decays was reduced by introducing a two-stage transition radiation detector as an additional identifier for electrons. With these improved data, the double ratio was measured with reduced uncertainty. Including the former result, the double ratio obtained is

$$R = 0.982 \pm 0.0039\ , \tag{5.132}$$

leading to a value

$$\Re e\left(\frac{\varepsilon'}{\varepsilon}\right) = (23.0 \pm 6.5) \times 10^{-4}\ , \tag{5.133}$$

or 3.5 standard deviations from zero.

5.7.3 The Experiment E731 at Fermilab

The principle of this experiment [42] differs from that of NA31 in two ways: while in NA31 charged and neutral decays were recorded concurrently, in E731 they were registered in separate runs with a slightly different detector. On the other hand, in E731 K_L and K_S decays were collected simultaneously using a split beam: in one half of the beam cross section, K_L mesons from the target were allowed to decay over a long decay region of 27 m (charged decays) or 42 m (neutral decays), while in the other half, the K_L beam hit a block of B_4C, whereby a beam of K_S mesons was regenerated.

The vertex distribution of the events from regenerated K_S was concentrated in a small region behind the regenerator, positioned at 123 m from the

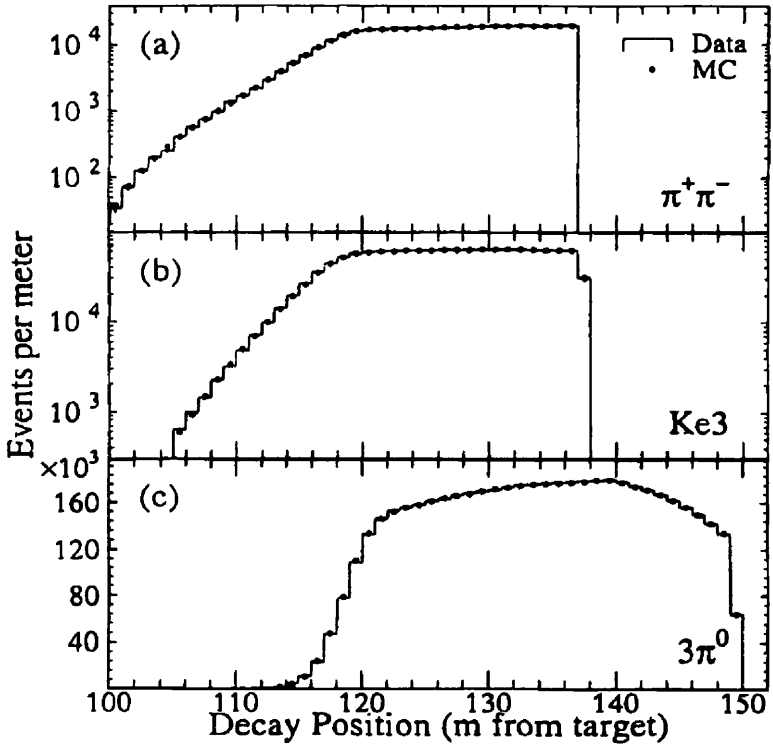

Fig. 5.25. Reconstructed K_L event vertex distributions for (**a**) $\pi^+\pi^-$ (full sample), (**b**) K_{e3} and (**c**) $3\pi^0$. The $\pi^+\pi^-$ Monte Carlo (MC) distribution is 25 times the data. The $3\pi^0$ and K_{e3} distributions have MC samples roughly equal to the data subsets, of a few million events. The acceptance falloff for upstream decays is due to a precision photon veto counter at 122 m. The overlays all have acceptable χ^2. (E731 experiment [42])

target, owing to the typical K_S decay length of 5 m. On the other hand, the vertex distribution of $K_L \to \pi^0\pi^0$ decays extended from 110 to 152 m from the target (see Fig. 5.25). The detector acceptances for K_L and K_S decays therefore were very different, and since the decay volumes for $K_L \to \pi^+\pi^-$ and $K_L \to \pi^0\pi^0$ were different, this acceptance correction does not cancel in the double ratio.

The $\pi^+\pi^-$ decays were selected by requiring the invariant $\pi\pi$ mass to be near the kaon mass and the transverse kaon momentum to satisfy $p_t^2 < 250\ \mathrm{MeV}^2/c^2$. The background from incoherent kaon regeneration amounted to $(0.155 \pm 0.014)\%$. In the $2\pi^0$ sample, the Monte Carlo simulation of the $3\pi^0$ background agrees with the shape of the distribution outside the K^0 mass peak (Fig. 5.26). The extrapolated $3\pi^0$ background under the peak

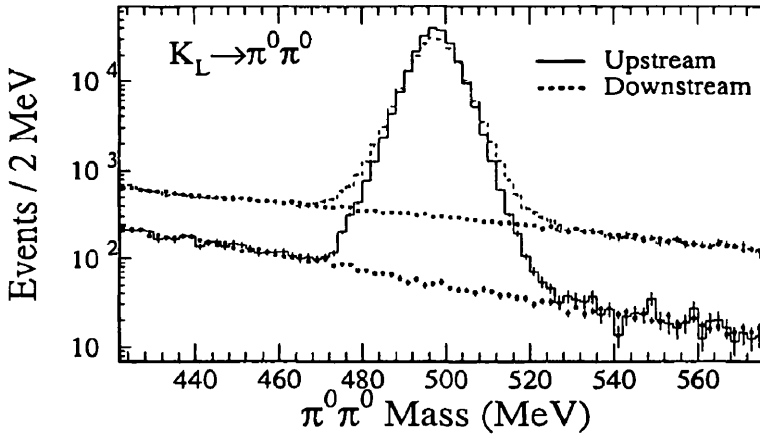

Fig. 5.26. Distribution as a function of $\pi^0\pi^0$ mass for $K_L \to 2\pi^0$ events upstream and downstream of the trigger plane. The *histogram* is the data; the *dots* are the $3\pi^0$ background MC simulation together with a small contribution from beam interactions. (E731 experiment [42])

is 1.78% and 0.049% in the vacuum and regenerator beams, respectively. Neutral background from incoherent scattering in the regenerator was subtracted by evaluating the distribution of the transverse center of energy of each event around the center of each beam. The shape of the distribution as a function of ring number was predicted from the measured $\pi^+\pi^-$ events. Figure 5.27 shows the distribution as a funbction of ring number for $2\pi^0$ events after subtraction of the $3\pi^0$ background. The arrow at ring number 120 indicates the cut, and the large dots show the extrapolation of the incoherent background under the signal peak. After this background subtraction, the event numbers in the vacuum beams were 327×10^3 $(\pi^+\pi^-)$ and 410×10^3 $(\pi^0\pi^0)$. In the regenerator beams, there were 1.06×10^6 $\pi^+\pi^-$ events and 0.800×10^6 $2\pi^0$ events. The regeneration amplitude was assumed to fall in accordance with a power of the kaon momentum, p^α. In the fit, the parameter α, the regeneration amplitude at 70 GeV/c momentum and $\Re e(\varepsilon'/\varepsilon)$ were varied. The results were

$$\alpha = -0.6025 \pm 0.0065 \tag{5.134}$$

and

$$\Re e\left(\frac{\varepsilon'}{\varepsilon}\right) = (7.4 \pm 5.2\ (\text{stat}) \pm 2.9\ (\text{syst})) \times 10^{-4}\,, \tag{5.135}$$

where the systematic uncertainty includes a part from acceptance calculations (1.19×10^{-4}) and from the energy calibration (1.6×10^{-4}). The authors of [42] deduce an upper limit $\Re e(\varepsilon'/\varepsilon) < 17 \times 10^{-4}$ (95% C.L.), which is at variance with the observation of the NA31 experiment.

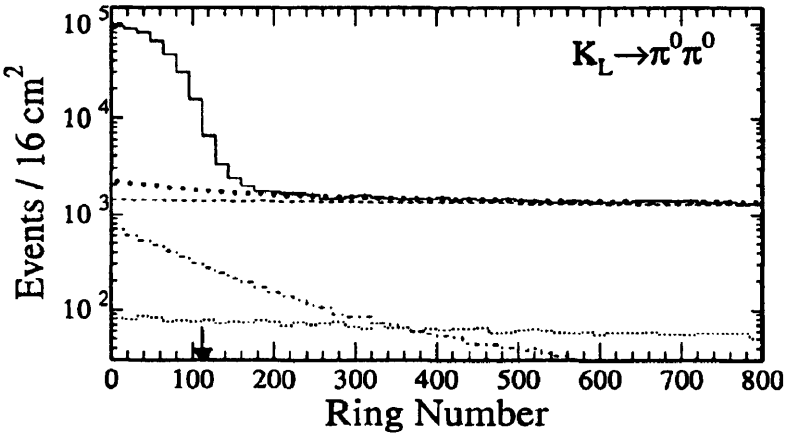

Fig. 5.27. Distribution as a function of the ring number for $3\pi^0$ background-subtracted $K_L \to 2\pi^0$ events. The *histogram* is the data; the *large dots* are the MC simulation for incoherent processes. Contributions from regenerator incoherent scattering (*dashed line*), diffractive scattering (*dash–dotted line*) and inelastic scattering (*small dots*) at the trigger plane are shown separately. The *arrow* shows the position of the cut. (E731 experiment [42])

5.7.4 The kTeV Experiment at Fermilab

The disagreement between the positive result of NA31 and the null result of E731 left an unsatisfactory state of affairs. For this reason, new experiments with a tenfold increase in data-taking capacity and reduced systematic uncertainty were designed, at both Fermilab and CERN.

The Fermilab experiment at the 800 GeV Tevatron, called kTeV, was described in Sect. 5.5.7. The main improvements compared with E731 are:

- all four decay modes are now measured concurrently;
- the electromagnetic calorimeter is now made of CsI, with much improved energy resolution;
- the regenerator at 123 m from the target is made of plastic scintillator, viewed by photomultipliers, such that inelastic regeneration can be detected by the recoiling nucleus;
- the kaon momentum range from 40 to 160 GeV/c and the decay vertex region from 110 m to 158 m from the target, are the same for all decay modes.

As in the E731 experiment, a double beam of K_L and regenerated K_S enters the decay volume. $K^0 \to \pi^+\pi^-$ decays are identified by their invariant mass. Semileptonic K_{e3} events are reduced by a factor of 1000 by requiring the ratio of the calorimetric energy E of a track to its momentum p to be less than

0.85. $K_{\mu 3}$ events are rejected by registering the muon penetrating the 4 m iron wall. $\Lambda \to p\pi$ events are rejected on the basis of their invariant $p\pi$ mass. The invariant-$\pi\pi$-mass distribution after background subtraction is shown in Fig. 5.15. The rms mass resolution is 1.6 MeV, and events in the range 488 to 508 MeV were selected. The low-mass tail is due to $\pi^+\pi^-\gamma$ events. Background from K_S produced in incoherent regeneration is suppressed mainly by vetoing events with a signal generated in the active regenerator indicating the recoil of a nucleus in the scattering process. Further reduction of this background is achieved by extrapolating the kaon direction back to the regenerator exit face and calculating the transverse momentum of the kaon relative to the line connecting this intercept with the target position. The distribution as a function of p_t^2 is shown in Fig. 5.28 for the data and the calculated background shapes. After a cut against the backgrounds from semileptonic decays and from collimator scattering, 11.1 million and 19.29 million $\pi^+\pi^-$ events remain in the vacuum beam and regenerator beam samples, respectively.

The selection of $2\pi^0$ events follows the lines described in Sect. 5.5.2. The best pairing of photons was chosen to reconstruct the $K^0 \to \pi^0\pi^0$ decay. Events with an invariant $\pi^0\pi^0$ mass between 490 and 505 MeV were selected (Fig. 5.15c), and background from $3\pi^0$ was further reduced by vetoing photons outside the decay region. Events in which a kaon scatters in the collimator or the regenerator were reduced by a cut in the ring number (RING), defined by the maximum deviation $\Delta x_{\rm coe}$ or $\Delta y_{\rm coe}$ (in cm) of the center of energy of all showers from the center of the corresponding beam spot at the CsI position, to which the event was assigned by use of the x-position of the center ofenergy:

$$\mathrm{RING} = 4 \times \mathrm{Max}(\Delta x_{\rm coe}^2, \Delta y_{\rm coe}^2) \ . \tag{5.136}$$

Since beam size at the CsI plane is 9×9 cm^2, this corresponds to a RING value at the edge of 81 cm^2. Figure 5.28 shows the RING distribution after all other $K^0 \to \pi^0\pi^0$ selection cuts. The signal was selected by the cut RING < 110 cm^2, while scattered events outside that cut were used to evaluate the background contribution by extrapolation. The largest background comes from regenerator scattering in the regenerator beam, 1.13%, adding up to a total of 1.235% in that beam. Also, in the vacuum beam, the events scattered in the nearby regenerator make to largest contribution to the background, 0.25%, which is 0.48% in total. After all cuts and background subtraction, the remaining signal consists of 3.3 million and 5.55 million events in the vacuum and regenerator beams, respectively. The 3.3 million $K_L \to \pi^0\pi^0$ are the limiting factor in the statistical uncertainty in the double ratio.

Since the vertex distributions of K_L decays (flat) and K_S decays (concentrated behind the regenerator) are very different, the raw double ratio has to be corrected by the double ratio of acceptances (Fig. 5.29). The quality of the Monte Carlo simulations for the acceptances was checked by reproducing the z vertex distributions of the vacuum beam data for different decay modes

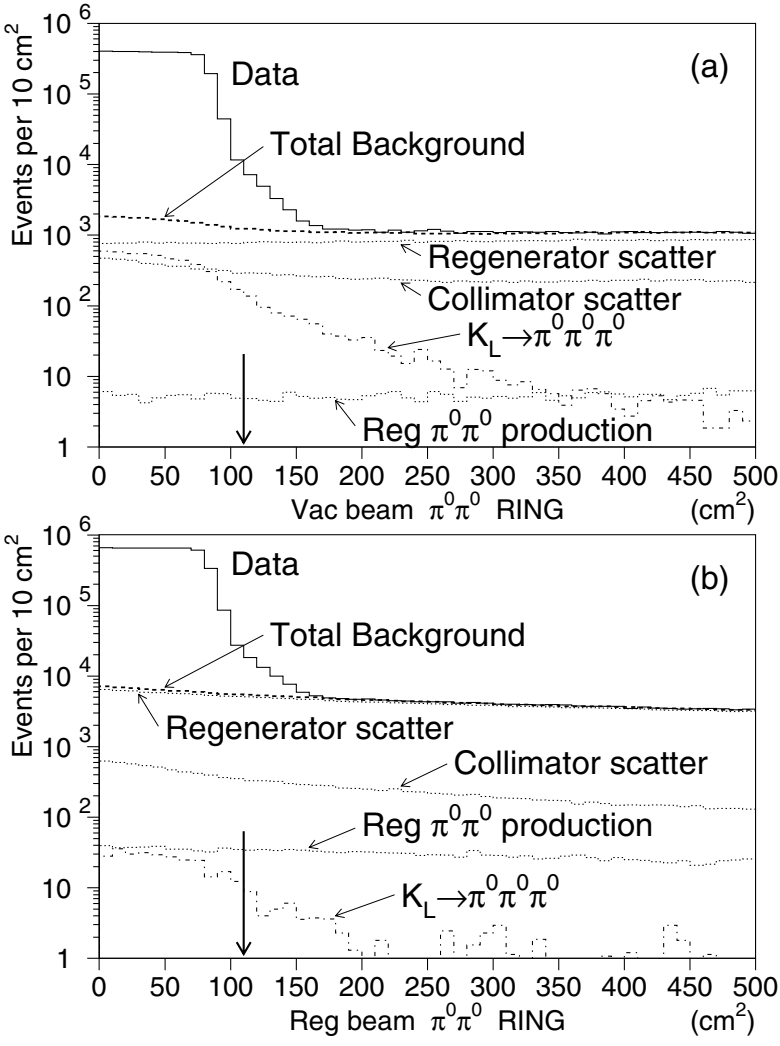

Fig. 5.28. The RING distribution (see text) after all $K \to \pi^0\pi^0$ selection cuts for (**a**) the vacuum beam and (**b**) the regenerator beam. The Monte Carlo predictions for the background components are overlaid. Events with RING < 110 cm^2 (*vertical arrow*) were included in the final $K \to \pi^0\pi^0$ sample (see [45])

(Fig. 5.30). In general the agreement is good, except that the $\pi^+\pi^-$ data show a slope of $(-0.70 \pm 0.30) \times 10^{-4}$/m.

The result for $\Re e(\varepsilon'/\varepsilon)$ is [45]

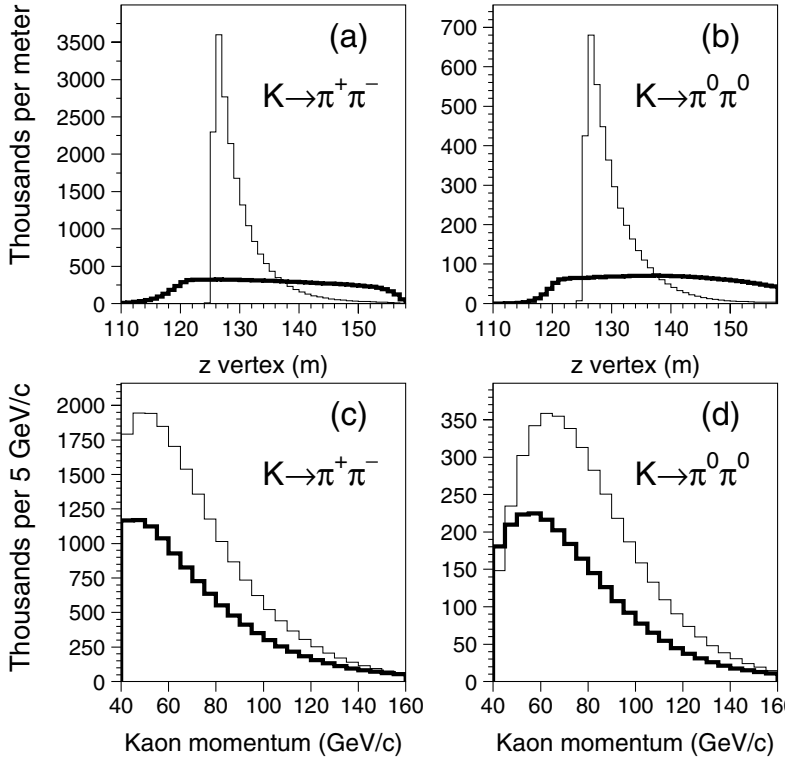

Fig. 5.29. (**a**) z vertex distribution for reconstructed $\mathrm{K} \to \pi^+\pi^-$ decays for the vacuum beam (*thick*) and regenerator beam (*thin histogram*). (**b**) z vertex distribution for reconstructed $\mathrm{K} \to \pi^0\pi^0$ decays. (**c**) Kaon momentum distribution for reconstructed $\mathrm{K} \to \pi^+\pi^-$ decays. (**d**) Kaon momentum distribution for reconstructed $\mathrm{K} \to \pi^0\pi^0$ decays. All $\mathrm{K} \to \pi\pi$ analysis cuts have been applied and background has been subtracted (see [45])

$$\begin{aligned} \Re e\left(\frac{\varepsilon'}{\varepsilon}\right) &= (20.71 \pm 1.48\ (\text{stat}) \pm 2.39\ (\text{syst})) \times 10^{-4} \\ &= (20.7 \pm 2.8) \times 10^{-4}\ . \end{aligned} \tag{5.137}$$

The systematic uncertainty for the neutral decays is mainly due to background, CsI energy calibration and acceptance corrections; for the charged decays, it is mainly due to uncertainties in the acceptance and trigger efficiency.

This result supersedes the earlier result [67] obtained from part of the same data, $(28.0 \pm 3.0 \pm 2.8) \times 10^{-4}$; the difference results from changes in the analysis.

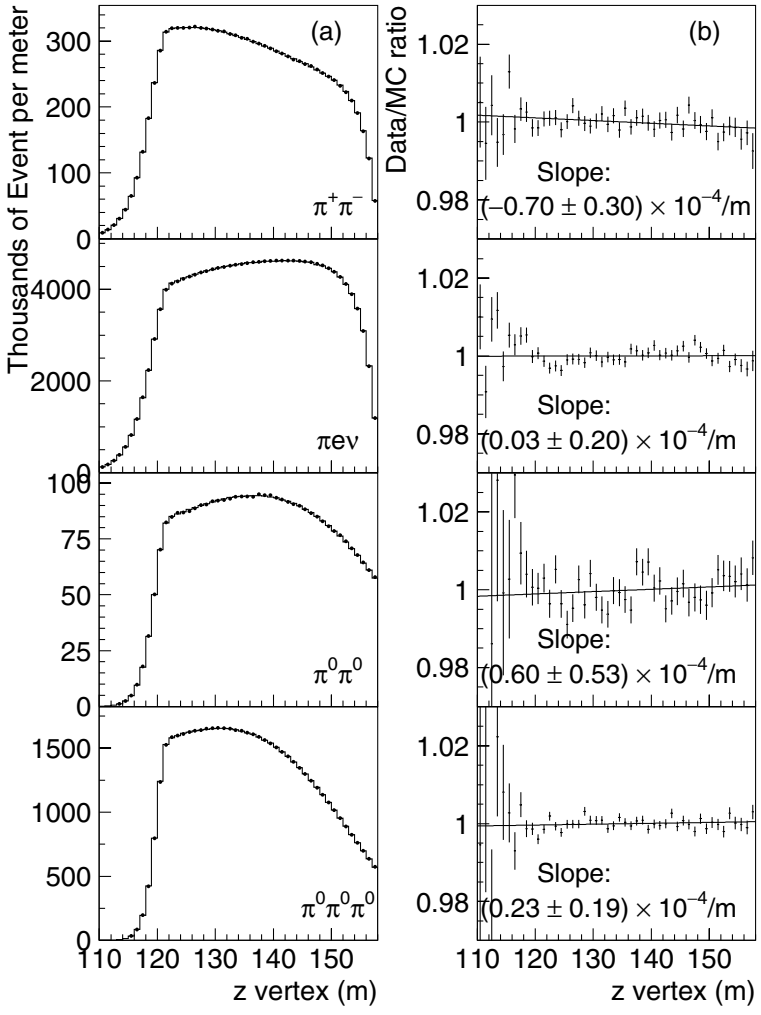

Fig. 5.30. (**a**) Comparison of the vacuum beam z distributions for data (*dots*) and MC calculations (*histograms*). The data-to-MC ratios (**b**) have been fitted to a line, and the z slopes are shown. The neutral distributions are for the combined 1996 + 1997 samples; the charged distributions are for 1997 only. (kTeV experiment [45])

The acceptance correction that has to be applied is about 5×10^{-2} for R or $\sim 80 \times 10^{-4}$ for $\Re e(\varepsilon'/\varepsilon)$, four times larger than the signal.

5.7.5 The NA48 Experiment

When the NA31 observation of a nonvanishing $\Re e(\varepsilon'/\varepsilon)$ was not confirmed by the result from the E731 experiment, the CERN-based collaboration set out

to construct a new, improved detector with the goal of achieving a precision measurement of $\Re e(\varepsilon'/\varepsilon)$ with a total uncertainty of 0.2×10^{-4}.

The new experiment was designed

- to measure all four decay modes concurrently by using two incident proton beams;
- to register at least ten times more data than in NA31 by use of an improved data-acquisition system;
- to improve on neutral-background rejection by developing a liquid-krypton electromagnetic calorimeter with substantially better energy resolution;
- to improve on charged-background rejection by using a magnetic spectrometer.

The resulting beam and detector have been described in Sect. 5.5.5. Data were taken in 1997, 1998 and 1999 with 450 GeV protons with a 14.4 s cycle time and a 2.38 s spill length. The effective spill length including the duty cycle was 1.7 s. In 2001, a lower intensity run was performed with 400 GeV protons, 16.8 s cycle time and 5.2 s spill length. The effective spill length including the duty cycle was 3.6 s. In the design of the NA48 detector, the cancellation of systematic uncertainties in the double ratio was exploited as much as possible. Important properties of the experiment are

- two almost collinear beams, which lead to almost identical illumination of the detector, and
- the K_S lifetime weighting of the events defined as K_L events.

The K_L target was located 126 m upstream of the beginning of the decay region. As the decay lengths at the average kaon momentum of 110 GeV/c are $\lambda_S = 5.9$ m and $\lambda_L = 3400$ m, the neutral beam derived from this target was dominated by K_L. The K_S target was located only 6 m upstream of the decay region so that the beam here was dominated by K_S. The two beams were almost collinear: The K_S target was situated 7.2 cm above the center of the K_L beam. The relative angle of the beams was 0.6 mrad such that they converged at the position of the electromagnetic calorimeter.

The beginning of the K_S decay region was defined by an anti counter (known as AKS). This detector was used to veto kaon decays occurring upstream of the counter. The position of the AKS also defined the global kaon energy scale, as the energy is directly correlated with the distance scale (Fig. 5.32). The decay region itself was contained in a 90 m long evacuated tank.

The identification of K_S decays was done by a detector (tagger) consisting of an array of scintillators situated in the proton beam directed on to the K_S target. If a proton signal was detected within a time window of ± 2 ns with respect to a decay, the event was defined as K_S event. The absence of a proton signal defined a K_L event.

To identify events coming from the K_S target a coincidence window of ± 2 ns between the proton signal in the tagger and the event time was chosen

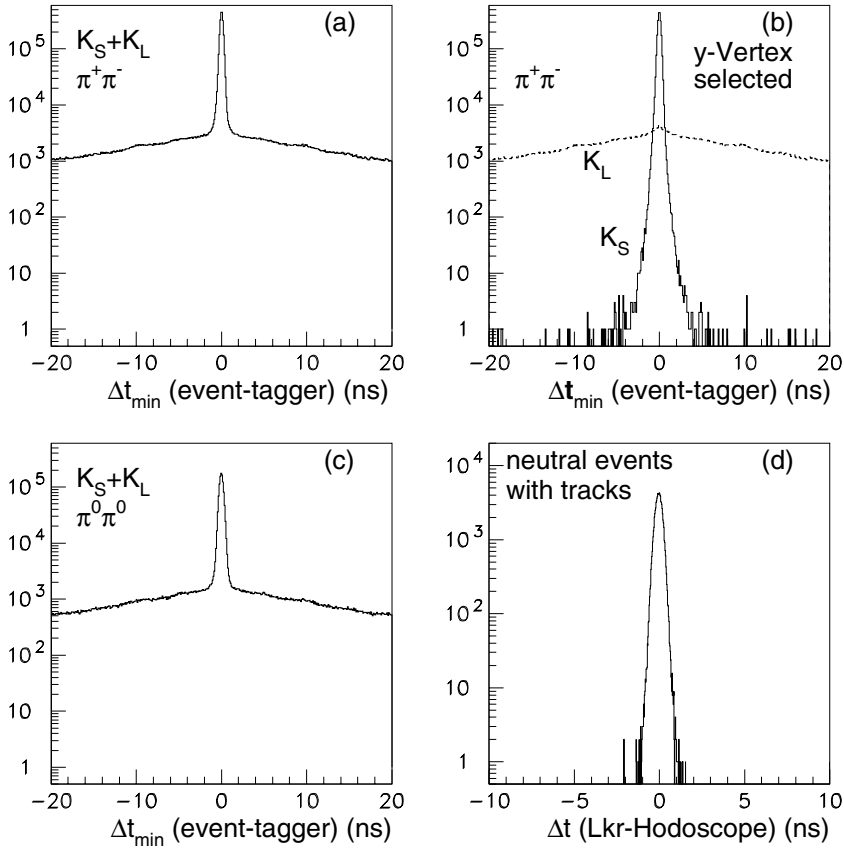

Fig. 5.31. (**a**), (**c**): Minimal difference between tagger time and event time ($\Delta t_{\min}$). (**b**) $\Delta t_{\min}$ for charged K_L and K_S events. (d) Comparison between charged and neutral event times. For this measurement, decays with tracks, selected by the neutral trigger, were used (γ conversion and Dalitz decays $K_S \to \pi^0\pi^0_D \to \gamma\gamma\gamma e^+e^-$) (NA48 experiment [68])

(see Fig. 5.31). Owing to inefficiencies in the tagger and in the proton reconstruction, a fraction α_{SL} of true K_S events are misidentified as K_L events. On the other hand, there is a constant background of protons in the tagger which have not led to a good K_S event. If those protons accidentally coincide with a true K_L event, this event is misidentified as a K_S decay. This fraction α_{LS} depends only on the proton rate in the tagger and the width of the coincidence window.

Both effects, α^{+-}_{SL} and α^{+-}_{LS}, can be measured (see Fig. 5.31b) in the charged mode, as K_S and K_L events can be distinguished by the vertical

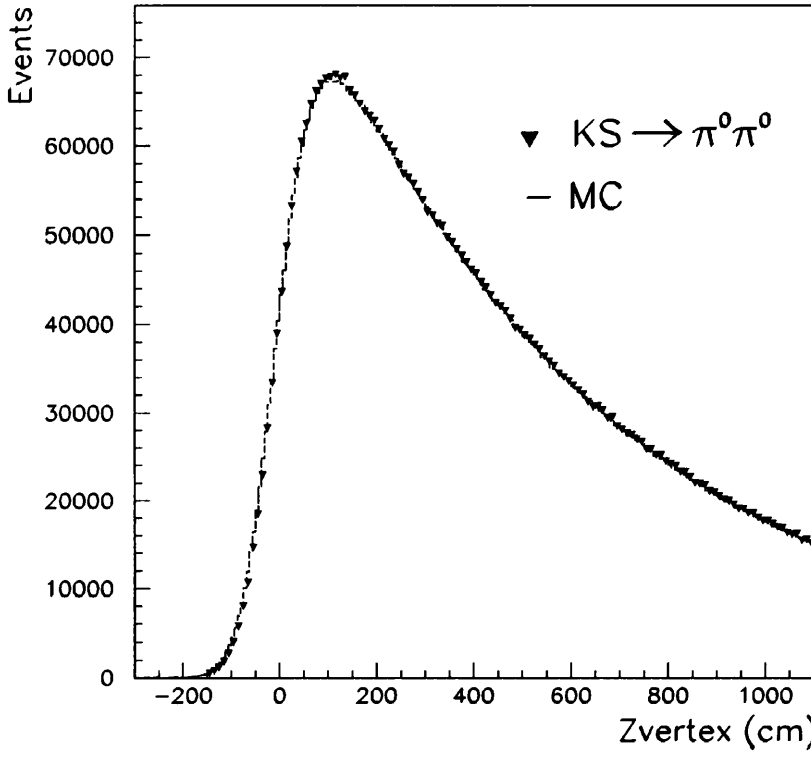

Fig. 5.32. Distribution of the reconstructed z vertex position of the $K_S \to \pi^0\pi^0$ candidates at the beginning of the decay volume. The origin of the z vertex axis has been set to the nominal AKS position. (NA48 experiment [68])

position of the decay vertex. The results are $\alpha_{SL}^{+-} = (1.63 \pm 0.03) \times 10^{-4}$ for the data from 1998/99 and $(1.12 \pm 0.03) \times 10^{-4}$ for the data from 2001. For the accidental-tagging rate, the value measured was $\alpha_{LS}^{+-} = (10.649 \pm 0.008)\%$ for the 1998/99 data sample and $(8.115 \pm 0.010)\%$ for the 2001 sample, owing to the lower instantaneous beam intensity. This means that about 11% or 8% of true K_L events are misidentified as K_S events; however, this quantity is precisely measured to the 10^{-4} level here. What is important for the measurement of R is the difference between the charged and the neutral decay modes $\Delta\alpha_{LS} = \alpha_{LS}^{00} - \alpha_{LS}^{+-}$. Proton rates in the sidebands of the tagging window were measured in both modes to determine $\Delta\alpha_{LS}$. The result is $\Delta\alpha_{LS} = (4.3 \pm 1.8) \times 10^{-4}$ for the 1998/99 event sample and $(3.4 \pm 1.4) \times 10^{-4}$ for the 2001 event sample. Several methods have been used to measure $\Delta\alpha_{SL}$, leading to the conclusion that there is no measurable difference between the mistaggings measured by different methods within an uncertainty of $\pm 0.5 \times 10^{-4}$.

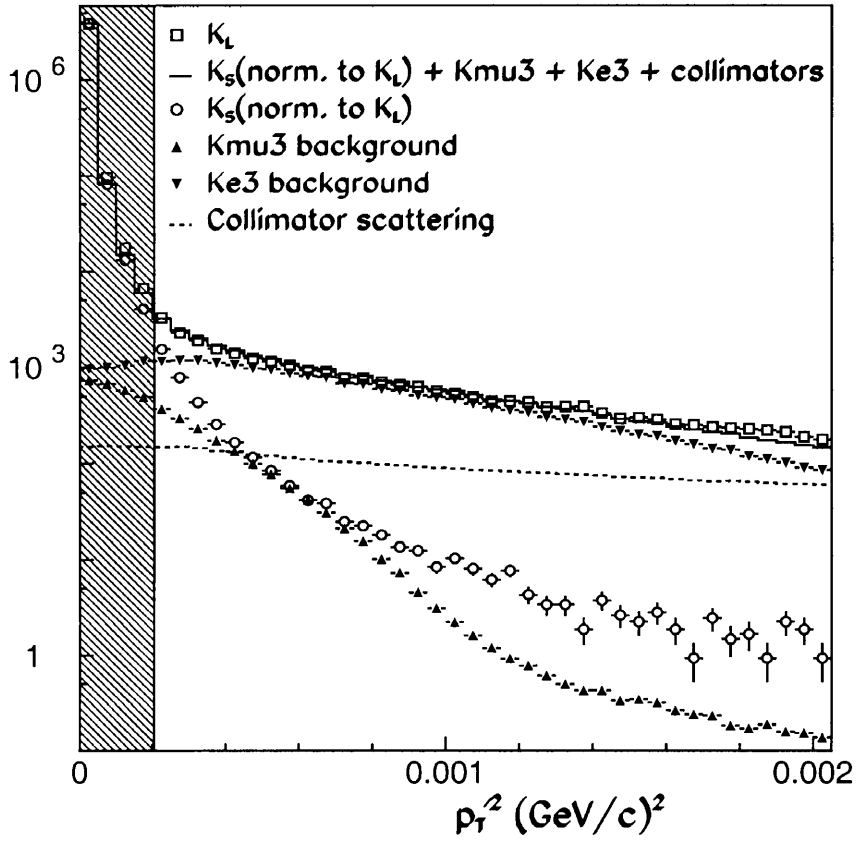

Fig. 5.33. Comparison of the $p_t'^2$ tail of the $K_L \to \pi^+\pi^-$ candidates with the sum of all known components. (NA48 experiment [68])

Another important correction is the background subtraction. Decays of the types $K_L \to \pi e\nu$ and $K_L \to \pi\mu\nu$ can be misidentified as $K \to \pi^+\pi^-$ decays, as the ν is undetectable. However, since the ν carries away momentum and energy, these events can be identified by their high transverse momentum p_t' and their reconstructed invariant mass. The remaining background can be measured by extrapolating the shape of the background in the $p_t'^2$ distribution into the signal region (Fig. 5.33). In this way, the charged background fraction leads to an overall correction to R of $(16.9 \pm 3.0) \times 10^{-4}$ for the 1998/99 data and $(14.2 \pm 3.0) \times 10^{-4}$ for the 2001 sample.

The reconstruction of $\pi^0\pi^0$ decays followed the principles described in Sect. 5.5.2. From the four shower energies and positions, the longitudinal distance z of the kaon decay vertex upstream from the calorimeter was calculated. Using z, the invariant masses of pairs of γ rays were obtained. The

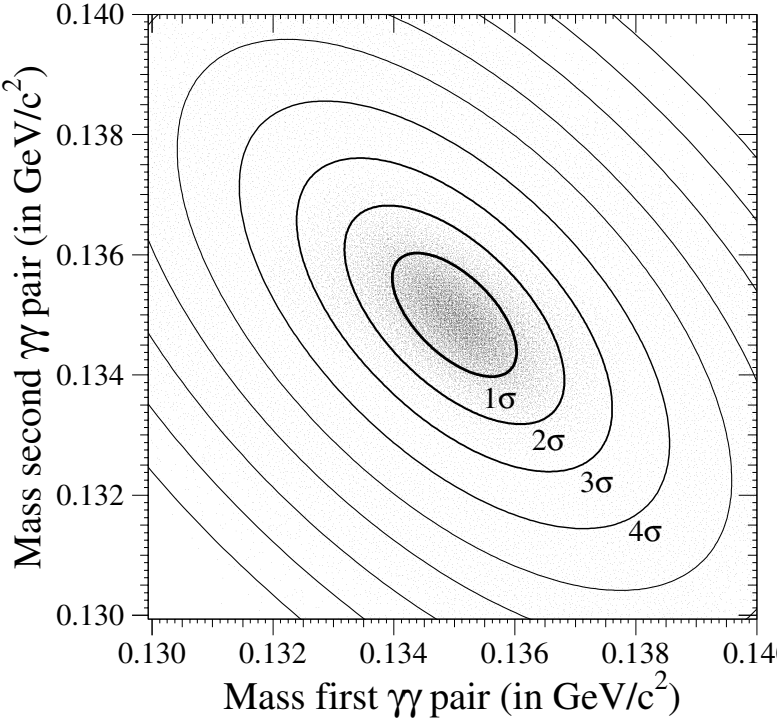

Fig. 5.34. Distribution of the $K_S \to \pi^0\pi^0$ candidates in the space of two reconstructed values of $m_{\gamma\gamma}$. The contours correspond to increments of one standard deviation. (NA48 experiment [68])

best shower pairing was obtained by choosing the one which agreed best with the $2\pi^0$ hypothesis. The two $\gamma\gamma$ masses are anticorrelated because of the constraint of the kaon mass (Fig. 5.34). The ellipses in Fig. 5.34 designate contours with increments of one standard deviation. The background from $3\pi^0$ decays with two undetected photons will be distributed with constant probability over each ellipse. The corresponding distribution of the background was simulated by Monte Carlo calculations. This leads to a correction to R of $(-5.9 \pm 2.0) \times 10^{-4}$ for the 1998/99 sample and $(-5.6 \pm 2.0) \times 10^{-4}$ for the 2001 sample.

The numbers of signal events after these corrections are summarized in Table 5.2.

The efficiency of the triggers used to record neutral and charged events has been determined. Independent triggers which accepted a downscaled fraction of events were used. In the neutral decay mode the efficiency was measured to be 0.99920 ± 0.00009, without any measurable difference between K_S and K_L decays. The $\pi^+\pi^-$ trigger efficiency was measured to be $(98.319 \pm 0.038)\%$

Table 5.2. Event numbers of the NA48 experiment after tagging correction and background subtraction [68, 69].

Event statistics ($\times 10^6$)					
	1998/99	2001		1998/99	2001
$K_S \to \pi^+\pi^-$	22.221	9.605	$K_L \to \pi^+\pi^-$	14.453	7.136
$K_S \to \pi^0\pi^0$	5.209	2.159	$K_L \to \pi^0\pi^0$	3.290	1.546

for K_L and $(98.353 \pm 0.022)\%$ for K_S decays. Here, a small difference between the trigger efficiencies for K_S and K_L decays was found. This leads to a correction to the double ratio of $(-4.5 \pm 4.7) \times 10^{-4}$ for the 1998/99 sample and $(5.2 \pm 3.6) \times 10^{-4}$ for the 2001 sample. The error in this measurement is dominated by the total number of events registered with the independent-trigger control samples. This error is one of the main contributions to the systematic error in the measurement of R.

Another systematic uncertainty, arising from limited knowledge of the energy scale, was estimated by using $K_S \to \pi^0\pi^0$ decays beginning at the anticounter position (Fig. 5.32). This measurement of the energy scale was checked using two-photon decays of η mesons produced by π^- beams in the decay volume. The uncertainty in the energy scale is $\pm 3 \times 10^{-4}$, corresponding to an uncertainty in R of $\pm 2 \times 10^{-4}$. Nonlinearities and other uncertainties in the calorimeter add up, together with the uncertainty from the energy scale, to a total of $\pm 5.8 \times 10^{-4}$ ($\pm 5.3 \times 10^{-4}$ for the 2001 data) for the neutral decays. For $\pi^+\pi^-$ decays, the agreement of the reconstructed anticounter position with the actual position is better than 2 cm for the 1998/99 (1 cm for 2001 the data). The overall uncertainty arising from the reconstruction of $\pi^+\pi^-$ decays in the double ratio is 2.8×10^{-4}.

Another systematic problem is the minimization of acceptance corrections by weighting of the K_L events. The difference in the lifetime between K_S and K_L events produces different illumination of the detector: there are more K_L events decaying closer to the detector, and they are therefore also measured at smaller radii, closer to the beampipe. NA48 weights the K_L events according to the measured K_S lifetime such that the distributions of the z position of the decay vertices of K_S and K_L events, and therefore the detector acceptances, become equal. Using this method, the influence of detector inhomogenities is minimized and the analysis becomes nearly independent of acceptance calculations by Monte Carlo methods. In fact, the acceptance correction due to the small detector differences is quite small. The price to pay for the gain in systematics is a loss in statistics.

Although the acceptances are almost equal, there are nevertheless small differences in the beam geometry and detector illumination between decays coming from the K_S and the K_L targets. These remaining differences have been corrected for with Monte Carlo methods. Using Monte Carlo methods

to calculate the double ratio R, the deviation from an input value 1 is $(26.7 \pm 5.7) \times 10^{-4}$ for the 1998/99 data sample and $(21.9 \pm 5.3) \times 10^{-4}$ for the 2001 data sample.

Summing all corrections to and systematic uncertainties in R, we find the amount to $(35.9 \pm 12.6) \times 10^{-4}$ for the 1998/99 data and $(35.0 \pm 11.0) \times 10^{-4}$ for the 2001 data.

The corresponding result for the direct-$\mathcal{CP}$-violation parameter is

$$\Re e \left(\frac{\varepsilon'}{\varepsilon} \right) = (15.3 \pm 2.6) \times 10^{-4} \tag{5.138}$$

for the data from 1997 [70] and 1998/99 [68], and

$$\Re e \left(\frac{\varepsilon'}{\varepsilon} \right) = (13.7 \pm 3.1) \times 10^{-4} \tag{5.139}$$

for the data from 2001 [69].

A comparison of these two values is significant because they were obtained at different average beam intensities. The combined final result from the NA48 experiment is

$$\begin{aligned} \Re e \left(\frac{\varepsilon'}{\varepsilon} \right) &= (14.7 \pm 1.4\ (\text{stat}) \pm 0.9\ (\text{syst}) \pm 1.5\ (\text{MC})) \times 10^{-4} \\ &= (14.7 \pm 2.2) \times 10^{-4}\,. \end{aligned} \tag{5.140}$$

5.7.6 Conclusions About Direct $\mathcal{CP}$ Violation, $\Re e(\varepsilon'/\varepsilon)$ and the Wu–Yang Triangle

The two experiments kTeV and NA48 have definitively confirmed the original observation of the NA31 team that direct $\mathcal{CP}$ violation exists. The results of all published experiments on ϵ'/ϵ are shown in Fig. 5.35. Therefore, $\mathcal{CP}$ violation as observed in the K meson system is a part of the weak interaction, due to weak quark mixing. Exotic, new interactions such as the superweak interaction are not needed. We therefore have a very precise experimental result for ε'/ε. The theoretical calculations of ε'/ε within the Standard Model, however, are still not very precise. This does not change the main conclusion of the experiments, that ε' is different from zero and positive, i.e. direct $\mathcal{CP}$ violation exists.

If we take into account the four relevant experiments NA31, E731, NA48 and kTeV, the weighted average comes out to be

$$\Re e \left(\frac{\varepsilon'}{\varepsilon} \right) = (16.7 \pm 1.6) \times 10^{-4}\,. \tag{5.141}$$

The consistency of the result is not completely satisfactory, since $\chi^2/\text{ndf} = 6.3/3$. If the phase of ε' as defined in (5.22), $\arg \varepsilon' = (42.3 \pm 1.5)^\circ$ [1], is

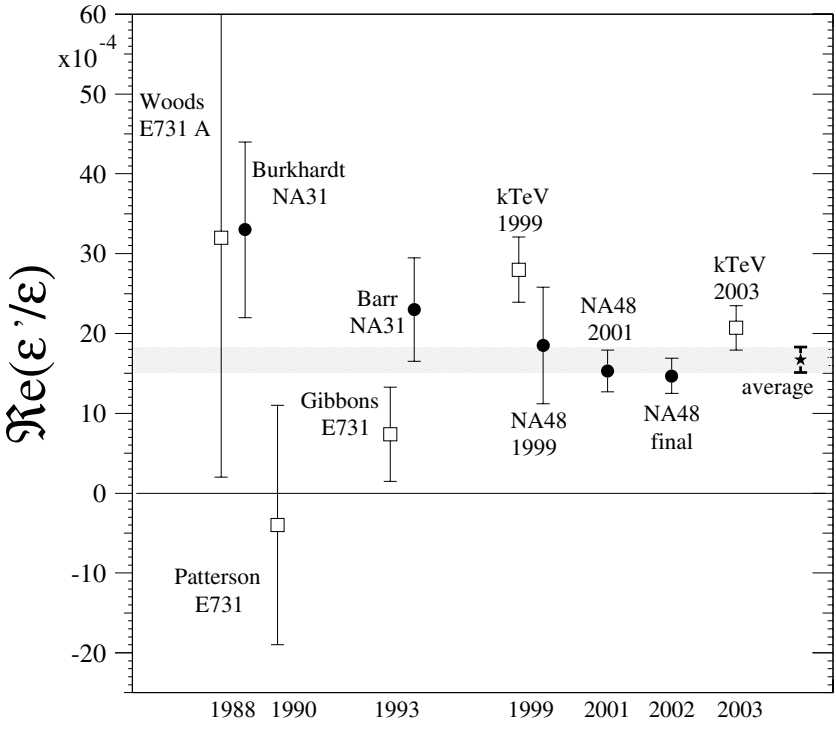

Fig. 5.35. Time sequence of published measurements of the parameter $\Re e(\varepsilon'/\varepsilon)$ of direct $\mathcal{CP}$ violation. The experiments at CERN are marked by *filled circles* and the experiments at Fermilab are marked by *open squares*. The kTeV result from 2003 is a reanalysis of the data from the kTeV 1999 result. (See [71] and also [45, 67, 68, 69, 70])

inferred, then a more precise value for the component of ε' transverse to ε can be derived.

We have done a complete fit to the Wu–Yang triangle (5.20), using as input

$$\Re e\left(\frac{\varepsilon'}{\varepsilon}\right) = (16.7 \pm 1.6) \times 10^{-4}, \quad \Re e\,\varepsilon = (1.658 \pm 0.0265) \times 10^{-3}\,,$$
$$\Phi_{+-} = 43.3^\circ \pm 0.4^\circ, \quad \Phi_{00} - \Phi_{+-} = (0.36 \pm 0.43)^\circ\,,$$
$$|\eta_{+-}| = (2.281 \pm 0.020) \times 10^{-3}, \quad |\eta_{00}| = (2.23 \pm 0.11) \times 10^{-3}\,,$$
$$\arg\,\varepsilon = 43.4 \pm 0.1^\circ, \quad \arg\,\varepsilon' = 42.3^\circ \pm 1.5^\circ\,.$$

The result of this fit is, with $\chi^2/\mathrm{ndf} = 0.8/4$

$$\Im m\left(\frac{\varepsilon'}{\varepsilon}\right) = (-3.3 \pm 4.4) \times 10^{-5} \tag{5.142}$$

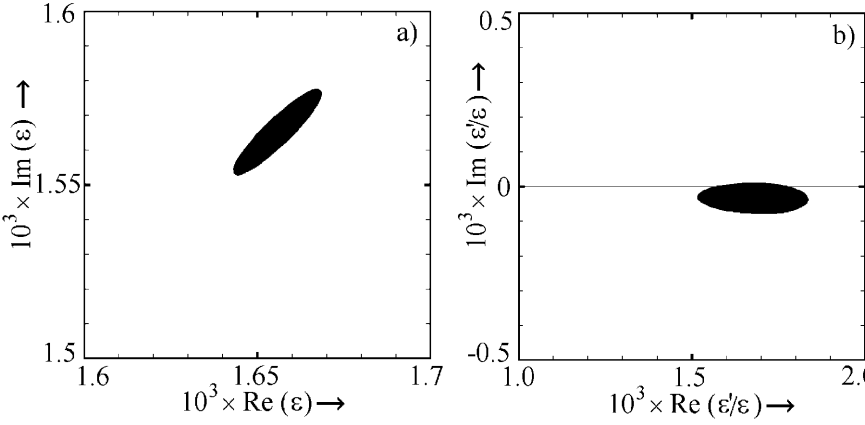

Fig. 5.36. Result of the fit to the Wu–Yang triangle relations between η_{+-}, η_{00}, ε and ε'. (**a**) Correlation of $\Re e\,\varepsilon$ and $\Im m\,\varepsilon$; (**b**) Correlation of $\Re e(\varepsilon'/\varepsilon)$ and $\Im m(\varepsilon'/\varepsilon)$. The boundaries of the black areas correspond to one-standard-deviation uncertainties

and

$$\Im m\,\varepsilon = (1.564 \pm 0.012) \times 10^{-3}\ . \tag{5.143}$$

Also, the real part of ε is constrained by the fit:

$$\Re e\,\varepsilon = (1.655 \pm 0.013) \times 10^{-3}$$

The result of this fit is expressed in correlation plots for $\Re e\,\varepsilon$ and $\Im m\,\varepsilon$ and for $\Re e(\varepsilon'/\varepsilon)$ and $\Im m(\varepsilon'/\varepsilon)$, in Fig. 5.36.

The result for direct $\mathcal{CP}$ violation (5.141) can also be quoted as a decay asymmetry between the K^0 and $\overline{\mathrm{K}^0}$ decay rates to a $\pi^+\pi^-$ final state. If the amplitudes are called $a = \mathrm{amp}(\mathrm{K}^0 \to \pi^+\pi^-)$ and $\overline{a} = \mathrm{amp}(\overline{\mathrm{K}^0} \to \pi^+\pi^-)$, then this asymmetry is

$$\begin{aligned} A &= \frac{\Gamma(\mathrm{K}^0 \to \pi^+\pi^-) - \Gamma(\overline{\mathrm{K}^0} \to \pi^+\pi^-)}{\Gamma(\mathrm{K}^0 \to \pi^+\pi^-) + \Gamma(\overline{\mathrm{K}^0} \to \pi^+\pi^-)} \\ &= \frac{|a|^2 - |\overline{a}|^2}{|a|^2 + |\overline{a}|^2}\ . \end{aligned} \tag{5.144}$$

Since $\overline{a}/a = 1 - 2\varepsilon'$, we obtain

$$\left|\frac{\overline{a}}{a}\right|^2 = 1 - 4\,\Re e\,\varepsilon' \tag{5.145}$$

and

$$A = 2\,\Re e\,\varepsilon' = 2\left(\Re e\,\varepsilon\,\Re e\left(\frac{\varepsilon'}{\varepsilon}\right) - \Im m\,\varepsilon\,\Im m\left(\frac{\varepsilon'}{\varepsilon}\right)\right)$$
$$= (5.6 \pm 0.6) \times 10^{-6}\,. \tag{5.146}$$

This very small decay rate asymmetry can be compared with the large values of some similar observables in the B system.

References

1. G. Colangelo, J. Gasser, H. Leutwyler, *Nucl. Phys. B* **603**, 125 (2001) 29, 89
2. W. Ochs, π *N Newsletter* **3**, 25 (1991); J. L. Basdevant, C. D. Frogatt, J. L. Petersen, *Phys. Lett. B* **41**, 178 (1972) 29
3. M. F. Losty *et al.*, *Nucl. Phys. B* **69**, 185 (1974); W. Hoogland *et al.*, *Nucl. Phys. B* **126**, 109 (1977) 29
4. G. Grayer *et al.*, *Nucl. Phys. B* **75**, 189 (1974) 29
5. M. Metcalf *et al.*, *Phys. Lett. B* **40**, 703 (1972) 30
6. V. V. Barmin *et al.*, *Phys. Lett. B* **46**, 465 (1973)
7. R. Wanke, presented at 38th Rencontres de Moriond, Electroweak Interactions and Unified Theories (2003) 30, 70
8. A. Pais, O. Piccioni, *Phys. Rev.* **100**, 1487 (1955) 31
9. K. Kleinknecht, *Fortschr. Phys.* **21**, 57 (1973) 32
10. M. L. Good, *Phys. Rev.* **106**, 591 (1957) 32, 33
11. V. Fitch *et al.*, *Phys. Rev. Lett.* **15**, 73; *Phys. Rev.* **164**, 1711 (1965) 32, 38
12. C. Alff-Steinberger *et al.*, *Phys. Lett.* **21**, 595 (1966) 32, 38, 53
13. M. Bott-Bodenhausen *et al.*, *Phys. Lett.* **23**, 277 (1966) 32, 38, 53
14. H. Faissner *et al.*, *Phys. Lett. B* **30**, 204 (1969) 32, 38
15. M. Ya. Balats *et al.*, *Sov. J. Nucl. Phys.* **13**, 53 (1971) 32
16. R. K. Carnegie *et al.*, *Phys. Rev. D* **6**, 2335 (1972) 32
17. W.C. Carithers *et al.*, *Phys. Rev. Lett.* **34**, 1244 (1975) 59, 60, 71
18. S. Bennett *et al.*, *Phys. Lett. B* **27**, 239; *Phys. Lett. B* **29**, 317 (1968) 32
19. M. W. Strovink, PhD thesis, Tech. Rep. No. 6, Princeton University, Princeton, NJ, (1970) 32
20. W.C. Carithers *et al.*, *Phys. Rev. Lett.* **34**, 1240 (1975) 32, 59, 61
21. J. M. Gaillard *et al.*, *Phys. Rev. Lett.* **18**, 20 (1967) 32
22. T. D. Lee, C. S. Wu, *Annu. Rev. Nucl. Sci.* **16**, 511 (1966) 35, 36
23. K. Hagiwara *et al.*, Review of Particle Physics, *Phys. Rev. D* **66** (2002) 38, 69
24. J. H. Dieperink *et al.*, *Proceedings of the International Conference on Instrumentation in High-Energy Physics*, Dubna, 1970, Joint Institute for Nuclear Research, Dubna (1971), p.251 38, 39
25. J. H. Christenson, J. W. Cronin, V. L. Fitch, R. Turlay, *Phys. Rev. Lett.* **13**, 138 (1964) 38
26. S. Bennett *et al.*, *Phys. Rev. Lett.* **19**, 993 (1967) 38, 70
27. D. Dorfan *et al.*, *Phys. Rev. Lett.* **19**, 987 (1967) 38, 70
28. C. Geweniger *et al.*, *Phys. Lett. B* **48**, 487 (1974) 38, 40, 55, 57, 58, 62, 63, 65, 71
29. M. Holder *et al.*, *Phys. Lett. B* **40**, 141 (1972) 41, 42, 43
30. M. Banner *et al.*, *Phys. Rev. Lett.* **28**, 1597 (1972) 41, 42

31. B. Wolff *et al.*, *Phys. Lett. B* **36**, 517 (1971) 41
32. J. C. Chollett *et al.*, *Phys. Lett. B* **31**, 658 (1970) 41
33. H. Burkhardt *et al.*, *Nucl. Instrum. Methods Phys.*A **268**, 116 (1988) 45
34. G. Barbiellini *et al.*, *Phys. Lett. B* **43**, 529 (1973) 41
35. J. H. Christenson *et al.*, *Phys. Rev. B* **140**, 74 (1965) 54
36. S. H. Aronson *et al.*, *Phys. Rev. Lett.* **25**, 1057 (1970) 54
37. R. K. Carnegie *et al.*, *Phys. Rev. D* **4**, 1 (1971) 54
38. M. Cullen *et al.*, *Phys. Lett. B* **32**, 523 (1970) 54, 70
39. C. Geweniger *et al.*, *Phys. Lett. B* **52**, 108 (1974) 55, 56, 70
40. S. Gjesdal *et al.*, *Phys. Lett. B* **52**, 113 (1974) 55, 57, 58, 70
41. L. K. Gibbons *et al.*, *Phys. Rev. Lett.* **70**, 1199 (1993) 55, 59, 70, 71
42. L. K. Gibbons *et al.*, *Phys. Rev. Lett.* **70**, 1203 (1993) 75, 76, 77, 78
43. K. Kleinknecht, S. Luitz *Phys. Lett.*B **336**, 581 (1994); K. Kleinknecht, *Phys. Rev. Lett.* **75**, 4784 (1995) 33, 62
44. B. Schwingenheuer *et al.*, *Phys. Rev. Lett.* **74**, 4376 (1995) 55, 66, 70, 71
45. A. Alavi-Harati *et al.*, *Phys. Rev. D* **67**, 012005 (2003) 55, 59, 62, 63, 64, 66, 70, 71, 80, 81, 82, 90
46. R. Messner *et al.*, *Phys. Rev. Lett.* **30**, 876 (1973) 58
47. V. I. Genchev *et al.*, Paper No. 641 (1974); K. Kleinknecht, *Proceedings of the International Conference on High-Energy Physics, 17th*, London, Chilton, Dideot, UK: Sci. Res. Council (1974), p. III - 23 58
48. A. Apostolakis *et al.*, *Phys. Lett. B* **458**, 545 (1999) 59, 67, 70, 71
49. A. Böhm *et al.*, *Nucl. Phys. B* **9**, 605 (1965) 62
50. D. A. Jensen *et al.*, *Phys. Rev. Lett.* **23**, 615 (1965) 62
51. R. Carosi *et al.*, *Phys. Lett. B* **237**, 303 (1990) 66, 71
52. A. Angelopoulos *et al.*, *Phys. Rep.* **374**, 165 (2003) 68, 69
53. V. L. Fitch *et al.*, *Phys. Rev. Lett.* **31**, 1524 (1973) 68, 70
54. C. Geweniger *et al.*, *Phys. Lett. B* **48**, 483 (1974) 68, 70
55. A. Alavi-Harati *et al.*, *Phys. Rev. Lett.* **88**, 181601 (2002) 70
56. R. Piccioni *et al.*, *Phys. Rev. Lett.* **29**, 1412 (1972) 68, 70
57. H. H. Williams *et al.*, *Phys. Rev. Lett.* **31**, 1521 (1973) 68, 70
58. H. Burkhardt *et al.*, *Phys. Lett.*B **206**, 169 (1988). 72, 73, 74, 75
59. H. Saal, PhD thesis. Columbia University, New York (1969) 70
60. J. Marx *et al.*, *Phys. Lett. B* **32**, 219 (1970) 70
61. V. A. Ashford *et al.*, *Phys. Rev. Lett.* **31**, 47 (1972) 70
62. M. A. Paciotti, PhD thesis, UCRL-19446, University of California Radiation Laboratory, Berkeley (1969) 70
63. R. L. McCarthy *et al.*, *Phys. Rev. D* **7**, 687 (1973) 70
64. A. Lai *et al.*, *Phys. Lett. B* **537**, 28 (2002) 70
65. A. Angelopoulos *et al.*, *Phys. Lett. B* **503**, 49 (2001) 70
66. A. Apostolakis *et al.*,*Phys. Lett. B* **444**, 38 (1998) 70
67. A. Alavi-Harati *et al.*, *Phys. Rev. Lett.* **83**, 22 (1999) 38, 81, 90
68. A. Lai *et al.*, *Eur. Phys. J. C* **22**, 231 (2001) 38, 47, 84, 85, 86, 87, 88, 89, 90
69. J. R. Batley *et al.*, *Phys. Lett. B* **544**, 97 (2002) 88, 89, 90
70. V. Fanti *et al.*, *Phys. Lett. B* **465**, 335 (1999) 89, 90
71. M. Woods *et al.*, *Phys. Rev. Lett.* **60**, 1695 (1988); H. Burkhardt *et al.*, *Phys. Lett. B* **206**, 169 (1988); J. R. Patterson *et al.*, *Phys. Rev. Lett.* **64**, 1491 (1990); L. K. Gibbons *et al.*, *Phys. Rev. Lett.* **70**, 1203 (1993); G. D. Barr *et al.*, *Phys. Lett. B* **317**, 233 (1993); 90

6 The Neutral B Meson System

After the observation of direct $\mathcal{CP}$ violation in the neutral kaon system in 1988, it became clear that the Kobayashi–Maskawa mechanism of weak quark mixing was the most likely and most natural candidate for explaining this phenomenon. Although the calculation of hadronic matrix elements for the relevant penguin diagrams, Q_6 and Q_8, was difficult, at least the sign of $\Re e(\varepsilon'/\varepsilon)$ and its order of magnitude were predicted correctly, i.e. agreed with the experimental values.

It seemed natural, therefore, that the same mechanism would also produce observable $\mathcal{CP}$-violating effects in other neutral meson systems. The discovery of $\mathrm{B}^0 - -\overline{\mathrm{B}^0}$ mixing in 1987 made the B^0 system the evident candidate for observing $\mathcal{CP}$ violation in another physical system.

6.1 Phenomenology of Mixing in the Neutral B Meson System

The parameters of mixing in the neutral B system are different from those in the neutral K system. Mixing in the $\mathrm{B_d}(\mathrm{b\overline{d}})$ system was discovered by the ARGUS collaboration [1] after some indications had been seen in the UA1 experiment [2]. At that time, such a large mixing effect was not expected since the box diagrams of the type shown in Fig. 4.1 yield an amplitude proportional to the mass of the heaviest quark in the loop, and the top-quark mass was assumed to be around 30 GeV.

We define the complex parameters

$$\begin{aligned} \gamma_h &= \mathrm{i}m_h + \frac{\Gamma_h}{2} \,, \\ \gamma_l &= \mathrm{i}m_l + \frac{\Gamma_l}{2} \,, \end{aligned} \tag{6.1}$$

for the heavy (h) and light (l) meson states.

The time evolution of B states is (see (3.19) and (3.25))

$$\begin{aligned} \mathrm{B}_h(t) &= (p\mathrm{B}^0 - q\overline{\mathrm{B}^0})\mathrm{e}^{-\gamma_h t} \,, \\ \mathrm{B}_l(t) &= (p\mathrm{B}^0 + q\overline{\mathrm{B}^0})\mathrm{e}^{-\gamma_l t} \,. \end{aligned} \tag{6.2}$$

Konrad Kleinknecht: Uncovering $\mathcal{CP}$ Violation, STMP 195, 95–121 (2003)

The two initial states at $t = 0$, with a definite quantum number $\mathbb{B}$, are

$$\psi_{\mathrm{B}}(0) = \mathrm{B}^0 \quad \text{and } \psi_{\overline{\mathrm{B}}}(0) = \overline{\mathrm{B}^0} \,. \tag{6.3}$$

Their decay law is not exponential, but given by (6.2), which leads to

$$\begin{aligned} 2\psi_{B}(t) &= \mathrm{B}^0(\mathrm{e}^{-\gamma_h t} + \mathrm{e}^{-\gamma_l t}) - \frac{q}{p}\overline{\mathrm{B}^0}(\mathrm{e}^{-\gamma_h t} - \mathrm{e}^{-\gamma_l t}) \,, \\ 2\psi_{\overline{B}}(t) &= \overline{\mathrm{B}^0}(\mathrm{e}^{-\gamma_h t} + \mathrm{e}^{-\gamma_l t}) - \frac{p}{q}\mathrm{B}^0(\mathrm{e}^{-\gamma_h t} - \mathrm{e}^{-\gamma_l t}) \,. \end{aligned} \tag{6.4}$$

The probabilities P, for flavor change are contained in these decay laws, and we obtain

$$\begin{aligned} P(\mathrm{B}^0 \to \overline{\mathrm{B}^0}) &= \frac{1}{4}\left|\frac{q}{p}\right|^2 \left[\mathrm{e}^{-\Gamma_h t} + \mathrm{e}^{-\Gamma_l t} - 2\mathrm{e}^{-\Gamma t}\cos\left(\Delta m_d\, t\right)\right] \,, \\ P(\overline{\mathrm{B}^0} \to \mathrm{B}^0) &= \frac{1}{4}\left|\frac{p}{q}\right|^2 \left[\mathrm{e}^{-\Gamma_h t} + \mathrm{e}^{-\Gamma_l t} - 2\mathrm{e}^{-\Gamma t}\cos\left(\Delta m_d\, t\right)\right] \,. \end{aligned} \tag{6.5}$$

The lifetimes of the heavy and light states should be nearly equal (to within a few percent), because the numbers of decay channels are very close:

$$\Gamma_h = \Gamma_l = \Gamma = \frac{\Gamma_h + \Gamma_l}{2} \,. \tag{6.6}$$

Therefore, in this case $y = \Delta\Gamma/2\Gamma = 0$. Also, in the Standard Model, the $\mathcal{CP}$ violation in $\mathrm{B}\overline{\mathrm{B}}$ mixing is expected to be small, such that $|q/p| = 1$ within $\mathcal{O}(10^{-3})$. In this case the oscillation probabilities are equal, i.e.

$$P(\mathrm{B}^0 \to \overline{\mathrm{B}^0}) = P(\overline{\mathrm{B}^0} \to \mathrm{B}^0) \,, \tag{6.7}$$

and they can be approximated by (3.29)

$$\mathrm{e}^{-\Gamma t}\frac{1 - \cos(\Delta m_d\, t)}{2} = \frac{1}{2}\mathrm{e}^{-T}\left(1 - \cos xT\right) \,. \tag{6.8}$$

The probability for remaining in the original beauty state is, correspondingly,

$$P(\mathrm{B}^0 \to \mathrm{B}^0) = P(\overline{\mathrm{B}^0} \to \overline{\mathrm{B}^0}) = \mathrm{e}^{-\Gamma t}\frac{1 + \cos(\Delta m_d\, t)}{2} \tag{6.9}$$

If B meson pairs are produced in e^+e^- annihilations at the $\Upsilon(4\mathrm{S})$ resonance (with parity -1), then parity conservation requires the $\mathrm{B}\overline{\mathrm{B}}$ state to be of the form

$$\mathrm{B}^0(\theta)\overline{\mathrm{B}^0}(\pi - \theta) - \mathrm{B}^0(\pi - \theta)\overline{\mathrm{B}^0}(\theta) \,, \tag{6.10}$$

where θ is the production angle relative to the e^+ direction of flight.

If the two mesons decay at times t_1 and t_2 from the moment of production ($t = 0$), then the first decay defines the flavor by its decay products. Assume

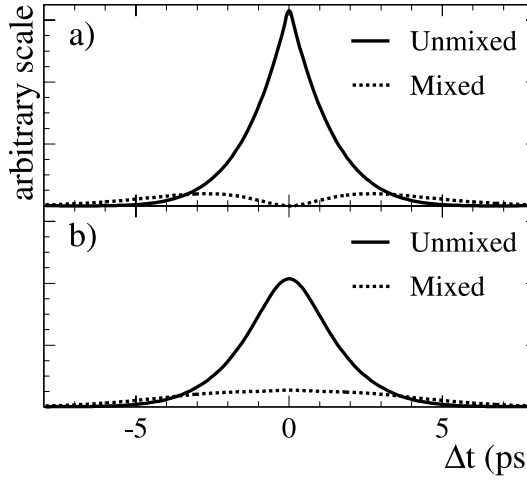

Fig. 6.1. Time dependence of unmixed and mixed pairs of neutral B mesons obtained from the $\Upsilon(4S)$ resonance, (**a**) without and (**b**) with experimental resolutions. *Solid curves* = unmixed, *dotted curves* = mixed

that the decay at t_1 corresponds to a B^0; at that time the flavor of the second meson is fixed to be a $\overline{\mathrm{B}^0}$. The time distribution of the second decay is then

$$\psi_2(t_2) = \overline{\mathrm{B}^0}\left(\mathrm{e}^{-\gamma_h(t_2-t_1)} + \mathrm{e}^{-\gamma_l(t_2-t_1)}\right) - \frac{q}{p}\mathrm{B}^0\left(\mathrm{e}^{-\gamma_h(t_2-t_1)} - \mathrm{e}^{-\gamma_l(t_2-t_1)}\right) . \tag{6.11}$$

This equation describes the time distribution of $\mathrm{B}\overline{\mathrm{B}}$ pair decays as a function of the time difference $\Delta t = t_2 - t_1$. The number of unmixed pairs is then (where C is a normalization constant)

$$N\left(\mathrm{B}^0\overline{\mathrm{B}^0}\right) = C\mathrm{e}^{-\Gamma|\Delta t|}\left[1 + \cos\left(\Delta m_d\,\Delta t\right)\right] , \tag{6.12}$$

and the number of mixed pairs is

$$N\left(\mathrm{B}^0\mathrm{B}^0\right) = N\left(\overline{\mathrm{B}^0\mathrm{B}^0}\right) = C\mathrm{e}^{-\Gamma|\Delta t|}\left[1 + \cos\left(\Delta m_d\,\Delta t\right)\right] . \tag{6.13}$$

If the flavor is falsely measured in $f\%$ of the cases, the relations are modified (using the abbreviation $\cos(\Delta m_d\,\Delta t) = \alpha$)

$$\begin{aligned} N\left(\mathrm{B}^0\overline{\mathrm{B}^0}\right) &= C\mathrm{e}^{-\Gamma|\Delta t|}\left[(1-f)(1+\alpha) + f(1-\alpha)\right] , \\ N\left(\mathrm{B}^0\mathrm{B}^0\right) &= C\mathrm{e}^{-\Gamma|\Delta t|}\left[1 - (1-2f)\alpha\right] . \end{aligned} \tag{6.14}$$

This leads to the time-dependent asymmetry

$$A(\Delta t) = \frac{N\left(\mathrm{B}^0\mathrm{B}^0\right) - N\left(\mathrm{B}^0\overline{\mathrm{B}^0}\right)}{N\left(\mathrm{B}^0\mathrm{B}^0\right) + N\left(\mathrm{B}^0\overline{\mathrm{B}^0}\right)} = (1-2f)\cos(\Delta m_d\,\Delta t) . \tag{6.15}$$

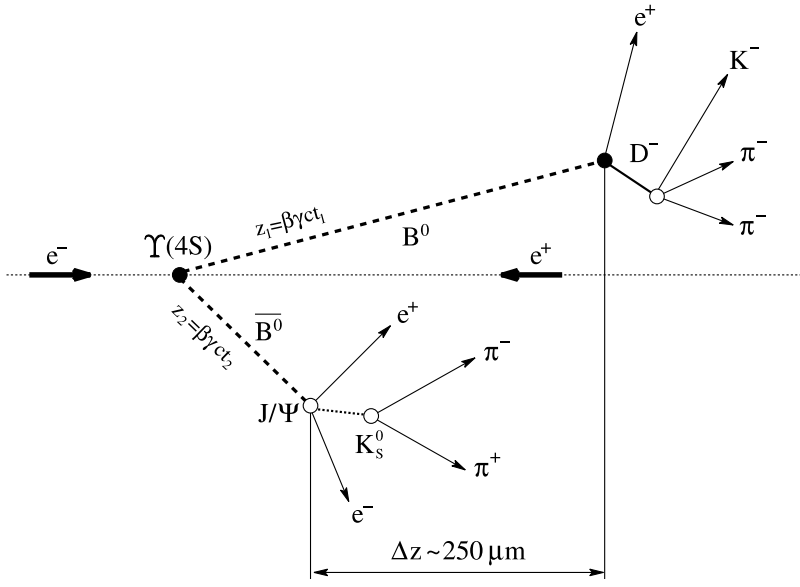

Fig. 6.2. Decay topology of $B^0\overline{B^0}$ pairs

This time dependence for mixed and unmixed pairs is shown in Fig. 6.1a for ideal conditions ($f = 0$). The corresponding curve for finite $f > 0$ and finite detector resolution for Δt is displayed in Fig. 6.1b.

The probability of mixing through a box diagram of the type shown in Fig. 4.1 is given by [3, 4, 5]

$$x \equiv \frac{\Delta m}{\Gamma} = \frac{G_F^2}{6\pi^2} B_B f_B^2 m_B \tau_B |V_{tb}^* V_{td}|^2 m_t^2 F\left(\frac{m_t^2}{M_W^2}\right) \eta_{QCD} \tag{6.16}$$

Here, B_B is the "bag factor" parameterizing the probability that d and $\overline{b}$ quarks will form a B_d hadron, f_B is the B meson decay constant, F is the calculated loop function, increasing with m_t^2, and $\eta_{QCD} \approx 0.8$ is a QCD correction.

6.2 Detection of B Meson Decays

Facilities especially designed for the production of B mesons are called B factories. Two machines with colliding electron and positron beams have been built for this purpose. Both are designed as asymmetric machines with different energies for the electron and positron beams. The center-of-mass energy of both machines is 10.58 GeV, which corresponds to the $\Upsilon(4S)$ resonance. This particular resonance was chosen because this $b\overline{b}$ bound state lies just above the $B\overline{B}$ threshold and decays predominately into $B\overline{B}$ pairs. Owing to

the asymmetric beam energies, the center-of-mass system moves along the electron direction and the $B\overline{B}$ pair is boosted by this motion. This is essential for the measurement of the difference between the decay times of the two B mesons, $t_1 - t_2$, which is necessary for the observation of a $\mathcal{CP}$-violating asymmetry. The boost also leads to an asymmetric design of the detectors. The experiments consist in detecting the decays of the pair of B mesons. The mass of the $\Upsilon(4S)$ $b\overline{b}$ state is (10.5800 ± 0.0035) GeV, and the cross section for its production in e^+e^- reactions is about 1.1 nb. It decays via the strong interaction to $B^0\overline{B^0}$ pairs (∼50%) or B^+B^- pairs (∼50%). The B meson pairs decay by a flavor-changing weak interaction into hadrons and leptons, with a mean lifetime around 10^{-12} s. Since the $\Upsilon(4S)$ is only slightly above the mass of two B mesons (masses of (5279.4 ± 0.5) MeV each), the kinetic energy of one B meson is only 11 MeV. The momentum of each B meson is 340 MeV/c, and its velocity $\beta^* = 0.064$. During their lifetime t, these B mesons fly over a distance $z = \beta\gamma ct$. For a lifetime of 1.5×10^{-12} s, this flight path would be about 30 μm. However, the asymmetric machine design leads to a moving $\Upsilon(4S)$, which gives the $B\overline{B}$ system an additional boost factor of $\beta\gamma = 0.56$ for the BaBar experiment and $\beta\gamma = 0.425$ for the Belle experiment. The geometrical pattern of such a decay of a pair of B mesons is shown in Fig. 6.2. It is now essential to measure the vertices of these two decays. This is done with silicon strip detectors with a typical resolution between 20 μm and 100 μm. The difference in the z positions of the two vertices along the beam direction is then measurable, and is typically $\Delta z \approx 250$ μm in these asymmetric machines. This difference is related to the decay time difference Δt:

$$\Delta z = z_2 - z_1 = \beta\gamma c(t_2 - t_1) = \beta\gamma c\,\Delta t\,. \tag{6.17}$$

The decay distribution for B^+B^- pairs without oscillation is given by

$$\begin{aligned} \mathrm{d}^2N &= \frac{N}{\tau^2}\mathrm{e}^{-(t_1/\tau)}\mathrm{e}^{-(t_2/\tau)}\mathrm{d}t_1\,\mathrm{d}t_2 \\ &= \frac{N}{\tau^2}\mathrm{e}^{-(\Delta t/\tau)}\mathrm{e}^{-(2t_2/\tau)}\mathrm{d}(\Delta t)\,\mathrm{d}t_2\,. \end{aligned} \tag{6.18}$$

Integrating over t_2 we obtain

$$\mathrm{d}N = \frac{N}{2\tau}\mathrm{e}^{-(|\Delta t|/\tau)}\mathrm{d}(\Delta t)\,. \tag{6.19}$$

There are pairs with positive and negative values of Δt, as visualized in Fig. 6.1.

6.3 Belle

One of the B factories is KEK B, located at at KEK, Tsukuba, and is associated with the detector Belle [24] (Fig. 6.3). The beam energies are 8 GeV for

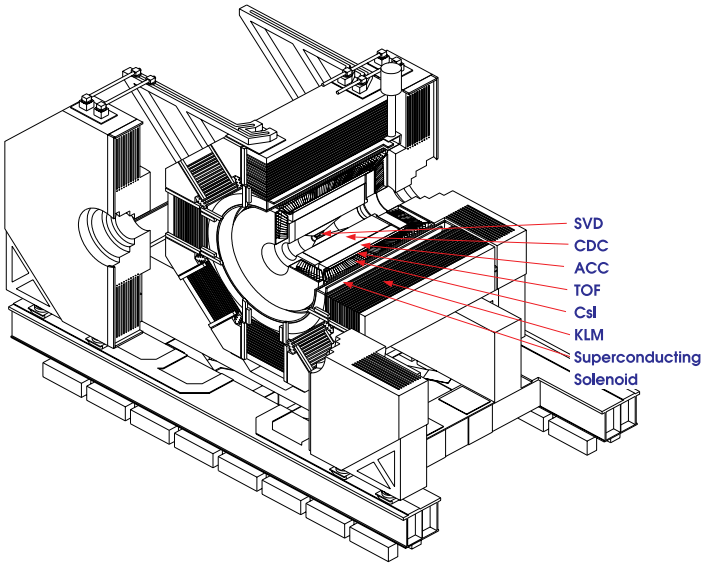

Fig. 6.3. The Belle detector with the silicon vertex detector (SVD), the central drift chamber (CDC), the aerogel Cerenkov counter (ACC), the CsI electromagnetic calorimeter and the K_L/μ detector (KLM). The detector is embedded in a magnetic field of 1.5 T produced by a solenoid with a length of 4.4 m and a diameter of 3.4 m [24]

the electrons and 3.5 GeV for the positrons. In order to reduce parasitic collisions the beams collide at a finite crossing angle of 22 mrad. This also makes the detector design easier and allows a short spacing between the bunches (0.6 m). The boost of the $\Upsilon(4S)$ in the lab frame is $\beta\gamma \simeq 0.425$.

Like all detectors at colliding-beam machines, the Belle detector has an onion-like design. The most important subdetector is the silicon vertex detector (SVD), because the decay points of the B's are reconstructed with the SVD. The SVD has three layers of 300 μm thick, double-sided silicon at distances from the beam of 3.0 cm, 4.55 cm and 6.05 cm. The readout pitch for the strips measuring the z component is 42 μm, and that for the ϕ component is 25 μm. This gives a total of 81 920 readout channels. The resolutions obtained for the impact parameters of tracks are

$$\sigma_{xy} = \left[19 \oplus \frac{50}{p\beta\sqrt{\sin^3\theta}} \right] \mu\text{m and} \tag{6.20}$$

$$\sigma_z = \left[36 \oplus \frac{42}{p\beta\sqrt{\sin^5\theta}} \right] \mu\text{m} \,. \tag{6.21}$$

The SVD is followed by the central drift chamber (CDC). The inner radius of the CDC is 8.3 cm and the outer radius is 88 cm. It consists of three cathode strip layers and 50 sense wire planes. The sense wire planes are organized in 11 superlayers, where six are axial and five are stereo superlayers. There are a total of 8400 sense wires (5280 axial and 3120 stereo) in the CDC. The drift chamber provides a measurement of the transverse momentum with a resolution of $\sigma_{p_t}/p_t = [(0.201 \pm 0.003)p_t \oplus (0.290 \pm 0.006)/\beta]\%$. The resolution for the $\mathrm{d}E/\mathrm{d}x$-measurement is about 7.8% for particle momenta between 0.4 GeV/c and 0.6 GeV/c.

Particle identification is provided by the aerogel Cerenkov counter (ACC). Each module of the ACC is made of five stacked aerogel tiles with a total size of $12 \times 12 \times 12$ cm^3. There are 960 counter modules in 60 cells in the ϕ direction in the barrel part (BACC) and 228 modules in five concentric layers in the forward end cap (EACC). To provide a 3σ K/π separation in the momentum region $0.7 < p_K < 2.4$ GeV/c different refractive indices are used. In the BACC, five different refractive indices n, 1.010, 1.013, 1.015, 1.020 and 1.028, depending on the polar angle, are used, while in the EACC, only one refractive index $n = 1.030$ is necessary.

The photon or electron energy is measured in the electromagnetic calorimeter (ECL). This consists of 8736 thallium-doped CsI crystals (6624 in the barrel, 1152 in the forward end cap, 960 in the backward end cap). The crystals have the shape of a truncated pyramid a front face of area 5.5×5.5 cm^2 and a back face of area 6.5×6.5 cm^2, and a length of 30 cm. The energy resolution of the ECL is $\sigma_E/E = 0.81\%/\sqrt[4]{E} \oplus 0.066/E\% \oplus 1.34\%$, and the electron identification efficiency is better than 90%.

All of the above subdetectors are embedded in a superconducting solenoid magnet of cylindrical shape, 3.4 m in diameter and 4.4 m in length, providing a magnetic field of 1.5 T.

The muon and K_L identification is provided by the K_L/μ detector (KLM). This consists of alternating layers of iron plates and resistive plate counters (RPCs). The RPCs have two parallel electrodes with a high intrinsic resistivity ($\geq 10^{10}\ \Omega\,\mathrm{m}$) with a gas-filled gap in between. For muon momenta higher than 1.5 GeV/c the detection efficiency is better than 90% and the fake rate is less than 2%. The position of a K_L is measured with an accuracy of $\Delta\phi = \Delta\theta = 30$ mrad and a timing resolution of a few nanoseconds.

6.4 BaBar

The second B factory is PEP II, located at SLAC, Stanford, and is associated with the detector BaBar [25] (Figs. 6.4 and 6.5. The beams collide head-on with an energy of 9 GeV for the electrons and 3.1 GeV for the positrons. This beam design requires dipole magnets that are close to the collision point to separate the beams after collision. These dipoles make the design of the

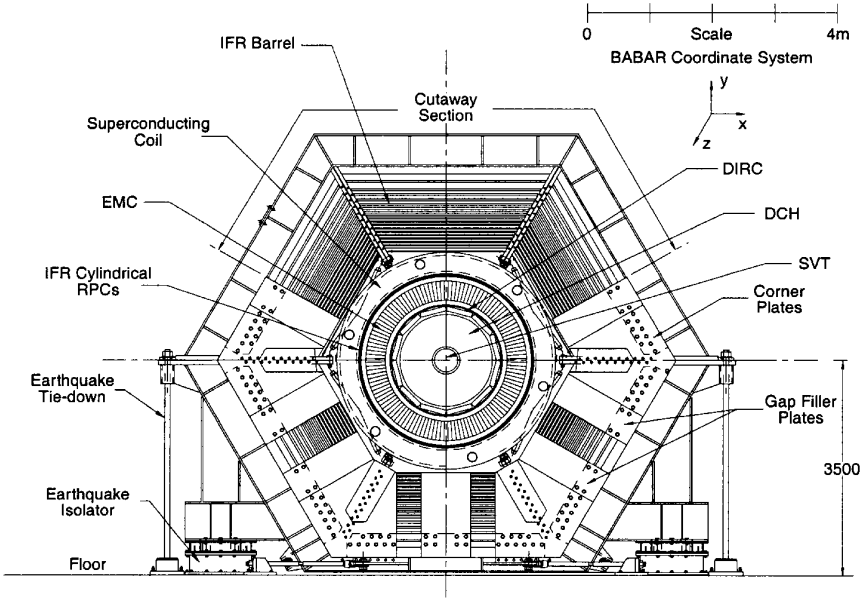

Fig. 6.4. The BABAR experiment front view [25]

detector more complicated, because they are positioned inside the detector. The boost of the $B\bar{B}$ pair in the lab frame is $\beta\gamma \simeq 0.55$.

Like in the Belle detector, the innermost subdetector serves for the identification of B decays. The silicon vertex tracker (SVT) consists of five layers of 300 μm thick, double-sided silicon at radii between 3.2 mm and 144 mm. For the readout strips measuring the z component, the readout pitch is 100 μm for layers 1 – 3 and 210 μm for layers 4 and 5. The readout pitch for the ϕ component is 100 μm for layers 1, 4, 5, and 110 μm for layers 2 and 3. With this vertex detector, a vertex resolution of 80 μm or better for fully reconstructed B mesons is achieved. The SVT has a total of 150 000 readout channels, an active silicon area of 0.96 m^2 and a combined efficiency of $\sim$97%.

At radii between 23.6 cm and 80.9 cm, the SVT is followed by the drift chamber (DCH). This consists of 40 layers of 11.9 mm $\times$ $\sim$19 mm hexagonal cells (total 7104), with 24 of these layers at small angles with respect to the z axis. The position resolution varies with the distance from the wire and is about 0.1 mm at 2–7 mm from the wire. This resolution increases to up to 0.25 mm at $<$ 2 mm from the wire and to up to 0.4 mm at 7–10 mm from the wire. The momentum resolution achieved is $\sigma_{p_t}/p_t = [(0.13 \pm 0.01)p_t \oplus (0.45 \pm 0.03)]\%$. The DCH also provides some information for particle identification by measuring the ionization energy loss with an rms resolution of the measured $\mathrm{d}E/\mathrm{d}x$ of $\sim$ 7.5%.

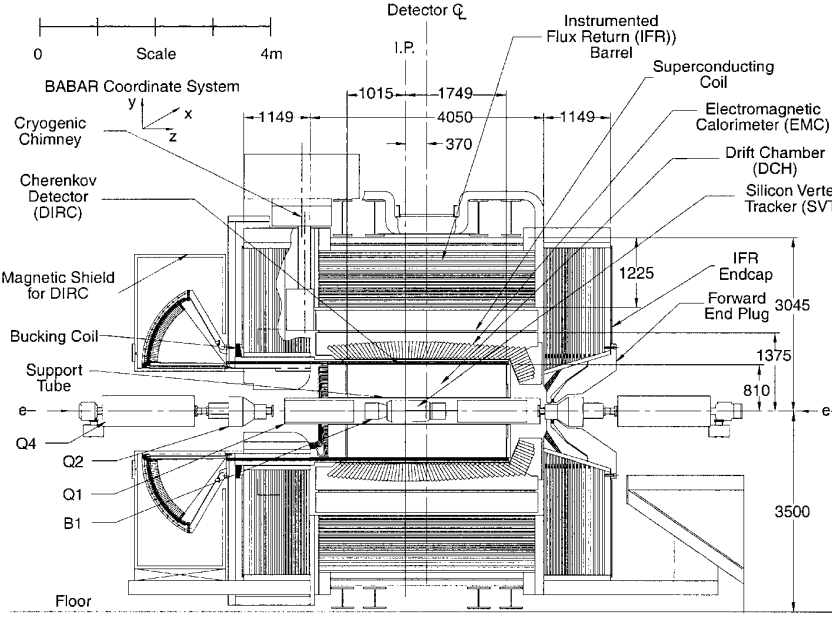

Fig. 6.5. The BABAR experiment side view [25]

The subdetector designed to provide a good π/K separation from 0.7 to 4 GeV is the detector of internally reflected Cerenkov light (DIRC). This novel detector consists of highly polished quartz bars (with a refractive index of $n = 1.473$) arranged regularly around the DCH, and a water-filled expansion volume for the Cerenkov ring covered with photomultiplier tubes (PMTs). Twelve quartz bars are grouped in hermetically sealed containers (bar boxes). The 12 bar boxes are arranged in a 12-sided polygonal barrel around the DCH. Each quartz bar is 17 mm thick, 35 mm wide and 4.9 m long (in four pieces, each 1.225 m long). At one end of the bar, a mirror reflects the Cerenkov light. At the other end of the bar, the light is emitted into an expansion volume (standoff box) filled with 6000 l of purified water (with a refractive index of $n = 1.346$). Each standoff box has 12 sectors for the PMTs, with 896 closely packed PMTs of 20 mm diameter per sector. The average resolution in the Cerenkov angle for a single track is about 2.5 mrad, resulting in a separation between kaons and pions of 4.2σ significance at 3 GeV/c and 2.5σ at 4.2 GeV/c.

The measurement of the energy of photons or electrons is done in the electromagnetic calorimeter (EMC). There is a total of 6580 thallium-doped (0.1%) CsI crystals, with 5760 crystals in the barrel part. The crystals have a front face of size 4.9×4.9 cm^2 and a back face of size 6.1×6.0 cm^2, with

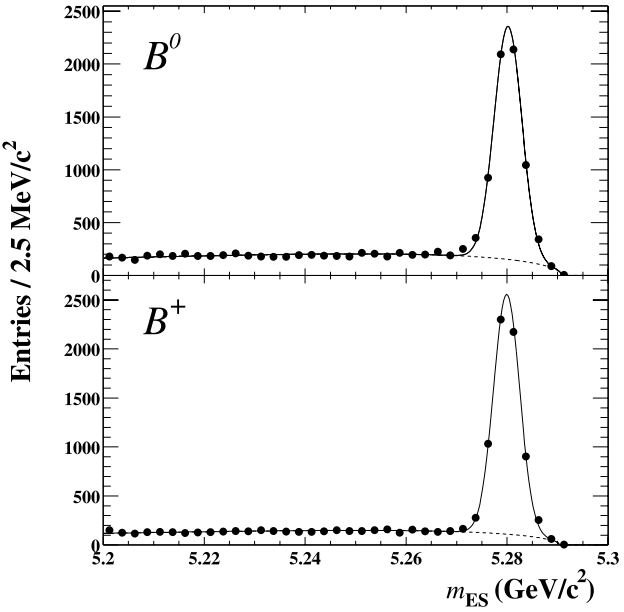

Fig. 6.6. $m_{\rm ES}$ distributions of the selected neutral (top) and charged (bottom) $\rm B_{rec}$ candidates.

a length in the forward direction of the detector of 32.4 cm and a length of 29.6 cm in the backward direction. The energy and position resolutions achieved with the EMC are

$$\frac{\sigma_E}{E} = \frac{(2.32 \pm 0.30)\%}{\sqrt[4]{E}} \oplus (1.85 \pm 0.04)\% \,, \tag{6.22}$$

$$\sigma_\theta = \sigma_\phi = \frac{3.67 \pm 0.07}{\sqrt{E}} \oplus (0.00 \pm 0.04) \text{ mrad} \,. \tag{6.23}$$

For π^0 mesons from $\rm B\overline{B}$ events, the mass resolution over the full range of photon energies is about 6.9 MeV.

All inner subdetectors are embedded in a superconducting magnet with a length of 3.5 m and a diameter of 3.1 m, providing a magnetic field of 1.5 T.

The instrumented flux return (IFR) detects neutral hadrons (primarily $\rm K_L$ and neutrons) and provides muon identification with high efficiency and good purity. The IFR consists of iron plates, which serve as the flux return for the magnet, and single-gap resistive plate chambers (RPCs), which serve as the active detectors. There are 19 layers with 342 modules in the barrel, and 18 layers with 432 modules in the two end doors. Between the EMC and the magnet cryostat, two layers of cylindrical RPCs with 32 modules are installed to detect particles exiting the EMC. An RPC consists of two 2 mm thick Bakelite sheets separated by a 2 mm gap, filled with a gas mixture with $\sim$8 kV across it.

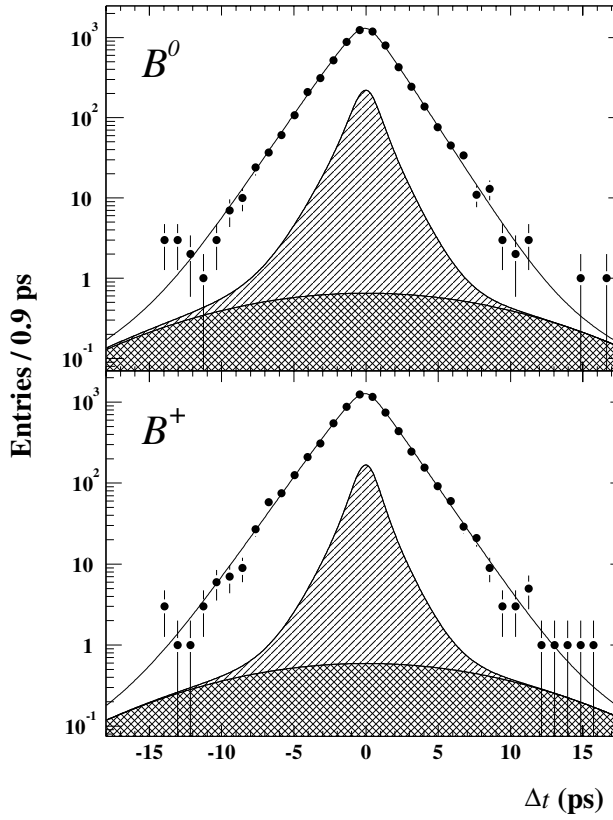

Fig. 6.7. Δt distribution for the B^0 (*top*) and B^+ (*bottom*) events within 2.5σ of the B mass in m_{ES}. The results of the fit are superimposed on the data. The *singly hatched areas* are the background components $\mathcal{B}$, and the *cross-hatched areas* represent the outlier contributions. (See [17])

6.5 Lifetime measurements

For charged B^+B^- meson pairs, the decay time distribution is exponential in the difference $\Delta t = t_2 - t_1$, of the decay times of the two mesons (6.19). A measurement of the B^+ lifetime therefore requires the kinematic reconstruction of hadronic decay modes. The reconstructed B^+ decay modes include $D^0\pi^+$, $D^{*0}\pi^+$, $J/\Psi K^+$ and $\Psi(2S)K^+$, and the charge-conjugate modes for the B^-. In the reconstruction, the beam energies are used as a constraint. For this purpose, the momenta of the decay particles are calculated in the center-of-mass system of the $\Upsilon(4S)$. Suppose that the B^+ decays into two particles with center-of-mass momenta $\boldsymbol{p}_1^*$ and $\boldsymbol{p}_2^*$; the "beam-energy-substituted mass" is then defined as

$$m_{ES} = \sqrt{\left(\frac{m_{\Upsilon(4S)}}{2}\right)^2 - (\boldsymbol{p}_1^* + \boldsymbol{p}_2^*)^2}\,. \tag{6.24}$$

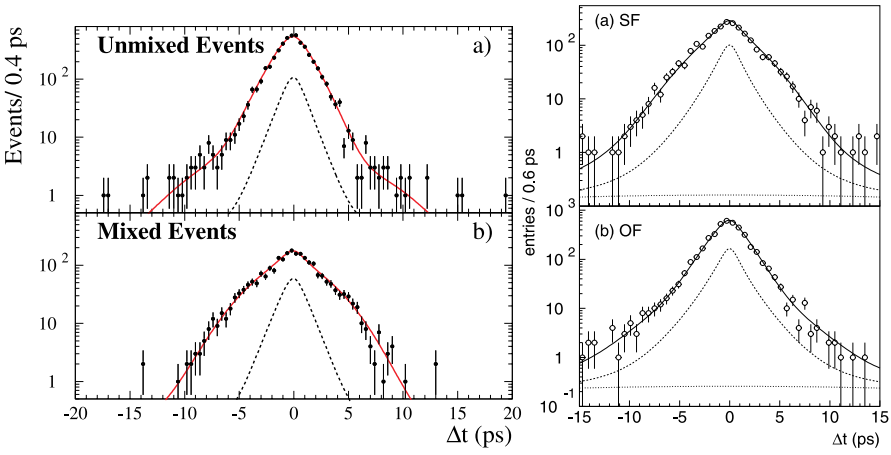

Fig. 6.8. Distributions of Δt in the data for selected (**a**) unmixed and (**b**) mixed events, with the likelihood fit (*solid*) and the contribution of the background (*dashed*) overlaid. *Left*, for the BABAR experiment [7], and *right* for the Belle experiment [9] (SF = same flavor; OF = opposite Flavor (unmixed events))

For a B decay, this mass has to agree with the B meson mass within the experimental resolution of about ±2.5 MeV. The second quantity defined is the "energy difference", which, for the example above, is

$$\Delta E = \boldsymbol{E}_1^* + \boldsymbol{E}_2^* - \frac{m_{\Upsilon(4S)}}{2} \,, \tag{6.25}$$

where $\boldsymbol{E}_1^*$ and $\boldsymbol{E}_2^*$ are the center-of-mass energies of the two decay particles. The definitions are modified for three or more decay particles.

Figure 6.6 shows, for samples of B^+B^- and $B^0\overline{B^0}$ candidate events, the m_{ES} distribution [17]. The corresponding distribution of Δt for these events is shown in Fig. 6.7, including a background of 7%. The lifetime is obtained from a fit of (6.19) to such a distribution for the charged B meson pairs. The lifetime distributions of neutral B mesons are more complicated, owing to oscillation phenomena, which have to be taken into account. However, if we add the time distributions for mixed and unmixed pairs given in (6.14), we obtain

$$\mathrm{d}N(\mathrm{B}^0) = 2C\mathrm{e}^{-\Gamma|\Delta t|}\mathrm{d}(\Delta t) \,, \tag{6.26}$$

which is again simply an exponential decay law. The results of the fits are

$$\begin{aligned} \tau_{\mathrm{B}^+} &= (1.673 \pm 0.032\ (\mathrm{stat}) \pm 0.023\ (\mathrm{syst}))\ \mathrm{ps} \,, \\ \tau_{\mathrm{B}^0_\mathrm{d}} &= (1.546 \pm 0.032\ (\mathrm{stat}) \pm 0.022\ (\mathrm{syst}))\ \mathrm{ps} \,, \end{aligned} \tag{6.27}$$

from the BABAR experiment.

The earlier measurements were averaged by the Particle Data Group (PDG) [19], and the present world averages are:

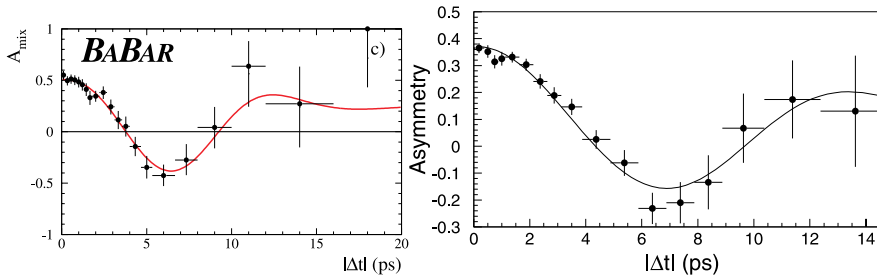

Fig. 6.9. *Left*: the time-dependent mixing asymmetry $\mathcal{A}_{\rm mix}(|\delta t|)$ observed by the BABAR experiment. *Right*: the observed time-dependent flavor asymmetry. The *curve* is the result of an unbinned maximum-likelihood fit. From the Belle experiment

$$\begin{aligned} \tau_{\rm B^+} &= (1.674 \pm 0.018)\ \text{ps}\ , \\ \tau_{\rm B^0_d} &= (1.542 \pm 0.016)\ \text{ps}\ , \\ \tau_{\rm B^0_s} &= (1.461 \pm 0.057)\ \text{ps}\ . \end{aligned} \tag{6.28}$$

6.6 Measurements of $\mathrm{B^0_d}$–$\overline{\mathrm{B^0_d}}$ Mixing

The mixing parameter Δm_d has been measured in e^+e^- collisions at LEP, SLD and the two new B factories. $\mathrm{B\overline{B}}$ pairs are produced in the $\Upsilon(4S)$ state, and the particle and antiparticle are identified by their decay to hadrons (jets) or to a final state containing leptons (e.g. $\mathrm{B} \to \mathrm{D}^{*+}\mathrm{X}l^-\overline{\nu}$). In this way, the probability of finding a BB or $\mathrm{\overline{BB}}$ pair ("like-sign events") can be compared with the total decay probability. The ratio of like-sign to total events, R, then shows a characteristic increase as the B mesons convert to $\overline{\mathrm{B}}$ and vice versa. The probabilities for flavor oscillation are given in (6.12) and (6.13) and Fig. 6.1.

Experimental data on this time dependence are shown in Fig. 6.8, from the BABAR experiment [7] and from the Belle experiment [9], for fully reconstructed, tagged B hadron pairs. The time-dependent asymmetry derived from these data is given in Fig. 6.9, again for both BABAR and Belle.

An alternative method for observing this time dependence is flavor tagging by observing leptons in the final state. This was also the method by which the ARGUS collaboration discovered $\mathrm{B^0_d}$–$\overline{\mathrm{B^0_d}}$ mixing. The beauty quark in the B meson is able to change its flavor by a weak semileptonic decay. The favored decay mode is $\overline{b} \to \overline{c}l^+\nu$, with a coupling strength $G_F|V_{cb}| \sim G_F \cdot 0.04$ (Chap. 7). The disfavored mode is $\overline{b} \to \overline{u}l^+\nu$, with a coupling strength $G_F|V_{ub}| \sim G_F \times 0.004$. In both cases, the b flavor is fixed by the sign of the lepton charge, which is either the muon or the electron charge. The total branching fraction for leptonic decays is 24%. There is also a cascade process, $b \to cX$ with $c \to dl^+\nu$, which yields a wrong-sign lepton with a

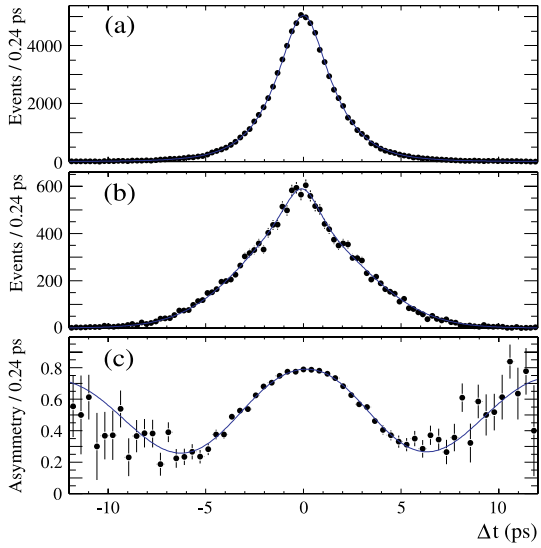

Fig. 6.10. Distributions of decay time difference for (**a**) opposite-sign and (**b**) same-sign dilepton events; (c) asymmetry between opposite- and same-sign dilepton events. The *points* are data and the *lines* correspond to the fit result. (BABAR experiment [8])

20% branching fraction, which reduces the accuracy of the tagging method. Another competing process, $b \to (c\overline{c})X$ with subsequent decay $(c\overline{c}) \to e^+e^-$ or $\mu^+\mu^-$, is much less frequent, with only a 1% branching fraction. If the fraction of leptons with the wrong charge from these sources is f, then the asymmetry is diluted by a factor $(1-2f)$, as in (6.15).

Data on the time dependence of opposite-sign and same-sign leptonic B pair decays from the BABAR experiment [8] are shown in Fig. 6.10. Similar data from the Belle experiment [10] display also the small amount of background (Fig. 6.11).

Alternative flavor-tagging methods use kaon tagging, jet charge tagging or same jet tags [11].

Kaon tagging is based on the appearance of a charged Kaon in the decay of a B meson, because the b quark decays predominantly to a c quark and this in turn decays predominantly to an s quark, which can hadronize as a K^- meson. Also, the direct process $b \to s$ is possible through a penguin graph. Here also, however competing processes dilute the tagging quality by producing a K^+, e.g. via the process $b \to XW^-$ and $W^- \to \overline{c} \to \overline{s} \to K^+$.

Jet charge tagging is based on the idea of measuring the charge of the b quark by statistical methods. For this purpose, a jet charge

$$Q_F = \frac{\sum_i W_i Q_i}{\sum W_i} \tag{6.29}$$

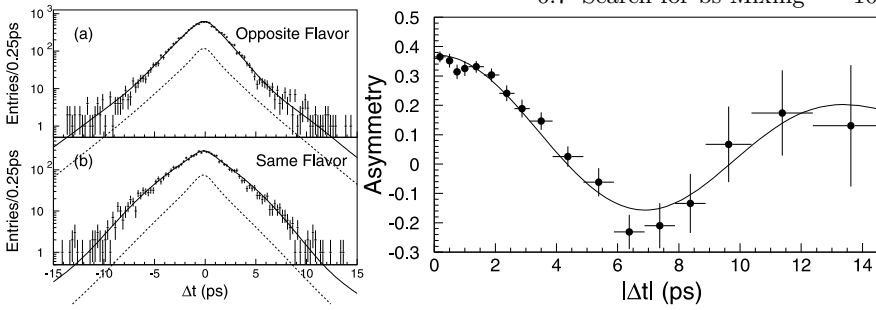

Fig. 6.11. *Left*: the Δt distributions for (**a**) opposite-flavor and (**b**) same-flavor dilepton events. The *solid lines* are the unbinned maximum-likelihood fits. The *dashed lines* show the background distribution. *Right*: the observed time-dependent flavor asymmetry. The *curve* is the result of an unbinned maximum-likelihood fit. (Belle experiment [10])

is defined by summing over the charges Q_i of jet particles weighted, for example, by their momentum. A practical example a weighting function is a power of the momentum component $p_\parallel$ parallel to the jet axis, $p_\parallel^{0.6}$.

Same-jet tags include the identification of a b flavored excited state which decays in accordance $\mathrm{B}^{**} \rightarrow \mathrm{B}\pi$. The π meson flies close to the direction of the B meson and can be identified. Another possibility is the definition of a jet charge for the remnant jet without the leading B^0 particle.

All these tagging methods can be used for identifying $\mathrm{B}\overline{\mathrm{B}}$ meson pairs and for measuring the oscillatory time behavior of $\mathrm{B_d}$ mesons. The fully reconstructed hadronic decays and the dileptonic events contribute most to the precision in the oscillation parameter Δm_d. The current world average for this is [20]

$$\Delta m_d = (0.489 \pm 0.008)\,\mathrm{ps}^{-1}\ . \tag{6.30}$$

Since the $\mathrm{B_d^0}$ lifetime is (1.542 ± 0.016) ps, the value of x_d is $\sim 0.76 \pm 0.02$. This is of similar magnitude to the value in the neutral kaon system, $x_\mathrm{K} = 0.945 \pm 0.002$. However, since the mass of the $\mathrm{B_d^0}$ meson is so large, the number of final states for decay is very similar for the two $\mathcal{CP}$ eigenstates B_h and B_l, and hence their lifetime is approximately the same, i.e. $\Gamma_h = \Gamma_l$, very different from the kaon system. Therefore, for the $\mathrm{B_d^0}$ system, $|y| \leq 0.01$, while for the kaon system, $y = -0.9966$.

6.7 Search for $\mathrm{B_s^0}$ Mixing

In principle, neutral $\mathrm{B_s^0} = (\overline{b}s)$ mesons can mix in a similar way to $\mathrm{B_d^0} = \overline{b}d$ mesons. In the box diagrams for $\mathrm{B_s^0}$ mixing, the d quark has to be replaced by an s quark (Fig. 6.12).

The expression for the mixing parameter x_s is similar to that in (6.16), except that all quantities related to the $\mathrm{B_d^0}$ meson are replaced by those for

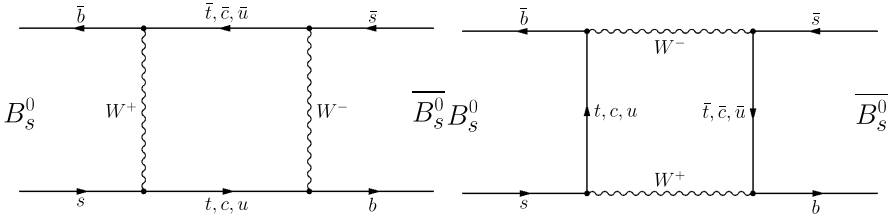

Fig. 6.12. Box diagrams for mixing between B_s^0 and $\overline{B_s^0}$ mesons

the B_s^0 meson, and the weak quark-coupling matrix elements are now $|V_{tb}^* V_{ts}|^2$ (see (7.26)).

The ratio of the mixing parameters x_s/x_d depends mainly on the ratio of these couplings, and therefore on $|V_{ts}/V_{td}|^2$. From the unitarity of the 3×3 CKM matrix and from experimental data on other decays, we deduce (Chap. 7) that this ratio is larger than 9 with a 90% confidence level. This means that we expect the mass difference Δm_s and the mixing parameter $\Delta m_s/\Gamma_s$ to be correspondingly larger, i.e. $x_s > 4.5$.

Therefore the B_s^0 oscillations are much faster than the B_d^0 oscillations, and harder to observe. The oscillation pattern obtained from (6.8) and (6.9), assuming $x_s = 15$, $y_s = 0.1$ and $|q/p| = 1$, is shown in Fig. 6.13.

After an initial hint from the UA1 collaboration of a time-integrated mixing probability of 0.12 ± 0.05, the LEP experiments ALEPH, DELPHI and OPAL, the SLD experiment at SLC, and the CDF experiment at Fermilab set out to measure this oscillation. The values of the B_s^0 oscillation amplitude A obtained from these five experiments were combined; the result is shown in Fig. 6.14. The amplitude A is 1 for true oscillations. A 95% C.L. lower limit can be calculated from the point where the $A = 1$ line crosses the 1.645σ line

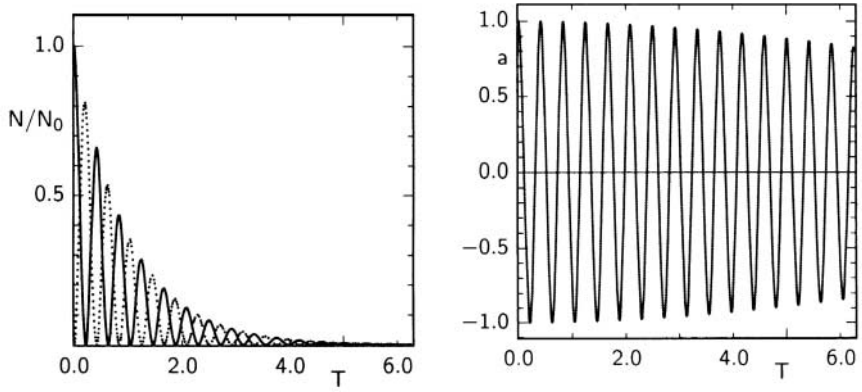

Fig. 6.13. *Left*: number of B_s^0 (*solid line*) and $\overline{B_s^0}$ (*dotted line*) mesons as a function of the unified time variable $T = \Gamma_{B_s^0} t$ for an initially pure B_s^0 state. *Right*: asymmetry function $a(T)$

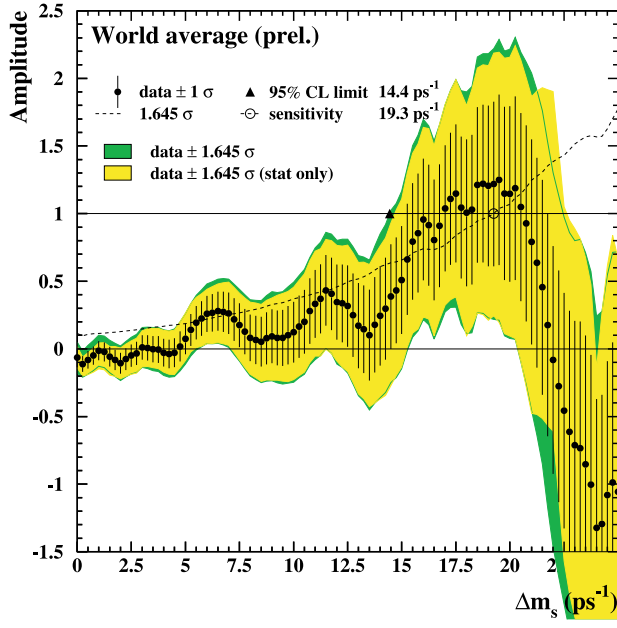

Fig. 6.14. Amplitude for B_s^0–$\overline{B_s^0}$ oscillations as a function of the oscillation frequency Δm_s [12]

from the data. While the most sensitive single experiments obtain a limit of $\Delta m_s > 6.6$ ps^{-1}, the combined fit gives a limit of $\Delta m_s > 14.4$ ps^{-1}, at 95% C.L. Using the B_s^0 lifetime $\tau_s = (1.47 \pm 0.06)$ ps, this present lower limit corresponds to a limit on the mixing parameter

$$x_s > 21 \quad \text{at 95\% C.L.} \tag{6.31}$$

In addition, the lifetime distribution of B_s^0 decays has been studied in order to look for evidence for two different lifetimes of the heavy and light mesons. No evidence has been seen, and an upper limit on $y = \Delta\Gamma/2\Gamma$ has been derived [13]:

$$|y_s| < 0.24 \quad \text{at 95\% C.L.} \tag{6.32}$$

6.8 Experiments on $\mathcal{CP}$ Violation in B^0 Decays

The most salient manifestation of $\mathcal{CP}$ violation in the $B^0/\overline{B^0}$ system is expected to be in the interference of mixing and decay, as discussed in Chap. 3. The largest effect is expected if we choose a $\mathcal{CP}$ eigenstate as the final state for the decay. Examples are the $\mathcal{CP}$ $(+1)$ state $\pi^+\pi^-$ (with angular momentum zero) and the $\mathcal{CP}$ (-1) state $J/\Psi K_S$. Here the $\mathcal{CP}$ eigenvalue of the J/Ψ

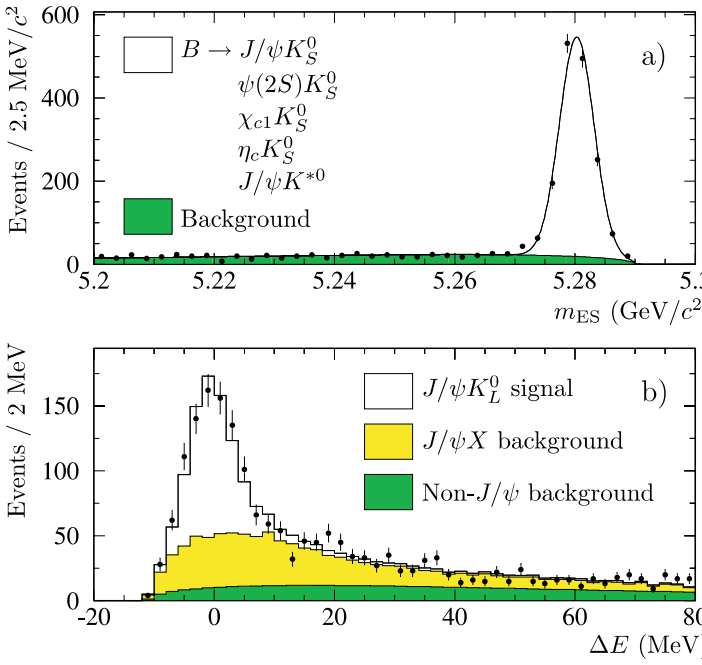

Fig. 6.15. Distributions for $B_{\mathcal{CP}}$ candidates satisfying the tagging and vertexing requirements: (**a**) $m_{\rm ES}$ for the final states $J/\Psi \mathrm{K_S}$, $\Psi(2\mathrm{S})\mathrm{K_S}$, $\chi_{c1}\mathrm{K_S}$, $\eta_c \mathrm{K_S}$ and $J/\Psi \mathrm{K}^{*0}$ ($\mathrm{K}^{*0} \to \mathrm{K_S}\pi^0$), and (**b**) ΔE for the final state $J/\Psi \mathrm{K_L}$. (BABAR experiment [21])

is $+1$, $\mathcal{CP}\,(\pi\pi) = +1$, and the angular momentum between the two systems (J/Ψ) and $\pi\pi$ must be $l = 1$ because the spins are $J(B) = J(K) = J(\pi\pi) = 0$ and $J(J/\Psi) = 1$.

We introduce as in (3.36) the decay amplitudes

$$\begin{aligned} A_f &= \langle f|T|\mathrm{B}^0\rangle \,, \\ \overline{A_f} &= \langle f|T|\overline{\mathrm{B}^0}\rangle \,. \end{aligned} \tag{6.33}$$

Using (6.4), we obtain the decay rates of initially pure B^0 and $\overline{\mathrm{B}^0}$ states:

$$\begin{aligned} \frac{\mathrm{d}N(t)}{\mathrm{d}t} &= \frac{1}{4}\left|\left(\mathrm{e}^{-\gamma_h t} + \mathrm{e}^{-\gamma_l t}\right) A_f - \frac{q}{p}\left(\mathrm{e}^{-\gamma_h t} - \mathrm{e}^{-\gamma_l t}\right)\overline{A_f}\right|^2 \,, \\ \frac{\mathrm{d}\overline{N}(t)}{\mathrm{d}t} &= \frac{1}{4}\left|\left(\mathrm{e}^{-\gamma_h t} + \mathrm{e}^{-\gamma_l t}\right)\overline{A_f} - \frac{p}{q}\left(\mathrm{e}^{-\gamma_h t} - \mathrm{e}^{-\gamma_l t}\right) A_f\right|^2 \,. \end{aligned} \tag{6.34}$$

Using the ratio (3.38)

$$\lambda = \frac{q\overline{A_f}}{pA_f} \tag{6.35}$$

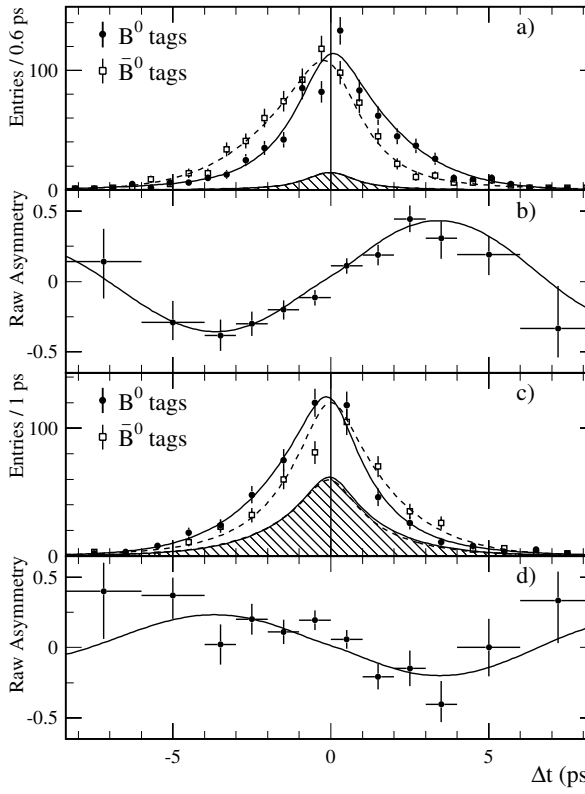

Fig. 6.16. (**a**) number of $\eta_f = -1$ candidates ($J/\Psi \mathrm{K_S}$, $\Psi(2\mathrm{S})\mathrm{K_S}$, $\chi_{c1}\mathrm{K_S}$, and $\eta_c \mathrm{K_S}$) in the signal region with a B^0 tag N_{B^0} and with a $\overline{\mathrm{B}^0}$ tag $N_{\overline{\mathrm{B}^0}}$, and (**b**) the raw asymmetry $(N_{\mathrm{B}^0} - N_{\overline{\mathrm{B}^0}})/(N_{\mathrm{B}^0} + N_{\overline{\mathrm{B}^0}})$, as functions of Δt. The *solid* and *dashed* curves represent the projection of the fit onto Δt for B^0 and $\overline{\mathrm{B}^0}$ tags, respectively. The *shaded regions* represent the background contributions. (**c**) and (**d**) contain the corresponding information for the $\eta_f = +1$ mode $J/\Psi \mathrm{K_L}$. (BABAR experiment [21])

and the approximate relations $\Gamma_h = \Gamma_l = \Gamma$ and $|q/p| = 1$, and defining $\Delta T = \Gamma\, \Delta t$ and $x = \Delta m\, \Gamma$ we obtain the following for the decay rates as a function of the time difference Δt, for B^0 tags and $\overline{\mathrm{B}^0}$ tags:

$$\frac{\mathrm{d}N(t)}{\mathrm{d}t} = \frac{|A_f|^2}{2} \mathrm{e}^{-\Delta T} \left[1 + \frac{1-|\lambda|^2}{1+|\lambda|^2} \cos(x\,\Delta T) - \frac{2\,\Im m\,\lambda}{1+|\lambda|^2} \sin(x\,\Delta T) \right] ,$$
$$\frac{\mathrm{d}\overline{N}(t)}{\mathrm{d}t} = \frac{|A_f|^2}{2} \mathrm{e}^{-\Delta T} \left[1 - \frac{1-|\lambda|^2}{1+|\lambda|^2} \cos(x\,\Delta T) + \frac{2\,\Im m\,\lambda}{1+|\lambda|^2} \sin(x\,\Delta T) \right] . \tag{6.36}$$

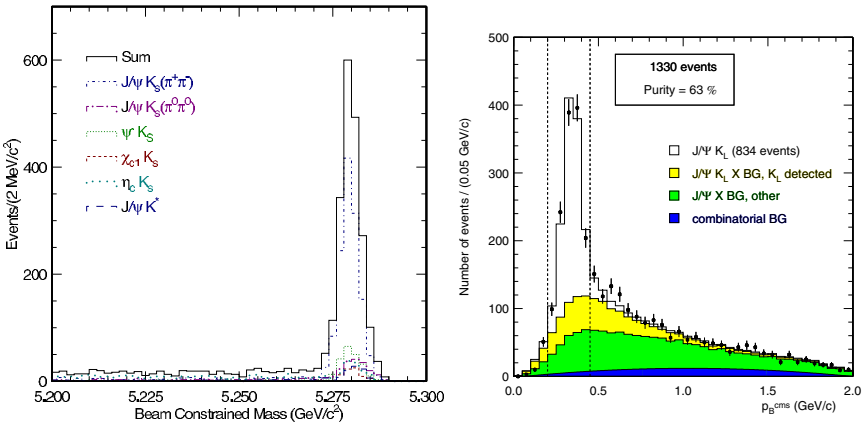

Fig. 6.17. The beam-energy-constrained mass distribution for all decay modes other than $J/\Psi \mathrm{K_L}$ (*left*). The $p_\mathrm{B}^\mathrm{cms}$ distribution for $\mathrm{B}^0 \to J/\Psi \mathrm{K_L}$ candidates, together with the results of the fit (*right*). (Belle experiment [22])

If f is a $\mathcal{CP}$ eigenstate, then $|\lambda| = 1$. In particular, for the final state $f = J/\Psi \mathrm{K_S}$, this yields [14]

$$\lambda_f = \mathrm{e}^{2\mathrm{i}\beta} \ , \tag{6.37}$$

and we obtain:

$$\begin{aligned} \frac{\mathrm{d}N(t)}{\mathrm{d}t} &= \frac{1}{2}\Gamma \mathrm{e}^{-\Gamma\Delta t}\left[1 - \sin(2\beta)\sin(\Delta m_d\,\Delta t)\right] \ , \\ \frac{\mathrm{d}\overline{N}(t)}{\mathrm{d}t} &= \frac{1}{2}\Gamma \mathrm{e}^{-\Gamma\Delta t}\left[1 + \sin(2\beta)\sin(\Delta m_d\,\Delta t)\right] \ . \end{aligned} \tag{6.38}$$

The decay asymmetry becomes

$$a_f(\Delta t) = \frac{\mathrm{d}\overline{N} - \mathrm{d}N}{\mathrm{d}\overline{N} + \mathrm{d}N} = \sin(2\beta)\sin(\Delta m_d\,\Delta t) \ . \tag{6.39}$$

The time integral over the asymmetry a_f vanishes, but a time-dependent measurement in an asymmetric B factory can reveal the effect. If other final states with a $\mathcal{CP}$ eigenvalue η_f are considered, the expression on the right-hand side for the asymmetries is multiplied by $(-\eta_f)$.

The experiment proceeds in the following way: events of the topology shown in Fig. 6.2 are selected by identifying lepton pairs (e^+e^- or $\mu^+\mu^-$) with the invariant mass of the J/Ψ, 3.1 GeV, and $\pi^+\pi^-$ pairs with the K^0 mass. From the J/Ψ and K, the first B^0 meson is reconstructed. The second B meson is flavor-tagged by identifying a lepton charge or a kaon charge. For both B mesons, the z position of the vertex along the beam direction is measured. The difference $z_2 - z_1$ gives the time difference between the two decays, $\Delta t = (z_2 - z_1)/\beta\gamma c$, and the distributions in the variable Δt for

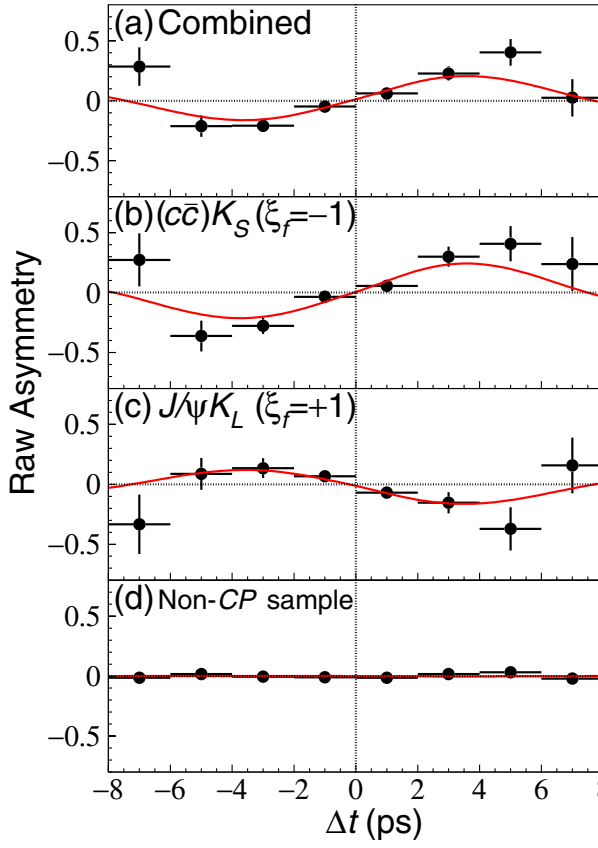

Fig. 6.18. (**a**) The raw asymmetry for all modes combined. The asymmetry for $J/\Psi \mathrm{K_L}$ and $J/\Psi \mathrm{K}^{*0}$ has been inverted to account for the opposite $\mathcal{CP}$ eigenvalue. The corresponding plots for (**b**) $(c\bar{c})\mathrm{K_S}$, (**c**) $J/\Psi \mathrm{K_L}$ and (**d**) non-$\mathcal{CP}$ control samples are also shown. The *curves* are the results of an unbinned maximum-likelihood fit applied separately to the individual data samples. (Belle experiment [22])

mixed and unmixed events, (6.38), and of their asymmetry (6.39), yield a measurement of the coefficient $\sin(2\beta)$ in front of the $\sin(\Delta m_d\, t)$ function. Backgrounds and mistagging have to be taken into account.

Such measurements have been presented by the BABAR collaboration. This collaboration used a sample of 88 million $\Upsilon(4\mathrm{S}) \to \mathrm{B\overline{B}}$ decays collected between 1999 and 2002 at the PEP-II asymmetric B factory [21]. Events with one neutral B meson fully reconstructed in a J/Ψ decay mode and the other B meson flavor-tagged by its decay products were studied. Five different decay modes into final states with definite $\mathcal{CP}$ eigenvalues are relevant for the analysis: $J/\Psi \mathrm{K_S}, \Psi(2S)\mathrm{K_S}$, $\chi_{c1}\mathrm{K_S}$ and $\eta_c \mathrm{K_S}$, with $\mathcal{CP}$ eigenvalues $\eta_f = -1$ (1506 events), and $J/\Psi \mathrm{K_L}$ with $\eta_f = +1$ (988 events).

Events were selected by two cuts in the "energy-substituted mass" $m_{\rm ES}$ and the "energy difference" ΔE, as defined in Sect. 6.5 ((6.24) and (6.25)). The distributions of candidates for B decay to $\mathcal{CP}$ eigenstates are shown in Fig. 6.15. Figure 6.15a contains the $m_{\rm ES}$ distribution for states with $\eta_f = -1$, and Fig. 6.15b the ΔE distribution for the final state $J/\Psi \mathrm{K_L}$ with $\eta_f = +1$. Also indicated is the amount of background and a simulation of the resolution for both quantities.

The time distributions of $\mathrm{B^0}$-tagged and $\overline{\mathrm{B^0}}$-tagged events are shown in Fig. 6.16a for the final states with $\eta_f = -1$, and the corresponding asymmetry as a function of Δt is given in Fig. 6.16b. From these, an unbinned maximum-likelihood fit yields a value of $\sin 2\beta$ of 0.76 ± 0.07. Figures 6.16c, d display the analogous distributions for events with $\eta_f = +1$. Here the value of $\sin 2\beta = 0.72 \pm 0.16$. Combining all channels, the result is

$$\sin 2\beta = 0.741 \pm 0.067\ (\mathrm{stat}) \pm 0.034\ (\mathrm{syst})\ . \tag{6.40}$$

The Belle experiment has collected 85 million $\mathrm{B\overline{B}}$ events [22]. Similarly to what was done by BABAR , each B meson decay to a $\mathcal{CP}$ eigenstate was reconstructed, and the accompanying B meson was identified from its decay products. The $\eta_f = -1$ states are $J/\Psi \mathrm{K_S}, \Psi(2\mathrm{S})\mathrm{K_S}, \chi_{c1}\mathrm{K_S}$ and $\eta_c \mathrm{K_S}$, and the $\eta_f = +1$ state is $J/\Psi \mathrm{K_L}$. The beam-energy-constrained mass $m_{\rm ES}$ for all decay modes except $J/\Psi \mathrm{K_L}$ is shown in Fig. 6.17a. For the $J/\Psi \mathrm{K_L}$ candidates, the B momentum in the $\Upsilon(4\mathrm{S})$ center-of-mass system, $p_{\rm B}^{\rm cms}$, is depicted in Fig. 6.17b. Also indicated is the cut applied and the background simulation. From this sample, the time difference Δt was calculated for each event, for B-tagged and $\overline{\mathrm{B}}$-tagged pairs. Figure 6.18 shows the asymmetry of the two distributions for three classes of events: Fig. 6.18b, charmonium–$\mathrm{K_S}$ events with $\eta_f = -1$; Fig. 6.18c, $J/\Psi \mathrm{K_L}$ events with $\eta_f = +1$; and Fig. 6.18d, non-$\mathcal{CP}$ sample as a check. Fig. 6.18a shows the combined $\sin(x\,\Delta T)$ distribution. The $J/\Psi \mathrm{K_S}$ events yield $\sin 2\beta = 0.73 \pm 0.10$, the $J/\Psi \mathrm{K_L}$ events 0.78 ± 0.17. Combining all available information, the authors of [22] obtain

$$\sin 2\beta = 0.719 \pm 0.074\ (\mathrm{stat}) \pm 0.035\ (\mathrm{syst})\ . \tag{6.41}$$

The two experiments together give an average experimental value

$$\sin 2\beta = 0.731 \pm 0.055\ . \tag{6.42}$$

This is a clear observation of $\mathcal{CP}$ violation (through interference of oscillation and decay) in a second meson system. At the same time, this measurement determines, with little theoretical uncertainty, one of the angles in the unitarity triangle called β by BABAR and ϕ_1 by Belle. There are two solutions for this angle, $\beta_1 = (23.5 \pm 2.4)^\circ$ and $\beta_2 = (66.5 \pm 2.4)^\circ$. The lower solution agrees perfectly with the CKM unitary triangle, as determined from other sources (see Chap. 7). Another possibility to measure the angle β/ϕ_1 is the decay of the $\mathrm{B^0_d}$ meson to the $\mathcal{CP}$ eigenstate $\phi\ \mathrm{K_S}$. The corresponding asymmetry

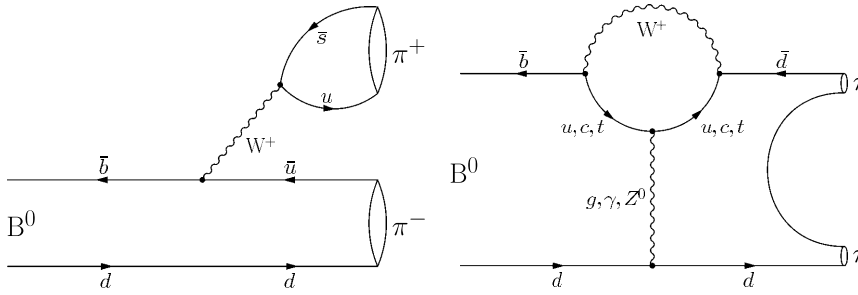

Fig. 6.19. Tree and penguin diagrams for the decay $B^0 \to \pi^+\pi^-$.

has been measured by the Belle and the BABAR collaborations [23]. The two collaborations obtain for $\sin 2\beta$ the values $+0.45 \pm 0.43\,(stat) \pm 0.07\,(syst)$ (BABAR) and $-0.96 \pm 0.50\,(stat) \pm 0.10\,(syst)$ (Belle). Clearly, the two results do not agree. The apparent deviation of the Belle value from the value (6.42) expected from the other measurements in the CKM scheme (see Chap. 7) remains, at this time, an open problem. The observation of direct $\mathcal{CP}$ violation in the B^0 system is much more difficult. It requires a measurement of the decay asymmetry in the decay $B^0 \to \pi^+\pi^-$, equivalent to a determination of the second angle in the unitarity triangle, called α by BABAR and ϕ_2 by Belle.

6.9 Search for Direct $\mathcal{CP}$ Violation in B^0 Decays

This search is performed by a measurement of the decay asymmetry in $B^0 \to \pi^+\pi^-$ decays. Unfortunately, the branching ratio is very small.

The decay can proceed through a tree diagram $b \to u\overline{u}d$, with an amplitude A_T proportional to $V_{ub}^* V_{ud}$ and through a penguin diagram $b \to d$, with an amplitude A_P proportional to $V_{tb}^* V_{td}$ (Fig. 6.19). The parameter λ for this final state is

$$\lambda_{\pi\pi} = \frac{q}{p}\frac{\overline{A_T} + \overline{A_P}}{A_T + A_P} \,. \tag{6.43}$$

The weak phases in the $\mathcal{CP}$ violation arising from the interference of A_T and A_P are given by the angle α:

$$\left(\frac{V_{ub}V_{ud}^*}{V_{tb}V_{td}^*}\right) = -e^{i\alpha}\left|\frac{V_{ub}V_{ud}}{V_{tb}V_{td}}\right| \,. \tag{6.44}$$

In the limit of vanishing penguin contributions, λ would be simply given by

$$\lambda = e^{2i\alpha} \,. \tag{6.45}$$

However, the "penguin pollution" makes the interpretation of an observed asymmetry more difficult. There are theoretical calculations described in [15] which relate the observed effective angle $\alpha_{\rm eff}$ to the true angle α.

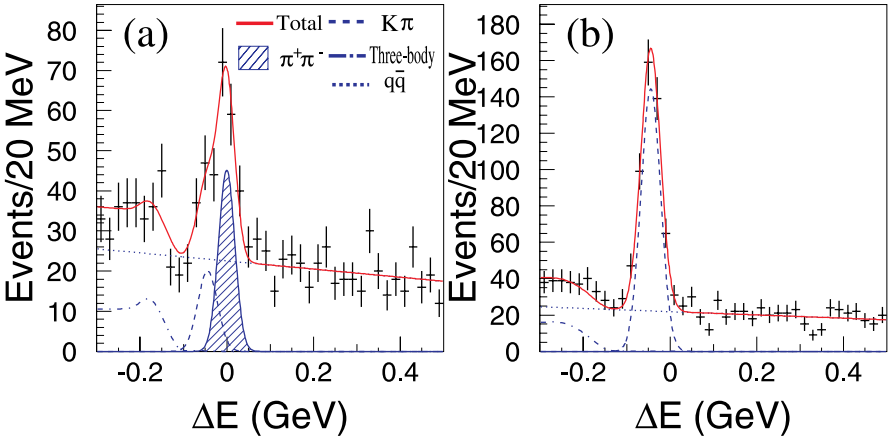

Fig. 6.20. ΔE distributions for (**a**) $\mathrm{B}^0 \to \pi^+\pi^-$ and (**b**) $\mathrm{B}^0 \to \mathrm{K}^+\pi^-$ candidates (see [16])

An alternative way to measure α is to use the decay channel $\mathrm{B}^0 \to \varrho\pi$, with common final states for B^0 and $\overline{\mathrm{B}^0}$ decay, $\pi^+\pi^-\pi^0$ and $\pi^0\pi^0\pi^0$.

Experiments on the decay $\mathrm{B}^0 \to \pi^+\pi^-$ have been done at the two B factories.

The Belle experiment, from data [16] with an integrated luminosity of 78 fb^{-1}, has reconstructed $\mathrm{B}\overline{\mathrm{B}}$ pairs that decayed to a $\pi^+\pi^-$ $\mathcal{CP}$ eigenstate, and the other B meson was identified from inclusive properties. The two vertex positions were constructed from information provided by the silicon vertex detector about the tracks. From this information, the decay time difference Δt was calculated. The decay rates for flavor $\mathbb{B} = +1$ (which tags a B^0) and $\mathbb{B} = -1$ (which tags a $\overline{\mathrm{B}^0}$) are

$$\mathrm{d}N(\Delta t) = \frac{\mathrm{e}^{-\frac{|\Delta t|}{\tau_\mathrm{B}}}}{4\tau_\mathrm{B}} \left[1 + \mathbb{B}\left\{S_{\pi\pi}\sin(\Delta m_d\,\Delta t) + A_{\pi\pi}\cos(\Delta m_d\,\Delta t)\right\}\right] , \quad (6.46)$$

where

$$S_{\pi\pi} = \frac{2\,\Im m\,\lambda}{|\lambda|^2 + 1} \quad (6.47)$$

and

$$A_{\pi\pi} = \frac{|\lambda|^2 - 1}{|\lambda|^2 + 1} . \quad (6.48)$$

B events were selected by a cut in the beam-constrained mass, $5271 < m_{\mathrm{ES}} < 5287$ MeV, and in the energy difference ΔE, $-0.3 < \Delta E < 0.5$ GeV. $\mathrm{B}^0 \to \mathrm{K}^+\pi^-$ candidates were collected at the same time, by identifying one track as a kaon and the other track as a pion in the Cerenkov detector. The ΔE distributions for $\pi\pi$ and $\mathrm{K}\pi$ events are shown in Fig. 6.20. The remaining

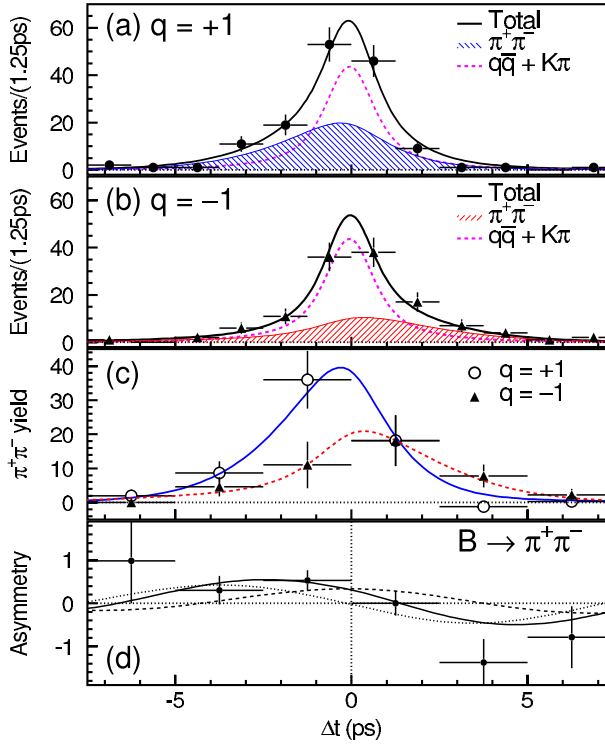

Fig. 6.21. The raw, unweighted Δt distributions for the 275 tagged $B^0 \to \pi^+\pi^-$ candidates: (**a**) 148 candidates with $q = +1$, i.e. the tag side was identified as B^0; (**b**) 127 candidates with $q = -1$; (**c**) $B^0 \to \pi^+\pi^-$ yields after background subtraction; (**d**) the $\mathcal{CP}$ asymmetry for $B^0 \to \pi^+\pi^-$ after background subtraction. In (**a**)–(**d**), the *curves* show the results of the unbinned maximum-likelihood fit to the Δt distributions of the 760 $B^0 \to \pi^+\pi^-$ candidates. In (**d**), the *solid curve* shows the resultant $\mathcal{CP}$ asymmetry, while the *dashed* and *dotted curves* show the contributions from the *cosine* and *sine* terms, respectively

sample consists of 760 $B^0 \to \pi^+\pi^-$ candidates. The raw Δt distributions for 148 B^0-tagged and 127 $\overline{B^0}$-tagged events are shown in Fig. 6.21. The result of the fit is

$$\begin{aligned} A_{\pi\pi} &= 0.77 \pm 0.27\ (\text{stat}) \pm 0.08\ (\text{syst})\ , \\ S_{\pi\pi} &= -1.23 \pm 0.41\ (\text{stat})^{+0.08}_{-0.07}\ (\text{syst})\ . \end{aligned} \tag{6.49}$$

The value of $S_{\pi\pi}$ is nonzero by three standard deviations, indicating $\mathcal{CP}$ violation. The corresponding experiment by the BABAR collaboration [26], with similar sensitivity, finds values which differ from those above,

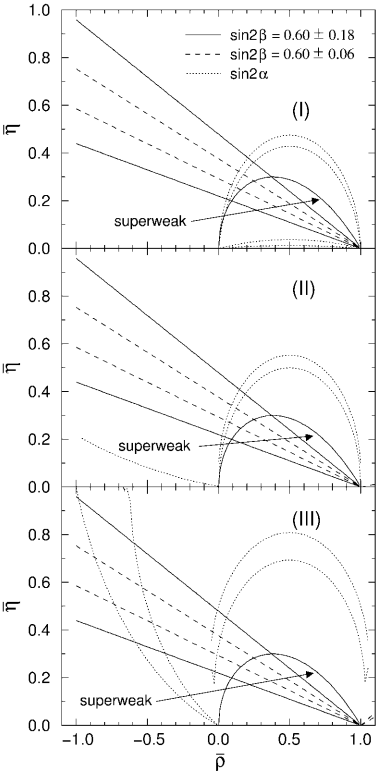

Fig. 6.22. Determination of the unitarity triangle in the $(\bar{\varrho}, \bar{\eta})$ plane by measuring $\sin(2\beta)$ and $\sin(2\alpha)$, For $\sin(2\alpha)$, we always find two solutions in the$(\bar{\varrho}, \bar{\eta})$ plane, and for $\sin(2\beta)$ we use only the solution consistent with $\mid V_{ub}/V_{cb} \mid \leq 0.1$. (See [6])

$$A_{\pi\pi} = 0.30 \pm 0.25 \pm 0.04 \,,$$
$$S_{\pi\pi} = 0.02 \pm 0.34 \pm 0.05 \,. \tag{6.50}$$

At this moment, it is therefore not yet possible to draw a conclusion about $\mathcal{CP}$ violation in this decay mode, or about the angle α or θ_2.

Using the constraints on the unitarity triangle from other experimental measurements (see Chap. 7), one can deduce that $\sin 2\alpha = -0.25 \pm 0.26$, which could give rise to a large decay asymmetry in $\mathrm{B}^0 \to \pi^+\pi^-$.

How it is possible, then, in the B meson system, to disentangle $\mathcal{CP}$ violation through mixing from the direct $\mathcal{CP}$ violation through the "Standard Model" KM mechanism? The answer is that one needs *two* precise angle measurements in order to see whether the upper corner of the unitarity triangle falls in a region allowed by the superweak model. This region, a curve from the point $(0, 0)$ to the point $(1, 0)$ in the $(\bar{\rho}, \bar{\eta})$ plane, is the geometrical location where $\sin 2\beta = -2 \sin 2\alpha$. If the corner falls in this region, then it is impossible to

distinguish the superweak $\mathcal{CP}$ violation from violation through the KM mechanism ("$\mathcal{CP}$ conspiracy"). This happens for $\bar{\rho} > 0$ and $\bar{\eta} = (1-\bar{\rho})[\bar{\rho}/(2-\bar{\rho})]^{1/2}$, and this corresponds to the curve labeled "superweak" in Fig. 6.22 [6, 27]. Clearly, the measurement of one angle, say β, alone cannot exclude the superweak model.

References

1. H. Albrecht *et al.*, *Phys. Lett.*B **192**, 245 (1987) 95
2. C. Albajar *et al.*, *Phys. Lett.*B **186**, 247 (1987); erratum *Phys. Lett.*B, **197**, 565 95
3. J. M. Gaillard, B. Lee, *Phys. Rev.*D **10**, 897 (1974) 98
4. I. I. Bigi, A. I. Sanda, *$\mathcal{CP}$ Violation*, Cambridge University Press, Cambridge (2000) 98
5. G. C. Branco, L. Lavoura, J. P. Silva, *$\mathcal{CP}$ Violation*, Oxford University Press, Oxford (1999) 98
6. A. J. Buras *et al.*, *Phys. Rev.*D **50**, 3433 (1994) 120, 121
7. B. Aubert *et al.*, *Phys. Rev. Lett.* **88**, 221802 (2002) 106, 107
8. B. Aubert *et al.*, *Phys. Rev. Lett.* **88**, 221803 (2002) 108
9. T. Tomura *et al.*, *Phys. Lett.*B **542**, 207 (2002) 106, 107
10. K. Hara *et al.*, *Phys. Rev. Lett.* **89**, 251803 (2002) 108, 109
11. R. Waldi, in *$\mathcal{CP}$ Violation in Particle, Nuclear, and Astrophysics*, ed. M. Beyer, Lecture Notes in Physics, Vol. 591, Springer. Berlin.Heidelberg (2002), p. 43 108
12. The LEP B Oscillation Working Group, CERN-EP-2001-050; and updates at www.cern.ch/LEPBOSC, Mar. 2003 111
13. DELPHI collaboration, *Eur. Phys. J.*C **18**, 229 (2000) 111
14. J. Nir, in *Heavy Flavor Physics*, ed. C. Davies, S. M. Playfer, Institute of Physics, Bristol (2002), p. 147 114
15. A. I. Sanda, K. Ukai, Prog. Theor. Phys. **107**, 421 (2002) 117
16. K. Abe *et al.*, *Phys. Rev.*D **68**, 012001 (2003) 118
17. B. Aubert *et al.*, *Phys. Rev. Lett.* **87**, 201803 (2001) 105, 106
18. K. Hagiwara *et al.*, Review of Particle Physics, *Phys. Rev. D* **66**, 010001 (2002)
19. L. Gibbons, K. Honscheid, in K. Hagiwara *et al.*, Review of Particle Physics, *Phys. Rev. D* **66**, 010001 (2002), p. 643; L. di Caccio *et al.*, preprint MPI-PhE/96-05 (1996), Max-Planck-Institut München 106
20. O. Schneider, in K. Hagiwara *et al.*, Review of Particle Physics, *Phys. Rev. D* **66**, 010001 (2002) , p. 670 109
21. B. Aubert *et al.*, *Phys. Rev. Lett.* **89**, 201802 (2002) 112, 113, 115
22. K. Abe *et al.*, *Phys. Rev.*D **66**, 071102(R) (2002) 114, 115, 116
23. T. Browder, talk at *Intl. Symposium on Lepton-Photon Interactions*, to be published in the proceedings, Chicago, Aug. 2003 117
24. A. Abashian *et al.*, *Nucl. Instrum. Methods*A **479**, 117 (2002) 99, 100
25. B. Aubert *et al.*, *Nucl. Instrum. Methods*A **479**, 1 (2002) 101, 102, 103
26. B. Aubert *et al.*, *Phys. Rev. Lett.* **89**, 281802 (2002) 119
27. B. Winstein, *Phys. Rev. Lett.* **68**, 1271 (1992) 121

7 Weak Quark Mixing and the CKM Matrix

Weak charged-current interactions of hadrons proceed through a Lagrangian of the current × current form

$$L = \frac{G}{\sqrt{2}} J^{+\alpha} \cdot j_\alpha^- + \text{h.c.} \tag{7.1}$$

Here j_α^- is the leptonic charged current

$$j_\alpha^- = \overline{l}\gamma_\alpha(1+\gamma_5)\nu_l \ , \tag{7.2}$$

where the lepton spinor is $\overline{l}$ and the neutrino spinor os ν_l.

The hadronic charged current $J^{+\alpha}$ connects one up-type $(2/3e)$ quark $U = (u, c, s)$ with one down-type $(-1/3e)$ quark $D = (d, s, b)$:

$$J^{+\alpha} = \overline{U}_i \gamma^\alpha (1+\gamma_5) D_k \cdot V_{ik} \ . \tag{7.3}$$

The coupling strength of quark currents is smaller than that of lepton currents. This was first observed in strangeness-changing processes, such as the decay of K mesons and Λ hyperons. The observed coupling V_{us} was about 5 times smaller than V_{ud} in neutron decay. This led Cabibbo [3] to postulate that the weak eigenstates of the then known quarks with $-1/3$ charge were not the flavor eigenstates d and s but a linear combination, rotated by an angle θ, the Cabibbo angle:

$$d_c = d\cos\theta + s\sin\theta \ . \tag{7.4}$$

The GIM mechanism, invented to cancel the $\mathrm{K_L} \to \mu^+\mu^-$ amplitude, required an orthogonal state

$$s_c = -d\sin\theta + s\cos\theta \ . \tag{7.5}$$

With charm complementing the two quark doublets, the hadronic charged current is then

$$J^{+\alpha} = (\overline{u}, \overline{c}) \begin{pmatrix} \cos\theta & \sin\theta \\ -\sin\theta & \cos\theta \end{pmatrix} \gamma_\alpha(1+\gamma_5) \begin{pmatrix} d \\ s \end{pmatrix} \ , \tag{7.6}$$

which contains a unitary (and real) 2×2 rotation matrix with one angle θ.

Konrad Kleinknecht: Uncovering $\mathcal{CP}$ Violation, STMP 195, 123–137 (2003)

For six quarks, this was generalized to a 3×3 unitary mixing matrix by Kobayashi and Maskawa [2]. We follow here a line of reasoning adapted from [1].

By convention, the mixing is often expressed in terms of a 3×3 unitary matrix V operating on mass eigenstates of quarks of charge $-1/3e$ (d, s and b):

$$\begin{pmatrix} d' \\ s' \\ b' \end{pmatrix} = \begin{pmatrix} V_{ud} & V_{us} & V_{ub} \\ V_{cd} & V_{cs} & V_{cb} \\ V_{td} & V_{ts} & V_{tb} \end{pmatrix} \begin{pmatrix} d \\ s \\ b \end{pmatrix} \quad . \tag{7.7}$$

The values of individual matrix elements can, in principle, all be determined from weak decays of the relevant quarks, or, in some cases, from deep inelastic neutrino scattering. Using the eight tree-level constraints discussed below together with unitarity, and assuming only three generations, the 90% confidence limits on the magnitude of the elements of the complete matrix are

$$\begin{pmatrix} 0.9741 \text{ to } 0.9756 & 0.219 \text{ to } 0.226 & 0.0025 \text{ to } 0.0048 \\ 0.219 \text{ to } 0.226 & 0.9732 \text{ to } 0.9748 & 0.038 \text{ to } 0.044 \\ 0.004 \text{ to } 0.014 & 0.037 \text{ to } 0.044 & 0.9990 \text{ to } 0.9993 \end{pmatrix} \quad . \tag{7.8}$$

The ranges shown are for the individual matrix elements. The constraints of unitarity connect different elements, so choosing a specific value for one element restricts the range of others.

There are several parameterizations of the Cabibbo–Kobayashi–Maskawa (CKM) matrix. We advocate a "standard" parameterization [4] of V that utilizes angles θ_{12}, θ_{23}, θ_{13} and a phase, δ_{13}

$$V = \begin{pmatrix} c_{12}c_{13} & s_{12}c_{13} & s_{13}\mathrm{e}^{-\mathrm{i}\delta_{13}} \\ -s_{12}c_{23} - c_{12}s_{23}s_{13}\mathrm{e}^{\mathrm{i}\delta_{13}} & c_{12}c_{23} - s_{12}s_{23}s_{13}\mathrm{e}^{\mathrm{i}\delta_{13}} & s_{23}c_{13} \\ s_{12}s_{23} - c_{12}c_{23}s_{13}\mathrm{e}^{\mathrm{i}\delta_{13}} & -c_{12}s_{23} - s_{12}c_{23}s_{13}\mathrm{e}^{\mathrm{i}\delta_{13}} & c_{23}c_{13} \end{pmatrix} \quad , \tag{7.9}$$

where $c_{ij} = \cos\theta_{ij}$ and $s_{ij} = \sin\theta_{ij}$ for the "generation" labels $i, j = 1, 2, 3$. This has distinct advantages in interpretation, for the rotation angles are defined and labeled in a way which relates to the mixing of two specific generations, and if one of these angles vanishes, so does the mixing between those two generations; in the limit $\theta_{23} = \theta_{13} = 0$ the third generation decouples, and the situation reduces to the usual Cabibbo mixing of the first two generations, with θ_{12} identified as the Cabibbo angle [3]. The real angles θ_{12}, θ_{23}, θ_{13} can all be made to lie in the first quadrant by an appropriate redefinition of quark field phases.

The matrix elements in the first row and third column, which have been directly measured in decay processes, are all of a simple form, and, as c_{13} is known to deviate from unity only in the sixth decimal place, $V_{ud} = c_{12}$, $V_{us} = s_{12}$, $V_{ub} = s_{13}\mathrm{e}^{-\mathrm{i}\delta_{13}}$, $V_{cb} = s_{23}$ and $V_{tb} = c_{23}$ to an excellent approximation. The phase δ_{13} lies in the range $0 \leq \delta_{13} < 2\pi$, with nonzero values generally breaking $\mathcal{CP}$ invariance for the weak interactions. The generalization to the n-generation case contains $n(n-1)/2$ angles and $(n-1)(n-2)/2$ phases.

Using only tree-level processes as constraints, the matrix elements in (7.8) correspond to values of the sines of the angles $s_{12} = 0.2229 \pm 0.0022$, $s_{23} = 0.0412 \pm 0.0020$ and $s_{13} = 0.0036 \pm 0.0007$.

If we use the loop-level processes discussed below as additional constraints, the sines of the angles remain unaffected, and the CKM phase, sometimes referred to as the angle $\gamma = \phi_3$ of the unitarity triangle, is restricted to $\delta_{13} = (1.02 \pm 0.26)$ radians $= (59 \pm 15)^\circ$.

Kobayashi and Maskawa [2] originally chose a parameterization involving the four angles θ_1, θ_2, θ_3 and δ:

$$\begin{pmatrix} d' \\ s' \\ b' \end{pmatrix} = \begin{pmatrix} c_1 & -s_1 c_3 & -s_1 s_3 \\ s_1 c_2 & c_1 c_2 c_3 - s_2 s_3 \mathrm{e}^{\mathrm{i}\delta} & c_1 c_2 s_3 + s_2 c_3 \mathrm{e}^{\mathrm{i}\delta} \\ s_1 s_2 & c_1 s_2 c_3 + c_2 s_3 \mathrm{e}^{\mathrm{i}\delta} & c_1 s_2 s_3 - c_2 c_3 \mathrm{e}^{\mathrm{i}\delta} \end{pmatrix} \begin{pmatrix} d \\ s \\ b \end{pmatrix} , \tag{7.10}$$

where $c_i = \cos\theta_i$ and $s_i = \sin\theta_i$ for $i = 1, 2, 3$. In the limit $\theta_2 = \theta_3 = 0$, this reduces to the usual Cabibbo mixing where θ_1 is identified (up to a sign) with the Cabibbo angle [3]. Note that in this case V_{ub} and V_{td} are real and V_{cb} is complex, illustrating a different placement of the phase than in the standard parameterization. Different forms of the Kobayashi–Maskawa parameterization are found in the literature and referred to as "the" Kobayashi–Maskawa form; some care about which one is being used is needed when the quadrant in which δ lies is under discussion.

The standard parametrization can be approximated in a way that emphasizes the hierarchy in the size of the angles, $s_{12} \gg s_{23} \gg s_{13}$ [5]. Setting $\lambda \equiv s_{12}$, the sine of the Cabibbo angle, one expresses the other elements in terms of powers of λ:

$$V = \begin{pmatrix} 1 - \lambda^2/2 & \lambda & A\lambda^3(\rho - \mathrm{i}\eta) \\ -\lambda & 1 - \lambda^2/2 & A\lambda^2 \\ A\lambda^3(1 - \rho - \mathrm{i}\eta) & -A\lambda^2 & 1 \end{pmatrix} + \mathcal{O}(\lambda^4) \, . \tag{7.11}$$

where A, ρ and η are real numbers that were intended to be of order unity. This approximate form is widely used, especially for B physics, but care must be taken, especially for $\mathcal{CP}$-violating effects in K physics, since the phase enters V_{cd} and V_{cs} through terms that are higher order in λ.

Another parameterization has been advocated [6] that arises naturally where one builds models of quark masses in which initially $m_u = m_d = 0$. With no phases in the third row or third column, the connection between measurements of $\mathcal{CP}$-violating effects for B mesons and individual CKM parameters is less direct than in the standard parameterization.

No physics can depend on which of the above parameterizations (or any other) is used, as long as a single one is used consistently and care is taken to ensure that no other choice of phases is in conflict.

Our present knowledge of the matrix elements comes from the following sources:

1. $|V_{ud}|$. Analyses have been performed comparing nuclear beta decays that proceed through a vector current with muon decay. Radiative corrections are essential to extracting the value of the matrix element. These analyses already include [7] effects of order $Z\alpha^2$, and most of the theoretical argument centers on the nuclear mismatch and structure-dependent radiative corrections [8, 9]. Further data have been obtained on superallowed $0^+ \to 0^+$ beta decays [10].
   Taking the complete data set, a value of $|V_{ud}| = 0.9740 \pm 0.0005$ has been obtained [11]. It has been argued [12] that the change in charge-symmetry violation for quarks inside nucleons that are in nuclear matter results in an additional change in the predicted decay rate of 0.075% to 0.2%, leading to a systematic underestimate of $|V_{ud}|$. This reasoning has been used [13] to explain quantitatively the binding-energy differences between the valence protons and neutrons of mirror nuclei. While it can be argued [11] that including this may involve double counting, we take this correction as an additional uncertainty to obtain a value of $|V_{ud}| = 0.9740 \pm 0.0005 \pm 0.0005$ where the first error is assumed to be Gaussian and the second one to be flat.
   The theoretical uncertainties in extracting a value of $|V_{ud}|$ from neutron decays are significantly smaller than those for decays of mirror nuclei, but the value depends both on the value of $g_{\rm A}/g_{\rm V}$ and on the neutron lifetime. Experimental progress has been made on $g_{\rm A}/g_{\rm V}$ using very highly polarized cold neutrons together with improved detectors. The recent experimental result [14], $g_{\rm A}/g_{\rm V} = -1.2739 \pm 0.0019$, by itself has a better precision than the former world average and results in $|V_{ud}| = 0.9713 \pm 0.0013$ if taken alone. Averaging over all recent experiments using polarizations of more than 90% [15] gives $g_{\rm A}/g_{\rm V} = -1.2720 \pm 0.0018$ and results in $|V_{ud}| = 0.9725 \pm 0.0013$ from neutron decay. Since most of the contributions to the errors in these two determinations of $|V_{ud}|$ are independent, we can average them to obtain

$$|V_{ud}| = 0.9734 \pm 0.0008 \ . \tag{7.12}$$

2. $|V_{us}|$. The original analysis of $\rm K_{e3}$ decays yielded [16]

$$|V_{us}| = 0.2196 \pm 0.0023 \ . \tag{7.13}$$

   With isospin violation in $\rm K^+$ and $\rm K^0$ decays taken into account, the extracted values of $|V_{us}|$ are in agreement at the 1% level. Radiative corrections have recently been calculated by chiral perturbation theory [17]. The combined effects of long-distance radiative corrections and nonlinear terms in the form factor can decrease the value of $|V_{us}|$ by up to 1% [18], and we take this into account by applying an additional correction of $(-0.5 \pm 0.5)\%$, which compensates the effect of radiative corrections in [17], to obtain

$$|V_{us}| = 0.2196 \pm 0.0026 \ , \tag{7.14}$$

in very good agreement with the former analysis. The analysis [19] of hyperon decay data has larger theoretical uncertainties because of first-order SU(3) symmetry-breaking effects in the axial–vector couplings. This analysis has been redone, incorporating second-order SU(3) symmetry-breaking corrections, in models [20] applied to the WA2 data [21], to give a value of $|V_{us}| = 0.2176 \pm 0.0026$, which is consistent with (7.14), obtained using the "best-fit" model. Since the values obtained in these models differ by more than the error estimates and generally do not give good fits, however, we retain the value of $|V_{us}|$, given in (7.14).

3. $|V_{cd}|$. The magnitude of $|V_{cd}|$ may be deduced from neutrino and antineutrino production of charm off valence d quarks. The dimuon production cross sections obtained by the CDHS group [22] yield $\overline{\mathrm{B}}_{\mathrm{c}}\,|V_{cd}|^2 = (0.41 \pm 0.07) \times 10^{-2}$, where $\overline{\mathrm{B}}_{\mathrm{c}}$ is the semileptonic branching fraction of the charmed hadrons produced. The corresponding value from the more recent CCFR Tevatron experiment [23], where a next-to-leading-order QCD analysis has been carried out, is $0.534 \pm 0.021^{+0.025}_{-0.051} \times 10^{-2}$, where the last error is from the scale uncertainty. Assuming a similar scale error for the CDHS measurement and averaging these two results gives $(0.49 \pm 0.05) \times 10^{-2}$. Supplementing this with data [24] on the mix of charmed-particle species produced by neutrinos and with PDG values for their semileptonic branching fractions (to give [23] $\overline{\mathrm{B}}_c = 0.099 \pm 0.012$) yields

$$|V_{cd}| = 0.224 \pm 0.016\ . \tag{7.15}$$

4. $|V_{cs}|$. Values for $|V_{cs}|$ obtained from neutrino production of charm and from semileptonic D decays have errors due to theoretical uncertainties that exceed 10%. These values have been superseded by direct measurements [25] of $|V_{cs}|$ in charm-tagged W decays, which give $|V_{cs}| = 0.97 \pm 0.09\ (\mathrm{stat}) \pm 0.07\ (\mathrm{syst})$. A tighter determination follows from the ratio of hadronic W decays to leptonic decays, which has been measured at LEP with the result [26] that $\sum_{i,j} |V_{ij}|^2 = 2.039 \pm 0.025 \pm 0.001$, where the sum extends over $i = u, c$ and $j = d, s, b$ and the last error is from the knowledge of α_s. For a three-generation CKM matrix, unitarity requires that this sum has a value of 2. Since five of the six CKM matrix elements in the sum are well measured or contribute negligibly to the measured sum of the squares, the LEP measurement can be converted into a greatly improved result [26]:

$$|V_{cs}| = 0.996 \pm 0.013\ . \tag{7.16}$$

5. $|V_{cb}|$. The heavy-quark effective theory (HQET) [27] provides a nearly model-independent treatment of B semileptonic decays to charmed mesons, assuming that both the b and the c quarks are heavy enough for the theory to apply. Measurements of the exclusive decay $\mathrm{B} \to \bar{\mathrm{D}}^* \ell^+ \nu_\ell$ have been used primarily to extract a value of $|V_{cb}|$ using corrections based on the

HQET. Exclusive $B \to \bar{D}\ell^+\nu_\ell$ decays give a consistent, but less precise result. The analysis of inclusive decays, where the measured semileptonic bottom-hadron partial width is assumed to be that of a b quark decaying through the usual $V--A$ interaction, depends on going from the quark to the hadron level and involves an assumption about the validity of quark–hadron duality. The results for $|V_{cb}|$ from exclusive and inclusive decays are generally in good agreement. A much more detailed discussion and a list of references can be found in a mini-review in the Review of Particle Physics [29]. We add an uncertainty due to the assumption of quark–hadron duality [30] to the results from inclusive decays and average over the inclusive and exclusive results, with the theoretical uncertainties combined linearly, to obtain

$$|V_{cb}| = (41.2 \pm 2.0) \times 10^{-3} \ . \tag{7.17}$$

6. $|V_{ub}|$. The decay $b \to u\ell\bar{\nu}$ and its charge conjugate can be observed in the semileptonic decay of B mesons produced on the $\Upsilon(4S)$ $(b\bar{b})$ resonance by measuring the lepton energy spectrum above the endpoint of the $b \to c\ell\bar{\nu}_\ell$ spectrum. There the $b \to u\ell\bar{\nu}_\ell$ decay rate can be obtained by subtracting the background caused by nonresonant e^+e^- reactions. This continuum background is determined from auxiliary measurements off the $\Upsilon(4S)$. The interpretation of this inclusive result in terms of $|V_{ub}|$ depends fairly strongly on the theoretical model used to generate the lepton energy spectrum, especially that for $b \to u$ transitions. At LEP, the separation between u-like and c-like decays is based on up to 20 different event parameters, and while the extraction of $|V_{ub}|$ is less sensitive to theoretical assumptions, it requires a detailed understanding of the decay $b \to c\ell\bar{\nu}_\ell$. The CLEO collaboration [31] has recently employed an important technique that uses moments of measured distributions of $b \to s\gamma$ and $B \to D^*\ell\nu_\ell$ to fix the parameters in the inclusive distribution and thereby reduce the errors.
The value of $|V_{ub}|$ can also be extracted from exclusive decays, such as $B \to \pi\ell\nu_\ell$ and $B \to \rho\ell\nu_\ell$, but there is an associated theoretical model dependence in the values of the matrix elements of the weak current between exclusive states. A detailed discussion of and set of references for both the inclusive and exclusive the analyses can be found in the mini-review on $|V_{ub}|$ in the Review of Particle Physics [32]. We average the LEP and CLEO inclusive results, keeping the theoretical errors separate (and added linearly), to obtain $|V_{ub}| = (4.11 \pm 0.25 \pm 0.78) \times 10^{-3}$, which we combine with the exclusive result from CLEO of $|V_{ub}| = (3.25 \pm 0.32 \pm 0.64) \times 10^{-3}$ to obtain a result dominated by the theoretical uncertainties,

$$|V_{ub}| = (3.6 \pm 0.7) \times 10^{-3} \ . \tag{7.18}$$

7. V_{tb}. The discovery of the top quark by the CDF and D0 collaborations utilized in part the semileptonic decays of t to b. The CDF collaboration

has published a limit on the fraction of decays of the form $t \to b\ \ell^+\ \nu_\ell$, as opposed to semileptonic t decays that involve the light s or d quark, of [33]

$$\frac{|V_{tb}|^2}{|V_{td}|^2 + |V_{ts}|^2 + |V_{tb}|^2} = 0.94^{+0.31}_{-0.24}\ . \tag{7.19}$$

For most of the CKM matrix elements, the principal error is no longer experimental, but instead theoretical. This arises from explicit model dependence in the interpretation of inclusive data or in the direct use of specific hadronic matrix elements to relate decay rates for exclusive processes to weak transitions of quarks. This type of uncertainty is often even larger, at present, in extracting CKM matrix elements from loop diagrams, as discussed below. Such theoretical errors are not distributed in a Gaussian manner. We have judged what is a reasonable range when assigning the theoretical errors.

The issue of how to use appropriate statistical methods to deal with these errors has been intensively discussed over the last few years by a number of authors [34]. While we have used the central values with the quoted errors to make a best overall fit to the CKM matrix (interpreting a "1σ" range in a theoretical error as corresponding to a 68% confidence level that the true value lies within a range of "$\pm 1\sigma$" of the central value in making those fits), the result should be used with appropriate care. Our limited knowledge of some of the theoretical uncertainties makes us cautious about extending this procedure to results for multi-standard-deviation determinations of the allowed regions for CKM matrix elements. We have determined the best fit by searching for the minimum chi-squared, by scanning the parameter spaces of the four angles. The results for three generations of quarks, from (7.12), (7.14), (7.15), (7.16), (7.17), (7.18) and (7.19) plus unitarity, are summarized in the matrix in (7.8). The ranges given there are different from those given in (7.12)–(7.19) because of the inclusion of unitarity, but are consistent with the one-standard-deviation errors on the input matrix elements. Note in particular that the unitarity constraint has pushed $|V_{ud}|$ about one standard deviation higher than the value given in (7.12). If we had kept the error on $|V_{ud}|$ quoted in [11], we would have a violation of unitarity in the first row of the CKM matrix by about 2.7 standard deviations. While this deserves some attention and encourages another more accurate measurement of $|V_{us}|$ as well as more theoretical work, we do not see this yet as a major challenge to the validity of the three-generation Standard Model.

The data do not preclude there being more than three generations. Moreover, the entries deduced from unitarity might be altered if the CKM matrix is expanded to accommodate more generations. Conversely, the known entries restrict the possible values of the additional elements if the matrix is expanded to account for additional generations. For example, unitarity and the known elements of the first row require that any additional element in the first row has a magnitude $|V_{ub'}| < 0.10$. When there are more than three gen-

erations, the allowed ranges (at 90% C.L.) of the matrix elements connecting the first three generations are

$$\begin{pmatrix} 0.9721 \text{ to } 0.9747 & 0.215 \text{ to } 0.224 & 0.002 \text{ to } 0.005 \ldots \\ 0.209 \text{ to } 0.227 & 0.966 \text{ to } 0.976 & 0.038 \text{ to } 0.044 \ldots \\ 0 \text{ to } 0.09 & 0 \text{ to } 0.12 & 0.08 \text{ to } 0.9993 \ldots \\ \vdots & \vdots & \vdots \end{pmatrix} , \tag{7.20}$$

where we have used unitarity (for the expanded matrix) and the measurements of the magnitudes of the CKM matrix elements (including the constraint from hadronic W decays), resulting in the weak bound $|V_{tb}| > 0.08$.

Direct and indirect information about the smallest matrix elements of the CKM matrix can be neatly summarized in terms of the "unitarity triangle", one of six such triangles that correspond to the unitarity condition applied to two different rows or columns of the CKM matrix. Unitarity applied to the first and third columns yields

$$V_{ud}V_{ub}^* + V_{cd}V_{cb}^* + V_{td}V_{tb}^* = 0 \ . \tag{7.21}$$

The unitarity triangle is just a geometrical representation of this equation in the complex plane [35], as shown in Fig. 7.1a. We can always choose to orient the triangle so that $V_{cd}V_{cb}^*$ lies along the horizontal; in the standard parameterization, V_{cb} is real, and V_{cd} is real to a very good approximation in any case. Setting cosines of small angles to unity, (7.21) becomes

$$V_{ub}^* + V_{td} \approx s_{12}V_{cb}^* \ , \tag{7.22}$$

which is shown by the unitarity triangle. The sides of this triangle are of the order of 1% of the diagonal elements of the CKM matrix, which highlights the precision we are aiming to achieve in knowing each of these sides, a precision of a few percent.

The angles α, β and γ of the triangle are also referred to as ϕ_2, ϕ_1, and ϕ_3, respectively, with β and $\gamma = \delta_{13}$ being the phases of the CKM elements V_{td} and V_{ub} as per

$$V_{td} = |V_{td}|\mathrm{e}^{-\mathrm{i}\beta}, \quad V_{ub} = |V_{ub}|\mathrm{e}^{-\mathrm{i}\gamma} \ . \tag{7.23}$$

If we rescale the triangle so that the base is of unit length, the coordinates of the vertices A, B and C become, respectively,

$$\left(\frac{\Re e\,(V_{ud}V_{ub}^*)}{|V_{cd}V_{cb}^*|}, \ \frac{\Im m\,(V_{ud}V_{ub}^*)}{|V_{cd}V_{cb}^*|} \right), \ (1,0) \text{ and } (0,0) \ . \tag{7.24}$$

The coordinates of the apex of the rescaled unitarity triangle take the simple form $(\bar{\rho}, \bar{\eta})$, where $\bar{\rho} = \rho(1-\lambda^2/2)$ and $\bar{\eta} = \eta(1-\lambda^2/2)$ in the Wolfenstein parameterization [5], as shown in Fig. 7.1b.

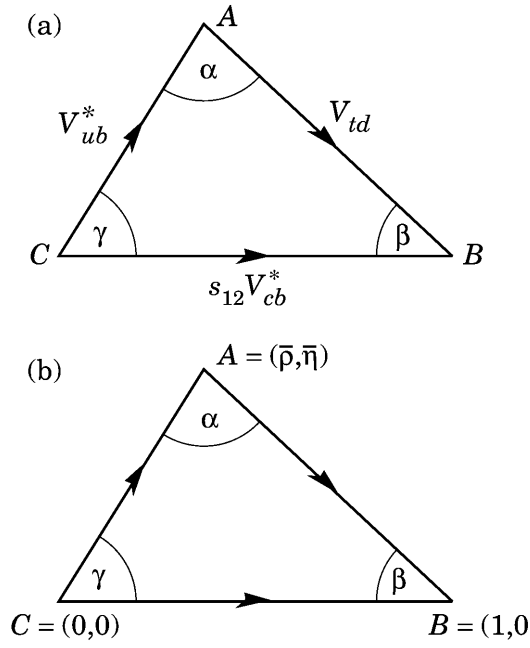

Fig. 7.1. (**a**) Representation in the complex plane of the triangle formed by the CKM matrix elements $V_{ud}V^*_{ub}$, $V_{td}V^*_{tb}$, and $V_{cd}V^*_{cb}$. (**b**) Rescaled triangle with vertices A, B and C at $(\bar{\rho}, \bar{\eta})$, $(1, 0)$ and $(0, 0)$, respectively

$\mathcal{CP}$-violating processes involve the phase in the CKM matrix, assuming that the observed $\mathcal{CP}$ violation is related solely to a nonzero value of this phase. More specifically, a necessary and sufficient condition for $\mathcal{CP}$ violation with three generations can be formulated in a parameterization-independent manner in terms of the nonvanishing of J, the determinant of the commutator of the mass matrices for the charge $2e/3$ and charge $-e/3$ quarks [36]. The $\mathcal{CP}$-violating amplitudes or differences of rates are all proportional to the product of CKM factors in this quantity, namely $s_{12}s_{13}s_{23}c_{12}c^2_{13}c_{23}\sin\delta_{13}$. This is just twice the area of the unitarity triangle.

Further information, particularly about CKM matrix elements involving the top quark, can be obtained from flavor-changing processes that occur at the one-loop level. This is visualized in Fig. 7.2, where the processes relevant to the various sides and angles of the unitarity triangle are indicated. We have not used this information up to this point, since the derivation of values for V_{td} and V_{ts} in this manner from, for example, B mixing or $b \to s\gamma$, requires an additional assumption that the top-quark loop, rather than new physics, gives the dominant contribution to the process in question. Conversely, when we find agreement between CKM matrix elements extracted from loop diagrams

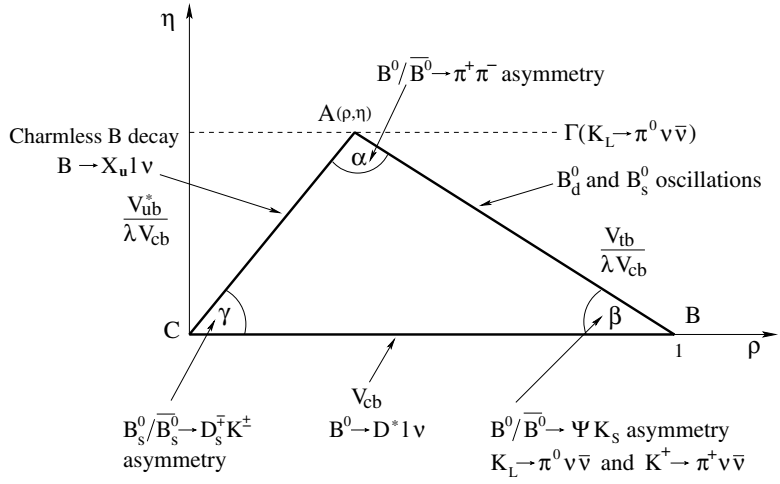

Fig. 7.2. CKM unitarity triangle for the B^0 system

and the values given above based on direct measurements plus the assumption of three generations, this can be used to place restrictions on new physics.

We consider first constraints from flavor-changing processes that are not $\mathcal{CP}$-violating. The measured value [37] of $\Delta m_{B_d^0} = 0.489 \pm 0.008$ ps^{-1} from $B_d^0 - - \overline{B_d^0}$ mixing can be turned into information about $|V_{tb}^* V_{td}|$, assuming that the dominant contribution to the mass difference arises from the matrix element between a B_d^0 and a $\overline{B_d^0}$ of an operator that corresponds to a box diagram with W bosons and top quarks as sides. Using the characteristic hadronic matrix element that then occurs, $\hat{B}_{B_d^0} f_{B_d^0}^2 = (1.30 \pm 0.12)(198 \pm 30 \text{ MeV})^2$, obtained from lattice QCD calculations [38]; next-to-leading-order QCD corrections ($\eta_{\text{QCD}} = 0.55$) [39]; and the running top-quark mass, $\overline{m}_t(m_t) = (166 \pm 5)$ GeV, as input, we obtain

$$|V_{tb}^* V_{td}| = 0.0079 \pm 0.0015 \ , \tag{7.25}$$

where the uncertainty comes primarily from the uncertainty in the hadronic matrix elements, whose estimated errors have been combined linearly.

In the ratio of the B_s^0 and B_d^0 mass differences, many common factors (such as the QCD correction and the dependence on the top-quark mass) cancel, and we have

$$\frac{\Delta m_s}{\Delta m_d} = \frac{\Delta m_{B_s^0}}{\Delta m_{B_d^0}} = \frac{m_{B_s^0}}{m_{B_d^0}} \frac{\hat{B}_{B_s^0} f_{B_s^0}^2}{\hat{B}_{B_d^0} f_{B_d^0}^2} \frac{|V_{tb}^* V_{ts}|^2}{|V_{tb}^* V_{td}|^2} \ . \tag{7.26}$$

With the experimentally measured masses, $\hat{B}_{B_s^0} f_{B_s^0}^2 / (\hat{B}_{B_d^0} f_{B_d^0}^2) = (1.15 \pm 0.06\, {}^{+0.07}_{-0.00})^2$, where the last, asymmetric error reflects the effect of the presence

of chiral logarithms in the unquenched calculations of f_B in lattice QCD [38], and the experimental lower limit [37] at 95% C.L. of $\Delta m_{B_s^0} > 13.1\ \mathrm{ps}^{-1}$ based on published data, we obtain

$$|V_{td}|/|V_{ts}| < 0.25\ . \tag{7.27}$$

Since, with three generations, $|V_{ts}| \approx |V_{cb}|$, this result converts to $|V_{td}| < 0.010$, which is a significant constraint by itself, (see Fig. 7.3).

The CLEO observation [40] of $b \to s\gamma$ is in agreement with the Standard Model prediction. This agreement can be translated into a constraint on $|V_{ts}|$ that is consistent with the result expected with three generations, but with a large uncertainty that is dominantly theoretical.

In the $K^+ \to \pi^+ \nu\bar{\nu}$ decay, there are significant contributions from loop diagrams involving both charm and top quarks. Experiments are just beginning to probe the level predicted in the Standard Model [41].

All these additional indirect constraints are consistent with the CKM elements obtained from the direct measurements plus unitarity, assuming three generations. Adding the results on B mixing together with theoretical improvements in lattice calculations reduces the range allowed for $|V_{td}|$.

Now we turn to $\mathcal{CP}$-violating processes. The added constraint from $\mathcal{CP}$ violation in the neutral kaon system, taken together with the restrictions above on the magnitudes of the CKM matrix elements, is tight enough to restrict considerably the range of angles and the phase of the CKM matrix. For example, the constraint obtained from the $\mathcal{CP}$-violating parameter ϵ in the neutral K system corresponds to the vertex A of the unitarity triangle lying on a hyperbola for fixed values of the (imprecisely known) hadronic matrix elements. [1].

In addition, following the initial evidence [44], it is now established that direct $\mathcal{CP}$ violation in the weak transition from a neutral K to two pions exists, i.e. the parameter ε' is nonzero [48]. While theoretical uncertainties in hadronic matrix elements whose amplitudes cancel presently preclude this measurement from giving a significant constraint on the unitarity triangle, this measurement supports the assumption that the observed $\mathcal{CP}$ violation is related to a nonzero value of the CKM phase.

Ultimately, in the neutral K system, the $\mathcal{CP}$-violating process $K_L \to \pi^0 \nu\bar{\nu}$ offers the possibility of a theoretically clean, high-precision measurement of the imaginary part of $V_{td}V_{ts}^*$ and the area of the unitarity triangle. Given $|V_{ts}|$, this will yield the altitude of the unitarity triangle. However, the experimental upper limit is presently many orders of magnitude away from the required sensitivity.

[1] The relevant QCD corrections, given to leading order in [42], have been extended to next-to-leading order in [39, 49]. The limiting curves in Fig. 7.3 arising from the value of $|\varepsilon|$ correspond to values of the hadronic matrix element, expressed in terms of the invariant parameter $\hat{B}_K$ of the renormalization group, from 0.75 to 1.10. See, for example, [43]

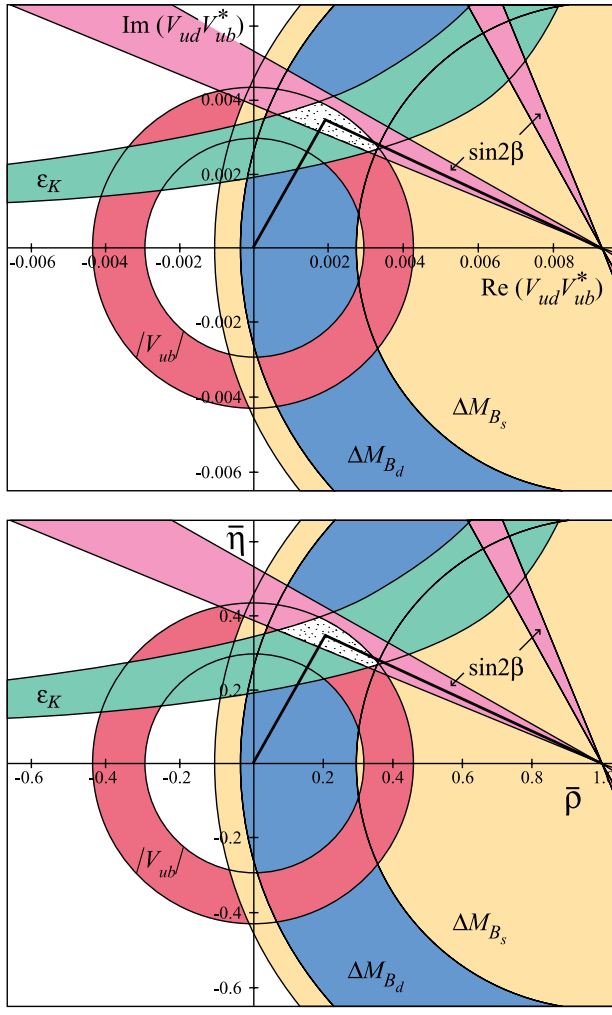

Fig. 7.3. Constraints from the text on the position of the apex, A, of the unitarity triangle following from $|V_{ub}|$, B mixing, ϵ, and $\sin 2\beta$. A possible unitarity triangle is shown with A in the preferred region.

Turning to the B meson system, for $\mathcal{CP}$-violating asymmetries of neutral B mesons decaying to $\mathcal{CP}$ eigenstates, the interference between mixing and a single weak decay amplitude for certain final states directly relates the asymmetry in a given decay to $\sin 2\phi$, where $\phi = \alpha, \beta, \gamma$ is an angle of the unitarity triangle [35]. A new generation of experiments has established a nonvanishing asymmetry in the decays $\mathrm{B_d}(\bar{\mathrm{B}}_\mathrm{d}) \to \mathrm{J}/\Psi\mathrm{K_S}$ and in other $\mathrm{B_d}$ decay modes,

where the asymmetry is given by $\sin 2\beta$. The present experimental results from BaBar [45] and Belle [46], when averaged, yield

$$\sin 2\beta = 0.731 \pm 0.055 \ . \tag{7.28}$$

While the limits on the leptonic charge asymmetry for $B_d^0 - -\overline{B_d^0}$ mixing (which measure the analogue of 2 $\Re e\ \epsilon$ in the neutral K system) have been reduced to the 1% level [37], they are still roughly an order of magnitude greater than the value expected without new physics. They provide no significant constraints on the CKM matrix for now [47].

The constraints on the apex of the unitarity triangle that follow from (7.18), (7.25), (7.27), (7.28) and ε are shown in Fig. 7.3. Both the limit on Δm_s and the value of Δm_d indicate that the apex lies in the first rather than the second quadrant. All constraints overlap nicely in one small area in the first quadrant, with the sign of ε measured in the K system agreeing with the sign of $\sin 2\beta$ measured in the B system.

Both the constraints from the lengths of the sides (from $|V_{ub}|$, $|V_{cb}|$, and $|V_{td}|$) and the contraints obtained independently from $\mathcal{CP}$-violating processes (ε from the K system and $\sin 2\beta$ from the B system) indicate the same region for the apex of the triangle.

From a combined fit using the direct measurements, B mixing, ϵ, and $\sin 2\beta$, we obtain:

$$\Re\mathrm{e}\ V_{td} = 0.0071 \pm 0.0008 \tag{7.29}$$

$$\Im\mathrm{m}\ V_{td} = -0.0031 \pm 0.0004 \tag{7.30}$$

$$\bar{\rho} = 0.21 \pm 0.10 \ , \tag{7.31}$$

$$\bar{\eta} = 0.35 \pm 0.05 \ . \tag{7.32}$$

All processes can be quantitatively understood by use of one value of the CKM phase $\delta_{13} = \gamma = (59 \pm 15)^\circ$. The value of $\beta = (23.0 \pm 2.2)^\circ$ from the overall fit is consistent with the value from the $\mathcal{CP}$ asymmetry measurements of $(23.5 \pm 2.4)^\circ$. The invariant measure of $\mathcal{CP}$ violation is $J = (3.0 \pm 0.3) \times 10^{-5}$.

The limit in (7.27) is not far from the value we would expect from the other information on the unitarity triangle. This limit is more robust theoretically, since it depends on ratios (rather than absolute values) of hadronic matrix elements and is independent of the top mass andr QCD corrections (which cancel in the ratio). Thus the significant increase in experimental sensitivity to B_s mixing that should become available in the next few years will lead either to an observation of mixing as predicted by our knowledge to date or to an indication of physics beyond the Standard Model. New physics could also be found in a variety of other measurements involving K and B mixing and/or decay.

References

1. F. Gilman, K. Kleinknecht, B. Renk, in K. Hagiwara *et al.*, Review of Particle Physics, *Phys. Rev. D* **66**, 010001 (2002) 124
2. M. Kobayashi, T. Maskawa, *Prog. Theor. Phys.* **49**, 652 (1973) 124, 125
3. N. Cabibbo, *Phys. Rev. Lett.* **10**, 531 (1963). 123, 124, 125
4. L.-L. Chau, W.-Y. Keung, *Phys. Rev. Lett.* **53**, 1802 (1984); H. Harari, M Leurer, *Phys. Lett.*B **181**, 123 (1986); H. Fritzsch, J. Plankl, *Phys. Rev.*D **35**, 1732 (1987); F. J. Botella, L.-L. Chao, *Phys. Lett.*B **168**, 97 (1986) 124
5. L. Wolfenstein, *Phys. Rev. Lett.* **51**, 1945 (1983) 125, 130
6. C. D. Frogatt, H. B. Nielsen, *Nucl. Phys.*B **147**, 277 (1979); H. Fritzsch, *Nucl. Phys.*B **155**, 189 (1979); S. Dimopoulos, L. J. Hall, S. Rabi, *Phys. Rev. Lett.* **68**, 1984 (1992); H. Fritzsch, Z.-Z. Xing, *Phys. Lett.*B **413**, 396 (1997) 125
7. W. J. Marciano, A. Sirlin, *Phys. Rev. Lett.* **56**, 22 (1986); A. Sirlin, R. Zucchini, *Phys. Rev. Lett.* **57**, 1994 (1986); W. Jaus, G. Rasche, *Phys. Rev.*D **35**, 3420 (1987); A. Sirlin, *Phys. Rev.*D **35**, 3423 (1987) 126
8. B. A. Brown, W. E. Ormand, *Phys. Rev. Lett.* **62**, 866 (1989) 126
9. F. C. Barker *et al.*, *Nucl. Phys.*A **540**, 501 (1992); F. C. Barker *et al.*, *Nucl. Phys.*A **579**, 62 (1994) 126
10. G. Savard *et al.*, *Phys. Rev. Lett.* **74**, 1521 (1995) 126
11. J. C. Hardy, I. S. Towner, talk at WEIN98, Santa Fe, June 14–21, 1998; nucl-th/9809087 126, 129
12. K. P. Saito and A. W. Thomas, *Phys. Lett.*B **363**, 157 (1995) 126
13. K. Tsushima, K. Saito, A. W. Thomas, nucl-th/9907101 126
14. H. Abele *et al.*, *Phys. Rev. Lett.* **88**, 211801 (2002) [a final result of J. Reich *et al.*, *Nucl. Instrum. Methods A* **440**, 535 (2000) and H. Abele *et al.*, *Nucl. Phys.*A **612**, 53 (1997)] 126
15. Yu. A. Mostovoi *et al.*, *Phys. Atomic Nucl.* **64**, 1955 (2001); P. Liaud, *Nucl. Phys.*A **612**, 53 (1997) 126
16. H. Leutwyler and M. Roos, *Z. Phys.*C **25**, 91 (1984) see also R. E. Shrock and L.-L. Wang, *Phys. Rev. Lett.* **41**, 1692 (1978) 126
17. V. Cirigliano *et al.*, *Eur. Phys. J.*C **23**, 121 (2002) 126
18. G. Calderon, G. Lopez Castro , *Phys. Rev.*D **65**, 073032 (2002) 126
19. J. F. Donoghue, B. R. Holstein, S. W. Klimt, *Phys. Rev.*D **35**, 934 (1987) 127
20. R. Flores-Mendieta, A. Garcia, G. Sanchez-Col'on, *Phys. Rev.*D **54**, 6855 (1996) 127
21. M. Bourquin *et al.*, *Z. Phys.*C **21**, 27 (1983) 127
22. H. Abramowicz *et al.*, *Z. Phys.*C **15**, 19 (1982) 127
23. S. A. Rabinowitz *et al.*, *Phys. Rev. Lett.* **70**, 134 (1993); A. O. Bazarko *et al.*, *Z. Phys.*C **65**, 189 (1995) 127
24. N. Ushida *et al.*, *Phys. Lett.*B **206**, 375 (1988). 127
25. P. Abreu *et al.*, *Phys. Lett.*B **439**, 209 (1998); R. Barate *et al.*, *Phys. Lett.*B **465**, 349 (1999) 127
26. LEP Collaborations, LEP Electroweak Working Group, SLD Heavy Flavour and Electroweak Groups, hep-ex/0112021v2 (2002) 127
27. N. Isgur, M. B. Wise, *Phys. Lett.*B **232**, 113 (1989); *Phys. Lett.*B **237**, 527 (1990) Erratum; E. Eichten, B. Hill, *Phys. Lett.*B **234**, 511 (1990); M. E. Luke, *Phys. Lett.*B **252**, 447 (1990)

28. K. Hagiwara *et al.*, Review of Particle Physics, *Phys. Rev. D* **66**, 010001 (2002) 127
29. M. Artuso, E. Barberio, Determination of V_{cb}, in K. Hagiwara *et al.*, Review of Particle Physics, *Phys. Rev. D* **66**, 010001 (2002) p. 701 128
30. A. Falk, presentation at the Fifth KEK Topical Conference, Tsukuba, Japan, November 20–22, 2001; hep-ph/0201094 128
31. A. Bornheim *et al.* (CLEO Collaboration), hep-ex/0202019 (2002) 128
32. M. Battaglia, L. Gibbons, Determination of V_{ub}, in K. Hagiwara *et al.*, Review of Particle Physics, *Phys. Rev. D* **66**, 010001 (2002) p. 706 128
33. T. Affolder *et al.*, *Phys. Rev. Lett.* **86**, 3233 (2001) 129
34. A. Hocker *et al.*, *Eur. Phys. J. C* 21 225 2001; C. Ciuchini *et al.*, *J. High Energy Phys.* **0107**, 013 (2001) 129
35. L.-L. Chau, W. Y. Keung, *Phys. Rev. Lett.* **53**, 1802 (1984); J. D. Bjorken, *Phys. Rev.*D **39**, 1396 (1989); C. Jarlskog and R. Stora, *Phys. Lett.*B **208**, 268 (1988); J. L. Rosner, A. I. Sanda, M. P. Schmidt, in *Proceedings of the Workshop on High Sensitivity Beauty Physics at Fermilab*, November 11 – 14, 1987, ed. A. J. Slaughter, N. Lockyer, M. Schmidt, Fermilab, Batavia, IL (1988), p. 165; C. Hamzaoui, J. L. Rosner, A. I. Sanda, in *Proceedings of the Workshop on High Sensitivity Beauty Physics at Fermilab*, November 11 – 14, 1987, ed. A. J. Slaughter, N. Lockyer, M. Schmidt, Fermilab, Batavia, IL (1988), p. 215 130, 134
36. C. Jarlskog, *Phys. Rev. Lett.* **55**, 1039 (1985); *Z. Phys.*C **29**, 491 (1985) 131
37. O. Schneider, $B^0 - \bar{B}^0$ Mixing, in K. Hagiwara *et al.*, Review of Particle Physics, *Phys. Rev. D* **66**, 010001 (2002) p. 670 132, 133, 135
38. S. Ryan, *Nucl. Phys. Proc. Suppl.* **106**, 86 (2002); hep-lat/01111010; A. Kronfeld, invited talk at the 9th International Symposium on Heavy Flavor Physics, September 10 – 13, 2001, Pasadena, California, FERMILAB-Conf-01/368-T; hep-ph/0111376 132, 133
39. A. J. Buras *et al.*, *Nucl. Phys.*B **347**, 491 (1990) 132, 133
40. S. Chen *et al.* (CLEO Collaboration), CLEO preprint 01-16; hep-ex/0108032, (2001) 133
41. S. Adler *et al.* (E787 Collaboration), hep-ex/0111091 (2001) 133
42. F. J. Gilman, M. B. Wise *Phys. Lett.*B **93**, 129 (1980); *Phys. Rev.*D **27**, 1128 (1983) 133
43. L. Lellouch *Nucl. Phys. Proc. Suppl.* **94**, 142 (2001) 133
44. H. Burkhardt *et al.*, *Phys. Lett.*B **206**, 169 (1988) 133
45. B. Aubert *et al.*, *Phys. Rev. Lett.* **89**, 201802 (2002) 135
46. K. Abe *et al.*, *Phys. Rev.*D **66**, 071102(R) (2002) 135
47. S. Laplace *et al.*, hep-ph/0202010 (2002(135
48. M. Woods *et al.*, *Phys. Rev. Lett.* **60**, 1695 (1988); H. Burkhardt *et al.*, *Phys. Lett. B* **206**, 169 (1988); J.R. Patterson *et al.*, *Phys. Rev. Lett.* **64**, 1491 (1990); L.K. Gibbons *et al.*, *Phys. Rev. Lett.* **70**, 1203 (1993); G.D. Barr *et al.*, *Phys. Lett. B* **317**, 233 (1993); A. Alavi-Harati *et al.*, *Phys. Rev. Lett.* **83**, 22 (1999); V. Fanti *et al.*, *Phys. Lett. B* **465**, 335 (1999); A. Lai *et al.*, *Eur. Phys. J. C* **22**, 231 (2001); J. R. Batley *et al.*, *Phys. Lett. B* **544**, 97 (2002); A. Alavi-Harati *et al.*, *Phys. Rev. D* **67**, 012005 (2003) 133
49. S. Herrlich and U. Nierste, *Nucl. Phys. B* **419**, 212 (1992); *Nucl. Phys. B* **476**, 27 (1996) 133

8 Conclusion

Nearly 40 years after the discovery of $\mathcal{CP}$ violation, the nature of the phenomenon has been clarified experimentally. In the K meson system, $\mathcal{CP}$ violation has been discovered in the mixing (ε), in the decay (ε'/ε, direct violation) and in the interference between mixing and decay ($\Im m\,\varepsilon$); in the B meson system, $\mathcal{CP}$ violation in the interference between mixing and decay has been observed ($\sin 2\beta$). All observations are consistent with the model of Kobayashi and Maskawa, where the weak 3×3 mixing matrix of six quarks has one nontrivial complex phase $\delta = (59 \pm 15)^\circ$. This leads to complex weak coupling constants of quarks, and to $\mathcal{T}$ violation and $\mathcal{CP}$ violation. The origin of the phase δ could be due, amongst other things, to the Higgs sector of the Standard Model or to right-handed currents.

Future experiments in the B sector will observe direct $\mathcal{CP}$ violation in B_d^0, mixing in B_s^0 and possibly $\mathcal{CP}$ violation in the B_s^0 system.

In cosmology, this $\mathcal{CP}$ violation in the quark sector, together with a large departure from thermal equilibrium via a first-order electroweak phase transition [1] and a baryon number violation by instantaneous processes [2], could in principle lead to the observed baryon asymmetry. The source would be the asymmetric interactions of quarks and antiquarks with the Higgs field [3]. However, the large lower bound of 114 GeV on the mass of the Higgs boson derived from LEP experiments makes this scenario very unlikely. One way out of this dilemma is the hypothesis that $\mathcal{CP}$ violation in the neutrino mixing matrix could cause a lepton asymmetry. (B+L)-violating processes before the electroweak phase transition could then convert this into a baryon asymmetry. This leptogenesis would proceed through the production of heavy Majorana neutrinos in the early Universe [4]. The measurement of such a $\mathcal{CP}$ violation in the neutrino sector, however, requires oscillation experiments over a distance of 3000 km, or, alternatively, at nuclear reactorsover a distance of about 3 km. In both cases the neutrino sources have to be very intense. For some time to come, the origin of the cosmological baryon asymmetry will remain an open question.

References

1. V. A. Rubakov, M. E. Shaposhnikov, *Phys. Uspekhi* **39**, 461 (1996) 139

Konrad Kleinknecht: Uncovering $\mathcal{CP}$ Violation, STMP 195, 139–140 (2003)

2. G. t' Hooft, *Phys. Rev. Lett.* **37**, 8 (1976); *Phys. Rev.*D **14**, 3422 (1976) 139
3. A. Riotto, M. Trodden, *Ann. Rev. Nucl. Part. Sci.* **49**, 35 (1999) 139
4. M. Fukugita, T. Yanagida, *Phys. Lett.*B **174**, 45 (1986); M. Flanz *et al.*, *Phys. Lett.*B **345**, 248 (1995); W. Buchmüller, *Ann. Phys.* (Leipzig) **10**, 95 (2001) 139

Index

Konrad Kleinknecht: Uncovering $\mathcal{CP}$ Violation, STMP 195, 141–142 (2003)

Springer Tracts in Modern Physics

156 **Growth Processes and Surface Phase Equilibria in Molecular Beam Epitaxy**
By N.N. Ledentsov 1999. 17 figs. VIII, 84 pages

157 **Deposition of Diamond-Like Superhard Materials**
By W. Kulisch 1999. 60 figs. X, 191 pages

158 **Nonlinear Optics of Random Media**
Fractal Composites and Metal-Dielectric Films
By V.M. Shalaev 2000. 51 figs. XII, 158 pages

159 **Magnetic Dichroism in Core-Level Photoemission**
By K. Starke 2000. 64 figs. X, 136 pages

160 **Physics with Tau Leptons**
By A. Stahl 2000. 236 figs. VIII, 315 pages

161 **Semiclassical Theory of Mesoscopic Quantum Systems**
By K. Richter 2000. 50 figs. IX, 221 pages

162 **Electroweak Precision Tests at LEP**
By W. Hollik and G. Duckeck 2000. 60 figs. VIII, 161 pages

163 **Symmetries in Intermediate and High Energy Physics**
Ed. by A. Faessler, T.S. Kosmas, and G.K. Leontaris 2000. 96 figs. XVI, 316 pages

164 **Pattern Formation in Granular Materials**
By G.H. Ristow 2000. 83 figs. XIII, 161 pages

165 **Path Integral Quantization and Stochastic Quantization**
By M. Masujima 2000. 0 figs. XII, 282 pages

166 **Probing the Quantum Vacuum**
Pertubative Effective Action Approach in Quantum Electrodynamics and its Application
By W. Dittrich and H. Gies 2000. 16 figs. XI, 241 pages

167 **Photoelectric Properties and Applications of Low-Mobility Semiconductors**
By R. Könenkamp 2000. 57 figs. VIII, 100 pages

168 **Deep Inelastic Positron-Proton Scattering in the High-Momentum-Transfer Regime of HERA**
By U.F. Katz 2000. 96 figs. VIII, 237 pages

169 **Semiconductor Cavity Quantum Electrodynamics**
By Y. Yamamoto, T. Tassone, H. Cao 2000. 67 figs. VIII, 154 pages

170 **d–d Excitations in Transition-Metal Oxides**
A Spin-Polarized Electron Energy-Loss Spectroscopy (SPEELS) Study
By B. Fromme 2001. 53 figs. XII, 143 pages

171 **High-T_c Superconductors for Magnet and Energy Technology**
By B. R. Lehndorff 2001. 139 figs. XII, 209 pages

172 **Dissipative Quantum Chaos and Decoherence**
By D. Braun 2001. 22 figs. XI, 132 pages

173 **Quantum Information**
An Introduction to Basic Theoretical Concepts and Experiments
By G. Alber, T. Beth, M. Horodecki, P. Horodecki, R. Horodecki, M. Rötteler, H. Weinfurter, R. Werner, and A. Zeilinger 2001. 60 figs. XI, 216 pages

174 **Superconductor/Semiconductor Junctions**
By Thomas Schäpers 2001. 91 figs. IX, 145 pages

175 **Ion-Induced Electron Emission from Crystalline Solids**
By Hiroshi Kudo 2002. 85 figs. IX, 161 pages

176 **Infrared Spectroscopy of Molecular Clusters**
An Introduction to Intermolecular Forces
By Martina Havenith 2002. 33 figs. VIII, 120 pages

Springer Tracts in Modern Physics

177 **Applied Asymptotic Expansions in Momenta and Masses**
By Vladimir A. Smirnov 2002. 52 figs. IX, 263 pages

178 **Capillary Surfaces**
Shape – Stability – Dynamics, in Particular Under Weightlessness
By Dieter Langbein 2002. 182 figs. XVIII, 364 pages

179 **Anomalous X-ray Scattering for Materials Characterization**
Atomic-Scale Structure Determination
By Yoshio Waseda 2002. 132 figs. XIV, 214 pages

180 **Coverings of Discrete Quasiperiodic Sets**
Theory and Applications to Quasicrystals
Edited by P. Kramer and Z. Papadopolos 2002. 128 figs., XIV, 274 pages

181 **Emulsion Science**
Basic Principles. An Overview
By J. Bibette, F. Leal-Calderon, V. Schmitt, and P. Poulin 2002. 50 figs., IX, 140 pages

182 **Transmission Electron Microscopy of Semiconductor Nanostructures**
An Analysis of Composition and Strain State
By A. Rosenauer 2003. 136 figs., XII, 238 pages

183 **Transverse Patterns in Nonlinear Optical Resonators**
By K. Staliūnas, V. J. Sánchez-Morcillo 2003. 132 figs., XII, 226 pages

184 **Statistical Physics and Economics**
Concepts, Tools and Applications
By M. Schulz 2003. 54 figs., XII, 244 pages

185 **Electronic Defect States in Alkali Halides**
Effects of Interaction with Molecular Ions
By V. Dierolf 2003. 80 figs., XII, 196 pages

186 **Electron-Beam Interactions with Solids**
Application of the Monte Carlo Method to Electron Scattering Problems
By M. Dapor 2003. 27 figs., X, 110 pages

187 **High-Field Transport in Semiconductor Superlattices**
By K. Leo 2003. 164 figs., XIV, 240 pages

188 **Transverse Pattern Formation in Photorefractive Optics**
By C. Denz, M. Schwab, and C. Weilnau 2003. 143 figs., XVIII, 331 pages

189 **Spatio-Temporal Dynamics and Quantum Fluctuations in Semiconductor Lasers**
By O. Hess, E. Gehrig 2003. 91 figs., XIV, 230 pages

190 **Neutrino Mass**
Edited by G. Altarelli, K. Winter 2003. 118 figs., XII, 248 pages

191 **Spin-orbit Coupling Effects in Two-dimensional Electron and Hole Systems**
By R. Winkler 2003. 66 figs., XII, 228 pages

192 **Electronic Quantum Transport in Mesoscopic Semiconductor Structures**
By T. Ihn 2003. 90 figs., XII, 280 pages

193 **Spinning Particles – Semiclassics and Spectral Statistics**
By S. Keppeler 2003. 15 figs., X, 190 pages

194 **Light Emitting Silicon for Microphotonics**
By S. Ossicini, L. Pavesi, and F. Priolo 2003. 206 figs., XII, 288 pages

195 **Uncovering *CP* Violation**
Experimental Clarification in the Neutral K Meson and B Meson Systems
By K. Kleinknecht 2003. 61 figs., XII, 142 pages